

Quantum

Optics

Winter Semester

2023/24

Igor Lesanovsky

## I Quantisation of the electromagnetic field ①

- the electromagnetic field is described by the variables  $\vec{E}$  (electric field) and  $\vec{B}$  (magnetic field)
- $\vec{E}$  and  $\vec{B}$  are solutions of Maxwell's equations
- despite  $\vec{E}$  and  $\vec{B}$  having each 3, i.e. in total 6, components only 4 of them are independent (gauge freedom)
- these independent degrees of freedom are typically expressed through the vector potential  $\vec{A}$  and the scalar potential  $\phi$
- in quantum optics we are often dealing with electromagnetic fields that are confined in finite volumes, e.g. in a cavity

- here it is convenient to decompose the fields into so-called modes, which are the solutions of Maxwell's equations with appropriate boundary conditions
- each mode has a periodic time-dependence and an energy that is quadratic in its amplitude
- there is a close analogy to the physics of harmonic oscillators

## I.1 Quantisation of a single mode

- we consider a plane wave of (angular) frequency  $\omega_k$  ↑ amplitude

$$\vec{E}(\vec{r}, t) = \hat{\epsilon} E_0 e^{i(\vec{k} \cdot \vec{r} - \omega_k t)} + \text{c.c.}$$

$$\vec{B}(\vec{r}, t) = \frac{\vec{k} \times \hat{\epsilon}}{ck} E_0 e^{i(\vec{k} \cdot \vec{r} - \omega_k t)} + \text{c.c.}$$

$\hat{\epsilon}$  ... polarisation vector, with  $|\hat{\epsilon}| = 1$

$\vec{k}$  ... wave vector, obeying  $|\vec{k}| = k = \frac{\omega_k}{c}$

- in vacuum, i.e. in the absence of sources (3)  
(charges  $\rho$  and currents  $\vec{j}$ ) Maxwell's equations read

$$\nabla \times \vec{E} = - \frac{\partial \vec{B}}{\partial t}$$

vacuum  
permeability  $\mu_0$  ↓      vacuum  
permittivity  $\epsilon_0$  ↓

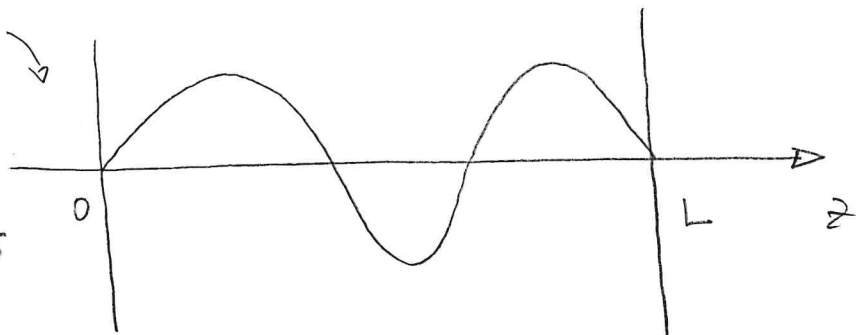
$$\nabla \times \vec{B} = \mu_0 \epsilon_0 \frac{\partial \vec{E}}{\partial t}$$

$$\nabla \cdot \vec{E} = 0$$

$$\nabla \cdot \vec{B} = 0$$

- we consider now a single mode in a one-dimensional box with perfectly conducting walls at  $z=0$  and  $z=L$

standing  
wave  
amplitude  
vanishes  
at  
boundaries



- only standing waves with nodes at 0 and L can exist inside the box
- we write the electric field as

$$E_x(\vec{r}, t) = \sqrt{\frac{2\omega^2}{V\epsilon_0}} q(+) \sin(kz)$$

$$E_y(\vec{r}, t) = 0$$

$$E_z(\vec{r}, t) = 0$$

↑ time-dependent  
amplitude

"normalisation" factor,  
that depends on the  
volume V

(4)

- the frequency  $\omega$  and the wave number  $k$  obey the relation

$$k = \frac{\omega_m}{c} = \frac{m\pi}{L}$$

with the mode index  $m = 1, 2, \dots$

- for the magnetic field we make the ansatz

$$B_x(\vec{r}, t) = 0$$

$$B_y(\vec{r}, t) = \left( \frac{\mu_0 \epsilon_0}{k} \right) \sqrt{\frac{2\omega^2}{V\epsilon_0}} \ddot{q}(t) \cos(kz)$$

$$B_z(\vec{r}, t) = 0$$

- plugging this into Maxwell's equations, yields

$$\nabla \times \vec{E} = \begin{pmatrix} \partial_y E_z - \partial_z E_y \\ \partial_z E_x - \partial_x E_z \\ \partial_x E_y - \partial_y E_x \end{pmatrix} = \sqrt{\frac{2\omega^2}{V\epsilon_0}} k q(t) \cos(kz) \begin{pmatrix} 0 \\ 1 \\ 0 \end{pmatrix} =$$

$$= - \frac{\partial \vec{B}}{\partial t} = - \frac{\mu_0 \epsilon_0}{k} \sqrt{\frac{2\omega^2}{V\epsilon_0}} \ddot{q}(t) \cos(kz) \begin{pmatrix} 0 \\ 1 \\ 0 \end{pmatrix}$$

$$\hookrightarrow \ddot{q}(t) = - \frac{k^2}{\mu_0 \epsilon_0} q(t) = - c^2 k^2 q(t)$$

$\hookrightarrow \ddot{q}(t) + \omega^2 q(t) = 0$ , only when the amplitude  $q(t)$  satisfies this differential equation (harmonic oscillator) Maxwell's equations are satisfied

$$\nabla \times \vec{B} = \begin{pmatrix} -\partial_z B_y \\ 0 \\ 0 \end{pmatrix} = \mu_0 \epsilon_0 \sqrt{\frac{2\omega^2}{\epsilon_0}} \dot{q} \sin(kz) \hat{e}_x$$

!!

$$\mu_0 \epsilon_0 \frac{\partial E}{\partial t} = \mu_0 \epsilon_0 \sqrt{\frac{2\omega^2}{\epsilon_0}} \dot{q} \sin(kz) \hat{e}_z$$

$\nabla \cdot \vec{B} = \nabla \cdot \vec{E} = 0$ , since  $E_x, B_y$  only depend on  $z$

perpendicular boundary conditions

$\hookrightarrow E_z, B_z = 0$  every where  $\rightarrow$  continuous

tangential boundary conditions of  $E$

$\hookrightarrow E_x = 0$  for  $z=0, L$ ; we can assume that the electric field is zero outside the cavity  $\rightarrow$  continuous

$\hookrightarrow E_y = 0$  everywhere  $\rightarrow$  continuous

(5)

- the equations  $\nabla \times \vec{B} = \mu_0 \epsilon_0 \frac{\partial \vec{E}}{\partial t}$  and  $\nabla \times \vec{E} = \nabla \times \vec{B} = 0$  are also satisfied
- note, concerning the boundary conditions:
  - perpendicular component of  $\vec{B}$  and tangential components of  $\vec{E}$  are continuous on perfectly conducting surface
  - additionally, for a charge-free and surface current-density free situation the perpendicular component of  $\vec{E}$  and the tangential components of  $\vec{B}$  are continuous, too
- in order to obtain the energy of the electromagnetic field, we calculate

$$\begin{aligned}
 H &= \frac{1}{2} \int dV (\epsilon_0 \vec{E}^2(\vec{r}, t) + \frac{1}{\mu_0} \vec{B}^2(\vec{r}, t)) \\
 &= \frac{1}{2} \int dV (\epsilon_0 E_x^2(\vec{r}, t) + \frac{1}{\mu_0} B_y^2(\vec{r}, t)) \\
 &= \frac{1}{2} \underbrace{\int_0^L A dz}_{\text{area of one wall}} \frac{2\omega^2}{V\epsilon_0} \left( \epsilon_0 q^2 \sin^2(kz) + \frac{\mu_0^2 \epsilon_0^2 q^2}{k^2} \dot{q}^2 \cos^2(kz) \right) \\
 &= \frac{1}{2} A \frac{2\omega^2}{V} \left( q^2 \frac{L}{2} + \frac{\mu_0 \epsilon_0}{k^2} \dot{q} \frac{L}{2} \right)
 \end{aligned}$$

(6)

- with  $V = A \cdot L$  one thus finds

$$H = \frac{1}{2} \omega^2 (q^2 + \frac{1}{\omega^2} \dot{q}^2) = \frac{1}{2} (p^2 + \omega^2 q^2),$$

where  $p = \dot{q}$  (we also used  $\epsilon_0 \mu_0 = \frac{1}{c^2}$ )

- this is the Hamilton function of a one-dimensional harmonic oscillator
- the system can be quantised using the substitution  $p \rightarrow \hat{p}$ ,  $q \rightarrow \hat{q}$ , where the operators  $\hat{p}$  and  $\hat{q}$  satisfy the canonical commutation relations

$$[\hat{q}, \hat{p}] = i\hbar$$

- this leads to the operators for the  $\vec{E}, \vec{B}$ -field:

$$\hat{E}_x(\vec{r}, t) = \sqrt{\frac{2\omega^2}{V\epsilon_0}} \hat{q}(t) \sin(kz)$$

$$\hat{B}_y(\vec{r}, t) = \frac{\mu_0 \epsilon_0}{k} \sqrt{\frac{2\omega^2}{V\epsilon_0}} \hat{p}(t) \cos(kz)$$

- note, that  $\hat{p}(t)$  and  $\hat{q}(t)$  are Heisenberg operators
- in the next step we introduce creation and annihilation operators:

$$a = \sqrt{\frac{1}{2\hbar\omega}} (\omega \hat{q} + i\hat{p}), \quad a^\dagger = \sqrt{\frac{1}{2\hbar\omega}} (\omega \hat{q} - i\hat{p})$$

with  $[a, a^\dagger] = 1$

(7)

- with these, we find

$$\hat{E}_x(\vec{r}, t) = E_0 (a(t) + a^*(t)) \sin(kz)$$

$$\hat{B}_y(\vec{r}, t) = B_0 \frac{1}{i} (a(t) - a^*(t)) \cos(kz),$$

with  $E_0 = \sqrt{\frac{t\omega}{\epsilon_0 V}}$  and  $B_0 = \frac{1}{c} E_0$

can be interpreted as  
electric / magnetic field  
per photon

- expression the Hamilton function in terms of the creation and annihilation operators yields

$$H = t\omega (a^\dagger a + \frac{1}{2})$$

- this allows us to find their time-evolution using the Heisenberg equations:

$$\frac{da}{dt} = \frac{i}{\hbar} [H, a] = \frac{i}{\hbar} t\omega [a^\dagger a, a] = -i\omega a$$

$$\hookrightarrow a(t) = e^{-i\omega t} a(0)$$

- lastly, we consider the eigenenergies and eigenstates, which are given by the stationary Schrödinger equation

$$H |4\rangle = E |4\rangle \rightarrow t\omega (a^\dagger a + \frac{1}{2}) |4\rangle = E |4\rangle$$

• applying  $a^+$  from the left, yields ⑧

$$\begin{aligned} \text{tw}(a^+ a a + \frac{1}{2}) |4\rangle &= \text{tw}(a^+ a a^+ - a^+ + \frac{a^+}{2}) |4\rangle \\ &= \text{tw}(a^+ a - \frac{1}{2}) a^+ |4\rangle \\ &= E a^+ |4\rangle \end{aligned}$$

↳  $\text{tw}(a^+ a + \frac{1}{2}) a^+ |4\rangle = (E + \text{tw}) a^+ |4\rangle$

↳ if  $|4\rangle$  is an eigenstate with energy  $E$ ,  
then  $a^+ |4\rangle$  is an eigenstate with energy  $E + \text{tw}$

• analogously, one shows that

$$\text{tw}(a^+ a + \frac{1}{2}) a |4\rangle = (E - \text{tw}) a |4\rangle$$

• since the energy of the harmonic oscillator  
is larger or equal than zero, there has to  
be a ground state:  $a |0\rangle = 0$

↳  $H |0\rangle = \underbrace{\frac{\text{tw}}{2} |0\rangle}_{\text{zero-point energy}}$

• continued application of  $a^+$  creates the  
excited states  $|n\rangle = C_n (a^+)^n |0\rangle$ , which obey

$$H |n\rangle = \text{tw}(a^+ a + \frac{1}{2}) |n\rangle = \text{tw}(n + \frac{1}{2}) |n\rangle$$

↳ number operator:  $\hat{n} = a a^+$

⑨

- the normalisation constant  $C_n$  is determined by noting that

$$a|n\rangle = d_n |n-1\rangle$$

$\uparrow$  n-dependent factor

$$\hookrightarrow |d_n|^2 \underbrace{\langle n-1|n-1\rangle}_1 = \langle n|a^\dagger a|n\rangle = n$$

$$\hookrightarrow d_n = \sqrt{n} \quad (\text{phase is chosen to be zero})$$

$$\hookrightarrow a|n\rangle = \sqrt{n}|n-1\rangle$$

- likewise, one finds  $a^\dagger|n\rangle = \sqrt{n+1}|n+1\rangle$

- iterating this expression yields

$$|n\rangle = \frac{(a^\dagger)^n}{\sqrt{n!}} |0\rangle \quad \text{and hence } C_n = \frac{1}{\sqrt{n!}}$$

- in quantum optics the states  $|n\rangle$  are also referred to as Fock states (generally, this term is used when considering more than one mode)

- they are orthonormal and complete:

$$\langle n|n'\rangle = \delta_{nn'} , \quad \sum_{n=0}^{\infty} |n\rangle \langle n| = \mathbb{1}$$

- the (photon) number operator,  $n = a^\dagger a$ , counts the number of elementary excitations, a.k.a. photons, contained in the considered electro-magnetic field mode

## I. 2 Quantum fluctuations of a single mode

(10)

- electric and magnetic field of a single mode have a vanishing expectation value for a Fock state,

Since  $\langle n | a | n \rangle = \underbrace{\langle n | n-1 \rangle}_{=0} = 0$

$$\hookrightarrow \langle n | \hat{E}_x | n \rangle = \langle n | \hat{B}_y | n \rangle = 0$$

- however, both fields have non-vanishing fluctuations:

$$\begin{aligned} \langle n | \hat{E}_x^2 | n \rangle &= E_0^2 \sin^2(kz) \langle n | (a^\dagger + a)^2 | n \rangle \\ &= - - - \underbrace{\langle n | (a^{+2} + a^\dagger a + a a^\dagger + a^2) | n \rangle}_{2a^\dagger a + 1} \\ &= E_0^2 \sin^2(kz) \langle n | (2a^\dagger a + 1) | n \rangle \\ &= 2E_0^2 \sin^2(kz) (n + \frac{1}{2}) \end{aligned}$$

$\hookrightarrow$  standard deviation

$$\Delta E_x = \sqrt{\langle \hat{E}_x^2 \rangle - \langle \hat{E}_x \rangle^2} = \sqrt{2} E_0 |\sin(kz)| \sqrt{n + \frac{1}{2}}$$

- the electric field is hence subject to fluctuations even in the vacuum state, i.e. when  $n = 0$

(11)

- to get a feeling for the order of magnitude of lets consider an optical frequency ( $\omega \approx 10^{14} \text{ Hz}$ ) and a cubic volume of  $V = 1 \text{ cm}^3 = 10^{-6} \text{ m}^3$

$$\hookrightarrow \Delta E_x \sim E_0 \sim \sqrt{\frac{t \omega}{\epsilon_0 V}} \sim \sqrt{\frac{10^{-34} \text{ Js} \cdot 10^{14} \text{ s}^{-1}}{10^{-11} \frac{\text{As}}{\text{Vm}} \cdot 10^{-6} \text{ m}^3}}$$

$$\sim 10^{-3/2} \frac{\text{V}}{\text{m}} \approx 3 \cdot 10^{-2} \frac{\text{V}}{\text{m}} = 3 \frac{\text{V}}{\text{cm}}$$

can be directly measured

- for the standard deviation of the magnetic field strength one obtains

$$\Delta B_y = \sqrt{2} B_0 |\cos(kz)| \sqrt{n + \frac{1}{2}}$$

- Since  $B_0 = \frac{E_0}{c}$  these fluctuations are about  $10^{-8}$ -times (in SI units) smaller than those of the electric field

### I.3 Quadrature operators for a single mode field

(12)

- the quadrature operators are defined as

$$\hat{X}_1 = \frac{1}{2} (a + a^\dagger) \text{ and } \hat{X}_2 = \frac{1}{2i} (a - a^\dagger)$$

- they are self-adjoint and obey the commutation relation

$$[\hat{X}_1, \hat{X}_2] = \frac{1}{4i} \left( [a, a^\dagger] + [a^\dagger, a] \right) = \frac{i}{2}$$

-1      -1

- the electric field expressed in terms of the quadrature operators reads

$$\begin{aligned}\hat{E}_x(\vec{r}, t) &= E_0 (a e^{-i\omega t} + a^\dagger e^{i\omega t}) \sin(kz) \\ &= 2E_0 \sin(kz) (\hat{X}_1 \cos \omega t + \hat{X}_2 \sin \omega t)\end{aligned}$$

- the quadrature operators are often used for the experimental measurement of quantum states of light

## I.4 Multimode fields

(13)

- let us come back to plane waves

$$\vec{E}(\vec{r}, t) = \hat{\epsilon} E_0 e^{i(\vec{k} \cdot \vec{r} - \omega_0 t)} + \text{c.c.}$$

$$\vec{B}(\vec{r}, t) = \frac{\mu_0 \epsilon_0}{c} \hat{\epsilon} E_0 e^{i(\vec{k} \cdot \vec{r} - \omega_0 t)} + \text{c.c.}$$

- these are solutions of Maxwell's equations in the absence of charges and currents

- $\vec{k}$  is the wave vector (indicating into which direction the wave is travelling) and  $\hat{\epsilon}$  is the polarisation vector

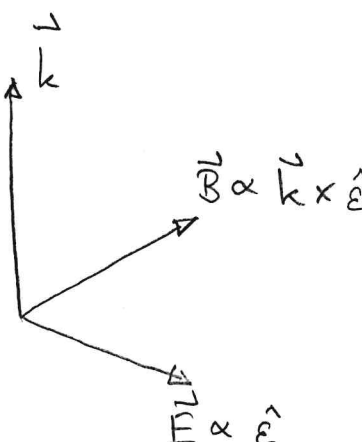
- the polarisation vector is perpendicular to the wave vector,  $\vec{k} \perp \hat{\epsilon}$

- assuming e.g. that  $\vec{k} = k \hat{e}_z$  we can parametrise the polarisation vector as

$$\hat{\epsilon} = \hat{\epsilon}_{k,s} = \epsilon_x \hat{e}_x + \epsilon_y \hat{e}_y$$

dependence on wave vector

index, which will be needed later to indicate the polarisation (two orthogonal polarisations are possible)



- linear polarisation:

$$\epsilon_x \hat{e}_x, \epsilon_y \hat{e}_y \in \mathbb{R}$$

- circular polarisation:

$$\text{e.g. } \hat{\epsilon}_{k,s} = \frac{1}{\sqrt{2}} (\hat{e}_x + i \hat{e}_y)$$

(14)

the energy of the electromagnetic field within a volume  $V$  is given by

$$H = \frac{1}{2} \int_V d^3r \left( \epsilon_0 \vec{E}^2(\vec{r}, t) + \underbrace{\frac{1}{\mu_0} \vec{B}^2(\vec{r}, t)}_{= \mu_0 \vec{H}^2(\vec{r}, t)} \right)$$

the energy of a plane wave with wave vector  $\vec{k}$  and linear polarisation  $s$  (polarisation vector  $\hat{e}_{k,s} \in \mathbb{R}$ ) reads

$$\begin{aligned} H_{k,s} &= \frac{1}{2} \int_V d^3r 4E_0^2 \left( \underbrace{\epsilon_0 \cos^2(\vec{k} \cdot \vec{r} - \omega t)}_{\text{electric field}} + \underbrace{\frac{1}{c^2 \mu_0} \cos^2(\vec{k} \cdot \vec{r} + \omega t)}_{\text{magnetic field}} \right) \\ &= \frac{\epsilon_0 E_0^2}{2} \cdot 4 \int_V d^3r 2 \cos^2(\vec{k} \cdot \vec{r} - \omega t) \quad \begin{matrix} \text{electric and mag. field} \\ \text{contribute same amount} \\ \text{of energy} \end{matrix} \\ &= \frac{\epsilon_0 E_0^2}{2} \cdot 4 \int_V d^3r \left( 1 - \underbrace{\cos(2[\vec{k} \cdot \vec{r} - \omega t])}_{\substack{\text{integral} \\ \text{yields } V}} \right) \quad \begin{matrix} \text{integral} \\ \text{averages} \end{matrix} \\ &= 2\epsilon_0 E_0^2 V \end{aligned}$$

another important quantity is the so-called Poynting vector,  $\vec{S} = \vec{E} \times \vec{H}$ , representing the energy flux

$$\begin{aligned} \hookrightarrow \vec{S}_{k,s} &= \frac{E_0^2}{c \epsilon_0 \mu_0} (\hat{e} \times (\vec{k} \times \hat{e})) 4 \cos^2(\vec{k} \cdot \vec{r} - \omega t) \quad \begin{matrix} \vec{a} \times (\vec{b} \times \vec{c}) = \\ = \vec{b}(\vec{c} \cdot \vec{a}) - \vec{c}(\vec{a} \cdot \vec{b}) \end{matrix} \\ &= \frac{2E_0^2}{c \mu_0} \vec{k} (1 + \cos(2[\vec{k} \cdot \vec{r} - \omega t])) \end{aligned}$$

the average energy flux into direction  $\frac{\vec{k}}{|\vec{k}|}$  is thus  $\frac{2E_0^2 k}{c \mu_0}$

## wave equation

$$\nabla \times \vec{B} = \mu_0 \epsilon_0 \frac{\partial \vec{E}}{\partial t} = \frac{1}{c^2} \frac{\partial^2 \vec{E}}{\partial t^2}$$

with  $\vec{B} = \nabla \times \vec{A}$  and  $\vec{E} = -\frac{\partial \vec{A}}{\partial t}$

$\hookrightarrow \underbrace{\nabla \times \nabla \times \vec{A}}_{-\Delta \vec{A} + \nabla(\nabla \cdot \vec{A})} = -\frac{1}{c^2} \frac{\partial^2}{\partial t^2} \vec{A}$

using the Coulomb gauge  $\nabla \cdot \vec{A} = 0$   
one thus finds the wave equation

$$\frac{1}{c^2} \frac{\partial^2}{\partial t^2} \vec{A} - \Delta \vec{A} = 0$$

(15)

- for quantising the multimode electric field it is convenient to consider the vector potential  $\vec{A}(\vec{r}, t)$  instead of the fields itself
- in the absence of charges and using the Coulomb gauge ( $\nabla \cdot \vec{A} = 0, \phi = 0$ ) the electric and magnetic fields are related to  $\vec{A}$  via

$$\vec{E} = - \frac{\partial \vec{A}}{\partial t}, \quad \vec{B} = \nabla \times \vec{A}$$

- the vector potential satisfies the wave equation

$$\frac{1}{c^2} \frac{\partial^2 \vec{A}}{\partial t^2} - \Delta \vec{A} = 0,$$

which is solved by plane waves

$$\vec{A}_k(\vec{r}, t) = \hat{E} A_0 e^{i(\vec{k} \cdot \vec{r} - \omega t)} + c.c.$$

assuming that the electromagnetic field is confined in a cubic volume  $V = L \times L \times L$ , the wave vector assumes discrete values:

$$\vec{k} = \frac{2\pi}{L} \vec{n} \quad \text{with } n_i \in \mathbb{Z} = 0, 1, 2, \dots$$

- the general solution of the wave equation (16) for many modes has the form

$$\vec{A}(\vec{r}, t) = \sum_{\substack{\vec{k} \\ \text{mode}}} \frac{A_{\vec{k}, s}}{\sqrt{V}} \hat{\epsilon}_{\vec{k}, s}^s e^{i(\vec{k} \cdot \vec{r} - \omega t)} + \text{c.c.}$$

↑ amplitude (in general complex valued)  
 ↑ mode  
 ↑ polarization →  
 ↑ normalisation      ↓ polarization vector

$$\hookrightarrow \vec{E}(\vec{r}, t) = i \sum_{\substack{\vec{k} \\ \text{mode}}} \frac{\omega_k A_{\vec{k}, s}}{\sqrt{V}} \hat{\epsilon}_{\vec{k}, s}^s e^{i(\vec{k} \cdot \vec{r} - \omega t)} + \text{c.c.}$$

$$\vec{B}(\vec{r}, t) = \sum_{\substack{\vec{k} \\ \text{mode}}} \frac{A_{\vec{k}, s}}{\sqrt{V}} : \vec{k} \times \hat{\epsilon}_{\vec{k}, s}^s e^{i(\vec{k} \cdot \vec{r} - \omega t)} + \text{c.c.}$$

$\frac{\omega_k}{c} \hat{\vec{k}} \times \hat{\epsilon}_{\vec{k}, s}^s$  with  $\hat{\vec{k}} = \frac{\vec{k}}{|\vec{k}|}$

- in the next step we calculate the energy of the electromagnetic field as a function of the vector potential amplitudes  $A_{\vec{k}, s}$
- this will be the starting point for the field quantisation
- since the  $A_{\vec{k}, s}$  are in general complex, we slightly modify the expression for the energy

$$H = \frac{1}{2} \int d^3 r \left( \epsilon_0 \vec{E} \cdot \vec{E}^* + \frac{1}{\mu_0} \vec{B} \cdot \vec{B}^* \right)$$

inserting the expansions of  $\vec{E}$  and  $\vec{B}$  yields (17)

$$H = \frac{1}{2V} \int d^3r \sum_{\vec{k} \in \vec{k}'_s} \left\{ \left[ \epsilon_0 \omega_k \omega_{k'} \hat{\vec{E}}_{\vec{k},s} \cdot \hat{\vec{E}}_{\vec{k}',s'} + \frac{\omega_k \omega_{k'}}{m_e c^2} (\vec{k} \times \hat{\vec{E}}_{\vec{k},s}) \cdot (\vec{k}' \times \hat{\vec{E}}_{\vec{k}',s'}) \right] \right.$$

$$\left. \cdot (A_{\vec{k},s} e^{i(\vec{k} \cdot \vec{r} - \omega_k t)} - A_{\vec{k},s}^* e^{-i(\cdot)}) (A_{\vec{k}',s'}^* e^{-i(\vec{k}' \cdot \vec{r} - \omega_{k'} t)} - A_{\vec{k}',s'} e^{i(\cdot)}) \right\}$$

in the next step we use the relation

$$\frac{1}{V} \int d^3r e^{i(\vec{k} - \vec{k}') \cdot \vec{r}} = \delta_{\vec{k} \vec{k}'}$$

$$\hookrightarrow H = \frac{\epsilon_0}{2} \sum_{\substack{\vec{k} \in \vec{k}'_s \\ \vec{k} \neq \vec{k}'_s}} \omega_k \omega_{k'} [\hat{\vec{E}}_{\vec{k},s} \cdot \hat{\vec{E}}_{\vec{k}',s'} + (\vec{k} \times \hat{\vec{E}}_{\vec{k},s}) \cdot (\vec{k}' \times \hat{\vec{E}}_{\vec{k}',s'})]$$

$$\cdot \left[ (A_{\vec{k},s} A_{\vec{k}',s'}^* + A_{\vec{k},s}^* A_{\vec{k}',s'}) \delta_{\vec{k} \vec{k}'} \right.$$

$$\left. - (A_{\vec{k},s}^* A_{\vec{k}',s'}^* e^{i(\omega_k + \omega_{k'})t} + A_{\vec{k},s} A_{\vec{k}',s'} e^{-i(\omega_k + \omega_{k'})t}) \delta_{\vec{k} - \vec{k}'} \right]$$

$$= \frac{\epsilon_0}{2} \sum_{\vec{k} \in s} \omega_k^2 \underbrace{[\hat{\vec{E}}_{\vec{k},s} \cdot \hat{\vec{E}}_{\vec{k},s}]}_{\delta_{ss}} + \underbrace{(\vec{k} \times \hat{\vec{E}}_{\vec{k},s}) \cdot (\vec{k} \times \hat{\vec{E}}_{\vec{k},s})}_{\delta_{ss}} \left( A_{\vec{k},s} A_{\vec{k},s}^* + A_{\vec{k},s}^* A_{\vec{k},s} \right)$$

$$+ \frac{\epsilon_0}{2} \sum_{\vec{k} \in s'} \omega_k^2 \left[ \hat{\vec{E}}_{\vec{k},s} \cdot \hat{\vec{E}}_{-\vec{k},s'} + (\vec{k} \times \hat{\vec{E}}_{\vec{k},s}) \cdot (-\vec{k} \times \hat{\vec{E}}_{-\vec{k},s'}) \right] \cdot$$

$$\cdot (A_{\vec{k},s}^* A_{\vec{k},s'}^* e^{i2\omega_k t} + \text{c.c.})$$

(18)

- The second sum vanishes because

$$(\hat{k} \times \hat{\epsilon}_{\vec{k},s}) \cdot (-\hat{k} \times \hat{\epsilon}_{-\vec{k},s}) = - \underbrace{(\hat{k} \cdot \hat{k})}_{1} (\hat{\epsilon}_{\vec{k},s} \cdot \hat{\epsilon}_{-\vec{k},s}),$$

which follows from  $(\vec{a} \times \vec{b}) \cdot (\vec{c} \times \vec{d}) = (\vec{a} \cdot \vec{c})(\vec{b} \cdot \vec{d}) - (\vec{a} \cdot \vec{d})(\vec{b} \cdot \vec{c})$

- The final result is thus

$$H = \epsilon_0 \sum_{\vec{k},s} \omega_k^2 (A_{\vec{k},s} A_{\vec{k},s}^* + A_{\vec{k},s}^* A_{\vec{k},s})$$

- at this point the amplitudes  $A_{\vec{k},s}$  are still complex numbers and both terms can be gathered into one
- however, we will now quantise the electromagnetic field by introducing raising and lowering operators (creation and annihilation operators) for the field modes  $(\vec{k},s)$

$$A_{\vec{k},s} \rightarrow \sqrt{\frac{\hbar}{2\epsilon_0\omega_k}} a_{\vec{k},s}$$

$$A_{\vec{k},s}^* \rightarrow \sqrt{\frac{\hbar}{2\epsilon_0\omega_k}} a_{\vec{k},s}^+$$

(19)

- this turns the energy into the Hamiltonian

$$H = \sum_{\vec{k}, s} \frac{\hbar \omega_k}{2} (\hat{a}_{\vec{k}, s}^\dagger \hat{a}_{\vec{k}, s} + \hat{a}_{\vec{k}, s} \hat{a}_{\vec{k}, s}^\dagger)$$

- the creation / annihilation operators for different modes  $(\vec{k}, s)$  commute, while for the same mode they satisfy the algebra of the harmonic oscillator's raising and lowering operators:

$$[\hat{a}_{\vec{k}, s}, \hat{a}_{\vec{k}', s'}^\dagger] = \delta_{\vec{k}\vec{k}'} \delta_{ss'}$$

- exploiting this relation, the Hamiltonian can be rewritten as

$$H = \sum_{\vec{k}, s} \hbar \omega_k (\hat{a}_{\vec{k}, s}^\dagger \hat{a}_{\vec{k}, s} + \frac{1}{2})$$

- the operators for  $\vec{A}$ ,  $\vec{E}$  and  $\vec{B}$  are then

$$\vec{A}(\vec{r}, t) = \sum_{\vec{k}, s} \sqrt{\frac{\hbar}{2\epsilon_0 \omega_k V}} \hat{E}_{\vec{k}, s}^\dagger (\hat{a}_{\vec{k}, s} e^{i(\vec{k} \cdot \vec{r} - \omega_k t)} + h.c.)$$

$$\vec{E}(\vec{r}, t) = i \sum_{\vec{k}, s} \sqrt{\frac{\hbar \omega_k}{2\epsilon_0 V}} \hat{E}_{\vec{k}, s} (\hat{a}_{\vec{k}, s}^\dagger e^{i(\vec{k} \cdot \vec{r} - \omega_k t)} - h.c.)$$

$$\vec{B}(\vec{r}, t) = i \sum_{\vec{k}, s} \frac{1}{c} \sqrt{\frac{\hbar \omega_k}{2\epsilon_0 V}} \vec{k} \times \hat{E}_{\vec{k}, s}^\dagger (\hat{a}_{\vec{k}, s} e^{i(\vec{k} \cdot \vec{r} - \omega_k t)} - h.c.)$$

- one often decomposes the fields into their positive and negative frequency components, e.g.

$$\vec{E}(\vec{r},+) = \vec{E}^{(+)}(\vec{r},+) + \vec{E}^{(-)}(\vec{r},+)$$

with  $\vec{E}^{(+)}(\vec{r},+) = i \sum_{k,s} E_k a_{k,s}^+ e^{+i(\vec{k} \cdot \vec{r} - \omega t)}$

and  $\vec{E}^{(-)}(\vec{r},+) = [\vec{E}^{(+)}(\vec{r},+)]^+$  ↑  $\sqrt{\frac{4\pi\epsilon}{2\epsilon_0 V}}$  electric field of an elementary excitation

- with these considerations the electromagnetic field can apparently be considered as a collection of harmonic oscillators
- the operator  $a_{k,s}^+$  creates an excitation (photon) in the mode  $(\vec{k}, s)$
- the operator  $\hat{n}_{k,s} = a_{k,s}^+ a_{k,s}$  is the number operator of the mode  $(\vec{k}, s)$  and measures the number of excitations contained in it
- energy eigenstates of the electromagnetic field are Fock states

$$|n_{k_1,s_1}\rangle \otimes |n_{k_2,s_2}\rangle \otimes \dots = |\underbrace{n_{k_1,s_1}, n_{k_2,s_2}, \dots}_{\text{photon number in mode } (\vec{k}_1, s_1)}\rangle = |\{n_{k,s}\}\rangle$$

- application of the Hamiltonian onto the Fock state yields

$$H |\{n_{\vec{k},s}\}\rangle = E(\{n_{\vec{k},s}\}) |\{n_{\vec{k},s}\}\rangle$$

$$= \sum_{k,s} (\hbar\omega_k n_{\vec{k},s} + \frac{1}{2}) |\{n_{\vec{k},s}\}\rangle$$

- the action of creation and annihilation operators is defined via

$$\alpha_{\vec{k}_m, s_m}^+ |n_{\vec{k}_1, s_1}, \dots, n_{\vec{k}_m, s_m}\rangle = \overline{|n_{\vec{k}_m, s_m}+1\rangle} |n_{\vec{k}_1, s_1}, \dots, n_{\vec{k}_m, s_m}+1, \dots\rangle$$

$$\alpha_{\vec{k}_m, s_m}^- |n_{\vec{k}_1, s_1}, \dots, n_{\vec{k}_m, s_m}\rangle = \overline{|n_{\vec{k}_m, s_m}^{-1}\rangle} |n_{\vec{k}_1, s_1}, \dots, n_{\vec{k}_m, s_m}-1, \dots\rangle$$

## I. 5 Thermal fields

- the quantised form of the radiation field leads rather straight-forwardly to Planck's law of radiation, which is one of the huge successes of quantum mechanics
- to derive it we consider a single mode, which is sufficient since all modes are independent in the absence of interactions

(22)

- a thermal state of a single mode with frequency  $\omega$  is described by the density matrix

$$\rho_{\text{th}} = \frac{e^{-\beta H}}{Z} \quad \text{with} \quad H = \hbar\omega(\hat{n} + \frac{1}{2})$$

and  $\beta = \frac{1}{k_B T} \leftarrow \text{temperature}$

$\nwarrow$  Boltzmann's constant

- for the partition function  $Z$  we obtain

$$\begin{aligned} Z &= \text{tr } e^{-\beta H} = \sum_{n=0}^{\infty} \langle n | e^{-\beta H} | n \rangle \\ &= \sum_{n=0}^{\infty} e^{-\beta \hbar\omega(n + \frac{1}{2})} = e^{-\frac{\beta \hbar\omega}{2}} \frac{1}{1 - e^{-\beta \hbar\omega}} \end{aligned}$$

- the probability to find  $n$  photons in the mode is then given by

$$\begin{aligned} p_n &= \langle n | \rho_{\text{th}} | n \rangle = \frac{e^{-\beta \hbar\omega(n + \frac{1}{2})}}{e^{-\frac{\beta \hbar\omega}{2}}} (1 - e^{-\beta \hbar\omega}) \\ &= e^{-\beta \hbar\omega n} (1 - e^{-\beta \hbar\omega}) \end{aligned}$$

- the mean photon number is

$$\begin{aligned} \bar{n} &= \text{tr}(\hat{n} \rho_{\text{th}}) = \sum_{n=0}^{\infty} \langle n | \hat{n} \rho_{\text{th}} | n \rangle = \sum_n n p_n \\ &= (1 - e^{-\beta \hbar\omega}) \sum_n n e^{-\beta \hbar\omega n} \end{aligned}$$

- to calculate the sum we use

$$\sum_{n=0}^{\infty} n e^{-nx} = -\frac{\partial}{\partial x} \sum_{n=0}^{\infty} e^{-nx} = -\frac{\partial}{\partial x} \frac{1}{1-e^{-x}} \\ = \frac{e^{-x}}{(1-e^{-x})^2}$$

$$\hookrightarrow \bar{n} = \frac{e^{-\beta \hbar \omega}}{1 - e^{-\beta \hbar \omega}} = \frac{1}{e^{\beta \hbar \omega} - 1}$$

- to obtain Planck's radiation law, we have to understand how many modes there are that possess energy  $\hbar \omega$ .

- these are all the modes whose wave vector obeys  $c|\vec{k}| = \omega$ , and in addition there are two polarisations for each wave vector

- the energy density of all these modes is

$$\underbrace{u(\nu) d\nu}_{\substack{\text{energy density} \\ \text{at frequency } \nu}} = \overbrace{\bar{n} \hbar \omega}^{\substack{\text{energy of} \\ \text{the modes}}} \underbrace{2 \frac{d^3 k}{(2\pi)^3}}_{\substack{\text{number of} \\ \text{modes per} \\ \text{Volume}}} = \overbrace{\bar{n} \hbar \omega}^{\substack{\text{polar coordinates}}} \underbrace{2 \cdot \frac{4\pi k^2 dk}{(2\pi)^3}}_{\substack{\text{polar coordinates}}}$$

$$= \frac{8\pi}{(2\pi)^3} \frac{\hbar \omega \omega^2 d\omega}{(e^{\beta \hbar \omega} - 1) c^3} = \underbrace{\frac{8\pi \nu^2}{c^3} \frac{\hbar \nu}{e^{\beta \hbar \nu} - 1}}_{\substack{\text{energy density} \\ \text{according to Planck}}} d\nu$$

(24)

- to conclude, let us consider the fluctuations of a thermal radiation field

$$\Delta n = \sqrt{\langle \hat{n}^2 \rangle - \langle \hat{n} \rangle^2} = \sqrt{\bar{n}^2 - \bar{n}^2}$$

$$\begin{aligned} \hookrightarrow (\Delta n)^2 &= \underbrace{(1 - e^{-\beta \hbar \omega}) \sum_n n^2 e^{-\beta \hbar \omega n}}_{\frac{1 + e^{\beta \hbar \omega}}{(e^{\beta \hbar \omega} - 1)^2}} - \frac{1}{(e^{\beta \hbar \omega} - 1)^2} \\ &= \frac{e^{\beta \hbar \omega}}{(e^{\beta \hbar \omega} - 1)^2} = \bar{n}^2 e^{\beta \hbar \omega} = \bar{n}^2 \underbrace{\frac{(1 + \bar{n})}{\bar{n}}}_{= e^{\beta \hbar \omega}} \\ &= \bar{n}^2 + \bar{n} \end{aligned}$$

$$\hookrightarrow \Delta n = \sqrt{\bar{n}^2 + \bar{n}} = \bar{n} \sqrt{1 + \frac{1}{\bar{n}}} \underset{\bar{n} \rightarrow \infty}{\approx} \bar{n} + \frac{1}{2}$$

- fluctuations grow with increasing  $\bar{n}$ , such that  $\frac{\Delta n}{\bar{n}} \rightarrow 1$  when  $\bar{n} \rightarrow \infty$

## I. 6 Coherent states

(25)

- coherent states are non-stationary states and unlike the Fock states they aren't eigenstates of the number operator
- in the context of quantum optics they were introduced by Roy Glauber (Nobel prize 2005)
- coherent states are (approximately) produced by a laser and are in some sense the "most classical" pure quantum states of light
- we consider a single mode light field with Hamiltonian

$$\hat{H} = \hbar\omega(\hat{a}\hat{a} + \frac{1}{2})$$

- a coherent state  $|\alpha\rangle$  is defined as an eigenstate of the annihilation operator  $\hat{a}$

$$\hat{a}|\alpha\rangle = \alpha|\alpha\rangle \quad \text{with } \alpha \in \mathbb{C}$$

- the expansion of the coherent state in terms of Fock (particle number) states reads

$$\begin{aligned}
 |\alpha\rangle &= \underbrace{\sum_{n=0}^{\infty} |n\rangle \chi_n |\alpha\rangle}_{\text{II}} = \sum_{n=0}^{\infty} \frac{(\alpha^+)^n}{\Gamma(n!)} |0\rangle \langle 0| \frac{\alpha^n}{\Gamma(n!)} |\alpha\rangle \\
 &= \sum_{n=0}^{\infty} |n\rangle \langle 0| \frac{\alpha^n}{\Gamma(n!)} |\alpha\rangle = \sum_{n=0}^{\infty} \langle 0|\alpha\rangle \frac{\alpha^n}{\Gamma(n!)} |n\rangle
 \end{aligned}$$

- by demanding normalisation, we find

$$\begin{aligned}
 1 &= \langle \alpha | \alpha \rangle = |\langle 0 | \alpha \rangle|^2 \sum_{mn} \frac{(\alpha^*)^m \alpha^n}{\Gamma(m!) \Gamma(n!)} \underbrace{\langle m | n \rangle}_{\delta_{mn}} = \\
 &= |\langle 0 | \alpha \rangle|^2 \sum_{n=0}^{\infty} \frac{|\alpha|^{2n}}{n!} = |\langle 0 | \alpha \rangle|^2 e^{|\alpha|^2}
 \end{aligned}$$

$$\hookrightarrow |\langle 0 | \alpha \rangle|^2 \cdot e^{|\alpha|^2} = 1 \rightarrow |\langle 0 | \alpha \rangle|^2 = e^{-|\alpha|^2}$$

- up to an irrelevant phase, we thus find

$$|\alpha\rangle = e^{-\frac{|\alpha|^2}{2}} \sum_{n=0}^{\infty} \frac{\alpha^n}{\Gamma(n!)} |n\rangle$$

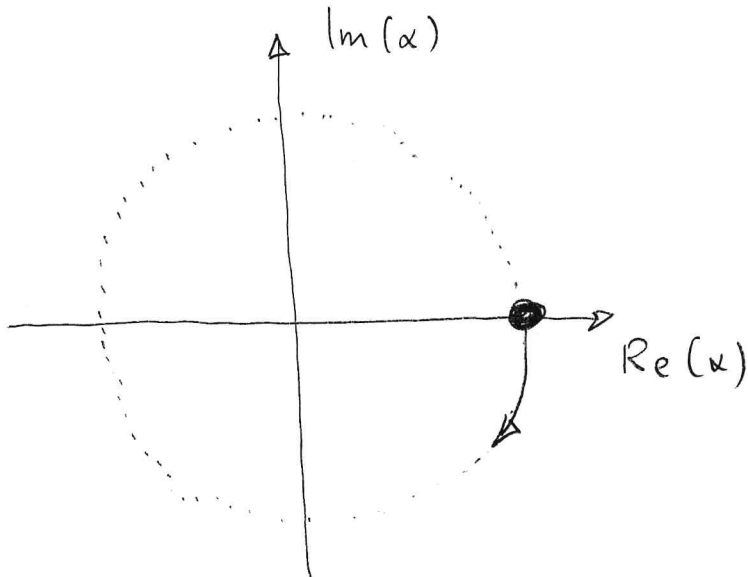
- in this representation it becomes apparent, that  $|\alpha\rangle$  is not a number eigenstate, but a superposition of infinitely many such eigenstates

- the time evolution of a coherent state is found by computing

$$\begin{aligned}
 |\alpha(t)\rangle &= e^{-\frac{iHt}{\hbar}} |\alpha\rangle = e^{-i\omega t(\alpha^{\dagger}\alpha + \frac{1}{2})} e^{-\frac{|\alpha|^2}{2}} \sum_{n=0}^{\infty} \frac{\alpha^n}{\Gamma(n!)} |n\rangle \\
 &= e^{-\frac{i\omega t}{2}} e^{-\frac{|\alpha|^2}{2}} \sum_{n=0}^{\infty} \frac{\alpha^n}{\Gamma(n!)} e^{-i\omega n t} |n\rangle \\
 &= e^{-\frac{i\omega t}{2}} e^{-\frac{|\alpha|^2}{2}} \sum_{n=0}^{\infty} \frac{(\alpha e^{-i\omega t})^n}{\Gamma(n!)} |n\rangle \\
 &= e^{-\frac{i\omega t}{2}} |\alpha e^{-i\omega t}\rangle
 \end{aligned}$$

- a coherent state remains a coherent state under time evolution

- it merely rotates in the complex  $\alpha$ -plane



- this rotation leads to harmonically oscillating electric and magnetic field components

$$\begin{aligned}
 \langle \alpha | E_x(\vec{r},+) | \alpha \rangle &= E_0 (\langle \alpha | a | \alpha \rangle e^{-i\omega t} + \langle \alpha | a^\dagger | \alpha \rangle e^{+i\omega t}) \sin(kz) \\
 &= E_0 (\alpha e^{-i\omega t} + \alpha^* e^{+i\omega t}) \sin(kz) \\
 &= 2E_0 \sin(kz) \operatorname{Re}(\alpha(+)) \\
 &\stackrel{\alpha(0) \in \mathbb{R}}{=} 2E \sin(kz) \cdot \alpha(0) \cdot \cos(\omega t)
 \end{aligned}$$

- an interesting aspect of coherent states is that they are minimum uncertainty states
- this statement is based on the so-called Heisenberg-Robertson uncertainty relation:

$$[A, B] = iC \Rightarrow \Delta A \cdot \Delta B \geq \frac{1}{2} |\langle C \rangle|,$$

with  $(\Delta A)^2 = \langle A^2 \rangle - \langle A \rangle^2$

(example:  $[p, q] = \frac{i}{\hbar} \rightarrow \Delta p \cdot \Delta q \geq \frac{\hbar}{2}$ )

- using the relation  $a = \sqrt{\frac{1}{2\hbar\omega}} (\omega q + ip)$  we can construct p and q operators for the light field

$$q = \sqrt{\frac{1}{2\hbar\omega}} (a + a^\dagger), \quad p = -i \sqrt{\frac{\hbar\omega}{2}} (a - a^\dagger)$$

- with  $\langle \alpha | q | \alpha \rangle = \sqrt{\frac{1}{2\hbar\omega}} (\alpha + \alpha^*)$

$$\langle \alpha | q^2 | \alpha \rangle = \frac{1}{2\hbar\omega} \langle \alpha | a^2 + a a^\dagger + a^\dagger a + a^2 | \alpha \rangle = \frac{1}{2\hbar\omega} (\alpha^2 + 1 + 2|\alpha|^2 + \alpha^{*2})$$

one finds

$$\begin{aligned} (\Delta q)^2 &= \langle q^2 \rangle - \langle q \rangle^2 = \frac{\hbar}{2\omega} (\alpha^2 + 1 + 2|\alpha|^2 + \alpha^{*2} - \alpha^2 - 2|\alpha|^2 - \alpha^{*2}) \\ &= \frac{\hbar}{2\omega} \end{aligned}$$

• likewise, one obtains  $(\Delta p)^2 = \frac{\hbar\omega}{2}$

$$\hookrightarrow \Delta p \cdot \Delta q = \frac{\hbar}{2}$$

$\hookrightarrow$  for coherent states the Heisenberg-Robertson uncertainty relation holds with an equal sign; this holds true for all times!

- the set of coherent states forms a (overcomplete) basis
- the resolution of the identity operation in terms of coherent states reads

$$\frac{1}{\pi} \int d^2\alpha |\alpha X_\alpha| = 1 , \text{ with } d^2\alpha = dx dy \\ \alpha = x + iy \\ -\infty \leq x, y \leq \infty$$

- this is shown as follows:

$$\begin{aligned} \int d^2\alpha |\alpha X_\alpha| &= \sum_{nm} \frac{1}{n!m!} \int d^2\alpha \alpha^m (\alpha^{*})^n |X_m| e^{-|\alpha|^2} \\ &= \sum_{nm} \frac{1}{n!m!} \int_0^\infty dr r \underbrace{\int_0^{2\pi} d\varphi r^{n+m}}_{e^{i\varphi(n-m)}} \underbrace{|X_m| e^{-r^2}}_{2\pi dnm} \\ &= 2\pi \sum_n \frac{1}{n!} \int_0^\infty dr r^{2n+1} e^{-r^2} |X_n| \end{aligned}$$

(30)

- with the substitution  $r^2 = u$  one finds

$$\int d^2\alpha | \alpha X \alpha | = \pi \sum_n \frac{1}{n!} \underbrace{\int_0^\infty du u^n e^{-u} \ln x_n}_{\Gamma(n+1) = n!}$$

$$= \pi \sum_n \ln x_n$$

- note, that coherent states are not orthogonal

$$\begin{aligned} \langle \alpha | \beta \rangle &= \sum_{nm} \frac{1}{\sqrt{n!m!}} (\alpha^*)^n \beta^m \langle n | m \rangle e^{-\frac{1}{2} |\alpha|^2 - \frac{1}{2} |\beta|^2} \\ &= \sum_n \frac{(\alpha^* \beta)^n}{n!} e^{-\frac{1}{2} |\alpha|^2 - \frac{1}{2} |\beta|^2} = e^{\alpha^* \beta - \frac{1}{2} |\alpha|^2 - \frac{1}{2} |\beta|^2} \\ &= e^{-\frac{1}{2} |\alpha - \beta|^2} e^{\frac{1}{2} (\beta \alpha^* - \alpha^* \beta)} \end{aligned}$$

- coherent states can be generated from the vacuum state  $|0\rangle$  by applying the so-called displacement operator  $D$ :

$$|\alpha\rangle = D(\alpha)|0\rangle \quad \text{with } D(\alpha) = e^{-\frac{|\alpha|^2}{2}} e^{\alpha a^\dagger} e^{-\alpha^* a}$$

- this is seen as follows:

$$\begin{aligned} |\alpha\rangle &= e^{-\frac{|\alpha|^2}{2}} \sum_n \frac{\alpha^n}{\sqrt{n!}} |n\rangle = e^{-\frac{|\alpha|^2}{2}} \sum_n \frac{\alpha^n}{\sqrt{n!}} \frac{(\alpha^\dagger)^n}{\sqrt{n!}} |0\rangle \\ &= e^{-\frac{|\alpha|^2}{2}} \sum_n \frac{(\alpha a^\dagger)^n}{n!} |0\rangle = e^{-\frac{|\alpha|^2}{2}} e^{\alpha a^\dagger} |0\rangle \\ &= e^{-\frac{|\alpha|^2}{2}} e^{\alpha a^\dagger} \underbrace{e^{-\alpha^* a}}_{|0\rangle} |0\rangle \end{aligned}$$

$$e^x e^y = e^{z(x,y)}$$

$$\begin{aligned} z(x,y) = & \quad x + y + \frac{1}{2}[x,y] + \frac{1}{12}[x,[x,y]] \\ & - \frac{1}{2}[y,[x,y]] - \frac{1}{24}[y,[x,[x,y]]] \end{aligned}$$

+ ...

(31)

- the displacement operator is a unitary operator, which satisfies

$$D^+(\alpha) = D(-\alpha) = D(\alpha)^{-1}$$

- it can also be written as

$$D(\alpha) = e^{\alpha a^\dagger - \alpha^* a} = e^{-\frac{|\alpha|^2}{2}} e^{-\alpha^* a} e^{\alpha a^\dagger},$$

which can be proven using the Baker-Campbell-Hausdorff theorem for the special case

$$[[A, B], A] = [[A, B], B] = 0 \quad \text{with } A = \alpha a^\dagger, B = -\alpha^* a \Rightarrow e^{A+B} = e^{-\frac{[A, B]}{2}} e^A e^B.$$

- the action of the displacement operator on the annihilation and creation operator is as follows:

$$D^+(\alpha) a D(\alpha) = a + \alpha$$

$$D^+(\alpha) a^\dagger D(\alpha) = a^\dagger + \alpha^*,$$

- e.g. when applied to the position operator  $q = \sqrt{\frac{\hbar}{2m}}(a + a^\dagger)$  this yields a displacement in real space:

$$D^+(\alpha) q D(\alpha) = q + 2 \sqrt{\frac{\hbar}{2m}} \operatorname{Re}(\alpha)$$

## II Quasi-probability distributions in phase space

(32)

- the motion of classical particles takes place in phase space which is spanned by all the momentum and position coordinates
- in quantum mechanics position and momentum are conjugate variables which obey an uncertainty relation
- both cannot be determined with arbitrary precision, which in statistical physics motivates the introduction of dimension phase space cells with volume  $(2\pi\hbar)^d$
- the idea behind quasi-probability distributions in quantum mechanics is to represent quantum states as "probability densities" in phase space.
- this builds a bridge between the probabilistic aspects of quantum mechanics and the description of classical dynamical systems in terms of phase space variables
- examples for such quasi-probability distributions are the Wigner function (introduced in 1932) and the P-function introduced by Glauber

- in quantum optics they play an important role for
  - visualising quantum states and their dynamics
  - calculating expectation values
  - assessing the non-classicality of states
  - quantum state tomography
- in this chapter we introduce the Wigner function  $W$ , as well as the so-called P- and Q-functions

## II.1 The Wigner function

- we begin by considering a particle in one dimension
  - the probability distribution of its position  $q$  is given by density matrix
- $$P_{\text{pos}}(q) = \text{tr } g \delta(q - \hat{q})$$
- $\nwarrow$  position operator
- $$= \int dq' \langle q' | g \delta(q - \hat{q}) | q' \rangle$$
- $\nwarrow$  position operator eigenstate
- $$= \int dq' \langle q' | g | q' \rangle = \langle q | g | q \rangle$$

- Similarly, the probability distribution for the momentum  $p$  is

$$\begin{aligned}
 P_{\text{momentum}}(p) &= \text{tr } g \delta(p - \hat{p}) \\
 &= \int dq \langle q | g \delta(p - \hat{p}) | q \rangle \\
 &= \int dq dq' dp' \underbrace{\langle q | g | q' \rangle}_{g(q, q')} \underbrace{\delta(p - \hat{p}) | p' \rangle}_{\frac{1}{2\pi\hbar} e^{-ip'q}} \underbrace{\langle p' | p' \rangle}_{\frac{1}{2\pi\hbar}} \\
 &= \frac{1}{2\pi\hbar} \int dq dq' g(q, q') e^{i\frac{p}{\hbar}(q' - q)}
 \end{aligned}$$

- one could now define a joint distribution function for  $p$  and  $q$  via  $P(q, p) = \text{tr } g \delta(p - \hat{p}) \delta(q - \hat{q})$
- however, since  $\hat{p}$  and  $\hat{q}$  do not commute this choice is certainly not unique
- moreover, since  $\hat{p}\hat{q}$  is not hermitian,  $P(q, p)$  is not even expected to be a real function
- the Wigner function overcomes this problem
- it is defined as

$$\begin{aligned}
 W(q, p) &= \frac{1}{2\pi\hbar} \int_{-\infty}^{\infty} d\xi e^{-\frac{i}{\hbar} p \xi} \langle q + \frac{1}{2}\xi | g | q - \frac{1}{2}\xi \rangle \\
 &= \frac{1}{\pi\hbar} \int d\xi e^{\frac{2i}{\hbar} p \xi} \langle q - \xi | g | q + \xi \rangle
 \end{aligned}$$

(35)

- according to this definition,  $W(q, p)$  is the Fourier transform of the off-diagonal elements of the density matrix in the position basis

- the Wigner function is real

$$W(q, p)^* = \frac{1}{2\pi\hbar} \int_{-\infty}^{\infty} d\xi e^{\frac{i}{\hbar} p \xi} \langle q - \frac{1}{2}\xi | \psi | q + \frac{1}{2}\xi \rangle$$

$$\stackrel{\xi \rightarrow -\xi}{=} \frac{1}{2\pi\hbar} \int_{-\infty}^{\infty} d\xi (-1) e^{-\frac{i}{\hbar} p \xi} \langle q + \frac{1}{2}\xi | \psi | q - \frac{1}{2}\xi \rangle$$

$$= W(q, p)$$

- the probability distribution for  $q$  is found by integrating  $W(q, p)$  over  $p$ , i.e.,  $P_{\text{pos}}(q)$  is the marginal distribution for  $q$

$$\begin{aligned} \int_{-\infty}^{\infty} dp W(q, p) &= \int_{-\infty}^{\infty} d\xi \langle q - \frac{1}{2}\xi | \psi | q + \frac{1}{2}\xi \rangle \underbrace{\frac{1}{2\pi\hbar} \int_{-\infty}^{\infty} dp e^{\frac{i}{\hbar} p \xi}}_{\delta(\xi)} \\ &= \langle q | \psi | q \rangle \end{aligned}$$

- the marginal distribution for  $p$  is obtained by integrating over  $q$

(33)

$$\text{P}(\text{momentum } p) = \int_{-\infty}^{\infty} dq W(q, p) = \frac{1}{2\pi\hbar} \int dq \int d\xi e^{-\frac{i}{\hbar} p \xi} \langle q + \frac{1}{2}\xi | g | q - \frac{1}{2}\xi \rangle$$

$$\left. \begin{array}{l} q'' = q + \frac{1}{2}\xi \\ q' = q - \frac{1}{2}\xi \end{array} \right\} = \frac{1}{2\pi\hbar} \int dq' \int dq'' e^{-\frac{i}{\hbar} p(q'' - q')} \langle q'' | g | q' \rangle$$

$$= \int dq' \int dq'' \langle p | q'' \rangle \langle q'' | p \rangle \langle q'' | g | q' \rangle$$

$$= \langle p | g | p \rangle$$

- to investigate the behaviour of  $W(q, p)$  under translations in (real) space, we introduce the translation operators

$$T_a |q\rangle = |q+a\rangle$$

↳ translated density matrix:  $T_a g T_a^\dagger$

↳ translated Wigner function.

$$\frac{1}{2\pi\hbar} \int d\xi e^{-\frac{i}{\hbar} p \xi} \underbrace{\langle q + \frac{\xi}{2} | T_a g T_a^\dagger | q - \frac{\xi}{2} \rangle}_{\langle q - a + \frac{\xi}{2} | g | q - a - \frac{\xi}{2} \rangle} = W(q-a, p)$$

- Similarly, a translation in momentum space, which is implemented via  $\psi(q) \rightarrow e^{i\frac{p}{\hbar} q} \psi(q)$ , yields  $W(q, p) \rightarrow W(q, p-p')$

(37)

- under reflection in space ( $q \rightarrow -q$ ) and
- (5) time reversal (complex conjugation) the Wigner function behaves as

$$\psi(q) \rightarrow \psi(-q) \Rightarrow W(q, p) \rightarrow W(-q, -p)$$

$$\psi(q) \rightarrow \psi^*(q) \Rightarrow W(q, p) \rightarrow W(q, -p)$$

- the overlap between two states  $\psi_1$  and  $\psi_2$  is related to their Wigner functions via

$$\begin{aligned} \text{tr}(\psi_1 \psi_2) &= 2\pi\hbar \int_{-\infty}^{\infty} dq \int_{-\infty}^{\infty} dp W_{\psi_1}(q, p) W_{\psi_2}(q, p) \\ &= 2\pi\hbar \int dq \int d\xi_1 \int d\xi_2 \underbrace{\frac{1}{(2\pi\hbar)^2} \int dp e^{-\frac{i}{\hbar} p(\xi_1 + \xi_2)}}_{2\pi\hbar \delta(\xi_1 + \xi_2)} \\ &\quad \times \left\langle q + \frac{\xi_1}{2} | \psi_1 | q - \frac{\xi_1}{2} \right\rangle \left\langle q + \frac{\xi_2}{2} | \psi_2 | q - \frac{\xi_2}{2} \right\rangle \end{aligned}$$

$$\begin{aligned} \left\{ \begin{array}{l} x' = q - \frac{\xi_1}{2} \\ x'' = q + \frac{\xi_1}{2} \end{array} \right\} &= \int dx' \int dx'' \left\langle x'' | \psi_1 | x' \right\rangle \left\langle x' | \psi_2 | x'' \right\rangle \\ &= \text{tr } \psi_1 \psi_2 \end{aligned}$$

- it turns out, that the properties (1-6) determine the Wigner function uniquely

- the last property can be used to estimate the area that a Wigner function is occupying in phase space
- to see that, we consider the purity of a state  $\rho$ :  $\text{tr } \rho^2 \leq 1$

$$\hookrightarrow 2\pi\hbar \int dq \int dp W_\rho^2(q, p) \leq 1$$

$$\hookrightarrow 2\pi\hbar \leq \frac{1}{\underbrace{\int dq \int dp W_\rho^2(q, p)}_{\substack{\text{area occupied} \\ \text{by the Wigner function}}}}$$

↓  
 area of  
 a phase  
 space cell  
 in 1d

- (7) the Wigner function never diverges, which can be seen by computing an upper bound of  $|W(q, p)|$  for the general state  $\rho = \sum_n p_n |4_n\rangle \langle 4_n|$

$$\begin{aligned}
 |W(q, p)| &= \frac{1}{2\pi\hbar} \left| \sum_n p_n \int_{-\infty}^{\infty} d\xi e^{-\frac{i}{\hbar} p \xi} \langle q - \frac{\xi}{2} | 4_n \rangle \langle 4_n | q + \frac{\xi}{2} \rangle \right| \\
 &\leq \frac{1}{\pi\hbar} \sum_n p_n \left| \frac{1}{2} \int_{-\infty}^{\infty} d\xi e^{-\frac{i}{\hbar} p \xi} \langle q - \frac{\xi}{2} | 4_n \rangle \langle 4_n | q + \frac{\xi}{2} \rangle \right| \\
 &= \frac{1}{\pi\hbar} \sum_n p_n \left| \int_{-\infty}^{\infty} dx \underbrace{e^{-\frac{i}{\hbar} 2px}}_{\alpha_n^*(x)} \underbrace{\langle q - x | 4_n \rangle}_{\beta_n(x)} \langle 4_n | q + x \rangle \right|
 \end{aligned}$$

$$= \frac{1}{\pi\hbar} \sum_n p_n |\langle \alpha_n | \beta_n \rangle| \leq \frac{1}{\pi\hbar} \sum_n p_n \underbrace{|\langle \alpha_n | \alpha_n \rangle|}_1 \cdot \underbrace{|\langle \beta_n | \beta_n \rangle|}_1 \quad (39)$$

$$\hookrightarrow |W(q, p)| \leq \frac{1}{\pi\hbar}$$

note, that  $W(q, p)$  is no probability distribution, since it can assume negative values for certain states  $\varrho$

to see this, we consider the two orthogonal pure states  $\varrho_1 = |\psi_1 \chi \psi_1|$  and  $\varrho_2 = |\psi_2 \chi \psi_2|$

$$\hookrightarrow 0 = \text{Tr } \varrho_1 \varrho_2 = 2\pi\hbar \int dq \int dp W_{\varrho_1}(q, p) W_{\varrho_2}(q, p)$$

if we assume that  $W_{\varrho_1}(q, p) > 0$ , then  $W_{\varrho_2}(q, p)$  must assume negative values, so that the integral can vanish

- in the following we consider Wigner functions in the context of harmonic oscillators due to their importance for characterising quantum states of the electromagnetic field

(40)

- using the raising and lowering operator, we can construct the position and momentum operators

$$\begin{aligned}\hat{q} &= \frac{1}{\sqrt{2}}(a + a^\dagger) \\ \hat{p} &= \frac{1}{i\sqrt{2}}(a - a^\dagger)\end{aligned}\quad \left\{ \quad [\hat{p}, \hat{q}] = i\right.$$

(note, that we have been „setting”  $\hbar = 1$ )

- in quantum optics one expresses the Wigner function rather in terms of coherent state amplitudes ( $a|\alpha\rangle = \alpha|a\rangle$ ) than through position and momentum

$$W(q, p) \rightarrow W(\alpha, \alpha^*) \text{ with } \alpha = \frac{q + ip}{\sqrt{2}}$$

- the common definition is

$$W(\alpha, \alpha^*) = \frac{1}{\pi^2} \int d^2\beta \operatorname{tr}(g D(\beta)) e^{-(\beta\alpha^* - \beta^*\alpha)}$$

where  $d^2\beta = d\operatorname{Im}(\beta) d\operatorname{Re}(\beta) = d\beta_2 d\beta_1$ ,  $\beta = \beta_1 + i\beta_2$

This can be seen as follows:

(41)

$$D(\beta) = e^{\beta a^+ - \beta^* a} = e^{\frac{1}{2}i(\beta_2 \hat{q} - \beta_1 \hat{p})}$$

↪ with  $\Gamma_2 \beta \rightarrow \beta$  and  $\text{tr } \cdot = \int d\xi \langle \xi | \cdot | \xi \rangle$   
 one finds  $\uparrow \quad \uparrow$   
 position eigenstates

$$W(\alpha, \alpha^*) = \frac{1}{2\pi^2} \int d^2 \beta \int d\xi \langle \xi | \rho | \xi \rangle \underbrace{e^{i(\beta_2 \hat{q} - \beta_1 \hat{p})}}_{e^{i\beta_2 \hat{q}} e^{-i\beta_1 \hat{p}}} \underbrace{e^{-i(\beta_2 q - \beta_1 p)}}_{e^{-\frac{i}{2}\beta_1 \beta_2}}$$

now, we use that

$$\begin{aligned} e^{-i\beta_1 \hat{p}} |\xi\rangle &= \int dp \underbrace{e^{-i\beta_1 \hat{p}}}_{\frac{1}{\sqrt{2\pi}} e^{-ip\xi}} |p\rangle \langle p | \xi \rangle \\ &= \frac{1}{\sqrt{2\pi}} \int dp e^{-ip(\xi + \beta_1)} |p\rangle = |\xi + \beta_1\rangle \end{aligned}$$

$$\begin{aligned} \hookrightarrow W(\alpha, \alpha^*) &= \frac{1}{2\pi^2} \int d^2 \beta \int d\xi \langle \xi | \rho | \xi + \beta_1 \rangle e^{i\beta_2(\xi + \beta_1)} e^{-i(\beta_2 q - \beta_1 p)} e^{-\frac{i\beta_1 \beta_2}{2}} \\ &= \frac{1}{2\pi^2} \int d\beta_1 e^{i\beta_1 p} \int d\xi \langle \xi | \rho | \xi + \beta_1 \rangle \underbrace{\int d\beta_2 e^{i\beta_2(\xi + \frac{\beta_1}{2} - q)}}_{2\pi \delta(\xi - (q - \frac{\beta_1}{2}))} \\ &= \frac{1}{\pi} \int d\beta_1 e^{i\beta_1 p} \langle q - \frac{\beta_1}{2} | \rho | q + \frac{\beta_1}{2} \rangle \\ &= 2 W(q, p) \end{aligned}$$

↑ different normalisation in  
 $\alpha, \alpha^*$  and  $q, p$  representation

- in the following we consider a few examples and technical details

(42)

### Coherent state

- to obtain the Wigner function for the coherent state  $|\gamma\rangle$ , we have to first evaluate

$$\text{tr}(g D(\beta)) = \langle \gamma | D(\beta) | \gamma \rangle = \langle \gamma | D(\beta) D(\gamma) | 0 \rangle$$

- the concatenation of two displacement operators yields

$$D(\alpha) D(\beta) = D(\alpha + \beta) e^{\frac{1}{2}(\alpha\beta^* - \alpha^*\beta)}$$

- the latter relation is shown as follows:

$$\begin{aligned} D(\alpha) D(\beta) &= e^{-\frac{|\alpha|^2}{2}} e^{\alpha a^\dagger} e^{-\alpha^* a} e^{\frac{|\beta|^2}{2}} e^{-\beta^* a^\dagger} e^{\beta a^\dagger} \\ &= e^{-\frac{|\alpha|^2}{2} + \frac{|\beta|^2}{2}} e^{\alpha a^\dagger} \underbrace{e^{-(\alpha^* + \beta^*) a^\dagger} e^{\beta a^\dagger}}_{e^{\beta a^\dagger} e^{-(\alpha^* + \beta^*) a^\dagger} e^{-(\alpha^* + \beta^*) \beta [a, a^\dagger]}} \\ &= e^{-\frac{|\alpha|^2}{2} - \frac{|\beta|^2}{2}} e^{(\alpha + \beta) a^\dagger - (\alpha^* + \beta^*) a} e^{-\alpha^* \beta} \end{aligned}$$

which should be compared to

$$D(\alpha + \beta) = e^{-\frac{|\alpha + \beta|^2}{2}} e^{(\alpha + \beta) a^\dagger - (\alpha^* + \beta^*) a} = e^{-\frac{|\alpha|^2}{2} - \frac{|\beta|^2}{2} - \frac{\alpha^* \beta - \alpha \beta^*}{2}} e^{(\alpha + \beta) a^\dagger - (\alpha^* + \beta^*) a}$$

- we then find

$$\begin{aligned} \text{tr}(g D(\beta)) &= \langle \gamma | D(\beta) | \gamma \rangle e^{\frac{1}{2}(\beta\gamma^* - \beta^*\gamma)} = e^{\gamma^*(\beta + \gamma) - \frac{1}{2}|\gamma|^2 - \frac{1}{2}|\gamma + \beta|^2 + \frac{1}{2}(\beta\gamma^* - \beta^*\gamma)} \\ &= e^{-\frac{1}{2}|\beta|^2} e^{\beta\gamma^* - \beta^*\gamma} \end{aligned}$$

- the Wigner function of the coherent state  $|y\rangle$  can thus be written as

$$W(x, \alpha^*) = \frac{1}{\pi^2} \int d\beta^2 e^{-\frac{1}{2}|\beta|^2} e^{\beta(\gamma^* - \alpha^*) - \beta^*(\gamma - x)}$$

- using the shifted Gaussian integral

$$\frac{1}{\pi} \int d\beta^2 e^{-\delta|\beta|^2} e^{\beta^*x - \beta\alpha^*} = \frac{1}{\delta} e^{-\frac{|x-\alpha|^2}{\delta}} \quad (\delta > 0),$$

one obtains the explicit expression

$$W(x, \alpha^*) = \frac{2}{\pi} e^{-2|x-y|^2}.$$

This is a Gaussian in the complex plane, centered at  $\alpha = y$

Note, that one often writes  $W(x)$  for the Wigner function instead of  $W(x, \alpha^*)$ .

In the following we introduce the 2D complex Fourier transform, which is useful for computing Wigner functions

for a function  $g(\xi)$  with complex variable  $\xi = u + iv$  this is defined as

$$\tilde{g}(x) = \int \frac{d^2\xi}{\pi} e^{x\xi^* - x^*\xi} g(\xi)$$

with  $d\xi^2 = du dv$

- writing  $\alpha = x+iy$  yields

$$\bar{g}(x+iy) = \iint_{-\infty}^{\infty} \frac{du dv}{\pi} e^{2i(xu-yv)} g(u+iv),$$

which is indeed very similar to the "usual" Fourier transform

- the inverse Fourier transform is actually performed with the very same formula, unlike in case of the "usual" Fourier transform, where complex conjugation has to be applied to the argument of the exponential function
- to show this we use the Fourier representation of the 2d - delta - function:

$$\begin{aligned} \delta(x) \delta(y) &= \iint_{-\infty}^{\infty} \frac{dk dk'}{(2\pi)^2} e^{i(xk+yk')} \stackrel{v=-\frac{k}{2}}{=} \iint_{-\infty}^{\infty} \frac{du dv}{\pi^2} e^{2i(xu-yv)} \\ &= \int \frac{d^2 \xi}{\pi^2} e^{\alpha \xi^* - \alpha^* \xi} = \delta^{(2)}(\alpha) \end{aligned}$$

- we now apply the complex Fourier transform twice to show that it is its own inverse:

$$\begin{aligned} \tilde{g}(\alpha) &= \int \frac{d^2 \xi}{\pi} e^{\alpha \xi^* - \alpha^* \xi} g(\xi) = \underbrace{\int \frac{d^2 \xi}{\pi} e^{\alpha \xi^* - \alpha^* \xi}}_{\tilde{g}(\xi)} \underbrace{\int \frac{d^2 \xi}{\pi} e^{\xi \xi^* - \xi^* \xi}}_{\tilde{g}(\xi)} \tilde{g}(\xi) \\ &= \int \frac{d^2 \xi}{\pi} \underbrace{\int \frac{d^2 \xi}{\pi} e^{\xi(\xi^* - \alpha^*) - \xi^*(\xi - \alpha)}}_{\pi \delta^{(2)}(\xi - \alpha)} \tilde{g}(\xi) = \tilde{g}(\alpha) \end{aligned}$$

(45)

- we can thus understand the Wigner function  $W(\alpha, \alpha^*) = \frac{1}{\pi^2} \int d^2 \beta \operatorname{tr}(g D(\beta)) e^{-(\beta \alpha^* - \beta^* \alpha)}$  as Fourier transform of  $\operatorname{tr}(g D(\beta))$
- $\operatorname{tr}(g D(\beta))$  is therefore the characteristic function of the Wigner function
- let us now derive another useful representation of Wigner function
- to this end we consider the complex Fourier transform of a function  $C(\beta, \beta^*)$  defined as

$$W(\alpha, \alpha^*) e^{-2|\alpha|^2} = \int C(\beta, \beta^*) e^{\beta \alpha^* - \beta^* \alpha} d^2 \beta$$

- the function  $C(\beta, \beta^*)$  can be found using the convolution theorem.

$$C(\beta, \beta^*) = \underbrace{\int \frac{d^2 \beta_1}{\pi^2} \operatorname{tr}(g e^{-(\beta - \beta_1) \alpha^* + (\beta^* - \beta_1^*) \alpha})}_{\mathcal{D}(\beta - \beta_1)} \underbrace{e^{-\frac{1}{2} |\beta|^2}}_{\text{Fourier transform of } e^{-2|\alpha|^2}}$$

(shifted) Fourier transform  
of the Wigner function  
 $W(\alpha, \alpha^*)$

- using  $\mathcal{D}(\beta - \beta_1) = e^{-(\beta - \beta_1) \alpha^*} e^{(\beta^* - \beta_1^*) \alpha} e^{-\frac{1}{2} |\beta - \beta_1|^2}$ , we write

$$\begin{aligned} C(\beta, \beta^*) &= \frac{1}{2\pi^5} \iiint \operatorname{tr}(g |\beta_2 \times \beta_3| e^{-(\beta - \beta_1) \alpha^*} e^{(\beta^* - \beta_1^*) \alpha} |\beta_2 \times \beta_3|) e^{-\frac{1}{2} |\beta - \beta_1|^2 - \frac{1}{2} |\beta_1|^2} \\ &= \frac{1}{2\pi^5} \iiint \langle \beta_3 | g | \beta_2 \rangle \langle \beta_2 | \beta_3 \rangle \exp [(\beta - \beta_1) \beta_2^* + (\beta^* - \beta_1^*) \beta_3 - \frac{1}{2} |\beta - \beta_1|^2 - \frac{1}{2} |\beta_1|^2] d\beta_1^2 d\beta_2^2 d\beta_3^2 \end{aligned}$$

- the integration over  $\beta_1$  involves the evaluation of a Gaussian integral

writing the remaining exponentials as overlaps eventually yields (46)

$$C(\beta, \beta^*) = \frac{1}{2\pi^4} \iint d\beta_2 d\beta_3 \langle \beta_3 | g | \beta_2 \rangle \langle \frac{\beta}{2} | \beta_3 \rangle \langle \beta_2 | -\frac{\beta}{2} \rangle$$

$$= \frac{1}{2\pi^2} \langle \frac{\beta}{2} | g | -\frac{\beta}{2} \rangle$$

making the variable change  $\beta \rightarrow -2\beta$   
and insertion into the initial expression yields

$$W(\alpha, \alpha^*) = \frac{2}{\pi^2} e^{2|\alpha|^2} \int d\beta \langle -\beta | g | \beta \rangle e^{-2(\beta\alpha^* - \beta^*\alpha)}$$

↳ the Wigner function is the Fourier transform of the off-diagonal elements of the density matrix in the coherent state basis

let us now use this result to calculate the Wigner function of a thermal state, which is defined as

$$\rho = \frac{e^{-\beta h_{\text{w}}}}{\text{tr}(e^{-\beta h_{\text{w}}})} = \sum_n \underbrace{\frac{\langle n \rangle^n}{(1 + \langle n \rangle)^{n+1}}}_{\text{average occupation number}} \underbrace{|n\rangle \langle n|}_{\text{projector on Fock state}}$$

average occupation number

$$\langle n \rangle = \text{tr}(\hat{a}^\dagger \hat{a} \rho) = (e^{\beta h_{\text{w}}} - 1)^{-1} = \left(\frac{1}{z} - 1\right)^{-1} = \frac{z}{1-z}$$

will need this later

To obtain the Wigner function we compute

$$\begin{aligned}
 & \text{compute} \\
 & \langle -\beta | g | \beta \rangle = \sum_n p_n \underbrace{\langle -\beta | n \rangle}_{\frac{\beta^n}{n!}} \underbrace{\langle n | \beta \rangle}_{e^{-|\beta|^2/2}} = \sum_n \frac{p_n}{n!} e^{-|\beta|^2} [(-\beta^*) \beta]^n \\
 & = \sum_n \frac{p_n}{n!} e^{-|\beta|^2} (-|\beta|^2)^n \\
 & = \frac{1}{1 + \langle n \rangle} \left( \sum_{n=0}^{\infty} \frac{1}{n!} \left( \frac{\langle n \rangle}{1 + \langle n \rangle} (-|\beta|^2) \right) \right)^n e^{-|\beta|^2} \\
 & = \frac{1}{1 + \langle n \rangle} e^{-\frac{\langle n \rangle}{1 + \langle n \rangle} |\beta|^2 - |\beta|^2} = \frac{1}{1 + \langle n \rangle} e^{-|\beta|^2} \frac{2\langle n \rangle + 1}{\langle n \rangle + 1}
 \end{aligned}$$

$$\hookrightarrow W(\alpha, \alpha^*) = \frac{2}{\pi^2} \frac{e^{2|\alpha|^2}}{1 + \langle n \rangle} \underbrace{\int d^2 \beta \exp \left[ -|\beta|^2 \frac{2\langle n \rangle + 1}{\langle n \rangle + 1} - 2(\beta \alpha^* - \beta^* \alpha) \right]}_{\text{Gaussian integral}}$$

- this Wigner function is centred at  $\alpha=0$  and has a width of  $\sqrt{\langle n \rangle + \frac{1}{2}}$
  - we can use this expression to calculate the Wigner function of a Fock state
  - the connection is established through the relation probabilities  $p_n = (1-z)z^n$

$$W_T(\alpha, \alpha^*) = \sum_{n=0}^{\infty} p_n W_n(\alpha, \alpha^*) = (1-z) \sum_{n=0}^{\infty} z^n W_n(\alpha, \alpha^*)$$

↑  
 ↑  
 Wigner function  
 of thermal state      Wigner function  
 of Fock state  $|n\rangle$

- expressing all expectation values  $\langle n \rangle$  in (48)  
 $W(\alpha, \alpha^*)$  through  $z$  one finds the relation

$$\sum_{n=0}^{\infty} z^n W_n(\alpha, \alpha^*) = \frac{2}{\pi(1+z)} e^{-2|\alpha|^2} e^{4|\alpha|^2 \frac{z}{1+z}}$$

- comparing the right hand side with the generating function of the Laguerre polynomials,

$$\sum_{n=0}^{\infty} L_n(x) (-z)^n = \frac{1}{1+z} e^{\frac{xz}{1+z}},$$

we can see that

$$W_n(\alpha, \alpha^*) = \frac{2(-1)^n}{\pi} e^{-2|\alpha|^2} L_n(4|\alpha|^2)$$

- the first three Laguerre polynomials are  
 $L_0 = 1$  ,  $L_1 = 1-x$  ,  $L_2 = \frac{1}{2}(2-4x+x^2)$
- indeed  $W_0(\alpha, \alpha^*) = \frac{2}{\pi} e^{-2|\alpha|^2}$  is identical to the result for a (nondisplaced) coherent state
- for  $|n=1\rangle$  one obtains

$$W_1(\alpha, \alpha^*) = \frac{2}{\pi} e^{-2|\alpha|^2} (4|\alpha|^2 - 1)$$

- this is a rotationally symmetric function which is negative for  $|\alpha| < \frac{1}{4}$
- this a manifestation of the non-classical character of this Fock state

## II.2 The Glauber - Sudarshan P-function

(49)

- the coherent states form an overcomplete basis and a resolution of the identity is given through  $\mathbb{1} = \frac{1}{\pi} \int d^2\alpha |\alpha\rangle\langle\alpha|$
- any density matrix can thus be expanded according to

$$\rho = \iint \frac{d^2\alpha}{\pi} \frac{d^2\beta}{\pi} |\alpha\rangle\langle\alpha| \rho |\beta\rangle\langle\beta|$$

- this yields the so-called Glauber R-representation

$$R(\alpha^*, \beta) = \langle \alpha | \rho | \beta \rangle e^{\frac{1}{2}(|\alpha|^2 + |\beta|^2)}$$

$$\rho = \iint \frac{d^2\alpha}{\pi} \frac{d^2\beta}{\pi} |\alpha\rangle\langle\alpha| R(\alpha^*, \beta) e^{-\frac{1}{2}(|\alpha|^2 + |\beta|^2)},$$

which is an "off-diagonal" representation of  $\rho$

- it actually turns out that  $\rho$  can be represented in terms of diagonal projectors on coherent states,  $|\alpha\rangle\langle\alpha|$
- the corresponding function  $P(\alpha, \alpha^*)$  is, in general, not simply a function, but often a distribution or derivative of a distribution
- in order to construct this so-called P-function, we first consider an operator in its normal ordered form

$$O_N(\alpha, \alpha^*) = \sum_{n,m} c_{nm} (\alpha^*)^n \alpha^m, \quad c_{nm} \in \mathbb{C}$$

creation operators  $\uparrow$        $\downarrow$  annihilation operators  
 to the left                          to the right

- any (operator-valued) function can be brought into this form, by repeated application of the commutator  $[a, a^\dagger] = 1$

↳ example:  $a^2 a^\dagger = a([a, a^\dagger] + a^\dagger a) = a(1 + a^\dagger a)$   
 $= a + ([a a^\dagger] + a^\dagger a)a$   
 $= a + (1 + a^\dagger a)a = a^\dagger a^2 + 2a$

- the procedure of normal ordering is often denoted by ' $:O:$ ', e.g.  $:a^2 a^\dagger: = a^\dagger a^2$   
 ↳ no use of commutator
- when an operator is normal ordered, one has

$$\langle \alpha | O_N(a, a^\dagger) | \alpha \rangle = \sum_{n,m} c_{nm} \langle \alpha | (a^\dagger)^n a^m | \alpha \rangle = \sum_{n,m} c_{nm} (\alpha^*)^n \alpha^m$$

$$= O_N(\alpha, \alpha^*)$$

↳ the expectation value of a normal ordered operator taken in a coherent state  $|\alpha\rangle$  is obtained by the replacement  $a \rightarrow \alpha, a^\dagger \rightarrow \alpha^*$

- we now consider the normal ordered distribution  $\delta(\alpha^* - a^\dagger) \delta(\alpha - a)$  to define the P-function

$$P(\alpha, \alpha^*) = \text{tr} (g \delta(\alpha^* - a^\dagger) \delta(\alpha - a))$$

which can be inverted to yield the density matrix  $g$ :

$$g = \int d^2\alpha \underbrace{P(\alpha, \alpha^*) | \alpha \rangle \langle \alpha |}_{\substack{\text{diagonal in} \\ \text{the coherent} \\ \text{state basis}}}$$

- the latter is shown by inserting the last expression into the previous one

$$\begin{aligned}
 \hookrightarrow P(\alpha, \alpha^*) &= \text{tr} \left( \int d\gamma^2 P(\gamma, \gamma^*) |\gamma\rangle \langle \gamma| \delta(\alpha^* - \alpha^+) \delta(\alpha - \alpha) \right) \\
 &= \int d\gamma^2 P(\gamma, \gamma^*) \langle \gamma | \delta(\alpha^* - \alpha^+) \delta(\alpha - \alpha) | \gamma \rangle \\
 &= \int d\gamma^2 P(\gamma, \gamma^*) \delta(\alpha^* - \gamma^*) \delta(\alpha - \gamma) = P(\alpha, \alpha^*)
 \end{aligned}$$

- the P-representation can be found for any operator after bringing it into anti-normal ordered form

$$O_A(\alpha, \alpha^*) = \sum_{nm} O_{nm} \alpha^n (\alpha^*)^m = \int \frac{d^2 \alpha}{\pi} \sum_{nm} O_{nm} \alpha^n (\alpha^*)^m |\alpha \rangle \langle \alpha|$$

- in practice  $P(\alpha, \alpha^*)$  can be calculated, similarly to  $W(\alpha, \alpha^*)$ , through a Fourier transform of off-diagonal elements of  $\hat{g}$

$$\begin{aligned}
 \hookrightarrow \langle -\beta | g | \beta \rangle &= \int d\alpha^2 P(\alpha, \alpha^*) \langle -\beta | \alpha \rangle \langle \alpha | \beta \rangle \\
 &= e^{-|\beta|^2} \int d\alpha^2 P(\alpha, \alpha^*) e^{-|\alpha|^2} e^{\beta \alpha^* - \beta^* \alpha}
 \end{aligned}$$

$P(\alpha, \alpha^*) e^{-|\alpha|^2}$  is the 2d complex Fourier transform of  $\langle -\beta | g | \beta \rangle e^{|\beta|^2}$

$$\hookrightarrow P(\alpha, \alpha^*) = \frac{e^{-|\alpha|^2}}{\pi^2} \int d\beta^2 \underbrace{\langle -\beta | g | \beta \rangle}_{e^{|\beta|^2}} e^{-|\beta|^2} e^{-\beta \alpha^* + \beta^* \alpha}$$

has to fall off more rapidly than  $e^{-|\beta|^2}$ , otherwise the result is to be interpreted as distribution

- expectation values of normal ordered operators are obtained from the P-function via

$$\begin{aligned} \langle O_N(\alpha, \alpha^*) \rangle &= \text{tr} (\overset{\uparrow}{g} O_N(\alpha, \alpha^*)) = \text{tr} \int d^2\alpha P(\alpha, \alpha^*) | \alpha X \alpha | O_N(\alpha, \alpha^*) \\ &\stackrel{\text{normal}}{\overbrace{\quad\quad\quad}} \quad \quad \quad = \int d^2\alpha P(\alpha, \alpha^*) O_N(\alpha, \alpha^*) \end{aligned}$$

- Examples:

- coherent state

$$g = |\gamma \times \gamma| \rightarrow P(\alpha, \alpha^*) = \delta^{(2)}(\alpha - \gamma)$$

- thermal state

$$g = \frac{e^{-\beta h w \alpha^*}}{\text{tr}(e^{-\beta h w \alpha^*})} = \sum_{n=0}^{\infty} \frac{\langle n \rangle^n}{(1 + \langle n \rangle)^{n+1}} |n X_n|$$

$$\begin{aligned} \hookrightarrow \langle -\beta | g | \beta \rangle &= \sum_{n=0}^{\infty} \frac{\langle n \rangle^n}{(1 + \langle n \rangle)^{n+1}} \langle -\beta | n X_n | \beta \rangle \\ &= \frac{e^{-|\beta|^2}}{1 + \langle n \rangle} \sum_{n=0}^{\infty} \frac{(-|\beta|^2)^n}{(1 + \langle n \rangle)^n} \frac{\langle n \rangle^n}{n!} = \frac{e^{-|\beta|^2}}{1 + \frac{1}{\langle n \rangle}} e^{-\frac{|\beta|^2}{1 + \frac{1}{\langle n \rangle}}} \end{aligned}$$

$$\begin{aligned} \hookrightarrow P(\alpha, \alpha^*) &= \frac{e^{|\alpha|^2}}{\pi^2 (1 + \langle n \rangle)} \int d^2\beta e^{-\frac{|\beta|^2}{1 + \frac{1}{\langle n \rangle}}} e^{-\beta \alpha^* + \alpha \beta^*} \\ &= \frac{e^{|\alpha|^2}}{\pi^2 (1 + \langle n \rangle)} \cdot \pi e^{-|\alpha|^2 (1 + \frac{1}{\langle n \rangle})} \left(1 + \frac{1}{\langle n \rangle}\right) \\ &= \frac{e^{-\frac{|\alpha|^2}{\langle n \rangle}}}{\pi \langle n \rangle} \end{aligned}$$

- the P-function is a Gaussian

- number state:

$$\mathcal{S} = \ln \chi_n$$

$$\hookrightarrow \langle -\beta \ln \chi_n | \beta \rangle = \frac{e^{-|\beta|^2} (-1)^n |\beta|^{2n}}{n!}$$

$$\begin{aligned} \hookrightarrow P(\alpha, \alpha^*) &= \frac{(-1)^n e^{|\alpha|^2}}{\pi^2 n!} \int d^2 \beta \, |\beta|^{2n} e^{-\beta \alpha^* + \beta^* \alpha} \\ &= \frac{e^{|\alpha|^2}}{\pi^2 n!} \frac{\partial^{2n}}{\partial \alpha^n \partial \alpha^{*n}} \int d^2 \beta \, e^{-\beta \alpha^* + \beta^* \alpha} \\ &= \frac{e^{|\alpha|^2}}{n!} \frac{\partial^{2n}}{\partial \alpha^n \partial \alpha^{*n}} \delta^{(2)}(\alpha) \end{aligned}$$

- the  $P$ -function can be expressed as the derivative of the  $\delta$ -function
- for  $n=0$  we obtain  $P(\alpha, \alpha^*) = e^{|\alpha|^2} \delta^{(2)}(\alpha) = \delta^{(2)}(\alpha)$ , which is consistent with the result we previously obtained for coherent states

## II.3 The Q-representation

- it turns out that the diagonal elements of  $\mathcal{S}$ , taken in coherent states, represent the density matrix in a unique way
- this motivates the Q-representation or Husimi function

$$Q(\alpha, \alpha^*) = \frac{1}{\pi} \langle \alpha | \mathcal{S} | \alpha \rangle$$

- one can obtain  $Q$  also in a similar way like  $P$ , but one needs to employ anti-normal ordering:

$$\begin{aligned}
 Q(\alpha, \alpha^*) &= \text{tr} (g \delta(\alpha - a) \delta(\alpha^* - a^*)) = \text{tr} \frac{1}{\pi} \int d\alpha' g \delta(\alpha - a) |\alpha' X_\alpha| \delta(a^* - a^*) \\
 &= \text{tr} \frac{1}{\pi} \int d\alpha' g \delta(\alpha - \alpha') \delta(\alpha^* - \alpha'^*) |\alpha' X_{\alpha'}| \\
 &= \frac{1}{\pi} \int d\alpha' \langle \alpha' | g | \alpha' \rangle \delta(\alpha - \alpha') \delta(\alpha^* - \alpha'^*) \\
 &= \frac{1}{\pi} \langle \alpha | g | \alpha \rangle
 \end{aligned}$$

- properties of the Husimi function

- $Q(\alpha, \alpha^*) \geq 0 \quad \forall \alpha \text{ and } Q(\alpha, \alpha^*) \in \mathbb{R}$

- $\int d^2\alpha Q(\alpha, \alpha^*) = \int d^2\alpha \frac{1}{\pi} \langle \alpha | g | \alpha \rangle = \text{tr} \underbrace{\int \frac{d^2\alpha}{\pi} | \alpha X_\alpha | g}_{\perp} = \text{tr } g = 1$

- upper bound: for  $g = \sum_i p_i |4_i\rangle \langle 4_i|$  one finds  $Q(\alpha, \alpha^*) = \frac{1}{\pi} \sum_i \underbrace{|\langle \alpha | 4_i \rangle|^2}_{\leq 1} \leq \frac{1}{\pi}$

- $Q(\alpha, \alpha^*)$  can be straightforwardly used for the evaluation of expectation values of anti-normal ordered expectation values

$$O_A(a, a^*) = \sum_{nm} \underset{\substack{\uparrow \\ \text{anti-normal ordered}}}{d_{nm}} a^n (a^*)^m$$

$$\begin{aligned}
 \hookrightarrow \langle O_A(a, a^*) \rangle &= \sum_{nm} d_{nm} \text{tr} (a^n (a^*)^m g) = \sum_{nm} d_{nm} \text{tr} \left( \frac{1}{\pi} \int d\alpha a^n |\alpha X_\alpha| (a^*)^m g \right) \\
 &= \sum_{nm} d_{nm} \frac{1}{\pi} \int d\alpha \alpha^n (a^*)^m \langle \alpha | g | \alpha \rangle = \int d\alpha Q(\alpha, \alpha^*) O_A(\alpha, \alpha^*)
 \end{aligned}$$

• Examples:

- coherent state

$$g = |\gamma \chi \gamma| \rightarrow Q(\alpha, \alpha^*) = \frac{1}{\pi} |\langle \alpha | \gamma \rangle|^2 = \underbrace{\frac{1}{\pi} e^{-|\alpha - \gamma|^2}}_{\text{Gaussian}}$$

- thermal state

$$\begin{aligned} Q(\alpha, \alpha^*) &= \frac{1}{\pi} \sum_{n=0}^{\infty} \frac{\langle n \rangle^n}{(1 + \langle n \rangle)^{n+1}} \underbrace{\langle \alpha | n \rangle \langle n | \alpha \rangle}_{e^{-|\alpha|^2} \frac{|\alpha|^{2n}}{n!}} \\ &= \frac{1}{\pi} \frac{e^{-|\alpha|^2}}{1 + \langle n \rangle} \sum_{n=0}^{\infty} \frac{1}{n!} \left( \frac{\langle n \rangle |\alpha|^2}{1 + \langle n \rangle} \right)^n \\ &= \frac{1}{\pi} \frac{e^{-|\alpha|^2}}{1 + \langle n \rangle} e^{\frac{\langle n \rangle}{1 + \langle n \rangle} |\alpha|^2} = \frac{1}{\pi} \frac{e^{-\frac{|\alpha|^2}{1 + \langle n \rangle}}}{1 + \langle n \rangle} \end{aligned}$$

- number state

$$Q(\alpha, \alpha^*) = \frac{1}{\pi} |\langle \alpha | n \rangle|^2 = \underbrace{\frac{1}{\pi} e^{-|\alpha|^2} \frac{|\alpha|^{2n}}{n!}}$$

(compare to Poisson distribution  $P_\lambda(n) = \frac{\lambda^n}{n!} e^{-\lambda}$ )

function is sharply peaked at  $|\alpha| \approx \sqrt{n}$

- the density matrix  $\rho$  can be computed from a given  $Q$ -function by using the representation

$$Q(\alpha, \alpha^*) = \sum_{n,m=0}^{\infty} Q_{nm} \underbrace{\alpha^m (\alpha^*)^n}_{\substack{\text{coefficients of} \\ \text{power series} \\ \text{expansion}}}$$

unifying notation:

$$F_k(\alpha, \alpha^*) = \frac{1}{\pi^2} \int d^2 \lambda e^{\alpha \lambda^* - \alpha^* \lambda} + (e^{\lambda \alpha^*} e^{-\lambda^* \alpha}) e^{\frac{1+k}{2} |\lambda|^2}$$

$k=0$   $\rightarrow$  Wigner function

$k=1$   $\rightarrow$  Glauber-Sudarshan P-function

$k=-1$   $\rightarrow$  Husimi Q-function

See, e.g., Sci Post Phys. 10, 045 (2021)

- with this we can write

$g = \pi \sum_{nm} Q_{nm} (\alpha^*)^n \alpha^m$ , which indeed yields the correct Q-function

$$Q(\alpha, \alpha^*) = \frac{1}{\pi} \langle \alpha | g(\alpha) \rangle = \sum_{nm} Q_{nm} (\alpha^*)^n \alpha^m$$

## II.4 Relationship between Wigner, P- and Q-distributions

- the different distributions have different "use cases":
  - the P-distribution allows to formulate a simple non-classicality criterion for quantum states of the radiation field
  - the Wigner function can be experimentally determined through quantum state tomography

- to establish relations between the distributions we consider the normal ordered quantum characteristic function

$$\chi(\lambda, \lambda^*) = \text{tr}(g e^{\lambda a^*} e^{-\lambda^* a})$$

- this function allows to calculate expectation values of normal ordered operators.

$$\langle (a^*)^r a^s \rangle = (-1)^s \frac{\partial^{r+s}}{\partial \lambda^r \partial (\lambda^*)^s} \chi(\lambda, \lambda^*) \Big|_{\lambda=0}$$

- using the Baker-Campbell-Hausdorff formula, (57)  
we can also write

$$\begin{aligned} \chi(\lambda, \lambda^*) &= \text{tr}(g e^{-\lambda^* \alpha} e^{\lambda \alpha^*} e^{i|\lambda|^2}) \\ &= \frac{e^{i|\lambda|^2}}{\pi} \int d^2 \alpha \underbrace{\text{tr}(g e^{-\lambda^* \alpha} |\alpha \times \alpha| e^{\lambda \alpha^*})}_{e^{-\lambda^* \alpha} e^{\lambda \alpha^*} |\alpha \times \alpha|} = e^{i|\lambda|^2} \int d^2 \alpha e^{\lambda \alpha^* - \lambda^* \alpha} Q(\alpha, \alpha^*) \end{aligned}$$

- inverting the Fourier transform yields then

$$Q(\alpha, \alpha^*) = \frac{1}{\pi^2} \int d^2 \lambda e^{-i|\lambda|^2} \chi(\lambda, \lambda^*) e^{-(\lambda \alpha^* - \lambda^* \alpha)}$$

- on the other hand, inserting the representation  
 $g = \int d^2 \alpha P(\alpha, \alpha^*) |\alpha \times \alpha|$  into the definition of  $\chi$   
yields

$$\begin{aligned} \chi(\lambda, \lambda^*) &= \int d^2 \alpha \langle \alpha | e^{\lambda \alpha^*} e^{-\lambda^* \alpha} | \alpha \rangle P(\alpha, \alpha^*) \\ &= \int d^2 \alpha e^{\lambda \alpha^* - \lambda^* \alpha} P(\alpha, \alpha^*) \end{aligned}$$

- inserting this into the expression for  $Q$  yields

$$Q(\alpha, \alpha^*) = \frac{1}{\pi^2} \int d^2 \lambda d^2 \beta e^{\lambda(\beta^* - \alpha^*) - \lambda^*(\beta - \alpha)} e^{-i|\lambda|^2} P(\beta, \beta^*)$$

- completing the square in the exponent and performing the Gaussian integral yields

$$Q(\alpha, \alpha^*) = \frac{1}{\pi} \int d^2 \beta e^{-i|\alpha - \beta|^2} P(\beta, \beta^*)$$

↳  $Q$  is obtained by convoluting  $P$  with a Gaussian

- The Wigner function is the Fourier transform of the characteristic function

$$X_w(\lambda, \lambda^*) = \text{tr}(g e^{i\lambda a - i\lambda^* a^*}) : W(\alpha, \alpha^*) = \frac{1}{\pi^2} \int d^2 \lambda e^{-i\lambda \alpha^* + i\lambda^* \alpha} X_w(\lambda, \lambda^*)$$

- a calculation analogous to the previous one, yields then

$$W(\alpha, \alpha^*) = \frac{2}{\pi} \int d^2 \beta e^{-2(\alpha - \beta)^2} P(\beta, \beta^*)$$

expectation values of symmetrically ordered operators

- we will now show, that  $W(\alpha, \alpha^*)$  allows to calculate the expectation values of symmetrically ordered operators, for example the operator  $O_s(aa^*) = \frac{1}{2}(a^*a + aa^*) = \{aa^*\}_{\text{sym}}$

$$\{a^2 a^*\}_{\text{sym}} = \frac{1}{3}(a^2 a^* + a a^* a + a^* a^2) \quad \text{or}$$

$$\{a^2 (a^*)^2\}_{\text{sym}} = \frac{1}{6}(a^2 a^{*2} + a a^{*2} a + a^{*2} a^2 + a a^* a a^* + a^* a^2 a^* + a a a^* a)$$

- in general, a term  $a^n (a^*)^k$  leads to  $\binom{n+k}{n}$  terms

- we now use that we can expand

$$\begin{aligned} \exp(\lambda a^* - \lambda^* a) &= \sum_{n=0}^{\infty} \frac{1}{n!} (\lambda a^* - \lambda^* a)^n \\ &= \sum_{n=0}^{\infty} \frac{1}{n!} \sum_{k=0}^n \binom{n}{k} \lambda^{n-k} (-\lambda^*)^k \{ (a^*)^{n-k} a^k \}_{\text{sym}} \\ &= \sum_{n=0}^{\infty} \sum_{k=0}^n \frac{1}{k! (n-k)!} \lambda^{n-k} (-\lambda^*)^k \{ a^k (a^*)^{n-k} \}_{\text{sym}} \end{aligned}$$

(58)

$$\hookrightarrow \exp(\lambda a^+ - \lambda^* a) = \sum_{r,s} \frac{1}{r! s!} \lambda^r (-\lambda^*)^s \left\langle \left\{ a^r (a^+)^s \right\}_{\text{sym}} \right\rangle$$

(59)

Note that summation is still constrained, since  $r$  and  $s$  are not independent.

$$\hookrightarrow \chi_w(\lambda, \lambda^*) = \text{tr} (pe^{\lambda a^+ - \lambda^* a}) = \sum_{r,s} \frac{1}{r! s!} \lambda^r (-\lambda^*)^s \left\langle \left\{ a^r (a^+)^s \right\}_{\text{sym}} \right\rangle.$$

Therefore, one finds

$$\left\langle \left\{ a^r (a^+)^s \right\}_{\text{sym}} \right\rangle = \frac{\partial^r}{\partial (-\lambda^*)^r} \frac{\partial^s}{\partial \lambda^s} \chi_w(\lambda, \lambda^*) \Big|_{\lambda = \lambda^* = 0}$$

using that

$$\chi_w(\lambda, \lambda^*) = \int d^2\alpha W(\alpha, \alpha^*) e^{\lambda \alpha^* - \lambda^* \alpha}$$

we thus see that applying derivatives with respect to  $\lambda, \lambda^*$  to both sides implies the relation

$$\left\langle \left\{ a^r (a^+)^s \right\}_{\text{sym}} \right\rangle = \int d^2\alpha W(\alpha, \alpha^*) \alpha^r (\alpha^*)^s$$

## (60)

### 11.5 Equations of motion for quasi-probability distributions

- the state of a quantum system evolves under the von Neumann equation:

$$\frac{\partial}{\partial t} \rho = -i [H, \rho]$$

we consider here systems, where the Hamiltonian depends on bosonic creation and annihilation operators,  
e.g.  $H = H(a, a^*)$

in the following we will show how the quasi-probability distributions allow to reexpress the von Neumann equation in terms of a partial differential equation for coherent state amplitudes

we start with the P-representation

$\rho = \int d^2x \, P(\alpha, \alpha^*) |x \alpha\rangle \langle x \alpha|$ , which allows us to calculate the action of an annihilation operator onto the left hand side:

$$a\rho = \int d^2x \, P(\alpha, \alpha^*) \alpha |x \alpha\rangle \langle x \alpha|$$

- more over, one finds that

$$g_{\alpha^+} = \int d^2\alpha' P(\alpha, \alpha') |\alpha' \rangle \langle \alpha'| \alpha'^*$$

- This allows to establish the correspondence

$$\alpha g \leftrightarrow \alpha P(\alpha, \alpha')$$

$$g_{\alpha^+} \leftrightarrow \alpha^* P(\alpha, \alpha')$$

- in the next step we will try to understand the action of the creation operator from the left
- to this end we introduce the so-called Bargmann - state,

$$|\alpha\rangle = e^{\frac{1}{2}|\alpha|^2} |\alpha\rangle = \sum_{n=0}^{\infty} \frac{\alpha^n}{\sqrt{n!}} |n\rangle$$

which is simply a non-normalised coherent state

- it is useful, because it is an analytic function, which only depends on  $\alpha$  (not on  $\alpha^*$ )

- one finds that

$$\alpha|n\rangle = \sum_{n=0}^{\infty} \frac{\alpha^n \sqrt{n+1}}{\sqrt{n!}} |n+1\rangle$$

$$\begin{aligned} \frac{\partial}{\partial \alpha} |\alpha\rangle &= \sum_{n=0}^{\infty} \frac{n \alpha^{n-1}}{\sqrt{n!}} |n\rangle = \sum_{n=1}^{\infty} \frac{\sqrt{n} \alpha^{n-1}}{\sqrt{(n-1)!}} |n\rangle \\ &= \sum_{n=0}^{\infty} \frac{\sqrt{n+1} \alpha^n}{\sqrt{n!}} |n+1\rangle \end{aligned}$$

and hence

$$a^\dagger |\alpha\rangle = \frac{\partial}{\partial \alpha} |\alpha\rangle$$

$$\begin{aligned} \hookrightarrow a^\dagger g &= \int d^2\alpha \left( \frac{\partial}{\partial \alpha} |\alpha\rangle \right) \langle \alpha | e^{-|\alpha|^2} P(\alpha, \alpha^*) \\ &\quad \text{not a function of } \alpha \text{ (but } \alpha^*) \\ &= - \int d^2\alpha |\alpha\rangle \langle \alpha | \left( \frac{\partial}{\partial \alpha} e^{-|\alpha|^2} P(\alpha, \alpha^*) \right) \\ &\quad + \underbrace{\langle \alpha | \alpha | e^{-|\alpha|^2} P(\alpha, \alpha^*) \rangle}_{-\infty} \Big|_{-\infty} \\ &\quad \text{is assumed to vanish} \\ &= - \int d^2\alpha |\alpha\rangle \langle \alpha | e^{-|\alpha|^2} \left( \frac{\partial}{\partial \alpha} - \alpha^* \right) P(\alpha, \alpha^*) \end{aligned}$$

we thus obtain the correspondence

$$a^\dagger g \leftrightarrow \left( \alpha^* - \frac{\partial}{\partial \alpha} \right) P(\alpha, \alpha^*)$$

$$ga \leftrightarrow \left( \alpha - \frac{\partial}{\partial \alpha^*} \right) P(\alpha, \alpha^*)$$

for the Q-function one obtains instead, using  $\frac{1}{\pi} \langle \alpha | a^\dagger g | \alpha \rangle = \alpha^* Q(\alpha, \alpha^*)$

$$a^\dagger g \leftrightarrow \alpha^* Q(\alpha, \alpha^*) , \quad ga \leftrightarrow \alpha Q(\alpha, \alpha^*) ,$$

and using

$$\begin{aligned} \langle \alpha | a^\dagger g | \alpha \rangle &= \langle \alpha | (a^\dagger g) |\alpha \rangle e^{-|\alpha|^2} = \left( \frac{\partial}{\partial \alpha^*} \langle \alpha | \right) g |\alpha\rangle e^{-|\alpha|^2} \\ &= \frac{\partial}{\partial \alpha^*} (\langle \alpha | g |\alpha \rangle e^{-|\alpha|^2}) + \alpha \langle \alpha | g |\alpha \rangle e^{-|\alpha|^2} \end{aligned}$$

one finds

$$ag \leftrightarrow \left( \alpha + \frac{\partial}{\partial \alpha^*} \right) Q(\alpha, \alpha^*) , \quad ga^\dagger \leftrightarrow \left( \alpha^* + \frac{\partial}{\partial \alpha} \right) Q(\alpha, \alpha^*)$$

(63)

for the Wigner function one finds

$$ag \leftrightarrow \left(\alpha + \frac{1}{2} \frac{\partial}{\partial \alpha^*}\right) W(\alpha, \alpha^*), \quad a^+g \leftrightarrow \left(\alpha^* - \frac{1}{2} \frac{\partial}{\partial \alpha}\right) W(\alpha, \alpha^*)$$

$$ga \leftrightarrow \left(\alpha - \frac{1}{2} \frac{\partial}{\partial \alpha^*}\right) W(\alpha, \alpha^*), \quad ga^+ \leftrightarrow \left(\alpha^* + \frac{1}{2} \frac{\partial}{\partial \alpha}\right) W(\alpha, \alpha^*)$$

let us now consider as an example the driven harmonic oscillator

$$H = H(a, a^+) = \omega \left( a a^+ + \frac{1}{2} \right) + \lambda a^+ + \lambda^* a$$

oscillator frequency      ↑      driving parameter

the von Neumann equation reads

$$i \frac{\partial g}{\partial t} = \omega [a a^+, g] + \lambda [a^+, g] + \lambda^* [a, g]$$

using the correspondence relations for the P-function one finds

$$\begin{aligned} i \frac{\partial P}{\partial t} &= \omega \left[ \left( \alpha^* - \frac{\partial}{\partial \alpha} \right) \alpha P - \left( \alpha - \frac{\partial}{\partial \alpha^*} \right) \alpha^* P \right] \\ &\quad + \lambda \left[ \left( \alpha^* - \frac{\partial}{\partial \alpha} \right) P - \alpha^* P \right] + \lambda^* \left[ \alpha - \left( \alpha - \frac{\partial}{\partial \alpha^*} \right) \right] P \end{aligned}$$

$$\hookrightarrow \frac{\partial P}{\partial t} = i \left[ \omega \left( \frac{\partial}{\partial \alpha} \alpha - \frac{\partial}{\partial \alpha^*} \alpha^* \right) + \lambda \frac{\partial}{\partial \alpha} - \lambda^* \frac{\partial}{\partial \alpha^*} \right] P$$

in the next step we change variables:

$$\begin{aligned} \alpha &= x + iy \\ \alpha^* &= x - iy \end{aligned} \quad \left\{ \rightarrow x = \frac{\alpha + \alpha^*}{2}, \quad y = \frac{\alpha - \alpha^*}{2i} \right. \quad \text{and} \quad \lambda = \mu + i\nu$$

using

$$\frac{\partial}{\partial x} = \frac{\partial x}{\partial x} \frac{\partial}{\partial x} + \frac{\partial y}{\partial x} \frac{\partial}{\partial y} = \frac{1}{2} \left( \frac{\partial}{\partial x} - i \frac{\partial}{\partial y} \right), \quad \frac{\partial}{\partial x^*} = \frac{1}{2} \left( \frac{\partial}{\partial x} + i \frac{\partial}{\partial y} \right)$$

then yields

$$\begin{aligned} \frac{\partial P}{\partial t} &= \frac{i}{2} \left[ \omega \left( \left( \frac{\partial}{\partial x} - i \frac{\partial}{\partial y} \right) (x+iy) - \left( \frac{\partial}{\partial x} + i \frac{\partial}{\partial y} \right) (x-iy) \right) \right. \\ &\quad \left. + (\mu + iv) \left( \frac{\partial}{\partial x} - i \frac{\partial}{\partial y} \right) - (\mu - iv) \left( \frac{\partial}{\partial x} + i \frac{\partial}{\partial y} \right) \right] P \\ &= \left[ \frac{\partial}{\partial y} (\omega x + \mu) - \frac{\partial}{\partial x} (\omega y + v) \right] P \end{aligned}$$

This partial differential equation can be solved by the 'method of characteristics', which we briefly summarise in the following

consider the partial differential equation for a function  $u(\vec{x})$ , with  $\vec{x}$  having  $N$  components

$$\sum_{i=1}^N a_i(\vec{x}, u) \frac{\partial u}{\partial x_i} = c(\vec{x}, u)$$

its solution can be found by parametrising

$$\vec{x} = \vec{x}(s), \quad u = u(\vec{x}(s), s)$$

and enforcing the ordinary differential equations

$$\underbrace{\frac{dx_i}{ds} = a_i(\vec{x}, u)}_{\text{ensures that}}$$

$$\text{and } \underbrace{\frac{du}{ds} = c(\vec{x}, u)}$$

ensures that

$$\sum_{i=1}^N \frac{dx_i}{ds} \frac{\partial u}{\partial x_i} = \frac{du}{ds}$$

expresses original partial differential in terms of total derivative with respect to  $s$

(65)

\* in our case, we have

$$-(\omega y + \nu) \frac{\partial}{\partial x} P(x,y,t) + (\omega x + \mu) \frac{\partial}{\partial y} P(x,y,t) - \frac{\partial}{\partial t} P(x,y,t) = 0$$

$$\hookrightarrow \frac{dx}{ds} = -(\omega y + \nu), \quad \frac{dy}{ds} = \omega x + \mu, \quad \frac{dt}{ds} = -1, \quad \frac{dP}{ds} = 0$$

\* we can choose  $s = -t$ , which yields

$$\frac{dx}{dt} = \omega y + \nu, \quad \frac{dy}{dt} = -(\omega x + \mu),$$

or, with  $\alpha = x + iy$

$$\frac{d\alpha}{dt} = \omega(y - ix) + \nu - i\mu = -i(\omega\alpha + \lambda)$$

\* the solution of this equation is

$$\begin{aligned} \alpha(t) &= \alpha(0) e^{-i\omega t} - i e^{-i\omega t} \int_0^t dt' e^{i\omega t'} \lambda(t') \\ &= \alpha(0) e^{-i\omega t} + \alpha_p(t) \end{aligned}$$

particular solution of  
inhomogeneous diff. equation

\* to determine  $P$ , we take into account that

$$\frac{dP}{dt} = 0, \text{ and hence } P(\alpha(t), t) = P(\alpha(0), 0)$$

$$\hookrightarrow P(\alpha(0), 0) = P((\alpha(t) - \alpha_p(t)) e^{i\omega t}, 0) = P(\alpha(t), t)$$

- let's consider a situation where the system is initially in a coherent state with amplitude  $\alpha(0)$  :

$$P(\alpha, 0) = \delta^{(2)}(\alpha - \alpha(0))$$

- using  $P(\alpha, +) = P((\alpha - \alpha_p(+)) e^{i\omega t}, 0)$  we then find

$$\begin{aligned} P(\alpha, +) &= \delta^{(2)}((\alpha - \alpha_p(+)) e^{i\omega t} - \alpha(0)) \\ &= \frac{1}{|e^{i\omega t}|} \delta^{(2)}(\alpha - \alpha(0) e^{-i\omega t} - \alpha_p(+)) \\ &= \delta^{(2)}(\alpha - [\alpha(0) e^{-i\omega t} + \alpha_p(+)]) \end{aligned}$$

↳ the state remains a coherent state

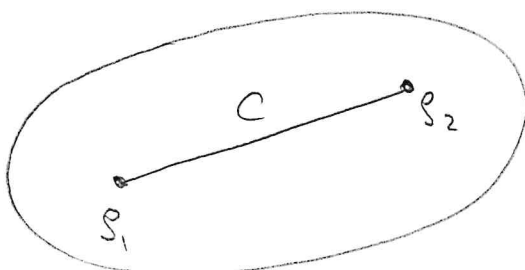
- if  $\lambda=0$  the coherent state rotates around the origin of the complex plane (phase space)
- changing  $\lambda$  allows to move the coherent state through phase space

(66)

## II. 6 Non-classicality of radiation fields

(67)

- definition: A radiation field is called "classical" if it can be described by a non-negative definite P-function no more singular than a  $\delta$ -function.
- it turns out that classical states form a convex set  $C$ : if  $\varrho_1, \varrho_2 \in C$ , then  $p\varrho_1 + (1-p)\varrho_2$  (with  $0 \leq p \leq 1$ )  $\in C$



- the extreme points of this set are the coherent states
- a measure for the "non-classical" character of a state  $\varrho$  is thus also given by its distance from  $C$ :

$$Q(\varrho) = \min_{\varrho_c \in C} \|\varrho - \varrho_c\|, \text{ with } \|\mathbf{A}\| = \text{tr}[(\mathbf{A}^\dagger \mathbf{A})^{1/2}]$$

- the properties of  $Q$  are
  - 1)  $Q(\bar{\varrho}_c) = 0$  for  $\bar{\varrho}_c \in C$
  - 2)  $Q(\varrho)$  is a convex function of  $\varrho$ , as any distance measure function on a convex set is a convex function

- the initial definition of classicality, i.e.

" $P(\alpha, \alpha^*) \geq 0$ " allows to derive a number of non-classicality conditions, which we discuss in the following

### Master parameter

$$Q_M = \frac{\underbrace{\langle (\hat{a}^\dagger \hat{a})^2 \rangle - \langle \hat{a}^\dagger \hat{a} \rangle^2}_{\text{variance of the photon number } n = \hat{a}^\dagger \hat{a} \text{ in a mode}}}{\underbrace{\langle \hat{a}^\dagger \hat{a} \rangle}_{\text{average photon number}}}$$

- using  $(\hat{a}^\dagger)^2 \hat{a}^2 = \hat{a}^\dagger (\hat{a} \hat{a}^\dagger) \hat{a} = (\hat{a}^\dagger \hat{a})^2 - \hat{a}^\dagger \hat{a}$  we can also write the normal ordered expression

$$\begin{aligned} Q_M &= \frac{\langle (\hat{a}^\dagger)^2 \hat{a}^2 \rangle - \langle \hat{a}^\dagger \hat{a} \rangle^2}{\langle \hat{a}^\dagger \hat{a} \rangle} \\ &= \frac{\langle \alpha^{*\dagger} \alpha^2 \rangle_p - \langle \alpha^{*\dagger} \alpha \rangle_p^2}{\langle \alpha^{*\dagger} \alpha \rangle_p} \quad \text{with } \langle \dots \rangle_p = \int d^2 \alpha P(\alpha, \alpha^*) \dots \end{aligned}$$

(if  $P$  is positive, then it can be interpreted as probability distrib.:  $\langle \alpha^{*\dagger} \alpha^2 \rangle_p - \langle \alpha^{*\dagger} \alpha \rangle_p^2$ )

↪ if  $P$  is a non-singular non-negative distribution then  $Q_M \geq 0$

↪ if  $Q_M < 0$ , then  $\alpha$  is non-classical

- for a coherent state  $|\alpha\rangle$  we found

$$\Delta n^2 = \langle (\hat{a}^\dagger \hat{a})^2 \rangle - \langle \hat{a}^\dagger \hat{a} \rangle^2 = |\alpha|^4, \quad \langle \hat{a}^\dagger \hat{a} \rangle = |\alpha|^2 \rightarrow Q_M = 0$$

- for a Fock state one instead obtains  $Q_M = -1$ , which is the lowest possible value  $Q_M$  can take

## Squeezing parameter

- we consider the generalised quadrature

$$X_\theta = \frac{a e^{-i\theta} + a^+ e^{i\theta}}{\sqrt{2}} \quad (X_{\theta=0} = X_1, \quad X_{\theta=\frac{\pi}{2}} = X_2)$$

- the squeezing parameter is then defined

as

$$\begin{aligned} S_\theta &= \underbrace{\langle : X_\theta^2 : \rangle}_{=} - \langle X_\theta \rangle^2 \\ &= \frac{1}{2} (a^2 e^{-i2\theta} + 2a^+ a + (a^+)^2 e^{-i2\theta}) \\ &= \langle X_\theta^2 \rangle - \langle X_\theta \rangle^2 - \frac{1}{2} \end{aligned}$$

- the minimum value  $S_\theta$  can assume is  $-\frac{1}{2}$
- for a positive definite P-function,  $P(\alpha, \alpha^*) \geq 0$ , we find

$$\begin{aligned} S_\theta &= \int d\alpha \left( \frac{\alpha e^{-i\theta} + \alpha^* e^{i\theta}}{\sqrt{2}} \right)^2 P(\alpha, \alpha^*) - \left( \int d\alpha P(\alpha, \alpha^*) \frac{\alpha e^{-i\theta} + \alpha^* e^{i\theta}}{\sqrt{2}} \right)^2 \\ &\geq 0 \end{aligned}$$

- if  $S_\theta < 0$  for any  $\theta$  is a signal for a state being non-classical
- note, that if  $P(\alpha, \alpha^*)$  does not exist in the sense that it is not a function no more singular than a  $\delta$ -distribution, this does not preclude the existence of  $S_\theta < 0$  (see later example of squeezed state)
- important:  $Q_\theta > 0$  and  $S_\theta > 0$  do not imply that a state is classical, i.e. these are only necessary criteria for classicality

## Necessary and sufficient criterion for classicality

- Bogoliubov's theorem: A continuous function  $\chi(\beta) = \int d\alpha^* P(\alpha, \alpha^*) e^{i\beta\alpha^* - \beta^*\alpha}$  with  $\chi(0)=1$  is a classical characteristic function, i.e. the Fourier transform of a genuine probability distribution  $P(\alpha, \alpha^*)$ , iff  $\chi(\beta)$  is positive semi-definite, i.e.

$$\sum_{ij=1}^n \underbrace{\chi(\beta_i - \beta_j)}_{C_{ij}} c_i^* c_j = \vec{c}^* C \vec{c} \geq 0,$$

for any set of complex numbers  $\{c_i\}$  and points  $\{\beta_i\}$ ,  $i=1, \dots, n$ .

This is the case iff all the following determinants are positive (or equal to zero) for all  $k$ : (Sylvester's criterion)

$$D^{(k)} = \begin{vmatrix} 1 & C_{12} & \dots & C_{1k} \\ C_{12}^* & 1 & \dots & C_{2k} \\ \vdots & \vdots & \ddots & \vdots \\ C_{1k}^* & C_{2k}^* & \dots & 1 \end{vmatrix}, \quad C_{ij} = \chi(\beta_i - \beta_j)$$

- The theorem leads to a whole hierarchy of non-classicality criteria: a quantum state is non-classical iff there exist values  $\beta_i$  ( $i=1 \dots k$ ) for which at least one of the determinants  $D^{(k)}$  ( $k=1, \dots, \infty$ ) is negative

## Bodmer's theorem:

$M(\theta)$  is a characteristic function (its Fourier transform is positive definite if

$$\int d\theta d\theta' M(\theta-\theta') \varphi(\theta) \varphi^*(\theta') \geq 0$$

$\varphi$  test function  
Fourier transform  
(shall be a positive function)

with  $M(\theta-\theta') = \int dx P(x) e^{i(\theta-\theta')x}$  one finds

$$\int d\theta d\theta' M(\theta-\theta') \varphi(\theta) \varphi(\theta') = \int d\theta d\theta' dx P(x) \varphi(\theta) \varphi^*(\theta') e^{i(\theta-\theta')x}$$

$$= \int dx P(x) \int d\theta \varphi(\theta) e^{i\theta} \int d\theta' \varphi^*(\theta') e^{-i\theta'}$$

$$= \int dx P(x) \underbrace{\left| \int d\theta \varphi(\theta) e^{i\theta} \right|^2}$$

positive if  $P(x)$  positive

## Sylvester's criterion

A  $n \times n$  Hermitian matrix  $M$  is positive if all the following matrices have a positive determinant:

upper left	$1 \times 1$	$n \times n$ corner of $M$	}
$\underline{\underline{M}}$	$\underline{\underline{M}}_{11}$	$\underline{\underline{M}}_{11 \dots 11}$	
$\underline{\underline{M}}$	$\underline{\underline{M}}_{11 \dots 11}$	$\underline{\underline{M}}_{11 \dots 11 \dots 11}$	

leading principal minors

$M$  itself

$$\hookrightarrow k=1 : \quad D^{(1)} = 1 > 0 \quad \text{always}$$

$$k=2 : \quad D^{(2)} \leq 0 \Leftrightarrow |C_{12}|^2 \geq 1$$

:

• Examples:

squeezed vacuum

- a squeezed state is created from a coherent state by applying the squeezing operator

$$S(\xi) = e^{\frac{1}{2}\xi^* a^2 - \frac{1}{2}\xi a^{*2}}, \quad \xi = r e^{i\theta}$$

$$\hookrightarrow |\alpha, \xi\rangle = S(\xi) \underbrace{D(\alpha)|0\rangle}_{\text{coherent state}} \xrightarrow{|\alpha|e^{i\theta}}$$

- This state has the following expectation values:

$$\langle a \rangle = \alpha \cosh(r) - \alpha^* e^{i\theta} \sinh(r)$$

$$\begin{aligned} \langle a^2 \rangle &= \langle (a^\dagger)^2 \rangle^* = \alpha^2 \cosh^2(r) + \alpha^{*2} e^{i2\theta} \sinh^2(r) \\ &\quad - 2|\alpha|^2 e^{i\theta} \sinh(r) \cosh(r) - e^{i\theta} \cosh(r) \sinh(r) \end{aligned}$$

$$\begin{aligned} \langle a^\dagger a \rangle &= |\alpha|^2 (\cosh^2(r) + \sinh^2(r)) - (\alpha^*)^2 e^{i\theta} \sinh(r) \cosh(r) \\ &\quad - \alpha^2 e^{i\theta} \sinh(r) \cosh(r) + \sinh^2(r) \end{aligned}$$

(72)

- to characterise the squeezed state we define the rotated quadrature operator  $Y_1 + i Y_2 = (X_1 + i X_2) e^{-i \frac{\theta}{2}}$

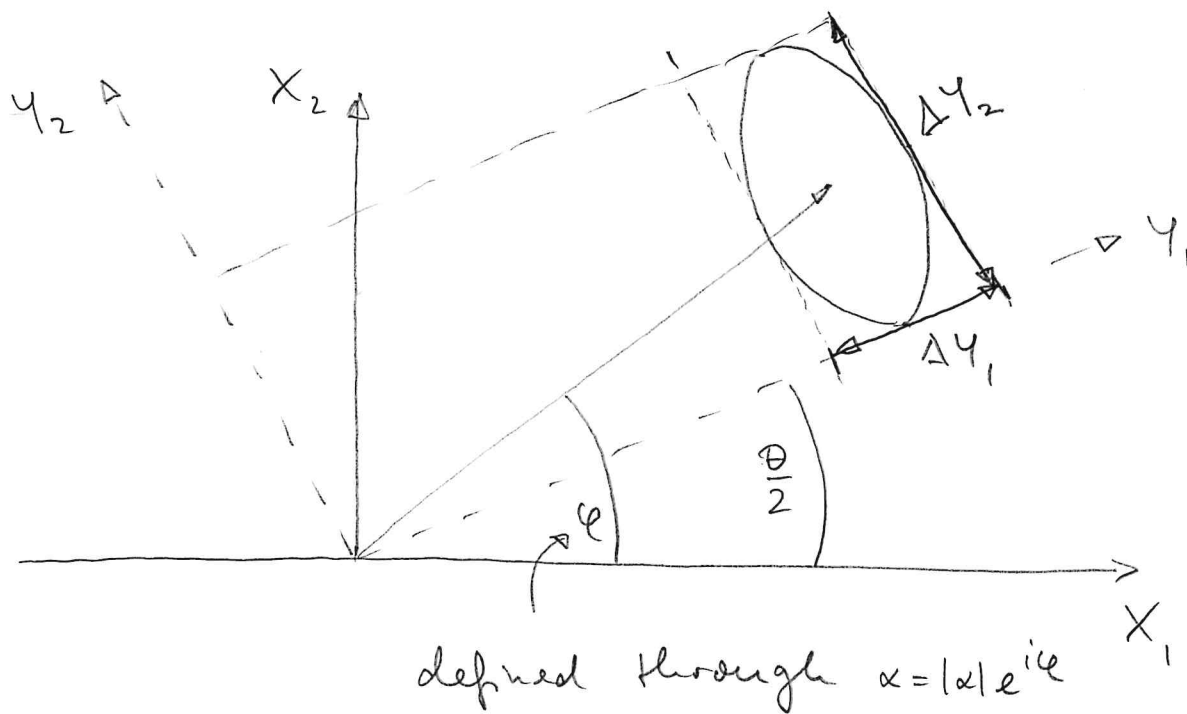
$$(\text{remember: } X_1 = \frac{1}{2}(a+a^\dagger), X_2 = \frac{1}{2i}(a-a^\dagger))$$

- we then find

$$\Delta Y_1^2 = \frac{1}{4} e^{-2\alpha}; \quad \Delta Y_2^2 = \frac{1}{4} e^{2\alpha}; \quad \Delta Y_1 \Delta Y_2 = \frac{1}{4}$$

$\uparrow$

squeezed direction  
of the state



- the uncertainty in  $Y_1$ -direction is reduced compared to the coherent state  
 ↳ "quantum noise" in this direction is smaller

for the squeezed vacuum state,  $S(\xi)|0\rangle$ , we (73) find in particular the following variances for the quadrature operator  $X_\Theta$ :

$$(\Delta X_{\frac{\Theta}{2}})^2 = \frac{1}{2} e^{2r}, \quad (\Delta X_{\frac{\Theta}{2} + \frac{\pi}{2}})^2 = \frac{1}{2} e^{-2r}$$

↑                              ↑  
note, that  $X_\Theta$  was defined with  
a ' $r_2$ ' and not a ' $z$ ' in the denominator

$$\hookrightarrow S_{\frac{\Theta}{2}} = \Delta X_{\frac{\Theta}{2}}^2 - \frac{1}{2} = \frac{1}{2}(e^{2r} - 1), \text{ but}$$

$$S_{\frac{\Theta}{2} + \frac{\pi}{2}} = \Delta X_{\frac{\Theta}{2} + \frac{\pi}{2}}^2 - \frac{1}{2} = \frac{1}{2}(e^{-2r} - 1) < 0 \quad \forall r > 0$$

↪ The squeezed vacuum state is non-classical!

This non-classicality is actually not detected by the Wigner function, which is a Gaussian:

$$W_\xi(x) = \frac{2}{\pi} \exp \left[ -2 |x \cosh(r) - \xi^* e^{i\theta} \sinh(r)|^2 \right],$$

and thus looks like a classical probability distribution

number states

- a number state satisfies  $a|n\rangle = n|n\rangle$
- for the Mandel parameter one thus finds

$$\Omega_n = \frac{\langle (a^\dagger a)^2 \rangle - \langle a^\dagger a \rangle^2 - \langle a^\dagger a \rangle}{\langle a^\dagger a \rangle} = \frac{n^2 - n^2 - n}{n} = -1$$

smallest possible value  $\downarrow$

- for the squeezing parameter one finds

$$\begin{aligned} S_\theta &= \langle (X_\theta)^2 \rangle - \langle X_\theta \rangle^2 - \frac{1}{2} \\ &= \frac{1}{2} \left[ \langle n | (a e^{i\theta} + a^\dagger e^{-i\theta})^2 | n \rangle - \underbrace{\langle n | a e^{-i\theta} + a^\dagger e^{i\theta} | n \rangle^2}_{0} - 1 \right] \\ &= \frac{1}{2} [\langle n | a a^\dagger + a^\dagger a | n \rangle - 1] = \frac{1}{2} [2n + 1 - 1] = n > 0 \end{aligned}$$

$\hookrightarrow S_\theta$  does not reveal non-classicality

Schrödinger cat state

$$|C\rangle = \frac{1}{N} (|\alpha\rangle + |-\alpha\rangle), \quad N = \sqrt{2(1 + e^{-2|\alpha|^2})}$$

$$X(\beta) = \text{tr}(g e^{\beta a^\dagger} e^{-\beta^* a}) = \frac{1}{N^2} (\langle \alpha | + \langle -\alpha |) e^{\beta a^\dagger} e^{-\beta^* a} (|\alpha\rangle + |-\alpha\rangle)$$

$$= \frac{1}{N^2} \left( e^{\beta a^\dagger - \beta^* \alpha} + e^{-\beta^* \alpha + \beta^* \alpha} + e^{\underbrace{\beta \alpha^* + \beta^* \alpha}_{e^{-2|\alpha|^2}} \langle \alpha | - \alpha \rangle} + e^{-\beta^* \alpha - \beta^* \alpha} \langle -\alpha | \alpha \rangle \right)$$

$$\left. \begin{array}{l} \alpha = \alpha_1 + i\alpha_2 \\ \beta = \beta_1 + i\beta_2 \end{array} \right\} = \frac{1}{N^2} \left( 2 \cos(2(\beta_1 \alpha_2 - \beta_2 \alpha_1)) + \left( e^{2(\beta_1 \alpha_1 + \beta_2 \alpha_2)} + e^{-2(\beta_1 \alpha_1 + \beta_2 \alpha_2)} \right) e^{-2|\alpha|^2} \right)$$

- for the sake of simplicity, we focus on real coherent state amplitudes:  $\alpha_2 = \beta_2 = 0$

$$\hookrightarrow \chi(\beta_1) = \frac{1 + \cosh(2\beta_1\alpha_1)e^{-2\alpha_1^2}}{1 + e^{-2\alpha_1^2}} > 1 \quad \forall \beta_1, \alpha_1 > 0$$

- non-classicality is revealed, since  $|C_{12}|^2 > 1$ , for all  $\alpha_1 \neq 0$

### photon added and subtracted states

- non-classical states can be obtained by adding or subtracting a photon to or from a state  $g$

photon  
subtracted :  $g^{(s)} = \frac{a g a^\dagger}{\langle a a^\dagger \rangle}$ , photon  
state added :  $g^{(a)} = \frac{a^\dagger g a}{\langle a a^\dagger \rangle}$

- photon subtraction cannot render a classical state into a non-classical state, since a positive P-function is converted into another positive P-function.

$$g^{(s)} = \int d^2\alpha \underbrace{\frac{|\alpha|^2 P(\alpha, \alpha^\dagger)}{\langle a a^\dagger \rangle}}_{|a \times a|} |a \times \alpha|$$

$P_s$  ... P-function of photon  
subtracted state

- photon subtraction can, however, enhance non-classicality

## ARTICLE

<https://doi.org/10.1038/s41467-021-24522-w>

OPEN

# Controlled multi-photon subtraction with cascaded Rydberg superatoms as single-photon absorbers

Nina Stiesdal<sup>1</sup>, Hannes Busche<sup>1</sup>, Kevin Kleinbeck<sup>2</sup>, Jan Kumlin<sup>1</sup>, Mikkel G. Hansen<sup>1</sup>, Hans Peter Büchler<sup>1,2</sup> & Sebastian Hofferberth<sup>1,3</sup>✉

The preparation of light pulses with well-defined quantum properties requires precise control at the individual photon level. Here, we demonstrate exact and controlled multi-photon subtraction from incoming light pulses. We employ a cascaded system of tightly confined cold atom ensembles with strong, collectively enhanced coupling of photons to Rydberg states. The excitation blockade resulting from interactions between Rydberg atoms limits photon absorption to one per ensemble and rapid dephasing of the collective excitation suppresses stimulated re-emission of the photon. We experimentally demonstrate subtraction with up to three absorbers. Furthermore, we present a thorough theoretical analysis of our scheme where we identify weak Raman decay of the long-lived Rydberg state as the main source of infidelity in the subtracted photon number and investigate the performance of the multi-photon subtractor for increasing absorber numbers in the presence of Raman decay.

<sup>1</sup>Department of Physics, Chemistry and Pharmacy, Physics@SDU, University of Southern Denmark, Odense, Denmark. <sup>2</sup>Institute for Theoretical Physics III and Center for Integrated Quantum Science and Technology, University of Stuttgart, Stuttgart, Germany. <sup>3</sup>Institut für Angewandte Physik, University of Bonn, Bonn, Germany. ✉email: hofferberth@sdu.dk

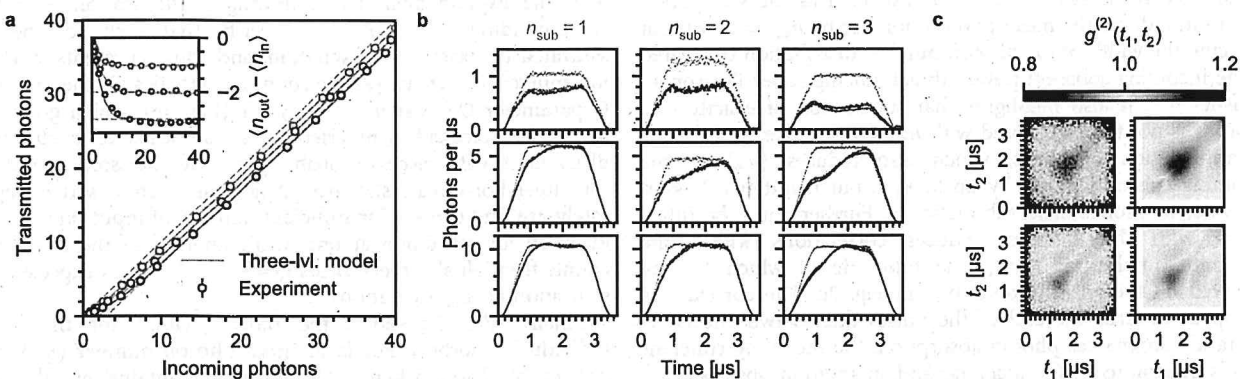


**Fig. 2 Effect of one, two and three single-photon absorbers on the probe transmission.** **a** Mean transmitted photons vs. mean incoming photon number. The inset shows the mean subtracted photons for the same data. All data are corrected for off-resonant absorption of the probe light and background counts. Error bars correspond to one standard error and are smaller than the markers for most data points. **b** Temporal profiles of probe light following transmission through  $n_{\text{sub}} = 1$  (left), 2 (centre) and 3 (right) absorbers for different mean photon numbers. The incoming pulses recorded in the absence of the superatom absorbers are shown in light grey. Besides the experimental data, we also show the results of the three-level model fitted to the experimental data (dark grey). **c**. Photon correlations following transmission through three superatom absorbers. Second-order correlation functions  $g^{(2)}(t_1, t_2)$  for  $R_{\text{in}} \approx 5.5 \mu\text{s}^{-1}$  (top) and  $10 \mu\text{s}^{-1}$  (bottom). Besides the experimental data (left), we also show the predictions of the three-level model (right).

at distances  $> 50 \mu\text{m} \gg r_B$  such that the superatoms do not blockade each other and act independently. We trap the ensembles at the foci of individual optical trapping beams that intersect perpendicularly with the probe and confine each ensemble within  $r_B$  along the probe axis. We use an acousto-optical deflector (AOD) to control the position and number of ensembles via the number and frequencies of radio-frequency (RF) signals applied<sup>40–42</sup>. A reservoir dipole trap (not shown in Fig. 1a) provides additional radial confinement ('Methods'). The ensembles have temperatures of  $\approx 10 \mu\text{K}$  with an extent  $< r_B$  along the probe axis and  $N \sim 10^4$  with exact numbers varying with  $n_{\text{sub}} = 3, 2, 1$ , respectively, due to variations in the trapping and cooling dynamics during ensemble preparation.

**Experimental results.** In the following, we experimentally demonstrate controlled subtraction of up to three photons by placing the corresponding number of absorbers  $n_{\text{sub}}$  in the probe path. We measure the transmission for coherent, Tukey-shaped probe pulses with a pulse length of  $\tau = 2.5 \mu\text{s}$  (FWHM, with  $1.0 \mu\text{s}$  rise/fall time) and  $\langle n_{\text{in}} \rangle \leq 40$ , where  $\langle n_{\text{in}} \rangle$  is the mean incoming photon number per pulse, using four single-photon counters in a Hanbury-Brown-Twiss configuration located behind a single-mode fibre. This configuration allows to analyse second-order photon correlations by calculating the correlation between all distinct pairs and averaging over the results. Without control field, we measure combined optical depths of the ensembles of  $\approx 11, 16$  and  $20$  for  $n_{\text{sub}} = 1, 2$  and  $3$  respectively, and find a probe transmission of  $> 0.99$  which is slightly reduced at finite  $\Delta/2\pi \approx 100 \text{ MHz}$  due to off-resonant scattering of the probe light and which the data below are corrected for.

First, we investigate the difference between  $\langle n_{\text{in}} \rangle$  and the mean transmitted photon number  $\langle n_{\text{out}} \rangle$  (Fig. 2a). For  $\langle n_{\text{in}} \rangle > 10$ , we observe the expected reduction by  $n_{\text{sub}}$ , while we subtract fewer photons for  $\langle n_{\text{in}} \rangle < 10$ . This behaviour is expected, as for low  $R_{\text{in}} \propto \langle n_{\text{in}} \rangle$ , the pulse area  $\sqrt{\kappa R_{\text{in}}} \tau$  is insufficient to drive the superatom population predominantly into  $|W\rangle$  and  $|D\rangle$ . This becomes particularly evident in the shape of the transmitted pulses for  $R_{\text{in}} \approx 1 \mu\text{s}^{-1}$  (top row in Fig. 2b) with transmission well below one at their end, whereas we observe the onset of saturation for  $R_{\text{in}} \approx 5 \mu\text{s}^{-1}$  (centre row). Importantly, the duration to reach saturation increases with  $n_{\text{sub}}$ , because the driving between  $|G\rangle$  and  $|W\rangle$  reduces alongside the probe intensity following each

absorber. For  $R_{\text{in}} \approx 10 \mu\text{s}^{-1}$  (bottom row), saturation sets in even faster, but we observe a slight oscillation in the subsequent transmission, which reflects the superatom dynamics as the probe drives Rabi oscillations between  $|G\rangle$  and  $|W\rangle$  with strong damping due to  $\gamma_D$ <sup>15</sup>. To suppress superradiant re-emission of absorbed photons in the forward direction after the probe pulse<sup>43,44</sup>,  $\gamma_D$  has to be sufficiently strong not only compared to  $1/\tau$ , but also compared to the coherent dynamics<sup>15,33</sup>. The dephasing is dominated by atomic motion, which is enhanced by the co-propagating probe and control beams compared to a counter-propagating configuration, with additional contributions from elastic scattering of the Rydberg electron by ground-state atoms<sup>45–47</sup> and the non-uniform AC-Stark shift induced by the trapping light ('Methods'), which can only be compensated for on average. To characterise the system, we determine  $\kappa$ ,  $\gamma_D$  and  $\Gamma$  by comparing the observed transmission to the predictions of a model of  $n_{\text{sub}}$  effective three-level atoms strongly coupled to a chiral waveguide ('Methods'), assuming that  $\kappa$ ,  $\gamma_D$  and  $\Gamma$  are equal for all absorbers. The results of the model are in good agreement with the experiment for both the subtracted photons (Fig. 2a) and pulse shape of the transmitted light (Fig. 2b) for  $\{\kappa, \Gamma, \gamma_D\} = \{0.49, 0.045, 2.3\} \mu\text{s}^{-1}$  for  $n_{\text{sub}} = 1$ ,  $\{0.33, 0.020, 3.2\} \mu\text{s}^{-1}$  for  $n_{\text{sub}} = 2$ , and  $\{0.35, 0.040, 2.4\} \mu\text{s}^{-1}$  for  $n_{\text{sub}} = 3$ .

A closer look at the number of subtracted photons (inset in Fig. 2a) reveals that it slightly exceeds  $n_{\text{sub}}$  at high  $\langle n_{\text{in}} \rangle$  indicating that a single absorber may subtract multiple photons. This excess cannot be explained by the deexcitation of the absorbers in the Rabi oscillation cycle as the associated spontaneous emission occurs back into the probe mode in forward direction with rate  $\kappa$ . Instead, it can be attributed to the small, but non-zero Raman decay  $0 < \Gamma < \kappa$ ,  $\gamma_D$ , which leads to spontaneous re-emission in random, rather than the forward direction. Its presence, even if weak, however, leads to reduced fidelity to subtract exactly one photon per absorber as we will discuss in detail in our theoretical analysis.

To further demonstrate manipulation of the quantum state of light at the single-photon level, we also investigate the effect of the subtraction on the correlations between transmitted photons. Figure 2c shows the second-order correlation function  $g^{(2)}(t_1, t_2) = \langle n(t_1)n(t_2) \rangle / (\langle n(t_1) \rangle \langle n(t_2) \rangle)$  for two of the transmitted pulses shown in Fig. 2b and  $n_{\text{sub}} = 3$  alongside the theory prediction for three cascaded three-level absorbers. Following initial antibunching, we observe  $g^{(2)}(t_2 - t_1 = 0) > 1$ , i.e. bunching of the

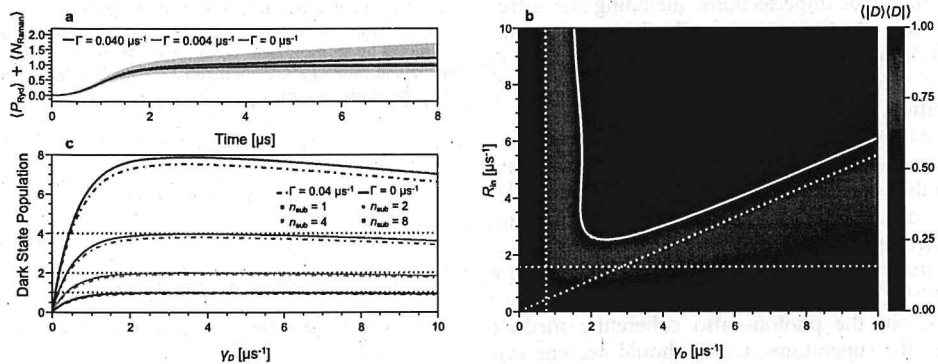


**Fig. 4 Theory prediction for the superatom dynamics.** All figures are at  $\kappa = 0.35 \mu\text{s}^{-1}$ . **a** Total number of subtracted photons vs. time, i.e. the sum of the dark-state population and Raman emitted photons, for a single superatom at  $R_{\text{in}} = 5 \text{ photons } \mu\text{s}^{-1}$  and dephasing rate  $\gamma_D = 2.4 \mu\text{s}^{-1}$ . Shaded regions indicate one standard deviation of the number of Raman emitted photons. **b** Dark-state population, here equal to the photon absorption probability, after driving a single superatom for  $\tau = 3 \mu\text{s}$  without Raman decay  $\Gamma = 0$ . The solid line indicates the 90% level. The dashed horizontal, vertical and diagonal lines correspond to  $\sqrt{\kappa R_{\text{in}}} \tau = \pi/2$ ,  $\exp(-\gamma_D \tau) = 0.1$  and  $\exp(-4\kappa R_{\text{in}} \tau / \gamma_D) = 0.1$ , respectively. **c** Mean dark-state population in a chain of 1, 2, 4 and 8 superatoms after driving the superatoms for  $\tau = 4 \mu\text{s}$  at a constant rate of  $R_{\text{in}} = 5 \text{ photons } \mu\text{s}^{-1}$ .

mean number of lost photons

$$\langle N_{\text{Raman}}(t) \rangle = \Gamma \int_{t_0}^t dt' P_{\text{Ryd}}(t'), \quad (1)$$

where  $P_{\text{Ryd}}(t)$  is the combined population of  $|W\rangle$  and  $|D\rangle$ . Figure 4a shows the total number of absorbed photons  $P_{\text{Ryd}}(t) + \langle N_{\text{Raman}}(t) \rangle$  together with one standard deviation  $\sqrt{\text{Var}(N_{\text{Raman}}(t))}$  ('Methods') for  $\Gamma = 0, 0.004$  and  $0.04 \mu\text{s}^{-1}$ , for a single superatom at constant driving. The fluctuations in photon absorption increase over time, highlighting that deterministic photon subtraction requires both low  $\Gamma$  and short duration  $\tau$ .

Consequently, we now analyse the dynamics of a single superatom at  $\tau = 3 \mu\text{s}$ , similar to the experiment. Figure 4b shows the population of  $|D\rangle$  vs.  $\gamma_D$  and  $R_{\text{in}}$  indicating a large parameter regime where photon absorption occurs with high probability. This regime is bounded by three processes with independent timescales, which we indicate by dashed lines. Firstly, the superatom is excited into  $|W\rangle$  with rate  $\sqrt{\kappa R_{\text{in}}}$  and the requirement  $\sqrt{\kappa R_{\text{in}}} \tau \gg 1$  gives a lower bound for the necessary photon rate. Similarly,  $|W\rangle$  decays into  $|D\rangle$  with rate  $\gamma_D$  and thus the dark state will only be populated for  $\gamma_D \tau \gg 1$ . However, at a large  $\gamma_D$ , the superatom dynamics enter an overdamped regime in which we can adiabatically eliminate  $|W\rangle$  ('Methods') and the effective absorption rate scales asymptotically as  $\gamma_{\text{eff}} \approx 4\kappa R_{\text{in}} / \gamma_D$ . Therefore, we also require  $\gamma_{\text{eff}} \tau \gg 1$ , limiting the maximal dephasing rate  $\gamma_D$ . This analysis is valid until we reach a large  $\sqrt{R_{\text{in}} \kappa \tau}$  where we expect that the blockade mechanism breaks down and the superatom starts to absorb more than one photon.

Lastly, we solve the master equation for a chain of up to  $n_{\text{sub}}$  driven superatoms. Figure 4c compares the total dark-state population for an ideal system with  $\Gamma = 0 \mu\text{s}^{-1}$  (solid lines) to  $\Gamma = 0.04 \mu\text{s}^{-1}$  (dashed lines) and shows the potential to extend our photon subtraction scheme up to  $n_{\text{sub}} = 8$ . In the simulation, we drive the superatoms with a mean number of 20 photons, which indicates that our set-up can work well even when the number of photons becomes comparable to  $n_{\text{sub}}$ . The dark-state population never reaches  $n_{\text{sub}}$  exactly, which is due to the short pulse duration  $\tau$  considered here and, by decreasing the Raman decay rate, higher absorption probabilities can be achieved.

## Discussion

The theoretical analysis of our experimental results reveals that the main contributions to imperfections in the subtracted photon

number are two-fold and are not necessarily unique to our scheme. First, a finite lifetime of the saturated state leads to excess absorption and the random nature of a decay process like Raman decay in our system introduces a probabilistic component into an initially deterministic scheme. This applies to any scheme which employs excited or metastable states and the severity of the impact depends on the decay strength compared to the absorber-photon coupling and the pulse duration. While the loss through Raman decay may initially seem as a disadvantage of our implementation, it should be noted that insertion loss into waveguides and cavities can lead to similar probabilistic fluctuations. Second, the slight deviation from  $n_{\text{sub}}$  for coherent input pulses of finite duration is more general and affects all subtraction schemes relying on irreversible transfer into a dark state or separate optical modes irrespective of the absorber nature, also including hybrid systems of waveguide- and cavity-coupled single quantum emitters<sup>14,56</sup>.

In our scheme, Raman decay could be further suppressed by reducing either  $\Omega_c$  or increasing  $\Delta$ , with the latter also reducing residual absorption on the probe transition. To compensate the associated reduction in  $\kappa$ , one can increase the number of atoms  $N$  per superatom via the ensemble density or increase the probe waist with  $r_B$  as upper constraint. Meanwhile, for increasing  $\kappa$  combined with fine-tuning of  $\gamma_D$ , the dark-state population converges towards  $n_{\text{sub}}$  shifting the curves in Fig. 4c upwards. In this context, performance limitations will ultimately occur for high  $R_{\text{in}}$  as power broadening causes a breakdown of the blockade.

While high-fidelity preparation of quantum states of light may require more substantial performance improvements, limitations are less stringent for other applications of our set-up. A more readily implementable application is number-resolved detection of up to  $n_{\text{sub}}$  photons based on the number of absorbers in a Rydberg state. Currently, performance would be limited by the low-efficiency  $\eta$  to detect the superatom state via field ionisation, but this could be significantly improved by replacing the MCP by another model or using optical detection<sup>57–59</sup>. By increasing  $n_{\text{sub}}$  well beyond the expected photon number, a weak photon-absorber coupling  $\kappa$  could also be compensated. Meanwhile, it is still important to minimise Raman decay as it reduces the detection efficiency for each absorber.

In summary, we have experimentally demonstrated controlled multi-photon subtraction from weak coherent probe pulses using a cascaded chain of saturable Rydberg superatom absorbers in free space. Our theoretical analysis has identified both technical

9. Ourjoumtsev, A., Tualle-Brouri, R., Laurat, J. & Grangier, P. Generating optical Schrödinger kittens for quantum information processing. *Science* **312**, 83–86 (2006).
10. Zavatta, A., Parigi, V., Kim, M. S. & Bellini, M. Subtracting photons from arbitrary light fields: experimental test of coherent state invariance by single-photon annihilation. *New J. Phys.* **10**, 123006 (2008).
11. Pinotsi, D. & Imamoglu, A. Single photon absorption by a single quantum emitter. *Phys. Rev. Lett.* **100**, 093603 (2008).
12. Hoi, I.-C. et al. Giant cross-Kerr effect for propagating microwaves induced by an artificial atom. *Phys. Rev. Lett.* **111**, 053601 (2013).
13. Gea-Banacloche, J. & Wilson, W. Photon subtraction and addition by a three-level atom in an optical cavity. *Phys. Rev. A* **88**, 033832 (2013).
14. Rosenblum, S. et al. Extraction of a single photon from an optical pulse. *Nat. Photon.* **10**, 19–22 (2016).
15. Paris-Mandoki, A. et al. Free-space quantum electrodynamics with a single Rydberg superatom. *Phys. Rev. X* **7**, 041010 (2017).
16. Saffman, M., Walker, T. G. & Mølmer, K. Quantum information with Rydberg atoms. *Rev. Mod. Phys.* **82**, 2313–2363 (2010).
17. Lukin, M. D. et al. Dipole blockade and quantum information processing in mesoscopic atomic ensembles. *Phys. Rev. Lett.* **87**, 037901 (2001).
18. Pritchard, J. D. et al. Cooperative atom-light interaction in a blockaded Rydberg ensemble. *Phys. Rev. Lett.* **105**, 193603 (2010).
19. Dudin, Y. O. & Kuzmich, A. Strongly interacting Rydberg excitations of a cold atomic gas. *Science* **336**, 887–889 (2012).
20. Peyronel, T. et al. Quantum nonlinear optics with single photons enabled by strongly interacting atoms. *Nature* **488**, 57–60 (2012).
21. Firstenberg, O., Adams, C. S. & Hofferberth, S. Nonlinear quantum optics mediated by Rydberg interactions. *J. Phys. B: At. Mol. Opt. Phys.* **49**, 152003 (2016).
22. Murray, C. & Pohl, T. Quantum and nonlinear optics in strongly interacting atomic ensembles. *Adv. At. Mol. Opt. Phys.* **65**, 321–372 (2016).
23. Ripka, F., Kübler, H., Löw, R. & Pfau, T. A room-temperature single-photon source based on strongly interacting Rydberg atoms. *Science* **362**, 446–449 (2018).
24. Ornelas-Huerta, D. P. et al. On-demand indistinguishable single photons from an efficient and pure source based on a Rydberg ensemble. *Optica* **7**, 813–819 (2020).
25. Gorniaczyk, H., Tresp, C., Schmidt, J., Fedder, H. & Hofferberth, S. Single-photon transistor mediated by interstate Rydberg interactions. *Phys. Rev. Lett.* **113**, 053601 (2014).
26. Tiarks, D., Baur, S., Schneider, K., Dürr, S. & Rempe, G. Single-photon transistor using a Förster resonance. *Phys. Rev. Lett.* **113**, 053602 (2014).
27. Gorshkov, A. V., Nath, R. & Pohl, T. Dissipative many-body quantum optics in Rydberg media. *Phys. Rev. Lett.* **110**, 153601 (2013).
28. Murray, C. R. et al. Photon subtraction by many-body decoherence. *Phys. Rev. Lett.* **120**, 113601 (2018).
29. Tiarks, D., Schmidt-Eberle, S., Stolz, T., Rempe, G. & Dürr, S. A photon-photon quantum gate based on Rydberg interactions. *Nat. Phys.* **15**, 124–126 (2019).
30. Thompson, J. D. et al. Symmetry-protected collisions between strongly interacting photons. *Nature* **542**, 206–209 (2016).
31. Busche, H. et al. Contactless nonlinear optics mediated by long-range Rydberg interactions. *Nat. Phys.* **13**, 655–658 (2017).
32. Distante, E. et al. Storing single photons emitted by a quantum memory on a highly excited Rydberg state. *Nat. Commun.* **8**, 14072 (2017).
33. Honer, J., Löw, R., Weimer, H., Pfau, T. & Büchler, H. P. Artificial atoms can do more than atoms: deterministic single photon subtraction from arbitrary light fields. *Phys. Rev. Lett.* **107**, 093601 (2011).
34. Tresp, C. et al. Single-photon absorber based on strongly interacting Rydberg atoms. *Phys. Rev. Lett.* **117**, 223001 (2016).
35. Dudin, Y. O., Li, L., Bariani, F. & Kuzmich, A. Observation of coherent many-body rabi oscillations. *Nat. Phys.* **8**, 790 (2012).
36. Ebert, M. et al. Atomic Fock state preparation using Rydberg blockade. *Phys. Rev. Lett.* **112**, 043602 (2014).
37. Weber, T. M. et al. Mesoscopic Rydberg-blockaded ensembles in the superatom regime and beyond. *Nat. Phys.* **11**, 157–161 (2015).
38. Zeiher, J. et al. Microscopic characterization of scalable coherent Rydberg superatoms. *Phys. Rev. X* **5**, 031015 (2015).
39. Kumlin, J., Hofferberth, S. & Büchler, H. P. Emergent universal dynamics for an atomic cloud coupled to an optical waveguide. *Phys. Rev. Lett.* **121**, 013601 (2018).
40. Roberts, K. O. et al. Steerable optical tweezers for ultracold atom studies. *Opt. Lett.* **39**, 2012–2015 (2014).
41. Barredo, D., de Léséleuc, S., Lienhard, V., Lahaye, T. & Browaeys, A. An atom-by-atom assembler of defect-free arbitrary two-dimensional atomic arrays. *Science* **354**, 1021–1023 (2016).
42. Endres, M. et al. Atom-by-atom assembly of defect-free one-dimensional cold atom arrays. *Science* **354**, 1024–1027 (2016).
43. Möhl, C. et al. Photon correlation transients in a weakly blockaded Rydberg ensemble. *J. Phys. B: At. Mol. Opt. Phys.* **53**, 084005 (2020).
44. Stiesdal, N. et al. Observation of collective decay dynamics of a single Rydberg superatom. *Phys. Rev. Res.* **2**, 043339 (2020).
45. Baur, S., Tiarks, D., Rempe, G. & Dürr, S. Single-photon switch based on Rydberg blockade. *Phys. Rev. Lett.* **112**, 073901 (2014).
46. Gaj, A. et al. From molecular spectra to a density shift in dense Rydberg gases. *Nat. Commun.* **5**, 4546 (2014).
47. Mirgorodskiy, I. et al. Electromagnetically induced transparency of ultra-long-range Rydberg molecules. *Phys. Rev. A* **96**, 011402 (2017).
48. Stiesdal, N. et al. Observation of three-body correlations for photons coupled to a Rydberg superatom. *Phys. Rev. Lett.* **121**, 103601 (2018).
49. Barnett, S. M., Ferenczi, G., Gilson, C. R. & Speirs, F. C. Statistics of photon-subtracted and photon-added states. *Phys. Rev. A* **98**, 013809 (2018).
50. Ates, C., Lesanovsky, I., Adams, C. S. & Weatherill, K. J. Fast and quasideterministic single ion source from a dipole-blockaded atomic ensemble. *Phys. Rev. Lett.* **110**, 213003 (2013).
51. Derevianko, A., Kómár, P., Topcu, T., Kroese, R. M. & Lukin, M. D. Effects of molecular resonances on Rydberg blockade. *Phys. Rev. A* **92**, 063419 (2015).
52. Ates, C., Pohl, T., Pattard, T. & Rost, J. M. Antiblockade in Rydberg excitation of an ultracold lattice gas. *Phys. Rev. Lett.* **98**, 023002 (2007).
53. Amthor, T., Giese, C., Hoffmann, C. S. & Weidemüller, M. Evidence of antiblockade in an ultracold Rydberg gas. *Phys. Rev. Lett.* **104**, 013001 (2010).
54. Pichler, H., Ramos, T., Daley, A. J. & Zoller, P. Quantum optics of chiral spin networks. *Phys. Rev. A* **91**, 042116 (2015).
55. Krämer, S., Plankensteiner, D., Ostermann, L. & Ritsch, H. QuantumOptics.jl: a Julia framework for simulating open quantum systems. *Comput. Phys. Commun.* **227**, 109–116 (2018).
56. Du, J., Li, W. & Bajcsy, M. Deterministic single-photon subtraction based on a coupled single quantum dot-cavity system. *Opt. Express* **28**, 6835–6845 (2020).
57. Olmos, B., Li, W., Hofferberth, S. & Lesanovsky, I. Amplifying single impurities immersed in a gas of ultracold atoms. *Phys. Rev. A* **84**, 041607 (2011).
58. Günter, G. et al. Interaction enhanced imaging of individual Rydberg atoms in dense gases. *Phys. Rev. Lett.* **108**, 013002 (2012).
59. Günter, G. et al. Observing the dynamics of dipole-mediated energy transport by interaction-enhanced imaging. *Science* **342**, 954–956 (2013).
60. Mahmoodian, S. et al. Strongly correlated photon transport in waveguide quantum electrodynamics with weakly coupled emitters. *Phys. Rev. Lett.* **121**, 143601 (2018).
61. Prasad, A. S. et al. Correlating photons using the collective nonlinear response of atoms weakly coupled to an optical mode. *Nat. Photon.* **14**, 719–722 (2020).

## Acknowledgements

This work has received funding from the European Union's Horizon 2020 programme under the ERC consolidator grants SIRPOL (grant no. 681208) and RYD-QNLO (grant no. 771417), the ErBeStA project (grant no. 800942), and under grant agreement no. 845218 (Marie Skłodowska-Curie Individual Fellowship to H.B.), the Deutsche Forschungsgemeinschaft (DFG) under SPP 1929 GiRyd project BU 2247/4-1, and the Carlsberg Foundation through the Semper Ardens Research Project QCool.

## Author contributions

N.S., H.B., M.G.H. and S.H. performed the experimental work, K.K., J.K. and H.P.B. conducted the theoretical analysis. All authors contributed to data analysis, discussion of the results, and the preparation of the manuscript.

## Funding

Open Access funding enabled and organized by Projekt DEAL.

## Competing interests

The authors declare no competing interests.

## Additional information

**Supplementary information** The online version contains supplementary material available at <https://doi.org/10.1038/s41467-021-24522-w>.

**Correspondence** and requests for materials should be addressed to S.H.

**Peer review information** *Nature Communications* thanks Gerard Higgins and the other, anonymous, reviewer(s) for their contribution to the peer review of this work. Peer review reports are available.

**Reprints and permission information** is available at <http://www.nature.com/reprints>

**Publisher's note** Springer Nature remains neutral with regard to jurisdictional claims in published maps and institutional affiliations.

- on the other hand, photon addition, can create non-classical states from classical ones

$$\hookrightarrow P^{(a)}(\alpha, \alpha^*) = \underbrace{\frac{1}{\langle aa^* \rangle}}_{\text{P-function after photon addition}} \left( \alpha^* - \frac{\partial}{\partial \alpha} \right) \left( \alpha - \frac{\partial}{\partial \alpha^*} \right) \underbrace{P(\alpha, \alpha^*)}_{\text{original P-function}}$$

- for a thermal state, one has, for instance, the P-function  $P_{th}(\alpha, \alpha^*) = \frac{1}{\pi \langle n \rangle} e^{-|\alpha|^2 / \langle n \rangle}$ , which upon photon addition becomes

$$P_{th}^{(a)} = \underbrace{\frac{(1 + \langle n \rangle)^2}{\langle n \rangle^2} \left[ |\alpha|^2 - \frac{\langle n \rangle}{1 - \langle n \rangle} \right]}_{\text{becomes smaller than zero}} P_{th}(\alpha, \alpha^*), \text{ for } \langle n \rangle \neq 0$$

- all photon added thermal states are non classical

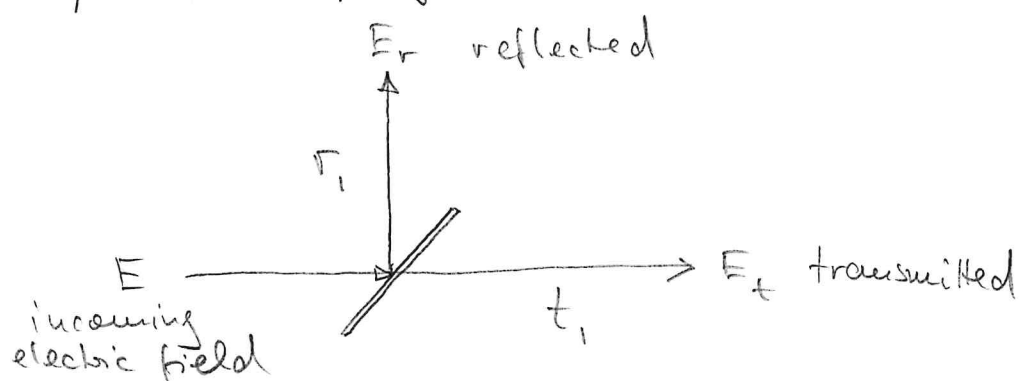
### III Quantum measurements of the electromag. field (77)

- our goal is to develop protocols, which allow the experimental measurement of electromagnetic field expectation values, e.g.  $\langle \vec{E} \rangle$ , their fluctuations,  $\Delta \vec{E}$
- we are also interested in measurements which allow to determine the non-classicality of a state and/or enable us to perform a full tomography of  $\rho$

#### III.1 Beam splitter physics

classical

beam splitter

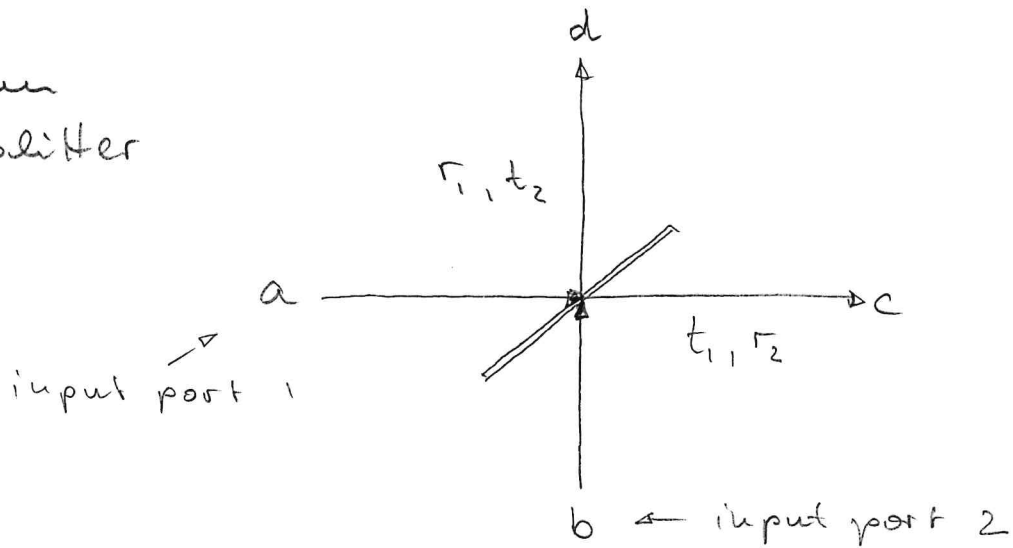


- with the transmission / reflection coefficient,  $t_i / r_i$  one can calculate the transmitted / reflected electric field amplitude

$$\text{transmitted: } E_t = t_i E$$

$$\text{reflected: } E_r = r_i E$$

quantum  
beam splitter



- the electromagnetic field is represented through creation and annihilation operators  
(we consider in the following their "positive frequency part" described via annihilation operators)
- unlike in the classical case, one always needs to consider 2 input ports (through one input port the vacuum state may enter)  
input modes:  $a, b \rightarrow$  output modes:  $c, d$
- the annihilation operators of the input and output are connected via

$$\begin{pmatrix} c \\ d \end{pmatrix} = \begin{pmatrix} t_1 & r_2 \\ r_1 & t_2 \end{pmatrix} \begin{pmatrix} a \\ b \end{pmatrix} = U \begin{pmatrix} a \\ b \end{pmatrix}$$

- when  $U$  is a unitary matrix, the output, just like the input operators obey canonical commutation relations

- for example:  $c = t_1 a + r_2 b$

$$\hookrightarrow [c, c^+] = [t_1 a + r_2 b, t_1^* a^+ + r_2^* b^+] \\ = |t_1|^2 [a, a^+] + |r_2|^2 [b, b^+] = |t_1|^2 + |r_2|^2 \stackrel{!}{=} 1$$

- likewise, one obtains  $t_1^* r_2 + r_2^* t_2 = 0$   
(this allows to show that  $U U^\dagger = \mathbb{1}$ )
- there are a number of convenient parametrisations of the beam splitter unitary:

- for  $|t_1| = |t_2| = |\cos \theta|$  and  $|r_1| = |r_2| = |\sin \theta|$  one has

$$U = \begin{pmatrix} \cos \theta & e^{i\varphi} \sin \theta \\ -e^{-i\varphi} \sin \theta & \cos \theta \end{pmatrix}$$

- for  $t_1 = t_2$  and  $r_1 = r_2$  one has to require, that  $e^{i\varphi} = -e^{-i\varphi} \Leftrightarrow \cos \varphi = 0 \rightarrow \varphi = \frac{\pi}{2}$ , which yields the so-called symmetric beam splitter

$$U = \begin{pmatrix} \cos \theta & i \sin \theta \\ i \sin \theta & \cos \theta \end{pmatrix}$$

- a 50-50 beam splitter one obtains for  $\theta = \frac{\pi}{4}$  and  $\varphi = \frac{\pi}{2}$ :

$$U = \frac{1}{\sqrt{2}} \begin{pmatrix} 1 & i \\ i & 1 \end{pmatrix}$$

$$e^{-i\theta(a^+L + b^+a)} \underset{a \in \mathbb{C}}{=} e^{i\theta(a^+b + b^+a)} =$$

$$= a + \underbrace{[-i\theta(a^+b + b^+a), a]}_{i\theta b} + \frac{1}{2} \underbrace{[-i\theta(a^+b + b^+a), i\theta b]}_{-\theta^2 a}$$

$$+ \frac{1}{3!} \underbrace{[-i\theta(a^+b + b^+a), -\theta^2 a]}_{-i\theta^3 b}$$

$$= a - \underbrace{\frac{\theta^2}{2} a}_{a \cos \theta} + \dots + \underbrace{i \left( \theta b - \frac{1}{3!} \theta^3 b^+ \right)}_{+ i b \sin \theta}$$

- the unitary, which describes the action of a beam splitter can be obtained from the Hamiltonian  $H = -(a^+b + b^+a)$

$$\hookrightarrow U(\theta) = e^{-i\theta H} = e^{i\theta(a^+b + b^+a)}, \text{ which yields}$$

$$c = a(\theta) = U^+(\theta)aU(\theta) = a \cos \theta + ib \sin \theta$$

$$d = b(\theta) = U^+(\theta)bU(\theta) = b \cos \theta + ia \sin \theta$$

- instead of studying the beam formation of operators, one can also apply the beam splitter operator to states

$$\underbrace{S_{\text{out}}}_{\text{output}} = \underbrace{U(\theta)}_{\text{input}} \circ U^+(\theta)$$

- lets consider an input which consists of two coherent states,  $|\alpha, \beta\rangle$

$$\begin{aligned} |\alpha, \beta\rangle_{\text{out}} &= U(\theta)|\alpha, \beta\rangle = U(\theta) \underbrace{e^{\alpha a^+ - \alpha^* a + \beta b^+ - \beta^* b}}_{\text{displaced vacuum at both input ports}} |q_0\rangle \\ &= U(\theta) e^{\dots} U^+(\theta) U(\theta) |0, 0\rangle \\ &= U(\theta) \left( \sum_{n=0}^{\infty} \frac{1}{n!} (\alpha a^+ - \beta b^+)^n \right) U^+(\theta) U(\theta) |0, 0\rangle \\ &= \sum_{n=0}^{\infty} \frac{1}{n!} [U(\theta)(\alpha a^+ - \beta b^+) U^+(\theta)]^n U(\theta) |0, 0\rangle \end{aligned}$$

$$\hookrightarrow |\alpha, \beta\rangle_{\text{out}} = \exp \left[ a^*(-\theta) \alpha - a(\theta) \alpha^* + b^*(-\theta) \beta - b(\theta) \beta^* \right] \underbrace{U(\theta)}_{|0,0\rangle} |0,0\rangle$$

using  $c = a(\theta) = a \cos \theta + i b \sin \theta$   
 $d = b(\theta) = b \cos \theta + i a \sin \theta$

and regrouping the coefficients in the exponent yields

$$|\alpha, \beta\rangle_{\text{out}} = \exp [a^* \alpha(\theta) - a \alpha^*(\theta) + b^* \beta(\theta) - b \beta^*(\theta)] |0,0\rangle$$

$$= |\alpha(\theta), \beta(\theta)\rangle, \text{ with } \begin{pmatrix} \alpha(\theta) \\ \beta(\theta) \end{pmatrix} = U \begin{pmatrix} \alpha \\ \beta \end{pmatrix}$$

- coherent states remain coherent states under the beam splitter operation and the coherent state amplitudes of the input and output are related by the classical relations
- in general, a density matrix  $\rho(a, b)$ , written in terms of the operators  $a$  and  $b$ , transforms under a beam splitter operation according to

$$\begin{aligned} \rho_{\text{out}} &= U(\theta) \rho(a, b) U^*(\theta) = \rho(U(\theta)a U^*(\theta), U(\theta)b U^*(\theta)) \\ &= \rho(a(\theta), b(\theta)) \end{aligned}$$

(82)

- lets consider in the following the formation of photon number states of the form  $|n, m\rangle$
  - the total number of photons is conserved by the beam splitter Hamiltonian:
- $$[H, \underbrace{a^\dagger a + b^\dagger b}_{\text{photon number at input port}}] \propto [a^\dagger b + a b^\dagger, a^\dagger a + b^\dagger b] = 0$$
- the output state must thus be of the form  $\sum_{p=0}^{n+m} f_p \underbrace{|p, n+m-p\rangle}_{\text{Fock states with total photon number } n+m}$
  - the amplitudes  $f_p$  are obtained via

$$\begin{aligned}
 |n, m\rangle_{\text{out}} &= U(\theta) |n, m\rangle = U(\theta) \frac{(a^\dagger)^n (b^\dagger)^m}{\sqrt{n! m!}} |0, 0\rangle = \frac{(a^\dagger(-\theta))^n (b^\dagger(-\theta))^m}{\sqrt{n! m!}} |0, 0\rangle \\
 &= \frac{(\cos \theta a^\dagger + i \sin \theta b^\dagger)^n (\cos \theta b^\dagger + i \sin \theta a^\dagger)^m}{\sqrt{n! m!}} |0, 0\rangle \\
 &= \sum_{q=0}^n \sum_{q'=0}^m \binom{n}{q} \binom{m}{q'} \frac{1}{\sqrt{n! m!}} (\cos \theta)^{n+q-q'} (\sin \theta)^{n-q+q'} (a^\dagger)^{q+q'} (b^\dagger)^{n+q-(q+q')} |0, 0\rangle \\
 &= \sum_{q, q'} \binom{n}{q} \binom{m}{q'} \sqrt{\frac{(q+q')! (n+m-q-q')!}{n! m!}} (\cos \theta)^{n+q-q'} (\sin \theta)^{n-q+q'} |q+q', n+m-q-q'\rangle
 \end{aligned}$$

- this state has indeed the anticipated form when identifying:  $p = q+q'$  and  $\sum_p = \sum_{q, q'}$

- for a single photon state, one finds

$$|1,0\rangle_{\text{out}} = \cos \theta |1,0\rangle + i \sin \theta |0,1\rangle$$

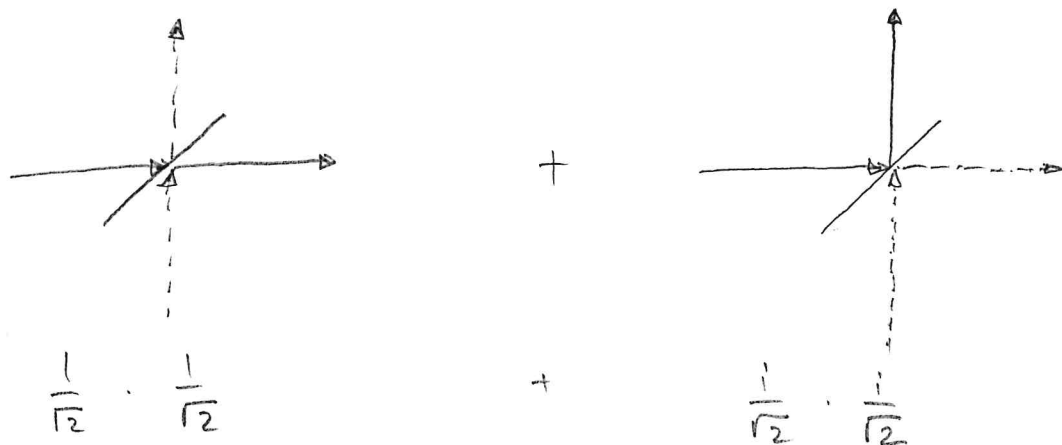
↳ a single photon (at input a) arrives "either" at output port c "or" d (note, that this is a superposition state)

- for two input photons in the state  $|1,1\rangle$  one obtains

$$|1,1\rangle_{\text{out}} = (\cos^2 \theta - \sin^2 \theta) |1,1\rangle + \sqrt{2} i \sin \theta \cos \theta (|2,0\rangle + |0,2\rangle)$$

apparently, a 50-50 beam splitter ( $\theta = \frac{\pi}{4}$ ) leads to a cancellation of the  $|1,1\rangle$ -amplitude  
 ↳ either both photons are found at port c or port d

- this is the so-called Hong-Ou-Mandel effect
- it is a consequence of destructive interference between two probability amplitudes that yield the state  $|1,1\rangle$  at the output



## Measurement of Subpicosecond Time Intervals between Two Photons by Interference

C. K. Hong, Z. Y. Ou, and L. Mandel

*Department of Physics and Astronomy, University of Rochester, Rochester, New York 14627*

(Received 10 July 1987)

A fourth-order interference technique has been used to measure the time intervals between two photons, and by implication the length of the photon wave packet, produced in the process of parametric down-conversion. The width of the time-interval distribution, which is largely determined by an interference filter, is found to be about 100 fs, with an accuracy that could, in principle, be less than 1 fs.

PACS numbers: 42.50.Bs, 42.65.Re

The usual way to determine the duration of a short pulse of light is to superpose two similar pulses and to measure the overlap with a device having a nonlinear response.<sup>1</sup> The latter might, for example, make use of the process of harmonic generation in a nonlinear medium. Indeed, such a technique was recently used<sup>2</sup> to determine the coherence length of the light generated in the process of parametric down-conversion.<sup>3</sup> The coherence time was found to be of subpicosecond duration, as predicted theoretically.<sup>4</sup> It is, however, in the nature of the technique that it requires very intense light pulses and would be of no use for the measurement of single photons. On the other hand, if we are dealing with two photons and wish to determine the time interval between them, which has a dispersion governed by the length of the photon wave packet, we are usually limited by the resolving time of the photodetector to intervals of order 100 ps or longer.<sup>5</sup>

We wish to report an experiment in which the time interval between signal and idler photons, and by implication the length of a subpicosecond photon wave packet, produced in parametric down-conversion was measured. The technique is based on the interference of two two-photon probability amplitudes in two-photon detection, and is easily able to measure a time interval of 50 fs, with an accuracy that could be 1 fs or better.

An outline of the experiment is shown in Fig. 1. A coherent beam of light of frequency  $\omega_0$  from an argon-ion laser oscillating on the 351.1-nm line falls on an 8-cm-long nonlinear crystal of potassium dihydrogen phosphate, where some of the incident photons split into two lower-frequency signal and idler photons of frequencies  $\omega_1$  and  $\omega_2$ , such that

$$\omega_0 = \omega_1 + \omega_2. \quad (1)$$

The two signal and idler photons are directed by mirrors M1 and M2 to pass through a beam splitter BS as shown, and the superposed beams interfere and are detected by photodetectors D1 and D2. We measure the rate at which photons are detected in coincidence, when the beam splitter is displaced from its symmetry position by various small distances  $\pm c\delta\tau$ . It should be em-

phasized that the signal and idler photons have no definite phase, and are therefore mutually incoherent, in the sense that they exhibit no second-order interference when brought together at detector D1 or D2. However, fourth-order interference effects occur, as demonstrated by the coincidence counting rate between D1 and D2.<sup>6-8</sup> The experiment has some similarities to another, recently reported, two-photon interference experiment in which fringes were observed and measured, but without the use of a beam splitter.<sup>6</sup>

Although the sum frequency  $\omega_1 + \omega_2$  is very well defined in the experiment, the individual down-shifted frequencies  $\omega_1, \omega_2$  have large uncertainties, that, in practice, are largely determined by the pass bands of the interference filters IF inserted in the down-shifted beams, as shown in Fig. 1. These pass bands are of order  $5 \times 10^{12}$  Hz, corresponding to a coherence time for each photon of order 100 fs. Needless to say, the two-photon probability amplitudes at the detectors D1, D2 are expected to interfere only if they overlap to this accuracy or better. We start by examining how this interference arises.

Let us label the field modes on the input sides of the beam splitter by 01,02 and on the output sides by 1,2 and suppose first that the light is monochromatic. If we take the state at the input resulting from one degenerate down-conversion to be the two-photon Fock state  $|1_{01}, 1_{02}\rangle$ , then one can show from general arguments<sup>7</sup> that the state on the output side of the beam splitter is

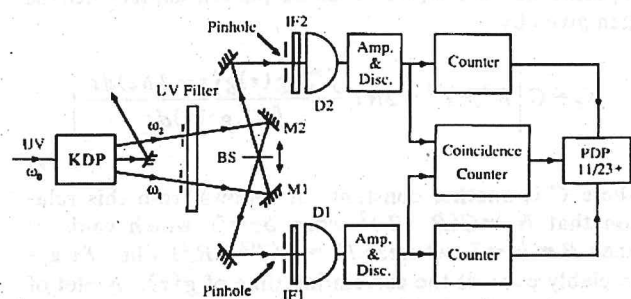


FIG. 1. Outline of the experimental setup.

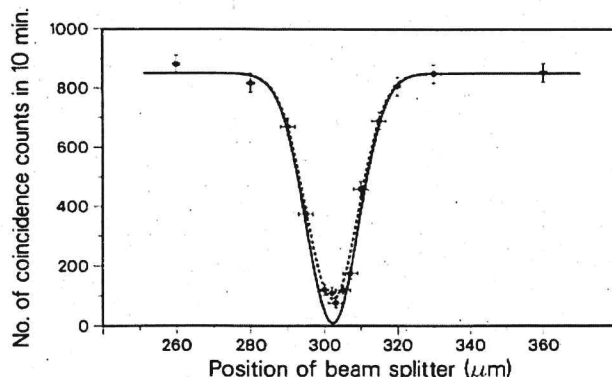


FIG. 2. The measured number of coincidences as a function of beam-splitter displacement  $c\delta\tau$ , superimposed on the solid theoretical curve derived from Eq. (11) with  $R/T=0.95$ ,  $\Delta\omega=3\times 10^{13}$  rad s $^{-1}$ . For the dashed curve the factor  $2RT/(R^2+T^2)$  in Eq. (11) was multiplied by 0.9 to allow for less than perfect overlap of the signal and idler photons. It will be seen that, except for the minimum, Eq. (11) is obeyed quite well, corresponding to a coherence time of about 100 fs.

time spread of the photoelectric pulses and the slewing of the discriminator pulses, a range of time intervals centered on zero delay was obtained with a spread of several nanoseconds. For the purpose of the measurement, pulse pairs received within a 7.5-ns interval were treated as "coincident." Pulse pairs received within an interval of 35 to 80 ns were regarded as accidentals, and when scaled by the factor 7.5/45 provided a measure of the number of accidental coincidences that occur within any 7.5-ns interval.

The results of the experiment are presented in Fig. 2, which is a plot of the number of observed photon coincidences, after subtraction of accidentals, as a function of the displacement of the beam splitter. It will be seen that for a certain symmetric position of the beam splitter, the two-photon coincidence rate falls to a few percent of its value in the wings, by virtue of the destructive interference of the two two-photon probability amplitudes. The width of the dip in the coincidence rate provides a measure of the length of the photon wave packet. It is found to be about 16  $\mu\text{m}$  at half height, corresponding to a time of about 50 fs, which should really be doubled to allow for the greater movement of the mirror image. This time is about what is expected from the passband of the interference filters.

Direct measurements of the beam-splitter reflectivity

and transmissivity show that  $R/T \approx 0.95$ , which makes the combination  $2RT/(R^2+T^2) \approx 0.999$ , and implies that  $N_c$  should fall close to zero when  $\delta\tau=0$ . That it does not fall quite that far is probably due to a slight lack of overlap of the signal and idler fields admitted by the two pinholes, causing less than perfect destructive interference. The solid curve in Fig. 2 is based on Eq. (11) with  $R/T=0.95$  and  $\Delta\omega=3\times 10^{13}$  rad/s  $\approx 5\times 10^{12}$  Hz, if we identify  $c\delta\tau$  with the beam-splitter displacement ( $x=302.5$ ) in micrometers. For the dashed curve the factor  $2RT/(R^2+T^2)$  in Eq. (11) was multiplied by 0.9 to allow for less than perfect overlap of the signal and idler photons. It will be seen that, except for the minimum, Eq. (11) is obeyed quite well, corresponding to a coherence time of about 100 fs.

We have therefore succeeded in measuring subpicosecond time intervals between two photons, and by implication the length of the photon wave packet, by a fourth-order interference technique. Unlike second-order interference, this method does not require that path differences be kept constant to within a fraction of a wavelength. The method is applicable to other situations in which pairs of single photons are produced, but becomes less efficient for more intense pulses of light, because the "visibility" of the interference is then reduced and cannot exceed 50% at high intensities.<sup>6</sup> In principle, the resolution could be better than 1  $\mu\text{m}$  in length or 1 fs in time.

This work was supported by the National Science Foundation and by the U.S. Office of Naval Research.

<sup>1</sup>See, for example, E. P. Ippen and C. V. Shank, in *Ultrashort Light Pulses*, edited by S. L. Shapiro (Springer-Verlag, Berlin, 1984), 2nd ed., p. 83.

<sup>2</sup>I. Abram, R. K. Raj, J. L. Oudar, and G. Dolique, Phys. Rev. Lett. **57**, 2516 (1986).

<sup>3</sup>D. C. Burnham and D. L. Weinberg, Phys. Rev. Lett. **25**, 84 (1970).

<sup>4</sup>C. K. Hong and L. Mandel, Phys. Rev. A **31**, 2409 (1985).

<sup>5</sup>S. Friberg, C. K. Hong, and L. Mandel, Phys. Rev. Lett. **54**, 2011 (1985).

<sup>6</sup>R. Ghosh and L. Mandel, Phys. Rev. Lett. **59**, 1903 (1987).

<sup>7</sup>Z. Y. Ou, C. K. Hong, and L. Mandel, to be published.

<sup>8</sup>R. Ghosh, C. K. Hong, Z. Y. Ou, and L. Mandel, Phys. Rev. A **34**, 3962 (1986).

<sup>9</sup>R. J. Glauber, Phys. Rev. **130**, 2529 (1963), and **131**, 2766 (1963).

## III.2 Measurement of the Wigner function

(84)

- in the following we will discuss so-called homodyne detection, which is a method to measure quadratures represented by

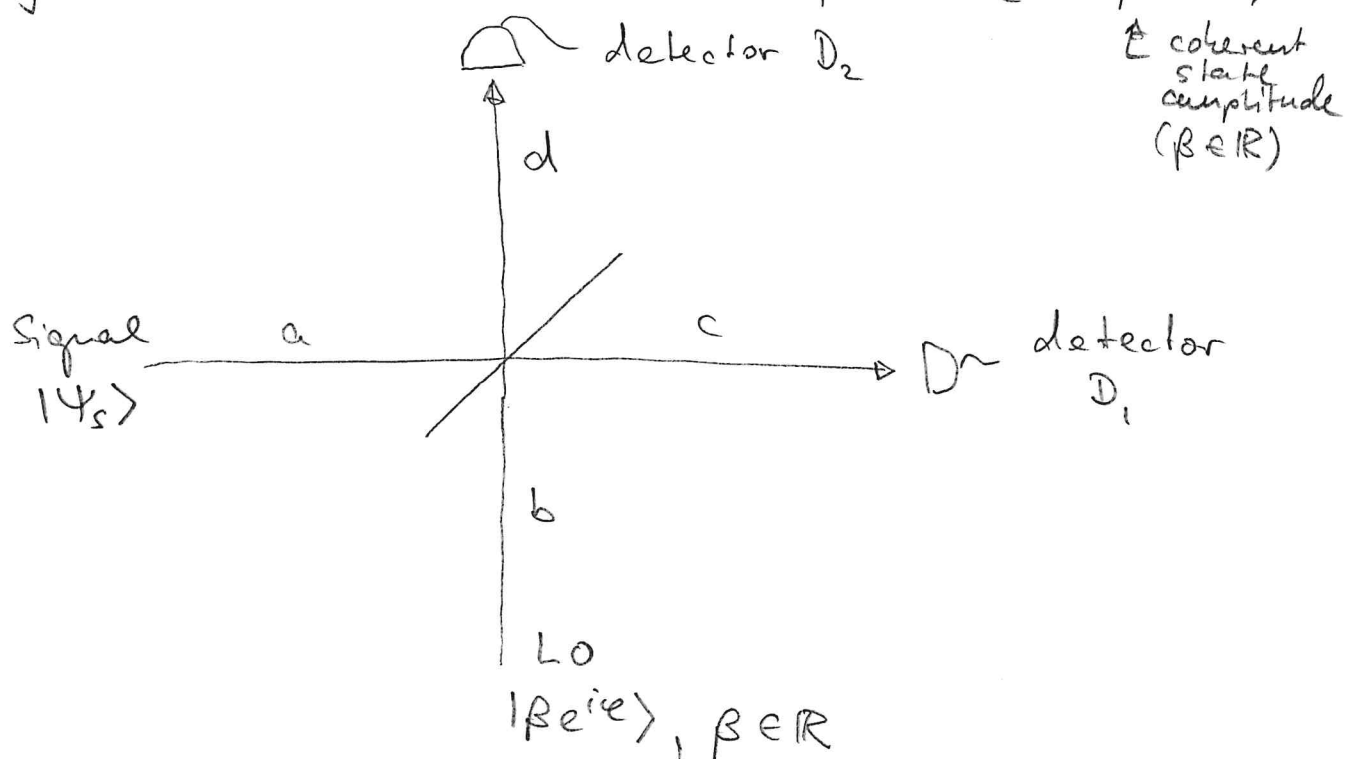
$$X(\varphi) = \frac{1}{2} (\alpha e^{-i\varphi} + \alpha^* e^{i\varphi})$$

not the operator,  
but value one  
is measuring

- the probability distribution  $P(X(\varphi))$  allows to reconstruct the Wigner function

- we consider a setting, where we feed into one input port of a beam splitter the signal state, whose Wigner function shall be determined

- into the other port we send the field of a local oscillator (LO) which is represented by a coherent state with phase  $\varphi$ :  $|\beta e^{i\varphi}\rangle$



(85)

the beam splitter mixes the input modes in the following way (standard homodyne detection):

$$c = \sqrt{T}a + i\sqrt{1-T}b \quad T \dots \text{transmittivity}$$

$$d = i\sqrt{1-T}a + \sqrt{T}b$$

- at the output ports we measure the intensity (proportional to the expectation value of the photon number) using the detectors  $D_1$  and  $D_2$

photons  
number  
of output  
modes

$$\left\{ \begin{array}{l} c^+c = T a^+a + (1-T)b^+b + i\sqrt{T(1-T)}(a^+b - b^+a) \\ d^+d = (1-T)a^+a + T b^+b - i\sqrt{T(1-T)}(a^+b - b^+a) \end{array} \right.$$

- calculating the expectation value of  $c^+c$  with the initial state  $|4\rangle_s \otimes |\beta e^{ie}\rangle_{\text{mode } a} \otimes |\beta e^{-ie}\rangle_{\text{mode } b}$  yields

$$\begin{aligned} \langle c^+c \rangle &= \langle 4 | c^+c | 4 \rangle = T \langle a^+a \rangle + (1-T) \langle b^+b \rangle \\ &\quad + i\sqrt{T(1-T)} (\langle a^+ \rangle \langle \beta e^{ie} | b | \beta e^{ie} \rangle - \text{c.c.}) \\ &= T \langle a^+a \rangle + (1-T) \beta^2 + i\sqrt{T(1-T)} \beta (\langle a^+ e^{ie} - a^- e^{-ie} \rangle) \\ &= T \langle a^+a \rangle + (1-T) \beta^2 + 2\sqrt{T(1-T)} \beta \langle X(\varphi + \frac{\pi}{2}) \rangle \end{aligned}$$

- if we now consider a parameter regime, where  $T \gg R = (1-T)$ , i.e. large transmittivity, and  $(1-T)\beta^2 \gg T \langle a^+a \rangle$ , i.e. a strong local oscillator, one has

$$\langle X(\varphi + \frac{\pi}{2}) \rangle = \frac{\langle c^+c \rangle - (1-T)\beta^2}{2\sqrt{T(1-T)}\beta}$$

- under the same assumptions also the operator identity is valid:

$$X(\varphi + \frac{\pi}{2}) |4\rangle = \frac{c^+ c - (1-T)\beta^2}{2 \sqrt{T(1-T)} \beta} |4\rangle$$

- this allows to access the statistics of measurements of  $X(\varphi + \frac{\pi}{2})$  through measuring the statistics of  $c^+ c$
- one is thus able to obtain  $P(X(\varphi))$
- somewhat more elegant expressions are obtained when considering balanced homodyne detection, which entails setting  $T = \frac{1}{2}$
- in this case one obtains

$$c^+ c - d^+ d = i(a^+ b - b^+ a)$$

and hence

$$\langle X(\varphi + \frac{\pi}{2}) \rangle = \frac{\langle c^+ c \rangle - \langle d^+ d \rangle}{2\beta}$$

- ↳ the quadrature  $X(\varphi + \frac{\pi}{2})$  and its distribution can be measured by measuring the photon count difference of the detectors  $D_1$  and  $D_2$

# Measurement of the quantum states of squeezed light

G. Breitenbach, S. Schiller & J. Mlynek

Fakultät für Physik, Universität Konstanz, D-78457 Konstanz, Germany

A state of a quantum-mechanical system is completely described by a density matrix or a phase-space distribution such as the Wigner function. The complete family of squeezed states of light (states that have less uncertainty in one observable than does the vacuum state) have been generated using an optical parametric amplifier, and their density matrices and Wigner functions have been reconstructed from measurements of the quantum statistics of their electric fields.

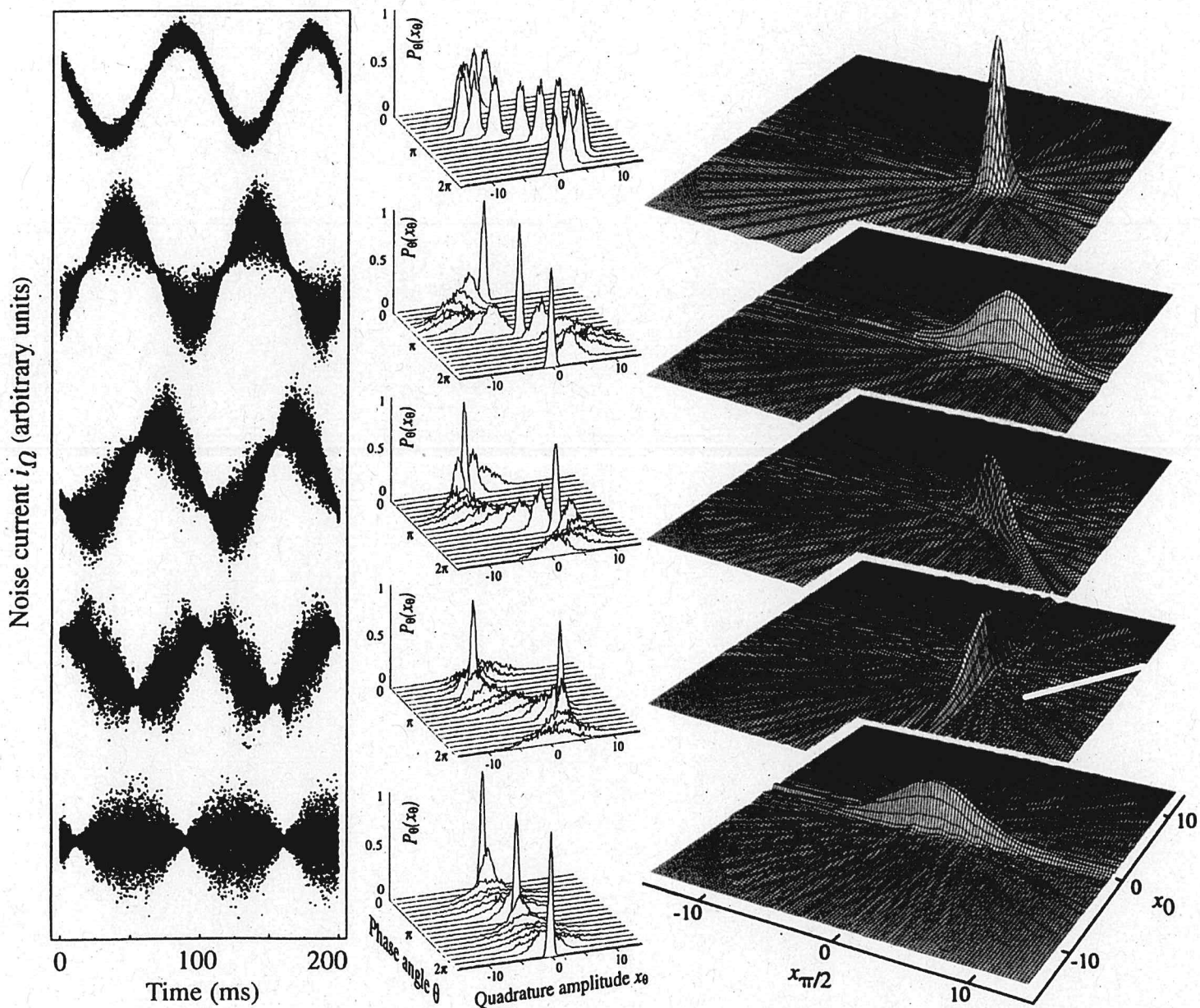


**Figure 2** Noise traces in  $i_D(t)$  (left), quadrature distributions  $P_\theta(x_0)$  (centre), and reconstructed Wigner functions (right) of generated quantum states. From the top: Coherent state, phase-squeezed state, state squeezed in the  $\phi = 48^\circ$ -quadrature, amplitude-squeezed state, squeezed vacuum state. The noise traces as a function of time show the electric fields' oscillation in a  $4\pi$  interval for the upper

four states, whereas for the squeezed vacuum (belonging to a different set of measurements) a  $3\pi$  interval is shown. The quadrature distributions (centre) can be interpreted as the time evolution of wave packets (position probability densities) during one oscillation period. For the reconstruction of the quantum states a  $\pi$  interval suffices.

# Measurement of the quantum states of squeezed light

G. Breitenbach, S. Schiller & J. Mlynek

Fakultät für Physik, Universität Konstanz, D-78457 Konstanz, Germany

**A state of a quantum-mechanical system is completely described by a density matrix or a phase-space distribution such as the Wigner function. The complete family of squeezed states of light (states that have less uncertainty in one observable than does the vacuum state) have been generated using an optical parametric amplifier, and their density matrices and Wigner functions have been reconstructed from measurements of the quantum statistics of their electric fields.**

A central theme in many fields of quantum physics is the development and application of theoretical and experimental tools for obtaining information about the states of quantum fields of matter and radiation. Although the state of an individual particle or system is unobservable, it is possible to determine the state of an ensemble of identically prepared systems by performing a large number of measurements<sup>1</sup>. Notable experimental success has recently been achieved in generating and determining states of various quantum-mechanical systems, employing newly developed methods of quantum state reconstruction (QSR)<sup>2-9</sup>. A single mode of light<sup>10-14</sup>, vibrational modes of a diatomic molecule<sup>15</sup> and of an ion in a Paul trap<sup>16</sup>, and the motional state of freely propagating atoms<sup>17</sup> have been characterized completely by determining their density matrix or, equivalently, their Wigner functions, a quantum-mechanical analogue of the classical phase-space distribution<sup>18</sup>.

A single spatial monochromatic mode of light represents a harmonic oscillator system for which non-classical states can be generated very efficiently using the interaction of laser light with nonlinear optical media. Squeezed states<sup>19</sup>, first generated about ten years ago<sup>20,21</sup>, have a reduced uncertainty in a specific quadrature (for example the amplitude quadrature) compared to that of the vacuum state. They have typically been characterized by measuring the variances of the electric field with a homodyne detector. A complete investigation of their quantum features, in particular their photon statistics (which at present cannot be measured directly owing to technical limitations of available photon counters) has only become possible through the recent development of theoretical tools for QSR. First experimental investigations analysed coherent and squeezed vacuum states<sup>10,11,13,14</sup>. Here we present a study of all types of squeezed states of light; squeezed vacuum, amplitude-squeezed states, phase-squeezed states and states squeezed in an arbitrary quadrature. For each of these states we construct 'portraits' in terms of both the Wigner functions (which are two-dimensional maps in appropriate phase-space coordinates) and the density matrices. These portraits contain all that one can know about the quantum-mechanical properties of the squeezed optical states.

## Optical homodyne tomography

How is the quantum state of an optical wave determined? The measurements to be performed on the state are measurements of the electric field operator  $E(\theta) \propto X_\theta = X \cos \theta + Y \sin \theta$  at all phase angles  $\theta$ . Here  $X = (a + a^\dagger)/\sqrt{2}$ ,  $Y = (a - a^\dagger)/\sqrt{2}i$  are the non-commuting quadrature operators of the electric field, with  $a$  and  $a^\dagger$  being the annihilation and creation operators.  $X$  and  $Y$  are analogous to position and momentum operators of a particle in a harmonic potential. To access experimentally the electric field, which oscillates with a frequency of  $\omega/2\pi$  of hundreds of THz, a balanced homodyne detector<sup>22</sup> is employed (see Fig. 1). In this

detector, the signal wave is spatially overlapped at a beamsplitter with a local-oscillator wave of the same frequency. The two fields emerging from the beamsplitter are proportional to the sum and the difference of the signal and local-oscillator fields. By detecting the difference of their fluxes, the natural oscillation of the signal state under investigation is converted to a low-frequency electrical signal  $i_\theta$ , which measures  $X_\theta$ , where  $\theta$  is the relative phase between signal and local oscillator. A large number of measurements of the observable  $X_\theta$  yields the probability distribution  $P_\theta(x_\theta)$  of its eigenvalues  $x_\theta$ . This procedure is repeated for a set of different phase angles  $\theta \in [0, \pi]$ .

The relation between the measured distributions and the density operator  $\rho$  is  $P_\theta(x_\theta) = \langle x | U^\dagger(\theta)\rho U(\theta) | x \rangle$ , where  $U(\theta) = \exp(-i\theta a^\dagger a)$  performs a rotation in phase space. As the optical state evolves freely with  $\omega$ ,  $U$  is equivalent to the time evolution operator with  $\theta = \omega t + \text{constant}$ , and the  $\theta$ -dependence of  $P_\theta$  is equivalent to the time dependence of the position probability density of the state (that is, of  $|\psi(x, t)|^2$ , if  $\rho = |\psi\rangle\langle\psi|$  is a pure state). Thus, homodyne detection maps out the time evolution of a harmonic oscillator state. Our measurements (shown below) may be regarded as an implementation of the oldest example of quantum dynamics, the motion of a wavepacket in a harmonic potential studied by Schrödinger in 1926<sup>23</sup>.

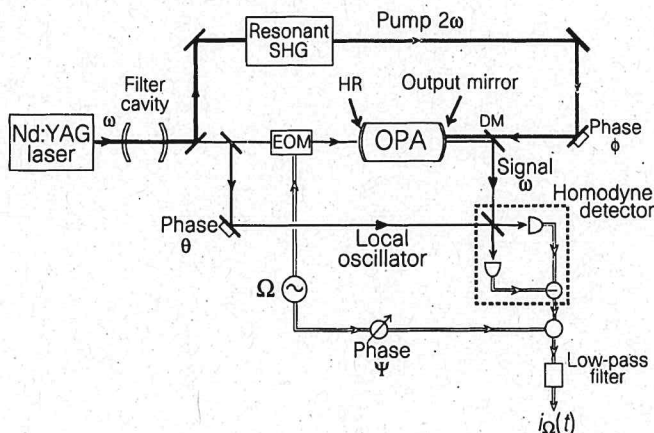


**Figure 1** Experimental scheme for generating bright squeezed light and squeezed vacuum with an optical parametric oscillator (OPA). The electric field quadratures are measured in the homodyne detector while scanning the phase  $\theta$ . A computer performs the statistical analysis of the photocurrent  $i_\theta$  and reconstructs the quantum states. EOM, electro-optic modulator; DM, dichroic mirror; SHG, second harmonic generator; HR, high reflector.

Of the various methods that have been proposed to reconstruct the quantum state numerically from the set of measured distributions  $P_\theta$ , two are employed here. The first method makes use of the fact that the distributions  $P_\theta(x_\theta)$  are the marginals of the Wigner function  $W(x, y)$  in rotated coordinates;

$$P_\theta(x_\theta) = \int_{-\infty}^{\infty} W(x_\theta \cos \theta - y_\theta \sin \theta, x_\theta \sin \theta + y_\theta \cos \theta) dy_\theta \quad (1)$$

where  $y_\theta = -x \sin \theta + y \cos \theta$ . Therefore  $W(x, y)$  can be obtained from the set  $P_\theta$  by back-projection via the inverse Radon transform<sup>2</sup>. The second method furnishes the elements of the density matrix in the Fock basis via integration of the distributions  $P_\theta$  over a set of pattern functions<sup>3,4</sup>. In contrast to the inverse Radon transform, this procedure does not involve any filtering of the experimental data and also allows an estimation of the propagation of statistical errors.

### The experiment

The experimental set-up is shown in Fig. 1. Central to the experiment is a monolithic standing-wave lithium-niobate optical

parametric oscillator (OPA)<sup>13,24</sup>, pumped by a frequency-doubled continuous-wave Nd:YAG laser (1,064 nm). The infrared laser wave is filtered by a high-finesse mode-cleaning cavity, which transmits 75% of the laser power. Its narrow linewidth of 170 kHz suppresses the high-frequency technical noise of the laser, yielding a shot-noise-limited local oscillator for light powers in the milliwatt range at frequencies  $\geq 1$  MHz (ref. 13). The pump wave  $2\omega$  (power  $\sim 20$ –30 mW) for the OPA is generated by resonant second harmonic generation.

In the past OPAs have been frequently used as sources of non-classical light<sup>10,13,25–28</sup>. Operated below threshold, the OPA is a source of squeezed vacuum. We studied the field's spectral components around a frequency offset by  $\Omega/2\pi = 1.5$  or 2.5 MHz from the optical frequency  $\omega$ , to avoid low-frequency laser excess noise. To generate bright light (that is, with non-vanishing average electric field at the frequencies  $\omega \pm \Omega$ ), we employ the OPA in a dual port configuration<sup>24</sup>. A very weak wave split off the main laser beam is phase-modulated by an electro-optic modulator (EOM) at the frequency  $\Omega$  (modulation index  $\beta \ll 1$ ) and injected into the

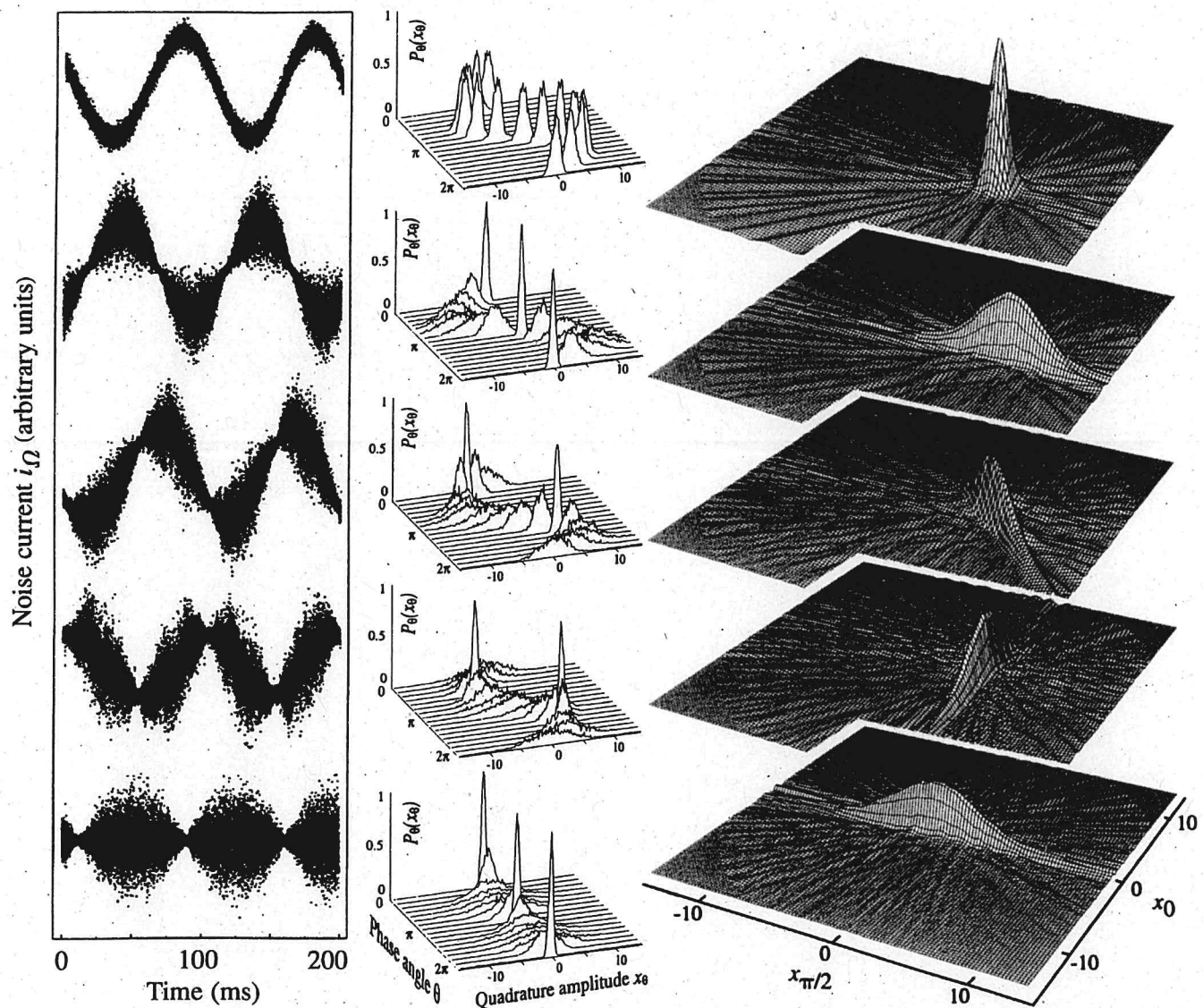


**Figure 2** Noise traces in  $i_\Omega(t)$  (left), quadrature distributions  $P_\theta(x_\theta)$  (centre), and reconstructed Wigner functions (right) of generated quantum states. From the top: Coherent state, phase-squeezed state, state squeezed in the  $\phi = 48^\circ$ -quadrature, amplitude-squeezed state, squeezed vacuum state. The noise traces as a function of time show the electric fields' oscillation in a  $4\pi$  interval for the upper

four states, whereas for the squeezed vacuum (belonging to a different set of measurements) a  $3\pi$  interval is shown. The quadrature distributions (centre) can be interpreted as the time evolution of wave packets (position probability densities) during one oscillation period. For the reconstruction of the quantum states a  $\pi$  interval suffices.

OPA through its high reflector (HR) port. The carrier frequency  $\omega$  is kept on-resonance with the cavity and the two 'bright' sidebands  $\omega \pm \Omega$  are well within the cavity bandwidth  $\Gamma/2\pi = 17$  MHz (HWHM). In the semiclassical picture we may write the Fourier components at the frequency  $\Omega'$  of the field's quadratures emitted from the output mirror as  $X(\Omega') = E_0(\Omega') + \beta E_0(\delta(\Omega' - \Omega) - \delta(\Omega' + \Omega)) + X_n(\Omega')$ ,  $Y(\Omega') = Y_n(\Omega')$ , where  $\delta$  is the Dirac delta-function,  $E_0$  is the amplitude of the emitted wave and  $X_n$ ,  $Y_n$  are the broad-band quantum fluctuations<sup>29</sup>. Due to the very small ratio of HR transmission (<0.1%) to output mirror transmission (2.1%), the transmitted sidebands and their quantum fluctuations are strongly attenuated. The quantum fluctuations of the signal wave inside the resonator originate essentially from the vacuum fluctuations entering through the output coupler. The injected seed-wave amplitude as well as the fluctuations are modified inside the resonator by the interaction with the  $2\omega$  pump wave: the quadrature fluctuations out-of-phase with the pump are deamplified (squeezed), the in-phase quadrature fluctuations are amplified. Similarly, the seed wave is deamplified if it is out of phase, and amplified if it is in phase, with the pump wave. As the relative phase  $\phi$  between seed wave and pump wave is controlled manually by a mirror attached to a piezoelectric actuator, deamplified amplitude-

squeezed light, amplified phase-squeezed light and light squeezed in an arbitrary quadrature are easily generated. The coherent excitation of the sidebands is controlled coarsely by changing the power of the seed wave (the photon flux of the carrier  $E_0$  at the OPA output port is about  $6 \times 10^8$  photons  $s^{-1} = 120$  pW), fine control is achieved by varying the modulation strength of the EOM. By turning the modulation off, we obtain squeezed vacuum, which has been described in detail previously<sup>13,14</sup>. By blocking the OPA pump wave, we are left with coherent states.

The signal is analysed at a homodyne detector, whose output current  $i_\Omega$  is mixed with an electrical local oscillator  $\sim \sin(\Omega t + \phi)$  phase-locked to the modulation frequency, and then low-pass filtered with 100 kHz bandwidth. We fix the phase of the electric local oscillator to  $\cos \phi = 1$ , so that the resulting current is;

$$i_\Omega(\theta, t) = (2\beta E_0 + X_n(\Omega, t) - X_n(-\Omega, t)) \sin \theta \\ + (Y_n(\Omega, t) - Y_n(-\Omega, t)) \cos \theta \quad (2)$$

where  $X_n(\Omega, t)$ ,  $Y_n(\Omega, t)$  are the noise fluctuations in a 100-kHz-wide band centred at  $\Omega$ . By variation of the optical local-oscillator phase  $\theta$ , any quadrature of the field difference at  $\omega + \Omega$  and  $\omega - \Omega$  can be accessed.

The  $i_\Omega$  data (about 500,000 points per trace) are taken with a high-speed 12 bit analogue-to-digital converter, while the local-oscillator phase is swept by  $2\pi$  in approximately 200 ms. Time traces of  $i_\Omega$  for coherent and squeezed states are shown in the left column of Fig. 2. They can be considered to be the experimental counterpart of the theoretical depictions of squeezed states introduced by Caves<sup>30</sup>.

The traces are subdivided into 128 equal-duration intervals within which the local-oscillator phase is approximately constant. These individual time traces may be regarded as the quantum trajectories of a particular quadrature  $X_\theta$ . The specific behaviour of the trajectory is unpredictable; its statistics however contain the information necessary and sufficient to calculate the quantum state properties. Experimentally, the statistics are obtained by forming histograms of 256 amplitude bins for each quantum trajectory and normalizing the absolute bin width using as reference the distribution of a vacuum state. The middle column of Fig. 2 shows selected measured quadrature probability distributions for the generated states. All distributions are found to be gaussians. This is expected, as the states are generated from a coherent state with a gaussian Wigner function via a second-order nonlinear interaction.

The variances of these distributions determine the amount of squeezing and anti-squeezing. A maximum of  $-6 \pm 0.25$  dB

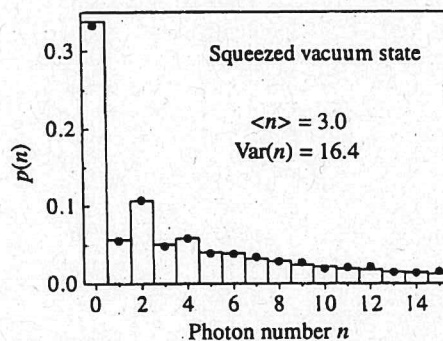
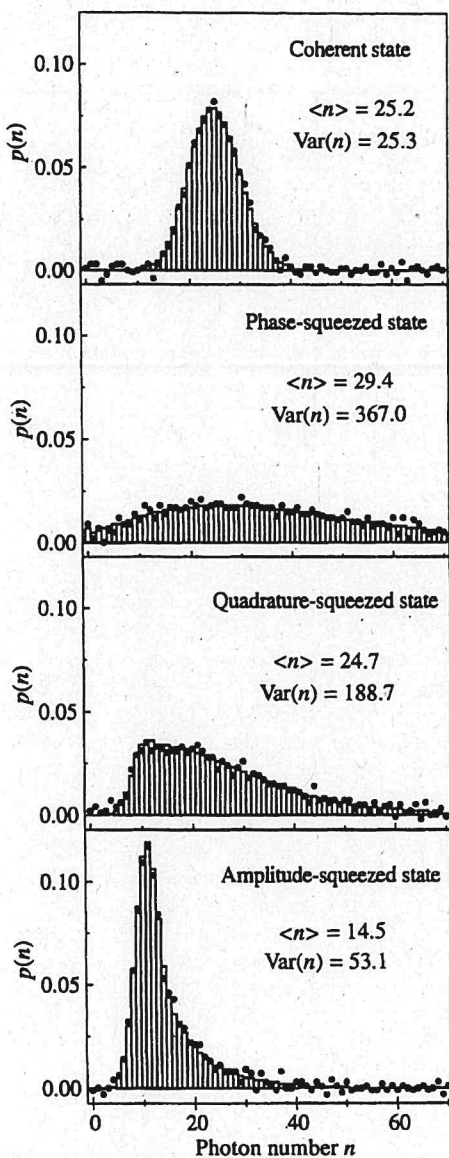


**Figure 3** Photon number distributions for the states of Fig. 2. Solid points refer to experimental data, histograms to theoretical expectations. Except for the poissonian distribution of the coherent state, all distributions are superpoissonian ( $\langle n \rangle < \text{Var}(n)$ ). The odd/even oscillations in the photon number distribution of the squeezed vacuum state are a consequence of the pair-wise generation of photons. They can also be explained by quantum interference effects in phase space<sup>37</sup>.

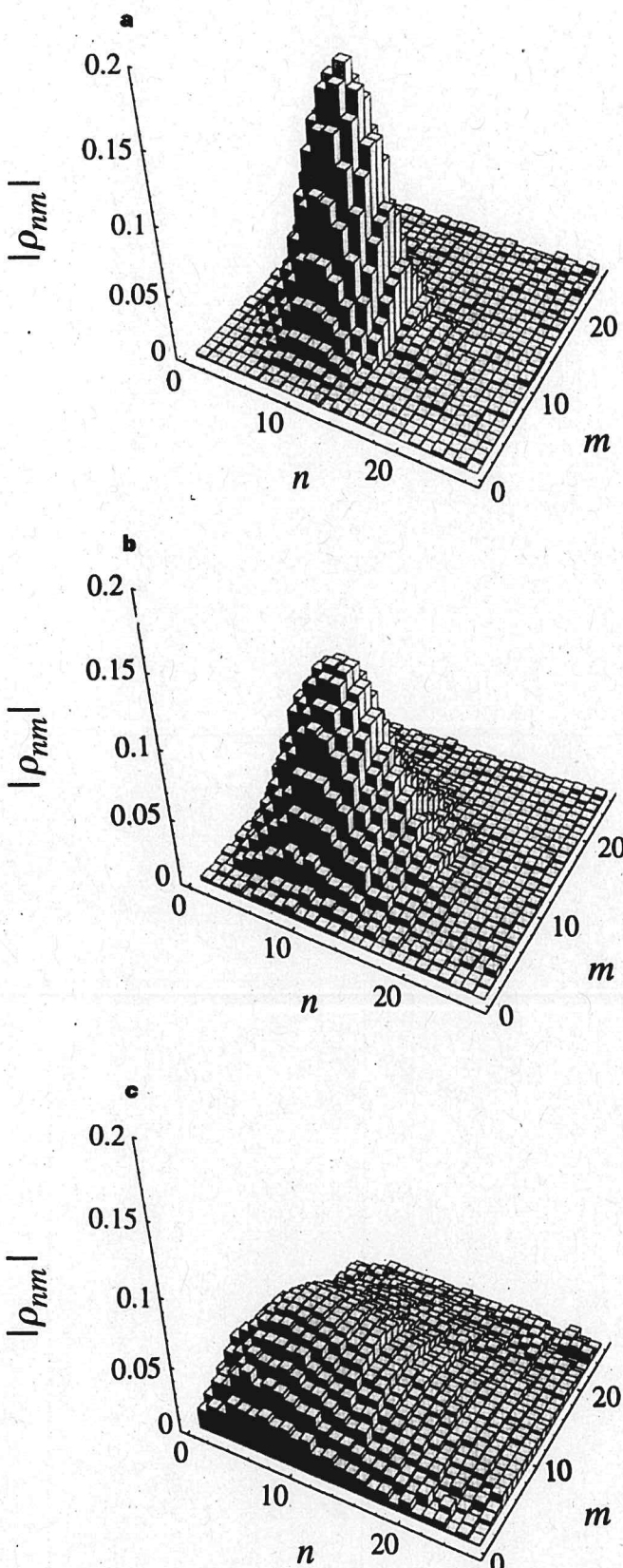


**Figure 4** Reconstructed density matrices (absolute values) of three states with approximately equal amplitude: **a**, sub-poissonian amplitude-squeezed state with  $\langle n \rangle = 8.9$ ,  $\text{Var}(n) = 4.9$ ; **b**, coherent state with  $\langle n \rangle = 8.4$ ,  $\text{Var}(n) = 8.6$ ; **c**, phase-squeezed state with  $\langle n \rangle = 8.4$ ,  $\text{Var}(n) = 24.6$ . The bump around  $n \approx 17, m \approx 12$  for the amplitude-squeezed state is a characteristic feature, where the matrix elements change sign.

(= 0.25) for the squeezed vacuum mode was detected. For the bright squeezed light only a maximum amount of squeezing of  $-5.2 \text{ dB}$  (= 0.3) was reached, due to slight phase instabilities of the seed wave. The anti-squeezing amounted to  $12-14 \text{ dB}$  (= 15.8–26.9) for the states presented. These values agree with the results of simultaneous measurements with a spectrum analyser.

#### Phase-space distributions of squeezed states

Applying the inverse Radon transform yields the Wigner distributions shown in the right column of Fig. 2. They agree well with the theoretical expression;

$$W(x, y) = \frac{1}{\pi ab} \exp \left( -\frac{(x - e_0 \cos \phi)^2}{a^2} - \frac{(y - e_0 \sin \phi)^2}{b^2} \right) \quad (3)$$

where  $x = x_0 \cos \phi + x_{\pi/2} \sin \phi$ ,  $y = -x_0 \sin \phi + x_{\pi/2} \cos \phi$  are the phase-space coordinates used in standard textbooks,  $a$  and  $b$  are respectively the minimum and maximum standard deviation of the quadrature fluctuations, and  $e_0 = 2\beta E_0$  is the state's amplitude. The commonly used depiction of squeezed states as ellipses in phase space, with half-axes  $a$  and  $b$ , corresponds to a horizontal section through the Wigner function. The area of the ellipse is a measure of the purity of the state, as  $\text{Tr} \rho^2 = 2\pi \int \int W(x, y)^2 dx dy$  equals  $1/ab$  for squeezed states (here  $\text{Tr}$  indicates the trace of a matrix).  $\text{Tr} \rho^2$  amounted to 1 for the (pure) coherent state and 0.41–0.46 for the squeezed states of Fig. 2. Their significantly mixed character arises mostly from loss experienced in the cavity of the OPA (escape efficiency 0.88) and during propagation and detection (overall detection efficiency  $\eta = 0.94$ ).

The quantum efficiency of the detection system is a critical issue in the field of QSR<sup>31</sup>. The loss suffered by the quantum state in propagation and detection is equivalent to a convolution of its original Wigner function with a gaussian. Thus for a given detection efficiency  $\eta$  only the  $s$ -parametrized phase-space distribution function  $W(x, y, s)$  (ref. 18) with  $s < 1 - (1/\eta)$ , can be reconstructed<sup>32</sup>. In a strict sense the Wigner function itself  $W(x, y) = W(x, y, s=0)$  is not accessible by tomographical methods, but with our high detection efficiency our reconstructions yield phase-space distributions with  $s = -0.064$ , which is very close to the Wigner function. An additional smoothing, also a convolution with a gaussian, occurs within the reconstruction algorithm in a filtering procedure with a quadratic regularization method<sup>33</sup>. However, its contribution to the total  $s$ -parameter can be made less than  $-0.01$ .

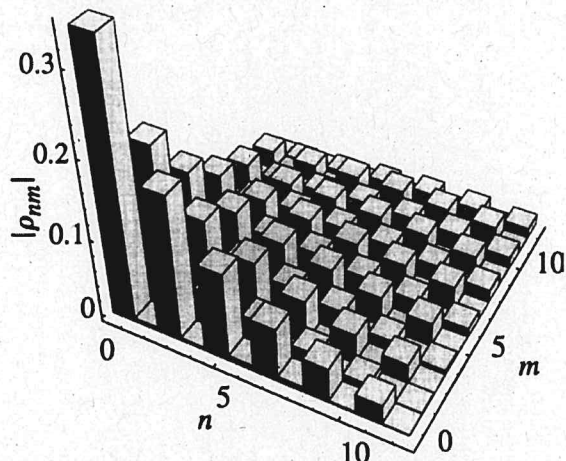


**Figure 5** Reconstructed density matrix of the squeezed vacuum state of Fig. 2: along the diagonal and the near off-diagonals the elements alternate in magnitude, which can be explained by quantum interference in phase space<sup>37</sup>. Odd off-diagonals are zero, owing to the symmetry of the state's distribution in phase space,  $W(x, y) = W(-x, -y)$ .

## Density matrices of squeezed states

An alternative view of the generated states is provided by their density matrices  $\rho$  in the Fock basis, because here the state is described in terms of energy eigenstates, in contrast to the description by field components discussed in the previous paragraph. The diagonal elements of the density matrix  $\rho_{nn} = p(n)$ , are the occupation probabilities of the number states  $|n\rangle$ . Here  $n$  is to be interpreted as the photon flux per unit bandwidth;  $p(n)$  is the probability that an ideal photon counter would register in 1 second  $n$  photons in a 1-Hz-wide spectral band. A state with  $\langle n \rangle$  photons corresponds to a photon flux of  $\langle n \rangle \times 10^5$  photons s<sup>-1</sup> ≈  $\langle n \rangle 0.02$  pW in the 100-kHz-wide spectral bands centred at  $\omega \pm \Omega$ .

Figure 3 shows the photon number distributions for the states from Fig. 2. As can be seen, a simple rotation of the squeezing ellipse (with respect to the coherent excitation in phase space) changes the photon distribution function substantially. Apart from the poissonian distribution of the coherent state, all distributions shown are strongly super-poissonian, that is, the photon number variance  $\text{Var}(n)$  exceeds its mean  $\langle n \rangle$ . For amplitude-squeezed light this seems counterintuitive, as reduced amplitude noise should imply reduced intensity (photon number) noise. An explanation is given by the expressions for photon number average and variance for general (non-minimum-uncertainty) squeezed states<sup>34</sup>:

$$\begin{aligned}\langle n \rangle &= \frac{1}{4}(a^2 + b^2 - 2) + \frac{1}{2}e_0^2 \\ \text{Var}(n) &= \frac{1}{8}(a^4 + b^4 - 2) + \frac{1}{2}e_0^2(a^2 \cos^2 \phi + b^2 \sin^2 \phi)\end{aligned}\quad (4)$$

For states with a large amplitude  $e_0$ , the variance of the amplitude quadrature  $a^2 \cos^2 \phi + b^2 \sin^2 \phi$  indeed determines the characteristics of the photon number distribution. However, in the regime of low amplitudes, when coherent excitation and quantum noise are comparable in size, the first terms in equation (4), figuratively the photon content of the quadrature fluctuations, play a significant role. We adjusted the experimental parameters to  $a^2 = 0.43$ ,  $b^2 = 3.3$  (reduced squeezing and anti-squeezing) and  $e_0 = 4.12$  to obtain amplitude-squeezed sub-poissonian light. Its Mandel-Q-parameter ( $\text{Var}(n) - \langle n \rangle)/\langle n \rangle = -0.45$ ) is to our knowledge the lowest value achieved so far using optical nonlinear frequency-conversion techniques<sup>35</sup>.

Figure 4 shows the density matrix up to  $n, m = 25$  for the sub-poissonian amplitude-squeezed state in comparison with those of a coherent and super-poissonian phase-squeezed state with approximately equal average photon numbers. Owing to their reflection symmetry in phase space, it is always possible to choose a basis in which the density matrices of these three states in the Fock representation are real. For the coherent state and the phase-squeezed state all elements  $\rho_{nm}$  are positive, for the amplitude-squeezed state the near-diagonals show oscillations. The density matrix of the squeezed vacuum, Fig. 5, exhibits the most interesting structure. Its typical 'chess-board' pattern is due to the down-conversion process occurring in the OPA, where photons are created in pairs. The deviations of the experimental density matrices presented here from the theoretical ones are of the order of 0.01 per element. Besides statistical effects, this is partly due to instabilities of the relative phases  $\theta$  and  $\phi$  and to fluctuations in the pump power.

We have carried out a complete experimental characterization of the whole family of squeezed states. Average photon number and orientation of the states in phase space were accurately controlled by macroscopic experimental parameters. In particular, this flexibility allowed us to generate amplitude-squeezed light with either sub- or super-poissonian photon statistics. The quantum state reconstructions were performed in quasi real-time, with a data acquisition time of 200 ms and an analysing time of ~20 s. Our results are in very good agreement with theory. Beyond the reconstructions

presented here, we have investigated the Pegg–Barnett phase distribution and incoherent superpositions of coherent states<sup>36</sup>.

Quantum state reconstruction by homodyne tomography has been developed into a reliable and accurate tool. We believe that this powerful method will stimulate experimental efforts to generate new quantum states with non-gaussian statistics using higher-order nonlinear processes. □

Received 10 January; accepted 15 April 1997.

1. Royer, A. Measurement of quantum states and the Wigner function. *Foundat. Phys.* **19**, 3–32 (1989).
2. Vogel, K. & Risken, H. Determination of quasiprobability distributions in terms of probability distributions for the rotated quadrature phase. *Phys. Rev. A* **40**, 2847–2849 (1989).
3. D'Ariano, G. M., Macchiavello, C. & Paris, M. G. A. Detection of the density matrix through optical homodyne tomography without filtered back projection. *Phys. Rev. A* **50**, 4298–4302 (1994).
4. Leonhardt, U., Munroe, M., Kiss, T., Richter, Th. & Raymer, M. G. Sampling of photon statistics and density matrix using homodyne detection. *Opt. Commun.* **127**, 144–160 (1996).
5. Leonhardt, U. & Raymer, M. G. Observation of moving wave packets reveals their quantum state. *Phys. Rev. Lett.* **76**, 1985–1989 (1996).
6. Richter, T. & Wünsche, A. Determination of occupation probabilities from time-averaged position distributions. *Phys. Rev. A* **53**, R1974–R1977 (1996).
7. Zucchetti, A., Vogel, W., Tasche, M. & Welsch, D.-G. Direct sampling of density matrices in field-strength bases. *Phys. Rev. A* **54**, 1–4 (1996).
8. Banaszek, K. & Wodkiewicz, K. Direct probing of quantum phase space by photon counting. *Phys. Rev. Lett.* **76**, 4344–4347 (1996).
9. Tan, S. M. An inverse problem approach to optical homodyne tomography. (spec. iss. on QSR) *J. Mod. Opt.* (submitted).
10. Smithy, D. T., Beck, M., Raymer, M. G. & Faridani, A. Measurement of the Wigner distribution and the density matrix of a light mode using optical homodyne tomography: application to squeezed states and the vacuum. *Phys. Rev. Lett.* **70**, 1244–1247 (1993).
11. Smithy, D. T., Beck, M., Cooper, J. & Raymer, M. G. Measurement of number-phase uncertainty relations of optical fields. *Phys. Rev. A* **48**, 3159–3167 (1993).
12. Munroe, M., Boggavarapu, D., Anderson, M. E. & Raymer, M. G. Photon number statistics from the phase-averaged quadrature field distribution: theory and ultrafast measurement. *Phys. Rev. A* **52**, R924–R927 (1995).
13. Breitenbach, G. et al. Squeezed vacuum from a monolithic optical parametric oscillator. *J. Opt. Soc. Am. B* **12**, 2304–2309 (1995).
14. Schiller, S., Breitenbach, G., Pereira, S. F., Müller, T. & Mlynek, J. Quantum statistics of the squeezed vacuum by measurement of the density matrix in the number state representation. *Phys. Rev. Lett.* **77**, 2933–2936 (1996).
15. Dunn, T. J., Sweetser, J. N. & Walmsley, I. A. Experimental determination of the quantum-mechanical state of a molecular vibrational mode using fluorescence tomography. *Phys. Rev. Lett.* **74**, 884–887 (1995).
16. Leibfried, D. et al. Experimental determination of the motional quantum state of a trapped atom. *Phys. Rev. Lett.* **77**, 4821–4825 (1996).
17. Kurnitski, C., Pfau, T. & Mlynek, J. Measurement of the Wigner function of an ensemble of helium atoms. *Nature* **386**, 150–153 (1997).
18. Hillery, M., O'Connell, R. F., Scully, M. O. & Wigner, E. P. Distribution functions in physics: fundamentals. *Phys. Rep.* **106**, 122–167 (1984).
19. Walls, D. Squeezed states of light. *Nature* **306**, 141–146 (1983).
20. Slusher, R. E., Hollberg, L. W., Yurke, B., Mertz, J. C. & Valley, J. F. Observation of squeezed states generated by four wave mixing in an optical cavity. *Phys. Rev. Lett.* **55**, 2409–2412 (1985).
21. Kimble, H. J. & Walls, D. F. (eds) (spec. iss. on squeezing light) *J. Opt. Soc. Am. B* **4**(10), (1987).
22. Yuen, H. P. & Chan, V. W. S. Noise in homodyne and heterodyne detection. *Opt. Lett.* **18**, 177–179 (1983).
23. Schrödinger, E. Der stetige Übergang von der Mikro- zur Makromechanik. *Naturwissenschaften* **14**, 664–666 (1926).
24. Breitenbach, G., Schiller, S. & Mlynek, J. 81% conversion efficiency in frequency-stable continuous-wave parametric oscillation. *J. Opt. Soc. Am. B* **12**, 2095–2101 (1995).
25. Wu, L.-A., Kimble, H. J., Hall, J. L. & Wu, H. Generation of squeezed states by parametric down conversion. *Phys. Rev. Lett.* **57**, 2520–2523 (1986).
26. Polzik, E. S., Carri, J. & Kimble, H. J. Spectroscopy with squeezed light. *Phys. Rev. Lett.* **68**, 3020–3023 (1992).
27. Kim, C. & Kumar, P. Quadrature-squeezed light detection using a self-generated matched local oscillator. *Phys. Rev. Lett.* **73**, 1605–1608 (1994).
28. Schneider, K., Bruckmeier, R., Hansen, H., Schiller, S. & Mlynek, J. Bright squeezed light generation by a continuous-wave semi-monolithic parametric amplifier. *Opt. Lett.* **21**, 1396–1397 (1996).
29. Collett, M. J. & Walls, D. F. Squeezing spectra for nonlinear optical systems. *Phys. Rev. A* **32**, 2887–2892 (1985).
30. Caves, C. M. Quantum limits on noise in linear amplifiers. *Phys. Rev. D* **26**, 1817–1839 (1982).
31. D'Ariano, G. M., Leonhardt, U. & Paul, H. Homodyne detection of the density matrix of the radiation field. *Phys. Rev. A* **52**, R1801–R1804 (1995).
32. Leonhardt, U. & Paul, H. Realistic optical homodyne measurements and quasiprobability distributions. *Phys. Rev. A* **48**, 4598–4604 (1993).
33. Janicke, U. & Wilkens, M. Tomography of atom beams. *J. Mod. Opt.* **42**, 2183–2199 (1995).
34. Dodonev, V. V., Man'ko, O. V. & Man'ko, V. I. Photon distribution for one-mode mixed light with a generic gaussian Wigner function. *Phys. Rev. A* **49**, 2993–3001 (1994).
35. Davidovich, L. Sub-Poissonian processes in quantum optics. *Rev. Mod. Phys.* **68**, 127–172 (1996).
36. Breitenbach, G. & Schiller, S. Homodyne tomography of classical and non-classical light. (spec. iss. on QSR) *J. Mod. Opt.* (submitted).
37. Schleich, W. & Wheeler, J. A. Oscillations in photon number distribution of squeezed states and interference in phase space. *Nature* **326**, 574–577 (1987).

**Acknowledgements.** We thank T. Müller and S. F. Pereira for their collaboration in the initial stage of the experiment, and A. Faridani and M. G. Raymer for providing the source code for the inverse Radon Transform. We also thank R. Bruckmeier, U. Leonhardt, W. P. Schleich, G. M. D'Ariano and S. M. Tan for discussions. This work was supported by the Deutsche Forschungsgemeinschaft and the EC Esprit programme.

**Correspondence and requests for materials** should be addressed to G.B. (e-mail: Gerd.Breitenbach@uni-konstanz.de). A video showing the time evolution of the quantum states presented here can be obtained from the authors.

from the distribution  $P(X(\varphi))$  we can reconstruct the Wigner function

starting point here is the relation

$$P(X(\varphi)) = \text{tr} (\underbrace{\delta(\hat{X}(\varphi) - X(\varphi))}_{\text{probability that the observable}} g)$$

$\hat{X}(\varphi)$  takes the value  $X(\varphi)$

(note, that we had to introduce the hat on top of the operator here)

$$= \text{tr} \left( \underbrace{\frac{1}{2\pi} \int d\lambda e^{i\lambda(\hat{X}(\varphi) - X(\varphi))}}_{\text{representation of the } \delta\text{-function}} g \right)$$

representation of the  $\delta$ -function

$$= \frac{1}{2\pi} \int d\lambda \underbrace{\text{tr}(e^{i\lambda \hat{X}(\varphi)} g)}_{\text{characteristic function}} e^{-i\lambda X(\varphi)}$$

characteristic function

the characteristic function reads

$$\chi(\lambda, \varphi) = \text{tr} (e^{i\frac{\lambda}{2} e^{i\varphi} a^\dagger + i\frac{\lambda}{2} e^{-i\varphi} a} g)$$

$$= \text{tr} (e^{\mu a^\dagger - \mu^* a} g) \quad \text{with } \mu = i\frac{\lambda}{2} e^{i\varphi}$$

$$= \chi_w(\mu) \quad \leftarrow \text{characteristic function of the Wigner function, i.e. } W(a, a^\dagger) = \frac{1}{\pi^2} \int d\mu \chi_w(\mu) e^{\mu a^\dagger - \mu a}$$

from  $P(X(\varphi))$  one can construct  $\chi(\lambda, \varphi)$ , from which one can calculate  $\chi_w(\mu)$  and then compute the Wigner function

Note, that one can show that the Wigner function and the probability distribution of the  $X(\varphi)$ -quadrature are related via the Radon transform

$$P(X(\varphi)) = \int_{-\infty}^{\infty} dY \ W(X(\varphi)\cos\varphi - Y\sin\varphi, X(\varphi)\sin\varphi + Y\cos\varphi)$$

### III.3 Theory of photon detection

(P)

- we consider the expansion of the electro-magnetic field in terms of plane waves

$$\vec{E}(\vec{r}, t) = \vec{E}^{(+)}(\vec{r}, t) + \vec{E}^{(-)}(\vec{r}, t),$$

with  $\vec{E}^{(+)}(\vec{r}, t) = \sum_{\vec{k}} \hat{\epsilon}_{\vec{k}} E_k a_{\vec{k}} e^{-i\omega_k t + i\vec{k} \cdot \vec{r}}$

and  $\vec{E}^{(-)}(\vec{r}, t) = (\vec{E}^{(+)}(\vec{r}, t))^+$

- at the heart of a typical photon detector lies the interaction between photons and matter, i.e. atoms
- considering an atom located at position  $\vec{r}$ , the interaction between the electromagnetic field and the atomic dipole  $\vec{d}$  is given by
- modelling the atom with two levels, the ground/excited state  $|g\rangle / |e\rangle$ , the dipole operator can be written as

$$\vec{d} = \sum_{m,n=e,g} \text{Im} X_m |\vec{d}| n X_n = \langle e | \vec{d} | g \rangle |e\rangle \langle g| + \text{h.c.}$$

$|e\rangle$  —

$\rightarrow$   
this can

also be  
an unbound  
state (ionisation)

$\vec{E}(\vec{r}, t)$

$|g\rangle$  —

- diagonal contributions vanish, since  $\vec{d} \propto \vec{r}_{\text{electrons}}$ ;  $\vec{d}$  is thus an operator with odd parity, whose expectation value vanishes when take with parity eigenstates

- we can now write for the interaction

Hamiltoian

$$H_{int} = -\vec{d} \cdot \vec{E} = -(\langle e | \vec{d} | g \rangle |e\rangle \otimes |g\rangle + \langle g | \vec{d} | e \rangle |g\rangle \otimes |e\rangle)$$

rotating

wave

approximation

$$\rightarrow (\vec{E}^{(+)}(\vec{r}, t) + \vec{E}^{(-)}(\vec{r}, t))$$

$$\approx -\langle e | \vec{d} | g \rangle \cdot \vec{E}^{(+)}(\vec{r}, t) |e\rangle \otimes |g\rangle - \langle g | \vec{d} | e \rangle \cdot \vec{E}^{(-)}(\vec{r}, t) |g\rangle \otimes |e\rangle$$

- photon detection now corresponds to the absorption of a photon by the atom

- denoting the initial and final state of the electromagnetic field as  $|i\rangle, |f\rangle$ , respectively, we find for the transition probability per time according to Fermi's Golden rule:

$$\frac{dP_{fi}}{dt} \propto \underbrace{|\langle f | \otimes \langle e |}_{\text{final light-matter state}} \underbrace{\langle e | H_{int} | i \rangle \otimes | g \rangle|}_{\text{initial light-matter state}}|^2$$

- for simplicity, we now assume  $\langle g | \vec{d} | e \rangle = d_e \in \mathbb{R}$  and write  $E_z(\vec{r}, t) = E$

$$\begin{aligned} \hookrightarrow \frac{dP_{if}}{dt} &\propto d^2 |\langle f | \otimes \langle e | (E^{(+)} |e\rangle \otimes |g\rangle + E^{(-)} |g\rangle \otimes |e\rangle) (|i\rangle \otimes |g\rangle)|^2 \\ &= d^2 |\langle f | E^{(+)} |i\rangle \langle e | e \rangle \langle g | g \rangle|^2 = d^2 |\langle f | E^{(+)} |i\rangle|^2 \end{aligned}$$

- the final state  $|f\rangle$  is not observed/resolved, and we have to sum over it in order to obtain the absorption rate  $\omega_i(\vec{r}, t)$

$$\begin{aligned}
 \hookrightarrow W_1(\vec{r}_1, t) &\propto \sum_f | \langle f | E^{(+)}(\vec{r}_1, t) | i \rangle |^2 \\
 &= \sum_f \langle i | E^{(-)}(\vec{r}_1, t) | f \rangle \langle f | E^{(+)}(\vec{r}_1, t) | i \rangle \\
 &= \langle i | E^{(-)}(\vec{r}_1, t) E^{(+)}(\vec{r}_1, t) | i \rangle
 \end{aligned}$$

for electrodynamic fields that are described by a mixed state  $\rho = \sum_i p_i |i\rangle\langle i|$  this formula generalises to

$$\begin{aligned}
 W_1(\vec{r}_1, t) &\propto \sum_i p_i \langle i | E^{(-)}(\vec{r}_1, t) E^{(+)}(\vec{r}_1, t) | i \rangle \\
 &= \text{tr} (\rho E^{(-)}(\vec{r}_1, t) E^{(+)}(\vec{r}_1, t))
 \end{aligned}$$

this formula motivates the introduction of the so-called first order correlation function

$$\begin{aligned}
 G^{(1)}(\vec{r}_1, \vec{r}_2, t_1, t_2) &= \text{tr} (\rho E^{(-)}(\vec{r}_1, t_1) E^{(+)}(\vec{r}_2, t_2)) \\
 &= \langle E^{(-)}(\vec{r}_1, t_1) E^{(+)}(\vec{r}_2, t_2) \rangle
 \end{aligned}$$

for the absorption / counting rate we can thus write

$$W_1(\vec{r}_1, t) \propto G^{(1)}(\vec{r}_1, \vec{r}_1, t_1, t)$$

let us now consider photo detection at two detectors, i.e. transitions of two atoms, which are positioned at  $\vec{r}_1$  and  $\vec{r}_2$

we also take into account, that the detection events take place at two different times:  $t_1 \leq t_2$

(92)

- the joint probability of observing a detection event (beamline ionisation) at  $\vec{r}_2$  within the interval  $[t_2, t_2 + dt_2]$  and at  $\vec{r}_1$  within the interval  $[t_1, t_1 + dt_1]$  is then

$$\begin{aligned} W_2(\vec{r}_1, t_1; \vec{r}_2, t_2) &\propto \sum_f |\langle f | E^{(+)}(\vec{r}_2, t_2) E^{(+)}(\vec{r}_1, t_1) | i \rangle|^2 \\ &= \text{tr} (g E^{(-)}(\vec{r}_1, t_1) E^{(-)}(\vec{r}_2, t_2) E^{(+)}(\vec{r}_2, t_2) E^{(+)}(\vec{r}_1, t_1)) \\ &= G^{(2)}(\vec{r}_1, \vec{r}_2, \vec{r}_2, \vec{r}_1; t_1, t_2, t_2, t_1) \end{aligned}$$

- in the last step we have introduced the second order correlation function

$$G^{(2)}(\vec{r}_1, \vec{r}_2, \vec{r}_3, \vec{r}_4; t_1, t_2, t_3, t_4) = \text{tr} (g E^{(-)}(\vec{r}_1, t_1) E^{(+)}(\vec{r}_2, t_2) E^{(+)}(\vec{r}_3, t_3) E^{(+)}(\vec{r}_4, t_4))$$

- note, that the first order correlation function is proportional to the intensity

$$\langle I(\vec{r}) \rangle \propto \langle E^{(-)}(\vec{r}, t) E^{(+)}(\vec{r}, t) \rangle,$$

but that "naively" calculating intensity correlations would yield the expression

$$\langle I(\vec{r}_1, t_1) I(\vec{r}_2, t_2) \rangle \propto \langle E^{(-)}(\vec{r}_1, t_1) E^{(+)}(\vec{r}_1, t_1) E^{(-)}(\vec{r}_2, t_2) E^{(+)}(\vec{r}_2, t_2) \rangle$$

which involves a different operator ordering compared with the second order correlation function obtained from a proper description of the two-point measurement

### III.4 Theory of optical coherence

(93)

- investigating correlations allows to quantify the "quantum nature" of the electromagnetic field
- to this end we introduce the normalized first order and second order coherence functions

$$g^{(1)}(\vec{r}_1, \vec{r}_2, \tau) = \frac{\langle E^{(-)}(\vec{r}_1, t) E^{(+)}(\vec{r}_2, t+\tau) \rangle}{\langle E^{(-)}(\vec{r}_1, t) E^{(+)}(\vec{r}_1, t) \rangle \langle E^{(-)}(\vec{r}_2, t+\tau) E^{(+)}(\vec{r}_2, t+\tau) \rangle}$$

$$g^{(2)}(\vec{r}_1, \vec{r}_2, \tau) = \frac{\langle E^{(-)}(\vec{r}_1, t) E^{(-)}(\vec{r}_2, t+\tau) E^{(+)}(\vec{r}_2, t+\tau) E^{(+)}(\vec{r}_1, t) \rangle}{\langle E^{(-)}(\vec{r}_1, t) E^{(+)}(\vec{r}_1, t) \rangle \langle E^{(-)}(\vec{r}_2, t+\tau) E^{(+)}(\vec{r}_2, t+\tau) \rangle}$$

- in case of a stationary single mode light field these expressions become

$$g^{(1)}(\tau) = \frac{\langle a^\dagger(t) a(t+\tau) \rangle}{\langle a a \rangle}, \quad g^{(2)}(\tau) = \frac{\langle a^\dagger(t) a^\dagger(t+\tau) a(t+\tau) a(t) \rangle}{\langle a a \rangle^2}$$

- for a free single mode field, which evolves according to  $a(t) = e^{-i\omega t} a(0)$  this yields

$$g^{(1)}(\tau) = e^{-i\omega\tau} \frac{\langle a^\dagger(0) a(0) \rangle}{\langle a^\dagger(0) a(0) \rangle} = e^{-i\omega\tau}$$

- for any freely evolving field, we thus get the same (trivial) first order coherence (this is not true for multi-mode fields)
- to calculate the second order coherence, we can make use of the P-function; e.g.

$$g^{(2)}(0) = \frac{\int d^2\alpha P(\alpha, \alpha^*) |\alpha|^4}{\left(\int d^2\alpha P(\alpha, \alpha^*) |\alpha|^2\right)^2}$$

equal time second order correlation

### examples:

- single mode thermal field

$$P(\alpha, \alpha^*) = \frac{1}{\pi \langle n \rangle} e^{-\frac{|\alpha|^2}{\langle n \rangle}}$$

↳ for such a Gaussian state, one finds,

$$\langle |\alpha|^4 \rangle = \langle \alpha^* \alpha \alpha^* \alpha \rangle = \langle \alpha^* \alpha \rangle \langle \alpha^* \alpha \rangle + \langle \alpha^* \alpha \rangle \langle \alpha^* \alpha \rangle = 2 \langle |\alpha|^2 \rangle^2$$

and hence

$$g^{(2)}(0) = 2$$

- single mode coherent state

$$P(\alpha, \alpha^*) = \delta^{(2)}(\alpha - \alpha_0)$$

$$\hookrightarrow g^{(2)}(0) = \frac{|\alpha_0|^4}{|\alpha_0|^4} = 1$$

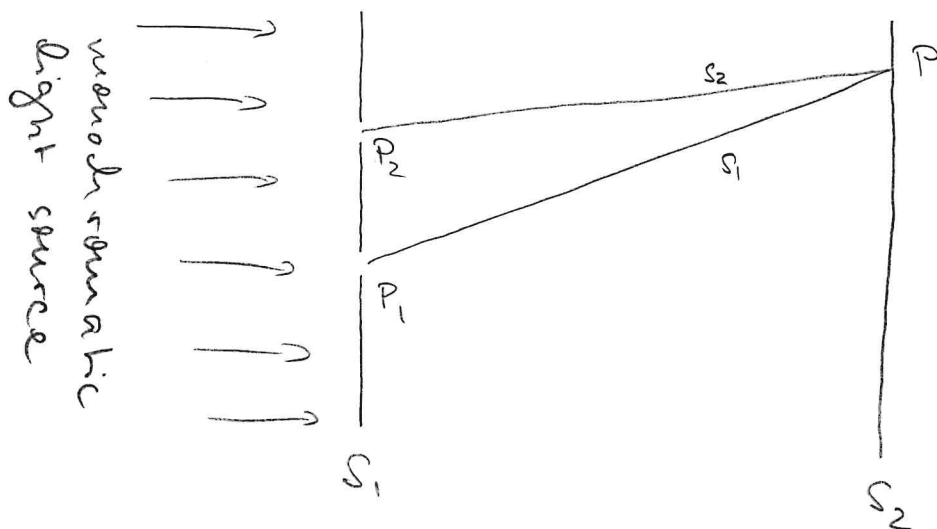
- Fock state

$$\hookrightarrow g^{(2)}(0) = \frac{\langle (\hat{a}^\dagger)^2 \hat{a} \rangle}{\langle \hat{a} \hat{a}^\dagger \rangle^2} = \frac{1}{n^2} n(n-1) = 1 - \frac{1}{n}$$

apparently, we can distinguish these three states from their second order coherence, despite them sharing the same first order coherence

next, we turn to the discussion of Young's double slit experiment and its relation to first order coherence

the field of a monochromatic light source is irradiated onto a screen  $S_1$ , with two pinholes at points  $P_1$  and  $P_2$



the positive frequency part of the field operator at a point  $P$  on the second screen  $S_2$  at time  $t$  may be expressed through the operators at points  $P_1$  and  $P_2$  at earlier times

$$E^{(+)}(r, t) = k_1 E^{(+)}(r_1, t-t_1) + k_2 E^{(+)}(r_2, t-t_2)$$

↑ geometric factors ↑

- here the times are given by  $t_i = \frac{s_i}{c}$ , which are the times needed for a photon to travel from  $P_i$  to  $P$
- a photo detector at  $P$  measures the intensity

$$\begin{aligned}\langle I(\vec{r}, t) \rangle &\propto \text{tr} (g E^{(-)}(\vec{r}_1, t) E^{(+)}(\vec{r}_1, t)) \\ &= |k_1|^2 \text{tr} (g E^{(-)}(\vec{r}_1, t-t_1) E^{(+)}(\vec{r}_1, t-t_1)) \\ &\quad + |k_2|^2 \text{tr} (g E^{(-)}(\vec{r}_2, t-t_2) E^{(+)}(\vec{r}_2, t-t_2)) \\ &\quad + 2 \text{Re} \left\{ k_1 k_2 \text{tr} (g E^{(-)}(\vec{r}_1, t-t_1) E^{(+)}(\vec{r}_2, t-t_2)) \right\}\end{aligned}$$

- in terms of the first order correlation functions  $G^{(1)}(\vec{r}_1, \vec{r}_2; t_1, t_2)$  this can be written as

$$\begin{aligned}\langle I(\vec{r}, t) \rangle &\propto |k_1|^2 G^{(1)}(\vec{r}_1, \vec{r}_1; t-t_1, t-t_1) + |k_2|^2 G^{(1)}(\vec{r}_2, \vec{r}_2; t-t_2, t-t_2) \\ &\quad + 2 \text{Re} \left\{ k_1 k_2 G^{(1)}(\vec{r}_1, \vec{r}_2, t-t_1, t-t_2) \right\}\end{aligned}$$

- for a single mode field the dependence on  $t$  cancels out and we can write

$$\langle I(\vec{r}, t) \rangle = \langle I^{(1)}(\vec{r}) \rangle + \langle I^{(2)}(\vec{r}) \rangle + 2 \underbrace{\left[ \langle I^{(1)}(\vec{r}) \rangle \langle I^{(2)}(\vec{r}) \rangle \right]}_{\text{interference term}} \text{Re} \{ g^{(1)}(\vec{r}_1, \vec{r}_2, \tau) \}$$

with  $\tau = t_1 - t_2 = \frac{s_1 - s_2}{c} \equiv \tau(\vec{r})$

- in the next step we write due to free evolution of field

$$g^{(1)}(\vec{r}_1, \vec{r}_2; \tau) = |g^{(1)}(\vec{r}_1, \vec{r}_2, \tau)| e^{i Q(\vec{r}_1, \vec{r}_2, \tau) - i \omega_0 \tau}$$

$$\hookrightarrow \langle I(\vec{r}, \tau) \rangle = \langle I^{(0)}(\vec{r}) \rangle + \langle I^{(2)}(\vec{r}) \rangle$$

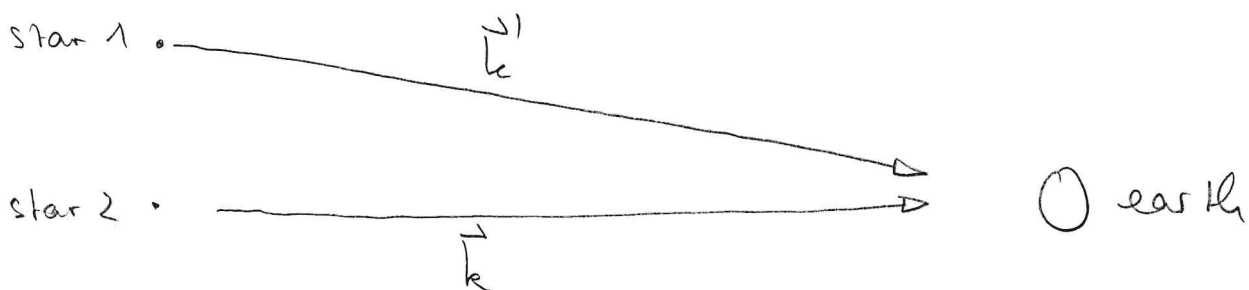
$$+ 2\overline{\langle I^{(1)}(\vec{r}) \rangle \langle I^{(2)}(\vec{r}) \rangle} |g^{(1)}(\vec{r}_1, \vec{r}_2, \tau)| \cos(\underbrace{\varphi(\vec{r}_1, \vec{r}_2, \tau)}_{\text{slowly varying with respect to position on } S_2} - \underbrace{w\tau}_{\text{rapidly varying}})$$

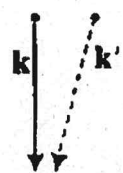
- from this expression it becomes apparent, that  $|g^{(1)}|$  is linked to the amplitude of the interference pattern / fringes on  $S_2$ ,
- for example, we can define the contrast

$$U = \frac{\langle I(\vec{r}, \tau) \rangle_{\max} - \langle I(\vec{r}, \tau) \rangle_{\min}}{\langle I(\vec{r}, \tau) \rangle_{\max} + \langle I(\vec{r}, \tau) \rangle_{\min}} \propto |g^{(1)}(\vec{r}_1, \vec{r}_2, \tau)|$$

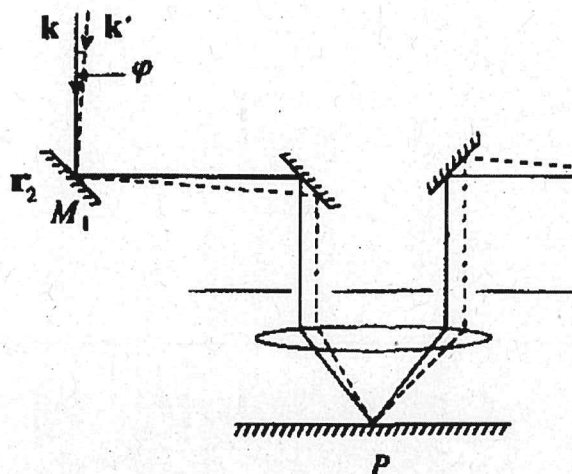
$\hookrightarrow$  the first order correlation function thus determines the visibility of the interference fringes

- as a further application of the theory of optical coherence and photon detection we discuss now Michelson's star interferometer

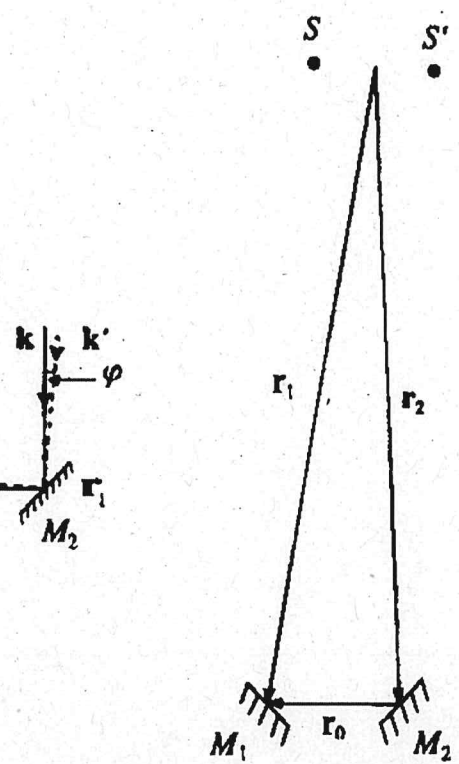




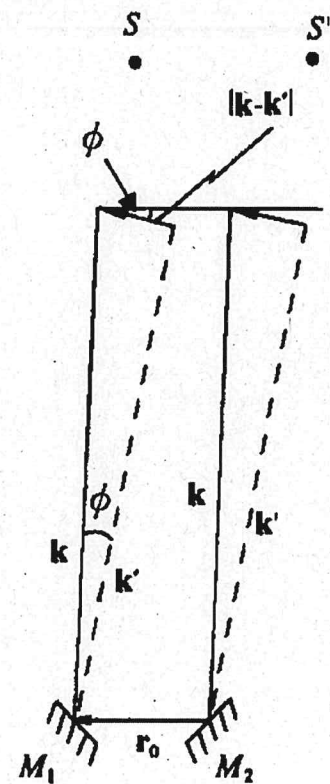
(a)



(b)



(c)



(d)

Taken from

Scully M.O. and Zubairy M.S.  
Quantum optics  
Cambridge University Press  
1997

The goal is to determine the angular separation  $\psi$  of two stars

We assume that the light is filtered, so that the wave vectors  $\vec{k}$  and  $\vec{k}'$  only differ direction but not in length (frequency)

The idea is to interfere the light that arrives from the stars at two different points ( $\vec{r}_1$  and  $\vec{r}_2$ ) on earth

This is achieved by using mirrors which divert the light rays arriving at the two points such that they meet at point P

here the intensity is

$$I_P \propto \langle |E_k (e^{i\vec{k} \cdot \vec{r}_1} + e^{i\vec{k} \cdot \vec{r}_2}) + E_{k'} (e^{i\vec{k}' \cdot \vec{r}_1} + e^{i\vec{k}' \cdot \vec{r}_2})|^2 \rangle$$

We assumed here that

$$\langle E_k^* E_{k'} \rangle = 0, \quad \text{which is valid for light emitted from 2 different stars}$$

assuming

$$|E_k|^2 = |E_{k'}|^2 \propto 2 + \cos(\vec{k} \cdot (\vec{r}_1 - \vec{r}_2)) + \cos(\vec{k}' \cdot (\vec{r}_1 - \vec{r}_2))$$

$$= 1 + \cos((\vec{k} + \vec{k}') \cdot \frac{(\vec{r}_1 - \vec{r}_2)}{2}) \cos((\vec{k} - \vec{k}') \cdot \frac{(\vec{r}_1 - \vec{r}_2)}{2})$$

$$\begin{aligned} \text{using } |\vec{k} - \vec{k}'| &= \sqrt{|\vec{k}|^2 + |\vec{k}'|^2 - 2\vec{k} \cdot \vec{k}'} = |\vec{k}| \cdot \sqrt{1 - \cos\psi} \\ &\approx |\vec{k}| \psi \end{aligned}$$

$$\text{and } (\vec{k} - \vec{k}') \cdot (\vec{r}_1 - \vec{r}_2) \approx |\vec{k} - \vec{k}'| \underbrace{|\vec{r}_1 - \vec{r}_2|}_{\text{d... distance between points from which light is interfered}} \approx |\vec{k}| \cdot d \psi$$

d... distance between points from which light is interfered

$$\hookrightarrow I_p \propto 1 + \underbrace{\cos\left(\frac{1}{2}(\vec{k} + \vec{k}') \cdot (\vec{r}_1 - \vec{r}_2)\right)}_{\text{interference term}} \cdot \underbrace{\cos\left(\frac{1}{2}kld \varphi\right)}_{\text{variation of } d}$$

(99)

variation of  $d$   
allows to infer  $\varphi$

- while in principle  $\varphi$  can be determined by varying the distance  $d$  between the mirrors, this scheme has a practical problem
- fluctuations in the atmospheric density lead to fluctuations in  $\vec{k}$  and  $\vec{k}'$   
these cancel in  $\vec{k} - \vec{k}'$  but not in  $\vec{k} + \vec{k}'$  and lead to a fluctuating prefactor  $\cos\left(\frac{1}{2}(\vec{k} + \vec{k}') \cdot (\vec{r}_1 - \vec{r}_2)\right)$ , which reduces the interference signal
- in fact, one can devise an interferometric scheme which removes the dependence on  $\vec{k} + \vec{k}'$
- this makes use of second order correlations that can be picked up by two spatially separated detectors; this is called the Hanbury-Brown-Twiss effect
- we consider two detector, positioned at  $\vec{r}_1$  and  $\vec{r}_2$ , with  $d = |\vec{r}_1 - \vec{r}_2|$

- the detected intensity correlations (at equal time) are proportional to  $G^{(2)}(\vec{r}_1, \vec{r}_2; t, t)$
- lets assume the two stars are sending out a photon each, i.e. the light field is described by the two-photon state  $|l_e l_{e'}\rangle$   
one photon in mode  $e$   
and one photon in mode  $e'$
- we then find

$$G^{(2)}(\vec{r}_1, \vec{r}_2; t, t) = \langle l_e l_{e'} | E^{(-)}(\vec{r}_1, t) E^{(-)}(\vec{r}_2, t) \underbrace{E^{(+)}(\vec{r}_2, t) E^{(+)}(\vec{r}_1, t)}_{\text{identity in photon Fock space}} | l_e l_{e'} \rangle$$

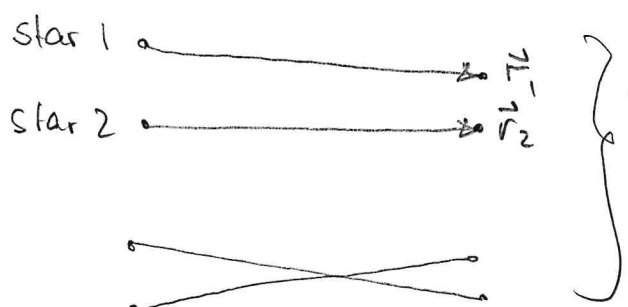
$\sum_{\{n\}} | \{n\} \rangle \langle \{n\} |$   
 $\downarrow$  only vacuum component survives

$$= \underbrace{\langle l_e l_{e'} | E^{(-)}(\vec{r}_1, t) E^{(-)}(\vec{r}_2, t) | 0\rangle_0}_{\Psi^{(2)*}(\vec{r}_1, \vec{r}_2; t)} | E^{(+)}(\vec{r}_2, t) E^{(+)}(\vec{r}_1, t) | l_e l_{e'} \rangle$$

$\Psi^{(2)*}(\vec{r}_1, \vec{r}_2; t) \dots$  two-photon wave function

$$= |\Psi^{(2)}(\vec{r}_1, \vec{r}_2; t)|^2$$

- with  $\Psi^{(2)}(\vec{r}_1, \vec{r}_2; t) \propto e^{-2i\omega t} (\underbrace{\langle 0 | a_k^{+} e^{ik \cdot \vec{r}_1} a_k^{+} e^{ik \cdot \vec{r}_2} | l_e l_{e'} \rangle}_{\omega = c|k|} + \underbrace{\langle 0 | a_k^{+} e^{ik \cdot \vec{r}_1} a_k^{+} e^{ik \cdot \vec{r}_2} | l_e l_{e'} \rangle}_{\text{amplitudes of two different pathways}})$



amplitudes of two  
different pathways

$$\hookrightarrow \Psi^{(2)}(\vec{r}_1, \vec{r}_2, t) \propto e^{-i\omega_0 t} (e^{i(\vec{k} \cdot \vec{r}_1 + \vec{k}' \cdot \vec{r}_2)} + e^{i(\vec{k}' \cdot \vec{r}_1 + \vec{k} \cdot \vec{r}_2)}) \quad (101)$$

- This yields

$$G^{(2)}(\vec{r}_1, \vec{r}_2; t) \propto 1 + \underbrace{\cos((\vec{k} - \vec{k}') \cdot (\vec{r}_1 - \vec{r}_2))}$$

interference term only  
depends on  $\vec{k} - \vec{k}'$ !

- to see the "robustness" of  $G^{(2)}$  measurements over  $G^{(1)}$  measurements lets consider the state

$$|4\rangle = \underbrace{|\text{vacuum}\rangle}_{\text{vacuum}} + \underbrace{|1\rangle (e^{i\theta} |1\rangle_{\vec{k}} + e^{i\theta'} |1\rangle_{\vec{k}'})}_{\text{single photon states}} + \underbrace{|2\rangle e^{i\phi} |1\rangle_{\vec{k}} |1\rangle_{\vec{k}'}}_{\text{two photon state}}$$

random phases

- calculating  $G^{(2)}$  yields the same result as above, since only the two photon state contributes for  $G^{(1)}$  one obtains

$$G^{(1)}(\vec{r}_1, \vec{r}_2; t) \propto \text{const} + 2 \cos\left(\frac{\vec{k}(\vec{r}_1 - \vec{r}_2)}{2}\right) \cos\left(\frac{\vec{k}'(\vec{r}_1 - \vec{r}_2)}{2}\right) \\ \times \underbrace{\cos\left(\frac{(\vec{k} - \vec{k}')}{2} \cdot (\vec{r}_1 + \vec{r}_2) - (\theta - \theta')\right)}_{\text{interference term}}$$

- averaging over the random phases, i.e. calculating,  $\frac{1}{2\pi} \int_0^{2\pi} d(\theta - \theta') G^{(1)}(\vec{r}_1, \vec{r}_2; t)$  makes the interference term vanish  $\rightarrow$  no robustness of the  $G^{(1)}$ -signal, unlike for the  $G^{(2)}$ -signal

(102)

- even for thermal light the  $G^{(2)}$  function leads to an interference pattern
  - ↳ defining  $a_{\epsilon}(j) = a_{\epsilon} e^{i k \vec{r}_j}$  yields
- $$G^{(2)} \propto \langle (a_{\epsilon}^+(1) + a_{\epsilon'}^+(1))(a_{\epsilon}^+(2) + a_{\epsilon'}^+(2))(a_{\epsilon}(2) + a_{\epsilon'}(2))(a_{\epsilon}(1) + a_{\epsilon'}(1)) \rangle$$
- This expression simplifies by noting that only contributions which involve pair annihilation and creation operators with the same  $k(k')$  yield a non-zero result; e.g.  $\langle a_{\epsilon}^+(1)a_{\epsilon'}^+(2)a_{\epsilon}(2)a_{\epsilon'}(1) \rangle = 0$

$$\begin{aligned} \hookrightarrow G^{(2)} &\propto \langle a_{\epsilon}^+(1)a_{\epsilon}^+(2)a_{\epsilon}(2)a_{\epsilon}(1) + (k \rightarrow k') \rangle \\ &+ \langle a_{\epsilon}^+(1)a_{\epsilon'}^+(2)(a_{\epsilon}(2)a_{\epsilon'}(1) + a_{\epsilon'}(2)a_{\epsilon}(1)) + (k \rightarrow k') \rangle \\ &\propto \langle (a_{\epsilon}^+)^2 a_{\epsilon}^2 + (a_{\epsilon'}^+)^2 a_{\epsilon'}^2 + \\ &+ a_{\epsilon}^+ a_{\epsilon'}^+ a_{\epsilon} a_{\epsilon'} (1 + e^{-i(\vec{k}-\vec{k}') \cdot (\vec{r}_1 - \vec{r}_2)}) + a_{\epsilon'}^+ a_{\epsilon}^+ a_{\epsilon'} a_{\epsilon} (1 + e^{i(\vec{k}-\vec{k}') \cdot (\vec{r}_1 - \vec{r}_2)}) \rangle \end{aligned}$$

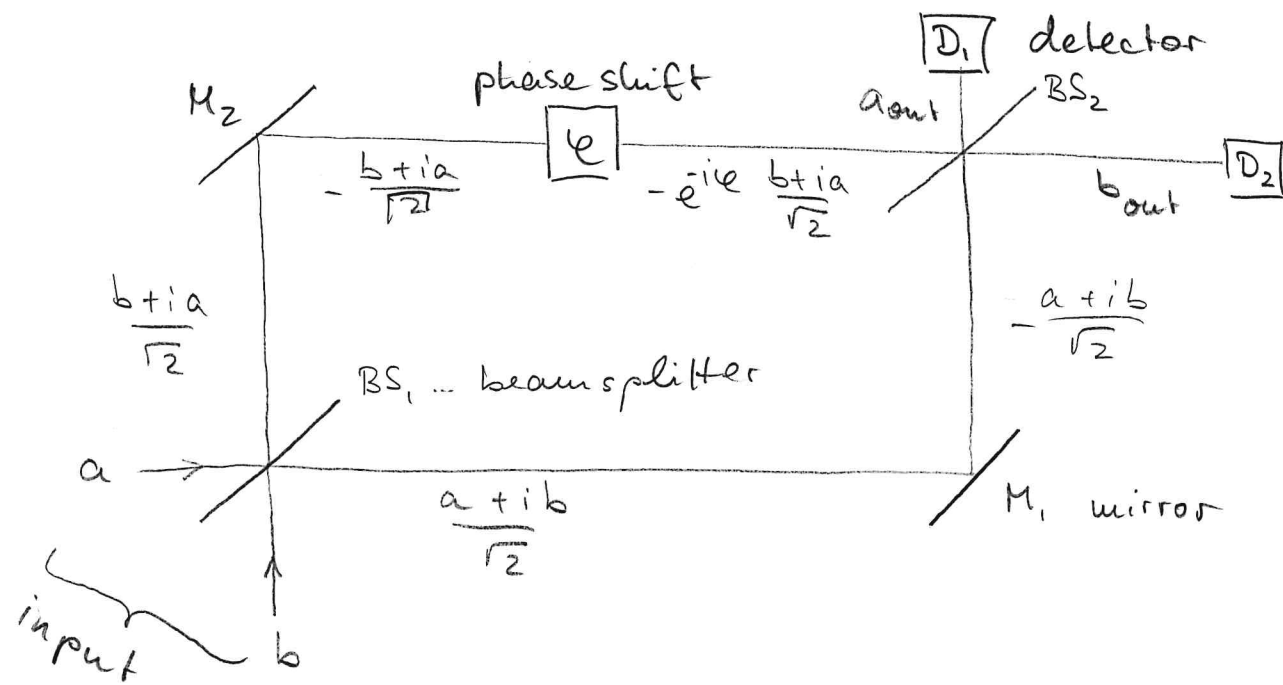
- assuming  $\langle n_{\epsilon} \rangle = \langle n_{\epsilon'} \rangle = \langle n \rangle$  and  $\langle n_{\epsilon}^2 \rangle = \langle n_{\epsilon'}^2 \rangle = \langle n^2 \rangle$ , this yields

$$\begin{aligned} G^{(2)} &\propto [\underbrace{\langle n^2 \rangle - \langle n \rangle}_{= 2\langle n \rangle^2} + \langle n \rangle^2 (1 + \cos((\vec{k}-\vec{k}') \cdot (\vec{r}_1 - \vec{r}_2)))] \\ &= 2\langle n \rangle^2 \text{ for thermal light} \end{aligned}$$

- ↳ "interference" fringes are produced, but not with 100% contrast

### III. 5 Noise in quantum-optical measurements (103)

- we consider a Mach-Zehnder interferometer



- In the ideal case the interferometer generates an interference pattern at each output, which has 100% contrast
- more accurately, the expectation value of the photon number, measured at the detectors exhibits full-contrast oscillations as a function of the parameter  $\varphi$  (phase shift)
- this allows in principle to measure  $\varphi$
- problem: expectation values can only be determined with arbitrary precision if one can conduct infinitely many measurements  
any finite set of measurements will reduce the accuracy with which  $\varphi$  can be determined

- this is due to the presence of quantum noise which leads to fluctuations in the output signal
- question: is it possible to choose specific quantum states of light as input for the interferometer, so that fluctuations are reduced?
- to answer this question let's first formulate a theoretical description of the interferometer
- input modes:  $a; b$
- output modes:  $a_{\text{out}}(D_1); b_{\text{out}}(D_2)$
- after the first beam splitter we have the two modes:  $\frac{1}{\sqrt{2}}(b+ia)$  and  $\frac{1}{\sqrt{2}}(a+ib)$
- reflection from the mirrors results in an overall phase shift of  $\pi$  (minus sign)  
 $\hookrightarrow -\frac{1}{\sqrt{2}}(b+ia)$  and  $-\frac{1}{\sqrt{2}}(a+ib)$
- the phase shift, which is acquired in the upper arm leads to  $e^{-i\phi}\frac{1}{\sqrt{2}}(b+ia)$  and the field in the other arm is unchanged
- at the detectors we then get

$$\begin{aligned}
 a_{\text{out}}(D_1) &= \frac{1}{\sqrt{2}}\left(-\frac{a+ib}{\sqrt{2}} - ie^{-i\phi}\frac{b+ia}{\sqrt{2}}\right) = \frac{1}{2}\left((e^{-i\phi})a - i(-e^{-i\phi} + 1)b\right) \\
 &= -ie^{-i\frac{\phi}{2}}\left(a \sin\left(\frac{\phi}{2}\right) + b \cos\left(\frac{\phi}{2}\right)\right)
 \end{aligned}$$

$$\text{and } b_{\text{out}}(D_2) = \frac{1}{\sqrt{2}} \left( -e^{-i\phi} \frac{b+ia}{\sqrt{2}} - i \frac{a+ib}{\sqrt{2}} \right)$$

$$= i e^{-i \frac{\varphi}{2}} \left( -a \cos\left(\frac{\varphi}{2}\right) + b \sin\left(\frac{\varphi}{2}\right) \right)$$

(105)

- for the number operators at each detector we then obtain

$$a_{out}^+ a_{out}^- = \sin^2 \frac{\varphi}{2} a^+ a + \cos^2 \frac{\varphi}{2} b^+ b + \sin \frac{\varphi}{2} \cos \frac{\varphi}{2} (a^+ b + a b^+)$$

$$b_{\text{out}}^{\dagger} b_{\text{out}} = \cos^2 \frac{\varphi}{2} a^{\dagger} a + \sin^2 \frac{\varphi}{2} b^{\dagger} b - \sin \frac{\varphi}{2} \cos \frac{\varphi}{2} (a^{\dagger} b + a b^{\dagger})$$

- note, that  $a_{\text{out}}^\dagger a_{\text{out}} + b_{\text{out}}^\dagger b_{\text{out}} = a^\dagger a + b^\dagger b$ , i.e. the number of photons is conserved
  - furthermore, note that the phase shift operation on a mode  $c$  is implemented via the unitary operator  $U_\varphi = e^{-i\varphi c}$
  - applying it to a coherent state yields  $U_\varphi |c\rangle = |e^{-i\varphi} c\rangle$ , which shows that a "classical" field is phase-shifted as "expected"
  - for the further discussion let us assume that light is only sent through the input part  $a$  and that the vacuum  $|0\rangle$  enters through part  $b$
  - we then have  $\langle a_{\text{out}}^\dagger a_{\text{out}} \rangle = \sin^2\left(\frac{\varphi}{2}\right) \langle a^\dagger a \rangle$   
and  $\langle b_{\text{out}}^\dagger b_{\text{out}} \rangle = \cos^2\left(\frac{\varphi}{2}\right) \langle a^\dagger a \rangle$

  
interference in the  
output intensity

- to get some insights into the role of noise let's study the difference between the photon counts in both detectors the corresponding operator is

$$\begin{aligned}\delta n_{\text{out}} &= b_{\text{out}}^+ b_{\text{out}} - a_{\text{out}}^+ a_{\text{out}} \\ &= \cos \varphi (a^\dagger a - b^\dagger b) + \sin \varphi (a^\dagger b + b^\dagger a)\end{aligned}$$

- in order to study noise, i.e. fluctuations, we need to evaluate the expectation value of

$$\begin{aligned}(\delta n_{\text{out}})^2 &= \cos^2 \varphi (a^\dagger a - b^\dagger b)^2 + \sin^2 \varphi (a^\dagger b + b^\dagger a)^2 \\ &\quad + \sin^2 \varphi ((a^\dagger a)^2 + (b^\dagger b)^2) + \\ &\quad + \sin \varphi \cos \varphi [(a^\dagger a - b^\dagger b)(a^\dagger b + b^\dagger a) + (a^\dagger b + b^\dagger a)(a^\dagger a - b^\dagger b)]\end{aligned}$$

- if the field entering port  $b$  is in the vacuum, we find that (assuming the input modes are prepared in a product state)

$$\begin{aligned}\langle (\delta n_{\text{out}})^2 \rangle &= \cos^2 \varphi \underbrace{\langle (a^\dagger a)^2 \rangle}_{\substack{\text{zero if} \\ \text{mode } b \\ \text{is in vacuum}}} + \sin^2 \varphi \left( \langle a^\dagger a \rangle \langle b^\dagger b \rangle + \langle a^\dagger b \rangle \langle b^\dagger a \rangle \right) \\ &\quad + 0\end{aligned}$$

quantum fluctuations of mode  $b$ :  $\langle b b^\dagger \rangle = 1$   
 quantum fluctuations of mode  $a$ :  $\langle a^\dagger a \rangle = \langle a^\dagger a \rangle + 1$

- defining  $n_a = a^\dagger a$  and using  $\langle \delta n_{\text{out}} \rangle = \cos \varphi \langle n_a \rangle$ , we find for the variance

$$\Delta \delta n_{\text{out}} = \langle \delta n_{\text{out}}^2 \rangle - \langle \delta n_{\text{out}} \rangle^2 = \underbrace{\cos^2 \varphi \Delta n_a}_{\substack{\text{variance of input} \\ \Delta n_a = \langle n_a^2 \rangle - \langle n_a \rangle^2}} + \sin^2 \varphi \langle n_a \rangle$$

- for the relative uncertainty we thus find

standard deviation →  $\frac{\sqrt{\Delta n_{\text{out}}}}{\langle d_{\text{out}} \rangle} = \frac{\sqrt{\Delta n_a + |\tan \varphi|^2 \langle n_a \rangle}}{\langle n_a \rangle}$

average signal →  $\langle d_{\text{out}} \rangle$

"quantum" uncertainty  
of photon number  
in initial state

contribution  
from  
quantum  
noise in  
mode b

- by sending a Fock state into the input port a we can achieve  $\Delta n_a = 0$

$$\hookrightarrow \frac{\sqrt{\Delta n_{\text{out}}}}{\langle d_{\text{out}} \rangle} = |\tan \varphi| \frac{1}{\sqrt{\langle n_a \rangle}}$$

- the precision with which  $\langle d_{\text{out}} \rangle$  can be determined increases with increasing input photon number; the noise to signal ratio decreases  $\propto \langle n_a \rangle^{-\frac{1}{2}}$

- this square root scaling is often referred to the standard quantum limit
- interestingly, the pre-factor of the  $\langle n_a \rangle^{\frac{1}{2}}$ -term can be improved by choosing particular input states

### III. 6 Introduction to quantum parameter estimation theory

- idea: determine parameters for which there is no immediate quantum observable (phase shift, temperature, external fields)
- to estimate the value of this parameter one measures a (quantum) observable, e.g. photon count rates, which depends on the parameter

#### Classical parameter estimation theory

- let  $p(x|\lambda)$  be the probability distribution of a random variable  $x$  depending on a parameter  $\lambda$
- i.e., given  $\lambda$ , the probability for the value of the random variable to lie in the interval  $[x, x+dx]$  is  $p(x|\lambda)dx$
- we suppose that  $p(x|\lambda)$  is known and that we can draw values  $x_i$  from it
- question: what is the best possible estimate for  $\lambda$  that can be obtained by drawing  $M$  samples?
- to formalise the question, we define the estimator function  $\hat{\lambda}$ :

$$\mathbb{R}^M \rightarrow \mathbb{R}; \quad \underbrace{\vec{x} = (x_1, \dots, x_M)}_{\text{Samples}} \rightarrow \underbrace{\hat{\lambda}(x_1, \dots, x_M)}_{\text{estimator function, which depends on sample}}$$

- note, we assume that the samples are drawn independently, i.e. the probability distribution factorises:

$$p(\vec{x}|\lambda) = \prod_{i=1}^n p(x_i|\lambda)$$

- the estimator function is a random variable itself due to its dependence on the random variables  $x_i$ :
- we request now that  $\hat{\lambda}$  shall be unbiased, i.e. its expectation value corresponds to the value of the sought parameter:

$$E(\hat{\lambda}(\vec{x})) = \int d\vec{x} p(\vec{x}|\lambda) \hat{\lambda}(\vec{x}) = \lambda$$

- moreover, we want that its mean square error (variance),  $E(\lambda) = E[(\hat{\lambda}-\lambda)^2]$ , is minimal
- such optimal estimator function saturates the so-called Cramér-Rao bound:

$$E(\lambda) \geq \frac{1}{M F(\lambda)} \quad \left. \begin{array}{l} \text{for an optimal estimator} \\ \text{number of samples } M \end{array} \right\} \begin{array}{l} \text{function the "}" sign} \\ \text{holds} \end{array}$$

$\uparrow$   
Fisher information

with the Fisher information being defined as

$$F(\lambda) = \underbrace{\int d\vec{x} p(\vec{x}|\lambda) \left( \frac{\partial \ln(p(\vec{x}|\lambda))}{\partial \lambda} \right)^2}_{E(V^2(\vec{x}|\lambda))} = \int d\vec{x} \frac{1}{p(\vec{x}|\lambda)} \left( \frac{\partial p(\vec{x}|\lambda)}{\partial \lambda} \right)^2$$

- the Fisher information is the expectation value of the square of the so-called score function :  $V(\vec{x}|\lambda) = \frac{\partial \ln(p(\vec{x}|\lambda))}{\partial \lambda}$

- the Cramer - Rao bound can be proven as follows
- using Schwartz' inequality ( $|\vec{a} \cdot \vec{b}|^2 \leq \|\vec{a}\|^2 \|\vec{b}\|^2$ ) one has

$$\begin{aligned} E([V(\vec{x}|\lambda) - E(V(\vec{x}|\lambda))] [\hat{\lambda} - E(\hat{\lambda})])^2 &\leq \\ &\leq \underbrace{E([V(\vec{x}|\lambda) - E(V(\vec{x}|\lambda))]^2)}_{\mathcal{E}(V(\vec{x}|\lambda))} \underbrace{E([\hat{\lambda} - E(\hat{\lambda})]^2)}_{\mathcal{E}(\hat{\lambda}(\vec{x}))} \quad (*) \end{aligned}$$

(here  $\vec{a} \cdot \vec{b} \triangleq \int d\vec{x} p(\vec{x}|\lambda) a^*(\vec{x}) b(\vec{x})$ )

- furthermore, one finds that

$$\begin{aligned} E(V(\vec{x}|\lambda)) &= \int d\vec{x} p(\vec{x}|\lambda) \frac{\partial \ln(p(\vec{x}|\lambda))}{\partial \lambda} = \int d\vec{x} \frac{\partial}{\partial \lambda} p(\vec{x}|\lambda) \\ &= \frac{\partial}{\partial \lambda} \int d\vec{x} p(\vec{x}|\lambda) = \frac{\partial}{\partial \lambda} 1 = 0 \end{aligned}$$

$$\begin{aligned} \hookrightarrow E(V(\vec{x}|\lambda) [\hat{\lambda} - E(\hat{\lambda})])^2 &= E(V(\vec{x}|\lambda) \hat{\lambda})^2 \\ &= \left( \int d\vec{x} p(\vec{x}|\lambda) \frac{\partial p(\vec{x}|\lambda)}{\partial \lambda} \frac{1}{p(\vec{x}|\lambda)} \hat{\lambda}(\vec{x}) \right)^2 \\ &= \left( \frac{\partial}{\partial \lambda} \int d\vec{x} p(\vec{x}|\lambda) \hat{\lambda}(\vec{x}) \right)^2 = \left( \frac{\partial}{\partial \lambda} E(\hat{\lambda}) \right)^2 \end{aligned}$$

- from (\*) we then find

$$\underbrace{(E(V(\vec{x}|\lambda) [\hat{\lambda} - E(\hat{\lambda})]))}_{\left( \frac{\partial}{\partial \lambda} E(\hat{\lambda}) \right)^2} - E(V(\vec{x}|\lambda)) \underbrace{E(\hat{\lambda} - E(\hat{\lambda}))^2}_{=0 \text{ for unbiased estimator}} \leq \mathcal{E}(V(\vec{x}|\lambda)) \mathcal{E}(\hat{\lambda})$$

$\left( \frac{\partial}{\partial \lambda} E(\hat{\lambda}) \right)^2 = \left( \frac{\partial}{\partial \lambda} \frac{1}{4} \right)^2 = 1$  if estimator is unbiased

Fisher information for factorising probability distribution

$$p(\vec{x}|\lambda) = \prod_{i=1}^M p(x_i|\lambda)$$

$$F(p(\vec{x}|\lambda)) = \int d\vec{x} \sum_{i=1}^M p(x_i|\lambda) \left( \frac{\partial \ln p(x_i|\lambda)}{\partial \lambda} \right)^2$$

$$= \int d\vec{x} \sum_{i=1}^M p(x_i|\lambda) \left( \sum_{k=1}^M \frac{\partial \ln p(x_k|\lambda)}{\partial \lambda} \right)^2$$

$$= \int d\vec{x} p(\vec{x}|\lambda) \sum_k \left( \frac{\partial \ln p(x_k|\lambda)}{\partial \lambda} \right)^2$$

$$+ \underbrace{\int d\vec{x} p(\vec{x}|\lambda) \sum_{k \neq m} \frac{\partial \ln p(x_k|\lambda)}{\partial \lambda} \frac{\partial \ln p(x_m|\lambda)}{\partial \lambda}}$$

$$\underbrace{\sum_{k \neq m} \int dx_k dx_m p(x_k|\lambda) p(x_m|\lambda) \frac{\partial \ln p(x_k|\lambda)}{\partial \lambda} \frac{\partial \ln p(x_m|\lambda)}{\partial \lambda}}$$

$$\left[ \int dx p(x|\lambda) \frac{\partial \ln p(x|\lambda)}{\partial \lambda} \right]^2 = \left[ \int dx \frac{p(x|\lambda)}{p(x|\lambda)} \frac{\partial p(x|\lambda)}{\partial \lambda} \right]^2$$

$$= \left[ \frac{\partial}{\partial \lambda} \int dx p(x|\lambda) \right]^2$$

$$= \left[ \frac{\partial}{\partial \lambda} 1 \right]^2 = 0$$

$$= \sum_{k=1}^M \int d\vec{x} p(\vec{x}|\lambda) \left( \frac{\partial \ln p(x_k|\lambda)}{\partial \lambda} \right)^2$$

$$= M \underbrace{\int dx p(x|\lambda) \left( \frac{\partial \ln p(x|\lambda)}{\partial \lambda} \right)^2}_{F(p(x|\lambda))}$$

Fisher information of  $p(x|\lambda)$

• using now that

(III)

$$\begin{aligned} E(V(\vec{x}|\lambda)) &= E(V(\vec{x}|\lambda)^2) - \underbrace{E(V(\vec{x}|\lambda))^2}_{=0} = M E(V(x,\lambda)^2) \\ &= M F(\lambda) \end{aligned}$$

we find  $1 \leq M F(\lambda) \cdot E(\hat{\lambda})$ , which yields the Cramér-Rao Bound

- in order to obtain estimates for functions, one can employ the method of maximum likelihood
- to this end one computes

$$p(\vec{x}|\lambda) = \prod_{i=1}^n p(x_i|\lambda)$$

and maximises its logarithm, which is called the "log-likelihood":

$$\ln \underbrace{L(\lambda|\vec{x})}_{\text{likelihood of } \lambda \text{ given } \vec{x}} = \ln p(\vec{x}|\lambda) = \sum_{i=1}^n \ln p(x_i|\lambda),$$

with respect to  $\lambda$

- as an example we consider a Gaussian distribution  $p(x|\mu, \sigma^2) = \frac{1}{\sqrt{2\pi\sigma^2}} e^{-\frac{(x-\mu)^2}{2\sigma^2}}$ , whose parameters are the mean  $\mu$  and the variance  $\sigma^2$

- the probability for obtaining a sequence of measurement outcomes  $\vec{x}$  is given

by  $p(\vec{x}|\mu, \sigma) = \prod_{i=1}^n p(x_i|\mu, \sigma) = \left(\frac{1}{2\pi\sigma^2}\right)^{\frac{n}{2}} e^{-\frac{1}{2\sigma^2} \sum_{i=1}^n (x_i - \mu)^2}$

$\hookrightarrow \ln L(\mu, \sigma | \vec{x}) = -\frac{n}{2} \ln(2\pi\sigma^2) - \frac{1}{2\sigma^2} \sum_i (x_i - \mu)^2$

$\hookrightarrow$  maximisation:  $0 = \frac{\partial}{\partial \mu} \ln L(\mu, \sigma | \vec{x}) = \frac{1}{\sigma^2} \sum_i (x_i - \mu)$

$$\hookrightarrow \sum_i x_i = n\mu$$

- from this follows that the maximum likelihood estimator  $\hat{\mu}(\vec{x})$  for  $\mu$  is given by  $\hat{\mu}(\vec{x}) = \frac{1}{n} \sum_{i=1}^n x_i$
- since  $E(\hat{\mu}) = \mu$  this estimator is unbiased
- an estimator for the variance we obtain via

$$0 = \frac{\partial}{\partial \sigma} \ln L(\mu, \sigma | \vec{x}) = -\frac{n}{\sigma} + \frac{1}{\sigma^3} \sum_{i=1}^n (x_i - \mu)^2$$

$$\hookrightarrow \sigma^2 = \frac{1}{n} \sum_{i=1}^n (x_i - \mu)^2$$

- hence, a good estimator for the variance appears to be  $\hat{\sigma}^2 = \frac{1}{n} \sum_{i=1}^n (x_i - \mu)^2$

+ inserting the estimator for  $\mu$  yields

$$\hat{\sigma}^2 = \frac{1}{M} \sum_{i=1}^M x_i^2 - \frac{1}{M^2} \sum_{i,j=1}^M x_i x_j$$

+ to check for a possible bias we evaluate

$$\begin{aligned} E(\hat{\sigma}^2) &= \frac{1}{M} \sum_{i=1}^M E(x_i^2) - \frac{1}{M^2} \sum_{i=1}^M E(x_i^2) - \frac{1}{M^2} \sum_{i \neq j} E(x_i) E(x_j) \\ &= \mu^2 + \sigma^2 - \frac{1}{M} (\mu^2 + \sigma^2) - \frac{M(M-1)}{M^2} \mu^2 \\ &= \frac{M-1}{M} \sigma^2 \quad \left. \begin{array}{l} \text{the current estimator is biased} \\ \text{when } M \text{ is finite} \end{array} \right\} \end{aligned}$$

- a non-biased estimator can be constructed via

$$(\hat{\sigma}^2)_0 = \frac{1}{M-1} \sum_{i=1}^M (x_i - \mu)^2$$

↑ unbiased maximum likelihood  
estimate of  $\sigma^2$ , not the empirical  
estimate of  $\sigma^2$

## Quantum parameter estimation theory

(114)

- in quantum mechanics all information on a system is contained in the density matrix  $\rho$
- measurements can be described with the help of a POVM (positive operator-valued measure)
- a POVM is a set of positive operators  $M_x$ , which "return" the outcome  $x$
- POVM measurements are generalisations of projective von Neumann measurements

$$\hat{A} = \sum_i a_i \underbrace{|i\rangle\langle i|}_\text{projector that "collapses" state when outcome $a_i$ is measured}$$

↑  
measurement operator  
(possible measurement outcome)

- when using a POVM the probability to find the outcome  $x$  is  $p(x) = \text{tr}(\rho M_x)$ ; in the above example with measurement operator  $\hat{A}$ , we have  $M_x = |x\rangle\langle x|$
  - the operators  $M_x$  obey the relation  $\sum_x M_x = \mathbb{1}$ , or for a continuous parameter
- $$\int dx M_x = \mathbb{1}$$
- given that the  $M_x$  are positive, they can be written as  $M_x = K_x^+ K_x$
  - when a measurement yields outcome  $x$ , the state collapses  $\rho \mapsto \frac{K_x \rho K_x^+}{\text{tr}(K_x \rho K_x^+)} = \frac{1}{p(x)} K_x \rho K_x^+$

- suppose the state on which we perform a measurement depends parametrically on  $\lambda : \mathcal{S} \rightarrow \mathcal{S}_\lambda$

- we then get for the probability to measure the value  $x$

$$p(x|\lambda) = \text{tr}(M_x \rho_\lambda)$$

- we can use this expression to calculate the Fisher information

$$\begin{aligned} F(\lambda) &= \int dx \frac{1}{p(x|\lambda)} \left( \frac{\partial p(x|\lambda)}{\partial \lambda} \right)^2 \\ &= \int dx \frac{1}{\text{tr}(M_x \rho_\lambda)} \left( \text{tr} \left( M_x \frac{\partial \rho_\lambda}{\partial \lambda} \right) \right)^2 \end{aligned}$$

- in order to compute the derivative of  $\rho_\lambda$  we introduce a hermitian operator  $L_\lambda$ , which satisfies the relation

$$\frac{\partial}{\partial \lambda} \rho_\lambda = \frac{1}{2} (L_\lambda \rho_\lambda + \rho_\lambda L_\lambda) \leftarrow \begin{array}{l} \text{implicit} \\ \text{equation} \\ \text{for } L_\lambda \end{array}$$

- $L_\lambda$  is called symmetric logarithmic derivative
- it can be considered as a "quantum score", which generalises the classical score function

$$\begin{aligned} V(x|\lambda) &: \text{tr} \left( M_x \frac{\partial \rho_\lambda}{\partial \lambda} \right) = \frac{1}{2} \left( \underbrace{\text{tr} (M_x L_\lambda \rho_\lambda)}_{\text{tr} (\rho_\lambda M_x L_\lambda)} + \underbrace{\text{tr} (M_x \rho_\lambda L_\lambda)}_{\text{tr} (L_\lambda M_x \rho_\lambda)} \right) = \text{tr} (\rho_\lambda (L_\lambda M_x)^*) \\ &= \text{Re} \{ \text{tr} (\rho_\lambda M_x L_\lambda) \} = \frac{\partial}{\partial \lambda} p(x|\lambda) = \text{tr} (\rho_\lambda M_x L_\lambda)^* \end{aligned}$$

$$\hookrightarrow F(\lambda) = \int dx \frac{1}{\text{tr}(g_\lambda M_x)} \text{Re} \left\{ \text{tr}(g_\lambda M_x L_\lambda) \right\}^2$$

- in the next step we aim to derive an upper bound for  $F(\lambda)$
- to this end we define the operators

$$A^\dagger = \frac{\sqrt{g_\lambda} \sqrt{M_x}}{\text{tr}(g_\lambda M_x)} \quad \text{and} \quad B = \sqrt{M_x} L_\lambda \sqrt{g_\lambda}$$

- This allows us to write

$$\begin{aligned} F(\lambda) &= \int dx \text{Re} \left\{ \text{tr}(A^\dagger B) \right\}^2 \leq \int dx |\text{tr}(A^\dagger B)|^2 \\ &\leq \int dx \text{tr}(A^\dagger A) + \text{tr}(B^\dagger B) \end{aligned}$$

- with  $\text{tr}(A^\dagger A) = \frac{\text{tr}(g_\lambda M_x)}{\text{tr}(g_\lambda M_x)} = 1$  and  $\text{tr}(B^\dagger B) = \text{tr}(M_x L_\lambda g_\lambda L_\lambda)$

one obtains

$$\begin{aligned} F(\lambda) &\leq \int dx \text{tr}(M_x L_\lambda g_\lambda L_\lambda) = \text{tr} \left( \underbrace{\int dx M_x L_\lambda}_{\mathbb{1}} g_\lambda L_\lambda \right) \\ &= \text{tr}(g_\lambda L_\lambda^2) \equiv F_g(\lambda) \end{aligned}$$

- the upper bound of  $F(\lambda)$  is given by the so-called quantum Fisher information  $F_g(\lambda)$
- $F_g(\lambda)$  can exhibit a scaling behaviour which allows to obtain signal to noise ratios that surpass the standard quantum limit

- to make this statement more concrete we consider in the following states of the form

$$g_\lambda = e^{-i\lambda X} |4\rangle \langle 4| e^{i\lambda X}$$

↗ hermitian operator  
 ↙ parameters  
 ↘ pure state that is to  
 (not dependent on  $\lambda$ ) be estimated

- here the parameter  $\lambda$  is imprinted on the state  $|4\rangle$  with a unitary involving the "generator"  $X$  (see e.g. phase shift discussed in the context of interferometry)
- for the sake of simplicity we focus on pure states at first
- to calculate the quantum Fisher information we need to compute the symmetric logarithmic derivative,  $L_\lambda$ , which satisfies

$$\begin{aligned} \frac{\partial}{\partial \lambda} g_\lambda &= -iX g_\lambda + i g_\lambda X = \frac{1}{2} (L_\lambda g_\lambda + g_\lambda L_\lambda) \\ &= -iX |4_\lambda \rangle \langle 4_\lambda| + i |4_\lambda \rangle \langle 4_\lambda| X = \frac{1}{2} (L_\lambda |4_\lambda \rangle \langle 4_\lambda| + |4_\lambda \rangle \langle 4_\lambda| L_\lambda) \end{aligned}$$

- to construct  $L_\lambda$  we introduce the set of states  $|\xi\rangle$ , which is orthogonal to  $|4_\lambda\rangle$ , i.e.  $\langle \xi | 4_\lambda \rangle = 0$
- multiplying the above expression from the left with  $\langle \xi |$  then yields

$$\langle \xi | L_\lambda | 4_\lambda \rangle \langle 4_\lambda | = -2i \langle \xi | X | 4_\lambda \rangle \langle 4_\lambda |$$

- likewise, multiplication from the right by  $|g\rangle\langle g|$  yields (118)

$$|4_\lambda X 4_\lambda| L_\lambda |g\rangle = 2 |4_\lambda X 4_\lambda| X |g\rangle$$

- we can thus construct  $L_\lambda$  as

$$L_\lambda = 2i \sum_g (|4_\lambda X 4_\lambda| X |g\rangle\langle g| - |g\rangle\langle g| X |4_\lambda X 4_\lambda|)$$

- the quantum Fisher information is then given by

$$\begin{aligned} F_q(\lambda) &= \text{tr}(S_\lambda L_\lambda^2) = \langle 4_\lambda | L_\lambda^2 | 4_\lambda \rangle \\ &= 4 \sum_{gg'} \langle 4_\lambda | (|4_\lambda X 4_\lambda| X |g\rangle\langle g| |g'\rangle\langle g'| X |4_\lambda X 4_\lambda|) | 4_\lambda \rangle \\ &= 4 \langle 4_\lambda | X \left( \sum_g |g\rangle\langle g| \right)^2 X | 4_\lambda \rangle \\ &= 4 \langle 4_\lambda | X (\mathbb{I} - |4_\lambda X 4_\lambda|) X | 4_\lambda \rangle \\ &= 4 (\langle 4_\lambda | X^2 | 4_\lambda \rangle - |\langle 4_\lambda | X | 4_\lambda \rangle|^2) = 4 (\Delta X)^2 \end{aligned}$$

↳ the quantum Fisher information is four times the variance of generator  $X$

- for a general state, which has the decomposition

$$S_\lambda = \sum_{i=1}^s p_i |4_i X 4_i|$$

$$F_q(\lambda) = \underbrace{\sum_{i=1}^s \frac{1}{p_i} \left( \frac{\partial}{\partial \lambda} p_i \right)^2}_{\text{classical Fisher information}} + \underbrace{\sum_{i=1}^s 4 p_i \left\langle \frac{\partial}{\partial \lambda} 4_i \middle| \frac{\partial}{\partial \lambda} 4_i \right\rangle - \sum_{i,j=1}^s \frac{8 p_i p_j}{p_i + p_j} \left| \left\langle 4_i \middle| \frac{\partial}{\partial \lambda} 4_j \right\rangle \right|^2}_{\text{quantum contribution}}$$

classical  
Fisher information

quantum contribution

- let us now investigate in what sense quantum effects, as quantified by the quantum Fisher information, allow us to perform measurements whose uncertainty is smaller than the standard quantum limit
- for the variance of an estimator for  $\lambda$  we found the Cramér-Rao bound

$$E(\lambda) \geq \frac{1}{M F(\lambda)} \geq \frac{1}{M F_q(\lambda)} = \frac{1}{4M(\Delta X)^2}$$

↑                      ↑                      ↑  
 number of      classical      quantum      variance of the  
 measurements      Fisher      Fisher      generator  $X$ :  
 information      information       $S_X = e^{-i\lambda X} / 4 \times 4! e^{i\lambda X}$

- suppose now that the state  $|4\rangle$  is the state of a system that is composed of  $N$  constituents, e.g.  $N$  spins, which is prepared in a product state:  $|4\rangle = \bigotimes_{i=1}^N |4\rangle_i = |4\rangle_1 |4\rangle_2 \dots |4\rangle_N = |4\rangle^{\otimes N}$

- the generator shall be the sum of single particle operators:  $X = \sum_{i=1}^N X_i$  (the  $X_i$  could be Pauli-matrices and  $\lambda$  could be the strength of an applied magnetic field)

- we then have  $(\Delta X)^2 = \underbrace{\langle 4 | \left( \sum_{i=1}^N X_i \right)^2 | 4 \rangle}_{N \langle x^2 \rangle + (N^2 - N) \langle x \rangle^2} - \underbrace{\left( \sum_{i=1}^N \langle 4 | X_i | 4 \rangle \right)^2}_{N^2 \langle x \rangle^2}$   
 $= N (\Delta x)^2$

$$\hookrightarrow E(\lambda) \geq \frac{1}{4MN(\Delta x)^2}$$

↓                      ↓  
 minimal achievable variance  
 scales with  $N^{-1}$ , which is  
 the standard quantum limit

(120)

- the scaling of  $(\Delta X)^2 \propto N$  is a manifestation of the central limit theorem given that  $X$  is a sum of random variables, which are independently distributed due to the fact that the system was prepared in a product state
- in the following we show that it is possible to prepare quantum correlated states which lead to a "better" scaling
- we consider the state (which is called GHZ-state)  
Greenberger-Horne-Zeilinger

$$|GHZ\rangle = \frac{1}{\sqrt{2}} \left( \underbrace{|-\xi\rangle_1 |-\xi\rangle_2 \dots |-\xi\rangle_N}_{|-\xi\rangle^{\otimes N}} + \underbrace{|+\xi\rangle_1 |+\xi\rangle_2 \dots |+\xi\rangle_N}_{|+\xi\rangle^{\otimes N}} \right),$$

where the single particle states are orthogonal eigenstates of  $x_i$ :  $x_i |\pm \xi\rangle_i = \pm \xi |\pm \xi\rangle_i$ ,  $\langle -\xi | \xi \rangle_i = 0$

$$\begin{aligned} \text{we find } \langle GHZ | X | GHZ \rangle &= \langle GHZ | \sum_i x_i | GHZ \rangle \\ &= \langle GHZ | \frac{1}{\sqrt{2}} (-N\xi | -\xi \rangle^{\otimes N} + N\xi | +\xi \rangle^{\otimes N}) = 0 \end{aligned}$$

$$\begin{aligned} \text{and } \langle GHZ | X^2 | GHZ \rangle &= \langle GHZ | \frac{1}{\sqrt{2}} (N^2 \xi^2 | -\xi \rangle^{\otimes N} + N^2 \xi^2 | +\xi \rangle^{\otimes N}) \\ &= N^2 \xi^2 \langle GHZ | GHZ \rangle = N^2 \xi^2 \end{aligned}$$

$$\hookrightarrow (\Delta X)^2 = N^2 \xi^2$$

- we thus obtain for the Cramér-Rao bound

$$E(\lambda) \geq \frac{1}{4MN^2\sigma^2} \propto \frac{1}{N^2}$$

- the GHZ state yields a  $\frac{1}{N^2}$  scaling, instead of  $\frac{1}{N}$ ,
- the minimal achievable variance is thus proportional to  $N^{-2}$ , which is referred to as the Heisenberg limit
- the enhancement of accuracy is related to the fact that the  $|GHZ\rangle$  state is an entangled state
- such states are challenging to prepare but they enable in principle quantum enhanced measurements

IV.1 Interaction between an atom and an electromagnetic field

- we consider an atom with a single active electron, e.g. hydrogen

- the Hamiltonian in the absence of external fields is given by

$$H_0 = \frac{1}{2m} \vec{p}^2 + V(\vec{r})$$

momentum operator  
 position operator  
 of electron (relative motion)

(reduced) mass  
 of the electron

interaction potential  
 between electron and ionic core (Coulomb potential in case of hydrogen)

- in the presence of external electromagnetic fields this Hamiltonian modifies to

$$H(\vec{r}, t) = \frac{1}{2m} \left( \vec{p} + e \vec{A}(\vec{r}, t) \right)^2 - e \phi(\vec{r}, t) + V(\vec{r})$$

vector potential      scalar potential  
 electronic charge

- the electric field  $\vec{E}(\vec{r}, t)$  and magnetic field  $\vec{B}(\vec{r}, t)$  are related to the vector potential  $\vec{A}(\vec{r}, t)$  and scalar potential  $\phi(\vec{r}, t)$  via

$$\vec{E}(\vec{r}, t) = -\nabla \phi(\vec{r}, t) - \frac{\partial \vec{A}(\vec{r}, t)}{\partial t}, \quad \vec{B}(\vec{r}, t) = \nabla \times \vec{A}(\vec{r}, t)$$

- note, that these relations are invariant under the gauge transformation
- $$\phi'(\vec{r}_1, t) = \phi(\vec{r}_1, t) - \frac{\partial \chi(\vec{r}_1, t)}{\partial t}, \quad \vec{A}'(\vec{r}_1, t) = \vec{A}(\vec{r}_1, t) + \nabla \chi(\vec{r}_1, t)$$
- ↑  
gauge function

- we will make use of this gauge invariance to simplify the atom-field Hamiltonian at the level of the Schrödinger equation the gauge transformation is implemented through the unitary  $R = \exp(-\frac{i e}{\hbar} \chi(\vec{r}_1, t))$

starting from it  $i\hbar \frac{\partial \psi(\vec{r}_1, t)}{\partial t} = H(\vec{r}_1, t) \psi(\vec{r}_1, t)$   
and applying  $R$ :  $\psi'(\vec{r}_1, t) = R \psi(\vec{r}_1, t)$ , we find

$$i\hbar \frac{\partial}{\partial t} \psi'(\vec{r}_1, t) = H'(\vec{r}_1, t) \psi'(\vec{r}_1, t)$$

with the transformed Hamiltonian

$$H'(\vec{r}_1, t) = R H R^+ - i\hbar R \frac{\partial}{\partial t} R^+ = \frac{1}{2m} (\vec{p} + e \vec{A}'(\vec{r}_1, t))^2 - e \phi'(\vec{r}_1, t) + V(\vec{r})$$

- to proceed, we fix the gauge in which we formulate the original Hamiltonian such that  
 $\nabla \cdot \vec{A} = 0$ , which is called the Coulomb gauge
- in this gauge  $\phi'(\vec{r}_1, t) = 0$  (in the absence of sources) and the Hamiltonian becomes

$$H(\vec{r}_1, t) = \frac{1}{2m} (\vec{p} + e \vec{A}(\vec{r}_1, t))^2 + V(\vec{r}) = \frac{\vec{p}^2}{2m} + \frac{e}{m} \vec{A} \cdot \vec{p} + \frac{e^2}{2m} \vec{A}^2 + V(\vec{r})$$

- applying the gauge transformation the Hamiltonian becomes

$$H'(\vec{r}, t) = \frac{1}{2m} (\vec{p} + e(\vec{A} + \nabla \chi))^2 + e \frac{\partial \chi}{\partial t} + V(\vec{r})$$

- in the Coulomb gauge the vector potential satisfies the wave equation (sources are absent)

$$\nabla^2 \vec{A} - \frac{1}{c^2} \frac{\partial^2}{\partial t^2} \vec{A} = 0$$

which is solved by plane waves

$$\vec{A}(\vec{r}, t) = \vec{A}_0 e^{i(\vec{k} \cdot \vec{r} - \omega t)} + \text{c.c.} \quad (c|\vec{k}| = \omega)$$

- considering that  $|\vec{k}| = \frac{2\pi}{\lambda}$  with  $\lambda = 400 \dots 700 \text{ nm}$  for optical transitions and  $|\vec{r}| \sim 1 \text{ nm}$  for typical states of atoms, we conclude  $\vec{k} \cdot \vec{r} \ll 1$
- we can thus approximate  $\vec{A}(\vec{r}, t) \approx \vec{A}_0 e^{-i\omega t} = \vec{A}(t)$ , which is the so-called dipole approximation
- in the final step we choose the gauge function  $\chi(\vec{r}, t) = -\vec{A}(t) \cdot \vec{r}$
- with  $\nabla \chi(\vec{r}, t) = -\vec{A}(t)$  and  $\frac{\partial \chi(\vec{r}, t)}{\partial t} = -\vec{r} \cdot \frac{\partial \vec{A}}{\partial t} = -\vec{r} \cdot \vec{E}(t)$  this yields the atom-light interaction Hamiltonian in the dipole approximation:

$$\begin{aligned} H &= \frac{\vec{p}^2}{2m} + V(r) + \underbrace{e\vec{r} \cdot \vec{E}}_{-\vec{d} \dots \text{dipole moment}} \\ &= H_0 - \vec{d} \cdot \vec{E}(t) \end{aligned}$$

## 10. 2 Atom driven by a classical light field (125)

- we consider a time-dependent electrical field  $\vec{E}(t) = \vec{E}_0 \cos \omega t$  where  $\omega$  is an optical frequency (this is modelling a laser)
- the Hamiltonian is then given by

$$H = H_0 - \vec{d} \cdot \vec{E}_0 \cos \omega t$$

- using the eigenbasis  $|n\rangle$  of  $H_0$  ( $H_0|n\rangle = \hbar\omega_n|n\rangle$ ) we can write

$$H = \sum_{n'n} |n'X_{n'}| H |nX_n| = \sum_n \hbar\omega_n |nX_n| - \sum_{n'n} \vec{E}_0 \cdot \langle n'|\vec{d}|n\rangle |n'X_{n'}| \cos \omega t$$

- when the eigenstates  $|n\rangle$  are eigenstates of the parity operator  $\Pi^{\dagger} \Pi = \hat{n}$ , i.e.  $\Pi|n\rangle = \pi_n|n\rangle$  with  $|\Pi_n|^2 = 1$ , we find

$$\begin{aligned} \langle n'|\vec{d}|n\rangle &\propto \langle n|\vec{r}|n\rangle = -\langle n|\Pi^{\dagger} \Pi|n\rangle \\ &= -|\Pi_n|^2 \langle n|\vec{r}|n\rangle = -\langle n|\vec{r}|n\rangle \end{aligned}$$

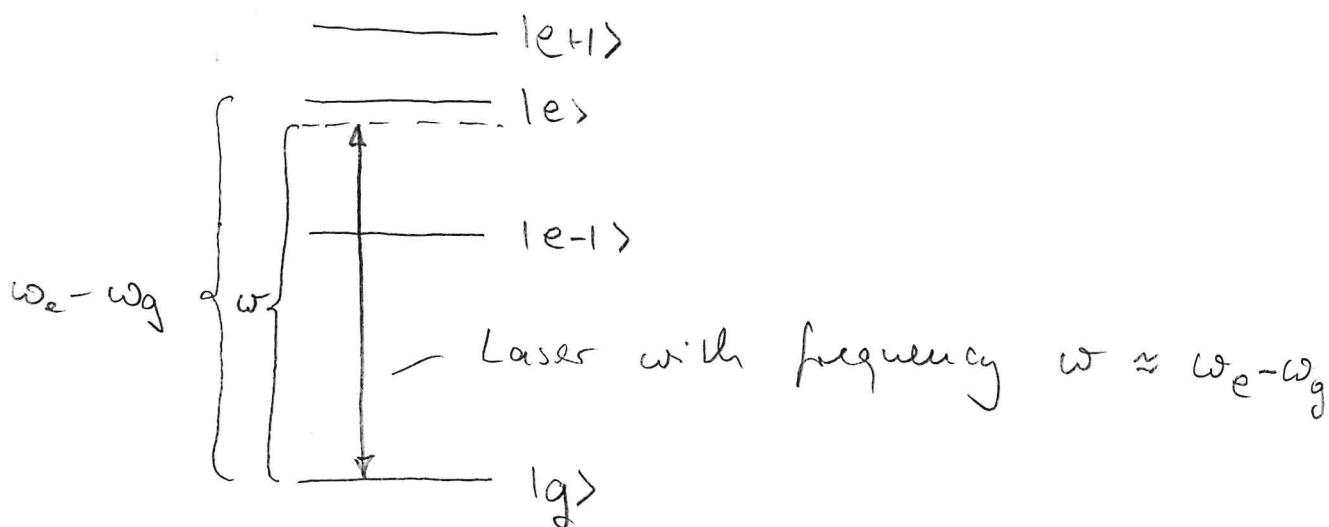
↳  $\langle n|\vec{d}|n\rangle = 0$

- hence, only off-diagonal elements of the dipole operator are non-zero (there is even more structure due to selection rules)

$$\begin{aligned} \hookrightarrow H &= \sum_n \hbar\omega_n |nX_n| - \sum_{n \neq n'} \underbrace{\vec{E}_0 \cdot \langle n'|\vec{d}|n\rangle}_{d_{n'n}} |n'X_{n'}| \cos \omega t \\ &\quad \text{transition dipole moment} \end{aligned}$$

(126)

- in the next step we simplify the problem by assuming that there are only two relevant states participating in the dynamics
- these are referred to as near-resonant states



- within this two-level approximation the Hamiltonian reads

$$H_{\text{2level}} = \omega_g |g\rangle\langle g| + \omega_e |e\rangle\langle e| - (\vec{d}_g \cdot \vec{E}_0 |e\rangle\langle g| + \vec{d}_e \cdot \vec{E}_0 |g\rangle\langle e|) \cos \omega t$$

next, we set  $\omega_g = 0$  and introduce the matrix notation; we also assume  $\vec{d}_g = \vec{d}_e = \vec{d}_0 \in \mathbb{R}$

$$|g\rangle = \begin{pmatrix} 0 \\ 1 \end{pmatrix} \quad \text{and} \quad |e\rangle = \begin{pmatrix} 1 \\ 0 \end{pmatrix}$$

$$\hookrightarrow H_{\text{2level}} = \begin{pmatrix} \omega_e & 0 \\ 0 & 0 \end{pmatrix} - \vec{d}_0 \cdot \vec{E}_0 \begin{pmatrix} 0 & 1 \\ 1 & 0 \end{pmatrix} \cos \omega t$$

- to deal with the time-dependence, we move into a rotating frame, using the unitary

$$R_w = \begin{pmatrix} e^{i\omega t} & 0 \\ 0 & 1 \end{pmatrix}$$

↪  $i\hbar \frac{\partial}{\partial t} |4\rangle = H_{\text{level}} |4\rangle$

↪  $i\hbar R_w \frac{\partial}{\partial t} R_w^+ R_w |4\rangle = R_w H_{\text{level}} R_w^+ R_w |4\rangle$

$|4\rangle$  .. wave function  
in rotating frame

↪  $i\hbar \frac{\partial}{\partial t} |4\rangle = \left[ i\hbar R_w \left( \frac{\partial}{\partial t} R_w^+ \right) + R_w H_{\text{level}} R_w^+ \right] |4\rangle$

$$= \left[ -\hbar \omega \begin{pmatrix} 1 & 0 \\ 0 & 0 \end{pmatrix} + \hbar \omega_e \begin{pmatrix} 1 & 0 \\ 0 & 0 \end{pmatrix} - \vec{d}_o \cdot \vec{E}_o \begin{pmatrix} 0 & e^{i\omega t} \\ e^{-i\omega t} & 0 \end{pmatrix} \cos \omega t \right] |4\rangle$$

$$= \left[ \begin{pmatrix} (\hbar(\omega_e - \omega)) & 0 \\ 0 & 0 \end{pmatrix} - \frac{\vec{d}_o \cdot \vec{E}_o}{2} \begin{pmatrix} 0 & 1 + e^{i2\omega t} \\ 1 + e^{-i2\omega t} & 0 \end{pmatrix} \right] |4\rangle$$

- the terms  $\propto e^{\pm i2\omega t}$  are rapidly oscillating at a frequency which is much faster than the internal dynamics of the two level atom which proceeds on the frequency scales  $\omega_e - \omega$  and  $\frac{\vec{d}_o \cdot \vec{E}_o}{\hbar}$
- these terms thus quickly average out and can be neglected, which is often referred to as rotating wave or secular approximation
- introducing furthermore the detuning:  $\hbar\Delta = \hbar(\omega_e - \omega)$ , and Rabi-frequency:  $\mathcal{R} = -\frac{\vec{d}_o \cdot \vec{E}_o}{2\hbar}$

yields the so-called Rabi model

(128)

$$H_{\text{Rabi}} = \hbar \begin{pmatrix} \Delta & \Omega \\ \Omega & 0 \end{pmatrix}$$

$$= \hbar \Delta \left( \frac{\sigma_z + 1}{2} \right) + \hbar \Omega \sigma^+ + \hbar \Omega \sigma^-$$

with the

Pauli spin matrices  $\sigma_z = \begin{pmatrix} 1 & 0 \\ 0 & -1 \end{pmatrix}$  and  $\sigma^+ = \begin{pmatrix} 0 & 1 \\ 0 & 0 \end{pmatrix}$ ,  $\sigma^- = \begin{pmatrix} 0 & 0 \\ 1 & 0 \end{pmatrix}$

- this model describes the interaction between an atom and a classical laser field
- the strength of the atom-light coupling is parameterised by the Rabi frequency, and the detuning is a measure for how resonant the laser is with respect to the atomic transition:

$$\Delta = \begin{cases} < 0 & \dots \text{red detuned} \\ 0 & \dots \text{resonant} \\ > 0 & \dots \text{blue detuned} \end{cases}$$

- we consider in the following the resonant case,  $\Delta = 0$

$$\hookrightarrow H_{\text{Rabi}} = \hbar \Omega \begin{pmatrix} 0 & 1 \\ 1 & 0 \end{pmatrix} \rightarrow U_{\text{Rabi}} = e^{-iH_{\text{Rabi}}t}$$

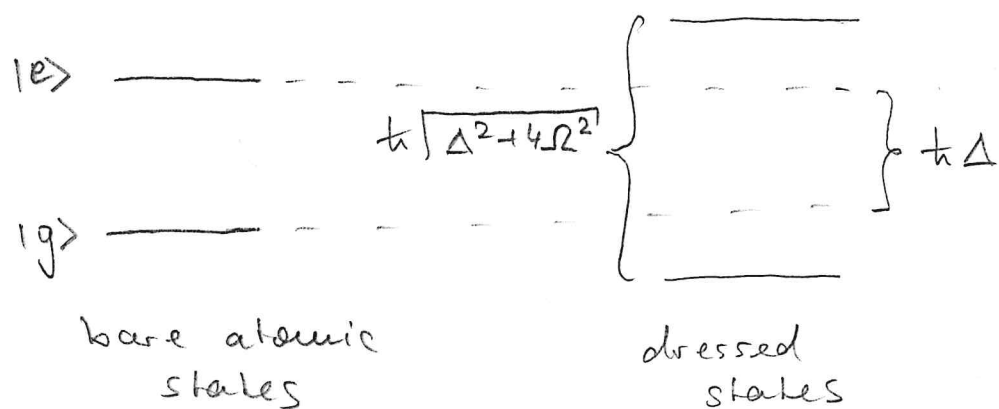
$$= \underbrace{\begin{pmatrix} \cos \Omega t & -i \sin \Omega t \\ -i \sin \Omega t & \cos \Omega t \end{pmatrix}}_{\text{time evolution operator}}$$

- when starting initially in the atomic ground state  $|g\rangle = |0\rangle$ , the application of the laser for a time  $t$  leads to the state

$$|g\rangle_t = U_{\text{Rabi}} |g\rangle = \begin{pmatrix} -i\sin\Omega t \\ \cos\Omega t \end{pmatrix} \\ = \cos\Omega t |g\rangle - i\sin\Omega t |e\rangle$$

- for  $t = \frac{\pi}{2\Omega}$  we thus find the atom in the excited state  $-i|e\rangle$  ( $\pi$ -pulse)
- for  $t = \frac{\pi}{2} \frac{1}{2\Omega}$  we obtain the superposition state  $\frac{1}{\sqrt{2}}(|g\rangle - i|e\rangle)$
- the eigenstates of the Rabi model are often referred to as dressed states
- their eigenenergies (for finite  $\Delta$ ) are given by

$$\mathcal{E}_{\pm} = \frac{\hbar}{2} \left( \Delta \pm \sqrt{\Delta^2 + 4\Omega^2} \right)$$



### IV. 3 Atom interacting with a quantised light field (130)

- we consider a single-mode light field, whose electric field operator (in the Schrödinger picture) is given by

$$\vec{E} = \sqrt{\frac{\hbar\omega}{\epsilon_0 V}} \vec{e} (a + a^\dagger) \underbrace{\sin(kz)}_{\substack{\text{field strength} \\ \text{per photon}}} \underbrace{\vec{e}}_{\substack{\text{polarisation} \\ \text{vector}}} \underbrace{\sin(kz)}_{\substack{\text{position} \\ \text{mode} \\ \text{function} \\ (\text{standing wave})}}$$

- given that the electric field is now a proper degree of freedom we also have to consider its Hamiltonian, which for a single mode is given by  $H_{\text{em}} = \hbar\omega a a^\dagger$  (we neglect the constant zero point energy)

- considering once more the atom with a two level approximation, we find the following Hamiltonian for the atom-light system

$$H_q = \underbrace{\hbar\omega_e n_e}_{\substack{\text{atomic} \\ \text{Hamiltonian}}} + \underbrace{\hbar\omega a a^\dagger}_{\substack{\text{light} \\ \text{Hamiltonian}}} + \underbrace{\lambda (s_+ + s_-)(a + a^\dagger)}_{\substack{\text{atom-light} \\ \text{coupling} \\ \text{Hamiltonian}}}$$

- here  $n_e = |0\rangle\langle 0| = \frac{1}{2}(s_2 + 1)$  is the projector on the excited atomic state and

$$\lambda = \vec{d}_0 \cdot \vec{e} \sqrt{\frac{\hbar\omega}{\epsilon_0 V}} \sin(kz_a) \quad \substack{\text{atomic position}}$$

is the atom-light coupling constant

- to simplify the Hamiltonian, we perform an approximation which resembles the rotating wave approximation
- to justify it, we remember that the creation and annihilation operators evolve under their free evolution as
$$a(t) = a(0) e^{-i\omega t}, \quad a^+(t) = a^+(0) e^{i\omega t}$$
- likewise one finds for the  $\sigma^\pm$ -operators of the atoms

$$\frac{d\sigma^\pm}{dt} = \frac{i}{\hbar} [\hbar\omega_e n_e, \sigma^\pm] = i\omega_e [n_e, \sigma^\pm] = \pm i\omega_e \sigma^\pm$$

$$\hookrightarrow \sigma^\pm(t) = \sigma^\pm(0) e^{\pm i\omega_e t}$$

- the operator products in the interaction term thus have the following time-dependence:

$$\sigma_+^+ a^- \sim e^{i(\omega_e - \omega)t}$$

$$\underbrace{\sigma_-^- a^+ \sim e^{-i(\omega_e - \omega)t}}_{\text{slowly evolving}}$$

$$\sigma_+^+ a^+ \sim e^{i(\omega_e + \omega)t}$$

$$\underbrace{\sigma_-^- a^- \sim e^{-i(\omega_e + \omega)t}}_{\text{rapidly oscillating}}$$

- neglecting the rapidly oscillating terms yields the so-called Jaynes-Cummings model

$$H_{JC} = \hbar\omega_e n_e + \hbar\omega_a a^+ a + \lambda (a^+ \sigma_-^- + a \sigma_+^+)$$

- This Hamiltonian conserves the number of excitations which is represented by the operator

$$N_{ex} = n_e + a^\dagger a$$

$$\begin{aligned} \hookrightarrow [N_{ex}, H_{JC}] &= \lambda [n_e a^\dagger a, \sigma^+ a + \sigma^- a^\dagger] \\ &= \lambda \left( \underbrace{[n_e, \sigma^+] a}_{\sigma^+} + \underbrace{[n_e, \sigma^-] a^\dagger}_{-\sigma^-} + \underbrace{\sigma^+ [a^\dagger a, a]}_{-a} + \underbrace{\sigma^- [a^\dagger a, a^\dagger]}_{a^\dagger} \right) \\ &= 0 \end{aligned}$$

- exploiting this conserved quantity, we can write the Jaynes-Cummings Hamiltonian as

$$H_{JC} = \hbar \omega_e (N_{ex} - a^\dagger a) + \hbar \omega a^\dagger a + \lambda (a^\dagger \sigma^- + a \sigma^+)$$

$$= \hbar \omega_e N_{ex} - \hbar \Delta a^\dagger a + \lambda (a^\dagger \sigma^- + a \sigma^+)$$

$\uparrow$   
detuning  $\omega_e - \omega$

- the ground state of  $H_{JC}$  is  $|g, 0\rangle$

$\uparrow$  atomic state  
 $\downarrow$  photon number

$$\hookrightarrow N_{ex}|g, 0\rangle = 0, a^\dagger a|g, 0\rangle = 0, (a^\dagger \sigma^- + a \sigma^+)|g, 0\rangle = 0$$

$$\hookrightarrow H_{JC}|g, 0\rangle = 0$$

- the excited states can be constructed from the state pairs  $|g, n\rangle, |e, n-1\rangle$  which are both eigenstates of  $N_{ex}$  with eigenvalue  $n$

- representing H<sub>ee</sub> in these pairs yields

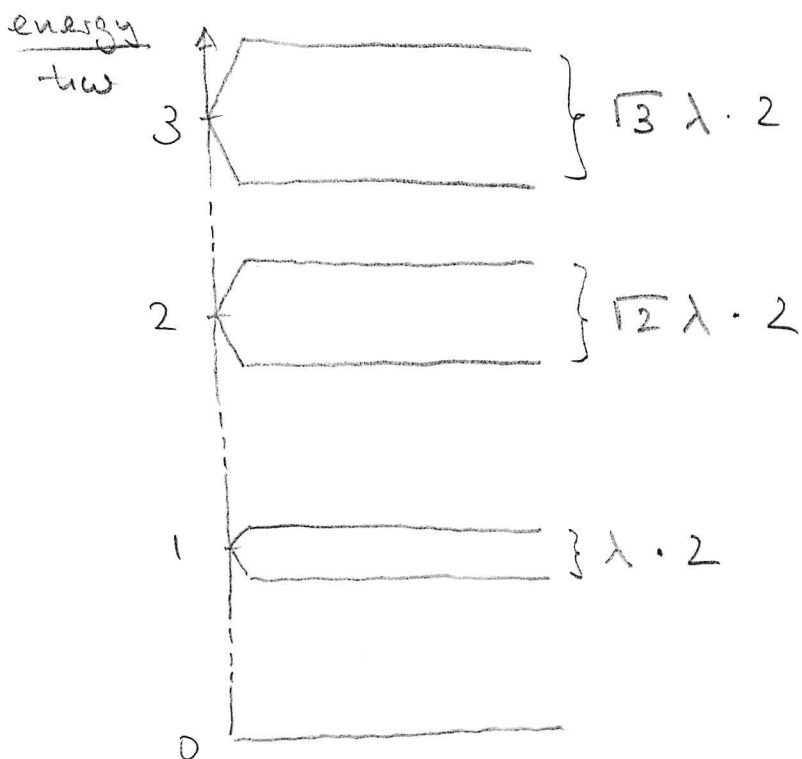
$$\begin{aligned}
 H_n = & \hbar\omega_e \begin{pmatrix} \langle e_{n-1} | N_{ex} | e_{n-1} \rangle & \langle e_{n-1} | N_{ex} | g_{in} \rangle \\ \langle g_{in} | N_{ex} | e_{n-1} \rangle & \langle g_{in} | N_{ex} | g_{in} \rangle \end{pmatrix} \\
 & \quad \circ \qquad \qquad \qquad \circ \\
 -\hbar\Delta & \begin{pmatrix} \langle e_{n-1} | \text{atale}_{n-1} \rangle & \langle e_{n-1} | \text{atalg}_{in} \rangle \\ \langle g_{in} | \text{atale}_{n-1} \rangle & \langle g_{in} | \text{atalg}_{in} \rangle \end{pmatrix} \\
 & \quad \circ \qquad \qquad \qquad \circ \\
 +\lambda & \begin{pmatrix} \langle e_{n-1} | (\alpha^{\pm} + \alpha^{\mp}) | e_{n-1} \rangle & \langle e_{n-1} | (\alpha^{\pm} + \alpha^{\mp}) | g_{in} \rangle \\ \langle g_{in} | (\alpha^{\pm} + \alpha^{\mp}) | e_{n-1} \rangle & \langle g_{in} | (\alpha^{\pm} + \alpha^{\mp}) | g_{in} \rangle \end{pmatrix} \\
 & \quad \circ \qquad \qquad \qquad \circ
 \end{aligned}$$

$$= \underbrace{\hbar\omega_e n}_{\hbar\omega n} - \underbrace{\hbar\Delta n}_{\hbar\omega n} + \begin{pmatrix} \hbar\Delta & \lambda\sqrt{n} \\ \lambda\sqrt{n} & 0 \end{pmatrix}$$

- up to an n-dependent constant this is the Hamiltonian of the Rabi model with n-dependent Rabi frequency  $\Omega_n = \frac{\lambda\sqrt{n}}{\hbar}$
- the eigenvalues (dressed state energies) are thus

$$E_{\pm}^n = \hbar\omega n + \frac{\hbar}{2} \left( \Delta \pm \sqrt{\Delta^2 + 4\frac{\lambda^2 n}{\hbar^2}} \right)$$

- The spectrum thus has the following structure (we show here the case  $\Delta=0$ )



- the splitting of the levels is non-linear
- for large  $n$  the relative difference of the level splitting decreases (i.e. the larger  $n$  the weaker is the dependence of  $\sqrt{n}$  on  $n$ )
- here the Jaynes-Cummings model approaches the Rabi model, which models a two level atom driven by a laser
- the laser can be described by a coherent state  $|\alpha\rangle$ , which for large  $\alpha$  is strongly peaked around the average photon number  $\bar{n} = |\alpha|^2$

in this case the interaction term of the Jaynes-Cummings model becomes

$$\begin{aligned}\lambda(a^\dagger \sigma^- + a \sigma^+) &\rightarrow \langle \alpha | \lambda(a^\dagger \sigma^- + a \sigma^+) | \alpha \rangle \\ &= \underbrace{\lambda \alpha \sigma^-}_{\hbar \omega} + \lambda \alpha^* \sigma^+ \\ &\text{hence Rabi frequency}\end{aligned}$$

- the non-linear nature of the spectrum of the Jaynes-Cummings model also manifests in the dynamics of the atom (which displays Rabi oscillations in case of the Rabi model)
- to see this, we consider again the resonant case ( $\delta=0$ ), in which case  $H_{\text{JC}}$  has the eigenstates

$$|n, \pm\rangle = \frac{1}{\sqrt{2}} (|g, n\rangle \pm |e, n-1\rangle) \quad \text{for } n > 0$$

$$|0\rangle = |g, 0\rangle \quad \text{for } n = 0$$

- the field shall be initially prepared in the state  $|4_f(0)\rangle = \sum_{n=0}^{\infty} c_n |n\rangle$ , and the atom shall be excited

- This initial state can be written as

(136)

$$\underbrace{|4_{af}(0)\rangle}_{\text{combined atom-field state}} = \sum_{n=0}^{\infty} c_n |e, n\rangle = \sum_{n=0}^{\infty} c_n \frac{1}{\sqrt{2}} (|n+1, +\rangle - |n+1, -\rangle)$$

$$\begin{aligned} \hookrightarrow |4_{af}(t)\rangle &= e^{-iH_{jet}t} |4_{af}(0)\rangle \\ &= \sum_{n=1}^{\infty} c_{n-1} \frac{1}{\sqrt{2}} (e^{-iH_{jet}t} |n, +\rangle - e^{-iH_{jet}t} |n, -\rangle) \\ &= \sum_{n=1}^{\infty} c_{n-1} \frac{e^{-i\omega_m t}}{\sqrt{2}} (e^{-i\frac{\lambda}{\hbar}t} |n, +\rangle - e^{+i\frac{\lambda}{\hbar}t} |n, -\rangle) \end{aligned}$$

- The probability for finding the atom in the state  $|e\rangle$  and the field in the Fock state  $|m\rangle$  is then given by

$$\begin{aligned} p_{me}(t) &= |\langle e, m | 4_{af}(t) \rangle|^2 = \left| c_{m-1} \frac{e^{-i\omega_m t}}{\sqrt{2}} \left( \frac{e^{-i\frac{\lambda}{\hbar}t} + e^{i\frac{\lambda}{\hbar}t}}{\sqrt{2}} \right) \right|^2 \\ &= |c_{m-1}|^2 \cos^2 \left( \frac{\lambda}{\hbar} t \right) \end{aligned}$$

- hence, the probability for the atom to be found in the excited state is

$$p_e(t) = \sum_{m=1}^{\infty} |c_{m-1}|^2 \cos^2 \left( \frac{\lambda}{\hbar} t \right)$$

- strictly periodic Rabi oscillations are therefore only found if the field is initially in a Fock state:  $c_{m-1} = \delta_{m, M_0}^{m_0}$  photon number of the initial Fock state

- for a light field in a coherent state  $|x\rangle$  we find

$$p_e(t) = \sum_{m=0}^{\infty} e^{-|\alpha|^2} \frac{|\alpha|^{2m}}{m!} \cos^2(\lambda \sqrt{m+1} t)$$

$$\alpha \gg 1 \approx \sum_{m=0}^{\infty} \frac{1}{\sqrt{2\pi|\alpha|}} e^{-\frac{(m-|\alpha|^2)^2}{2|\alpha|^2}} \cos^2(\lambda \sqrt{m+1} t)$$

$\ln\left(\frac{e^{-|\alpha|^2} |\alpha|^{2m}}{m!}\right) = -|\alpha|^2 + 2m \ln|\alpha| - \ln m!$ 
 $\propto -\frac{(m-|\alpha|^2)^2}{2|\alpha|^2} + \dots$ 
 $\hookrightarrow \frac{e^{-|\alpha|^2} |\alpha|^{2m}}{m!} \rightarrow \frac{1}{\sqrt{2\pi|\alpha|}} e^{-\frac{(m-|\alpha|^2)^2}{2|\alpha|^2}}$

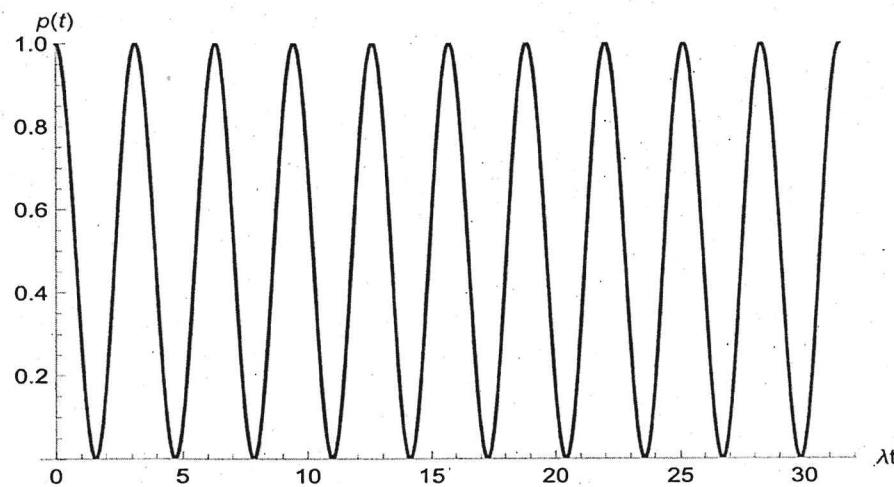
$$\approx \int_{-\infty}^{\infty} dx \underbrace{\frac{1}{\sqrt{2\pi|\alpha|}} e^{-\frac{(x-|\alpha|^2)^2}{2|\alpha|^2}}}_{\text{approaches } \delta(x-|\alpha|^2) \text{ for large } |\alpha|} \cos^2(\lambda \sqrt{x} t)$$

$$\xrightarrow{|\alpha|^2 \rightarrow \infty} \underbrace{\cos^2(\lambda |\alpha| t)}$$

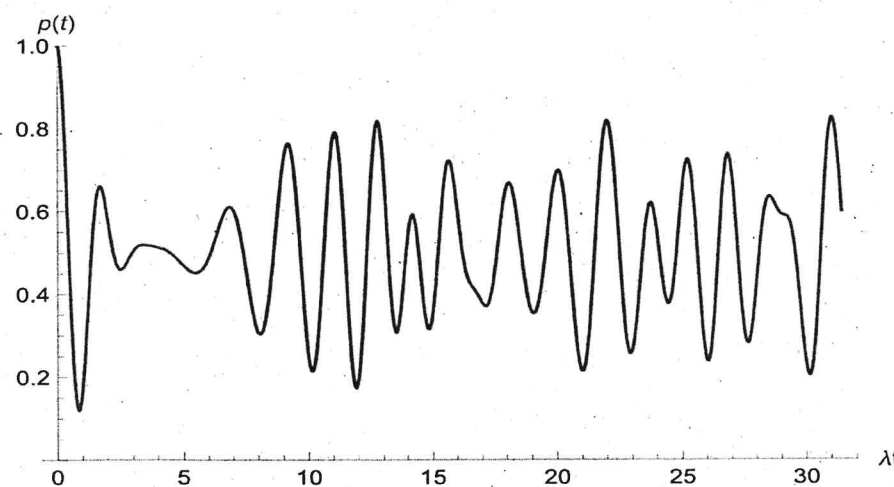
Rabi oscillations with Rabi frequency  $\lambda |\alpha| / \hbar$

- for finite values of  $\alpha$  the Rabi oscillations decay, which can be regarded as a manifestation of decoherence
- however, the oscillations may revive after some time (collapse and revival)

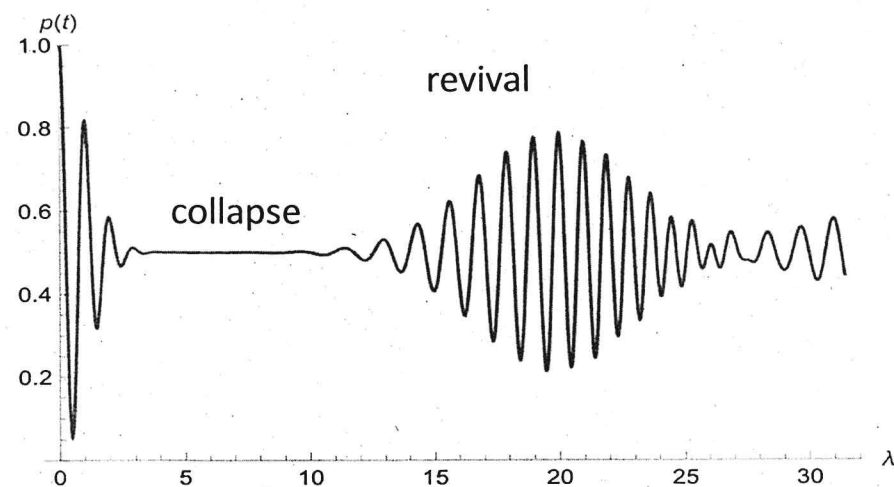
## Collapse and revival in the Jaynes-Cummings model



$$\alpha = 0$$



$$\alpha = 1.5$$

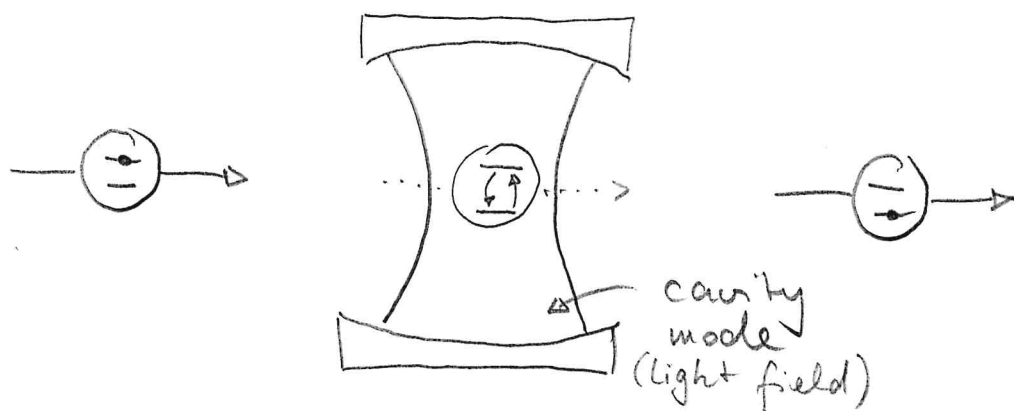


$$\alpha = 3$$

## IV. 4 Open system dynamics and decoherence

(138)

- in the following we will consider a situation in which a cavity, which contains a single mode light field, is "pumped" by a stream of incoming atoms, which pass the cavity volume one after the other

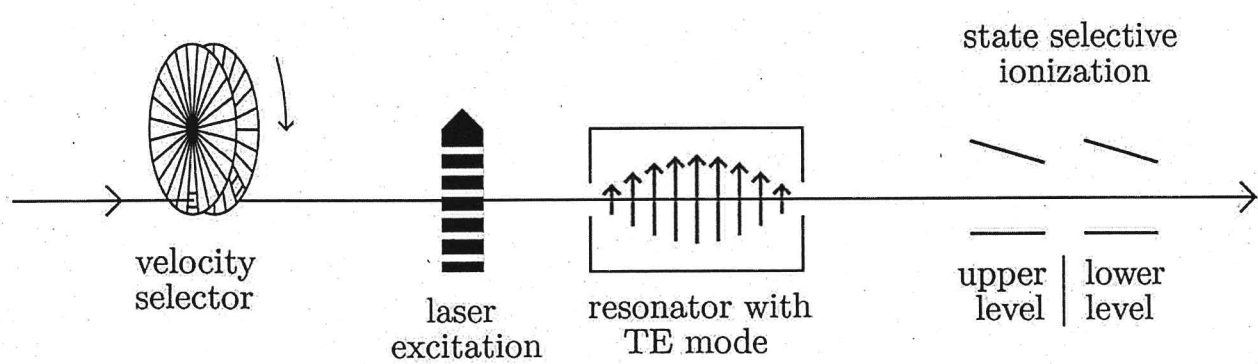


- depending on how long the atom remains inside the cavity it may deposit a quantum of excitation or remove one
- we assume that the cavity is in resonance with the atomic transition, i.e.  $\Delta = 0$
- the atom - cavity interaction is then described by the time-dependent Jaynes-Cummings Hamiltonian

$$H_{JC}(t) = \hbar \omega_{\text{ex}} N_{\text{ex}} + \lambda(t) (a^+ \sigma^- + a^- \sigma^+)$$

$\uparrow$   
coupling of atom to cavity  
mode while inside the cavity

# Micromaser setup



Taken from

Berthold-Georg Englert, Elements of micromaser physics, arXiv:quant-ph/0203052 (2002)

## LETTERS

# Reconstruction of non-classical cavity field states with snapshots of their decoherence

Samuel Deléglise<sup>1</sup>, Igor Dotsenko<sup>1,2</sup>, Clément Sayrin<sup>1</sup>, Julien Bernu<sup>1</sup>, Michel Brune<sup>1</sup>, Jean-Michel Raimond<sup>1</sup> & Serge Haroche<sup>1,2</sup>

The state of a microscopic system encodes its complete quantum description, from which the probabilities of all measurement outcomes are inferred. Being a statistical concept, the state cannot be obtained from a single system realization, but can instead be reconstructed<sup>1</sup> from an ensemble of copies through measurements on different realizations<sup>2–4</sup>. Reconstructing the state of a set of trapped particles shielded from their environment is an important step in the investigation of the quantum-classical boundary<sup>5</sup>. Although trapped-atom state reconstructions<sup>6–8</sup> have been achieved, it is challenging to perform similar experiments with trapped photons because cavities that can store light for very long times are required. Here we report the complete reconstruction and pictorial representation of a variety of radiation states trapped in a cavity in which several photons survive long enough to be repeatedly measured. Atoms crossing the cavity one by one are used to extract information about the field. We obtain images of coherent states<sup>9</sup>, Fock states with a definite photon number and ‘Schrödinger cat’ states (superpositions of coherent states with different phases<sup>10</sup>). These states are equivalently represented by their density matrices or Wigner functions<sup>11</sup>. Quasi-classical coherent states have a Gaussian-shaped Wigner function, whereas the Wigner functions of Fock and Schrödinger cat states show oscillations and negativities revealing quantum interferences. Cavity damping induces decoherence that quickly washes out such oscillations<sup>5</sup>. We observe this process and follow the evolution of decoherence by reconstructing snapshots of Schrödinger cat states at successive times. Our reconstruction procedure is a useful tool for further decoherence and quantum feedback studies of fields trapped in one or two cavities.

Engineering and reconstructing non-classical states of trapped light requires cavities that prevent the escape of even single photons during the preparation and read-out procedures. We have built a cavity made of highly reflecting superconducting mirrors<sup>12</sup> whose long damping time,  $T_c = 0.13$  s, allows the trapped field to interact with thousands of atoms crossing the cavity one by one. The interaction with atoms is used to turn an initial coherent field into a Fock or Schrödinger cat state and, subsequently, to reconstruct it. An ensemble of trapped photons becomes, like a collection of trapped atoms, an ‘object of investigation’ to be manipulated and observed for fundamental tests and quantum information purposes.

Our set-up is sketched in Fig. 1a. The cavity C, resonant at 51 GHz, is cooled to a temperature of 0.8 K (mean number of residual black-body photons,  $n_b = 0.05$ ). A coherent microwave field with a Poisson photon number distribution (mean,  $n_m$ ; standard deviation,  $\Delta n = \sqrt{n_m}$ ) is initially injected into C using a classical pulsed source S. Rubidium atoms from an atomic beam are prepared, in box B, in the circular Rydberg state with principal quantum number 50 ( $|g\rangle$ ).

The cavity is detuned from the transition between  $|g\rangle$  and the adjacent circular state with principal quantum number 51 ( $|e\rangle$ ) by an amount  $\delta$ , precluding atom-field energy exchange. The pulsed atom preparation produces Rydberg atoms with a velocity of 250 m s<sup>-1</sup>. Auxiliary microwave cavities R<sub>1</sub> and R<sub>2</sub> sandwiching C are connected to a microwave source S'. They are used to apply resonant pulses to the atoms. The R<sub>1</sub> pulse performs the  $|g\rangle \rightarrow (|e\rangle + |g\rangle)/\sqrt{2}$  transformation. The same pulse, differing by an adjustable phase shift  $\phi$ , is applied in R<sub>2</sub>. Atoms are counted by the detector D, discriminating  $|e\rangle$  and  $|g\rangle$  (one atom on average every 0.5 ms). For experimental details, see refs 13 and 14.

The R<sub>1</sub>–R<sub>2</sub> combination forms a Ramsey interferometer<sup>14</sup>. It is sensitive to the atomic-state-superposition phase shift induced by the atom’s interaction with the field in C, which is characterized by

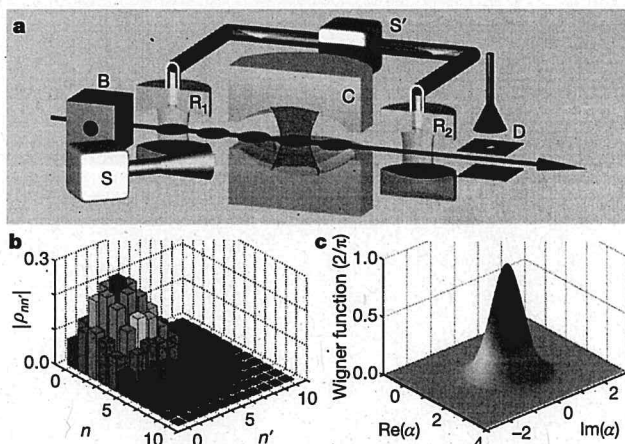


**Figure 1 | Reconstructing a coherent state.** **a**, The set-up, showing the stream of atoms prepared in box B and crossing the R<sub>1</sub>–R<sub>2</sub> interferometer in which the cavity C, made of two mirrors facing each other, is inserted. The source S, coupled to a waveguide, generates a coherent microwave pulse irradiating C on one side. By diffraction at the mirrors’ edges, it injects into C a small coherent field with controlled amplitude and phase. The field outside vanishes almost instantaneously when S is switched off. The source S is used to prepare an initial field in C and, later, to translate the field for state reconstruction. Another pulsed source, S', feeds the interferometer cavities R<sub>1</sub> and R<sub>2</sub>. Information is extracted from the field by state-selective atomic counting in D. **b**, Density matrix (modulus of matrix elements) of a coherent state of amplitude  $\beta = \sqrt{2.5}$ , reconstructed in an 11-dimensional Hilbert space. The reconstruction parameters are  $\delta/2\pi = 65$  kHz and  $\phi = -\Phi(0, \delta) + \pi$ . We sample 161 points in phase space and for each point detect  $\sim 7,000$  atoms over 600 realizations. The fidelity,  $F = \langle \beta | \rho | \beta \rangle$ , of the reconstructed state is 0.98. **c**, Wigner function (in units of  $2/\pi$ ) obtained from the density matrix shown in **b**.

<sup>1</sup>Laboratoire Kastler Brossel, Ecole Normale Supérieure, CNRS, Université Pierre et Marie Curie, 24 rue Lhomond, 75231 Paris Cedex 05, France. <sup>2</sup>Collège de France, 11 place Marcelin Berthelot, 75231 Paris Cedex 05, France.

the Rabi frequency  $\Omega/2\pi = 49$  kHz. This phase shift is described by an operator  $\Phi(N, \delta)$  that depends on  $\delta$  and the photon number operator  $N = a^\dagger a$  (where  $a$  and  $a^\dagger$  respectively denote the photon annihilation and creation operators). To lowest order,  $\Phi(N, \delta)$  is linear in  $N$ , but for the small  $\delta/\Omega$  values of our experiment, we take into account its exact nonlinear expression<sup>13</sup>. The interferometer measures  $\cos(\Phi(N, \delta) + \phi)$ , which is sensitive to the diagonal elements of the field density matrix in the Fock state basis, but contains no information about the coherences between these states. To obtain this information, we measure the phase shifts produced by the field after it has been translated in phase space, by mixing it with reference coherent fields of adjustable complex amplitudes  $\alpha$ . These translations, described by the operators  $D(\alpha) = \exp(\alpha a^\dagger - \alpha^* a)$  (where the asterisk denotes complex conjugation), are achieved by injecting a second field pulse into  $C$ .

We denote by  $\rho$  the density matrix of the field to be reconstructed (Fock-state-basis matrix elements,  $\rho_{nn'}$ ), by  $\rho^{(\alpha)} = D(\alpha)\rho D(-\alpha)$  the density matrix after field translation and by  $P_e$  and  $P_g$  the respective probabilities of finding in  $|e\rangle$  and  $|g\rangle$  the first atom that crosses the interferometer (experimentally obtained by averaging over many field realizations). The difference  $P_e - P_g = \text{Tr}[\rho^{(\alpha)} \cos(\Phi(N, \delta) + \phi)]$  is the expectation value in the translated state of the diagonal field operator  $\cos(\Phi(N, \delta) + \phi)$ . The measurement is non-demolition for the photon number<sup>15</sup>, and the ensemble average of first-crossing atoms does not change  $\rho_{nn'}^{(\alpha)}$ . Hence, the same  $P_e - P_g$  expression holds for the second (or any subsequent) atom. We thus determine  $P_e - P_g$  by averaging the detections of successive atoms for a single field realization with those measured for different realizations. A measuring sequence for each realization lasts 4 ms, which is short in comparison with the characteristic evolution time of the state. We also correct the raw  $P_e - P_g$  values by taking into account the known imperfections of the interferometer.

The  $P_e - P_g$  difference is also the expectation value of  $G(\alpha, \phi, \delta) = D(-\alpha) \cos(\Phi(N, \delta) + \phi) D(\alpha)$  in state  $\rho$ . By sampling  $\alpha$  values, we obtain the expectations  $g(\alpha, \phi, \delta)$  of an ensemble of non-commuting  $G(\alpha, \phi, \delta)$  operators satisfying:

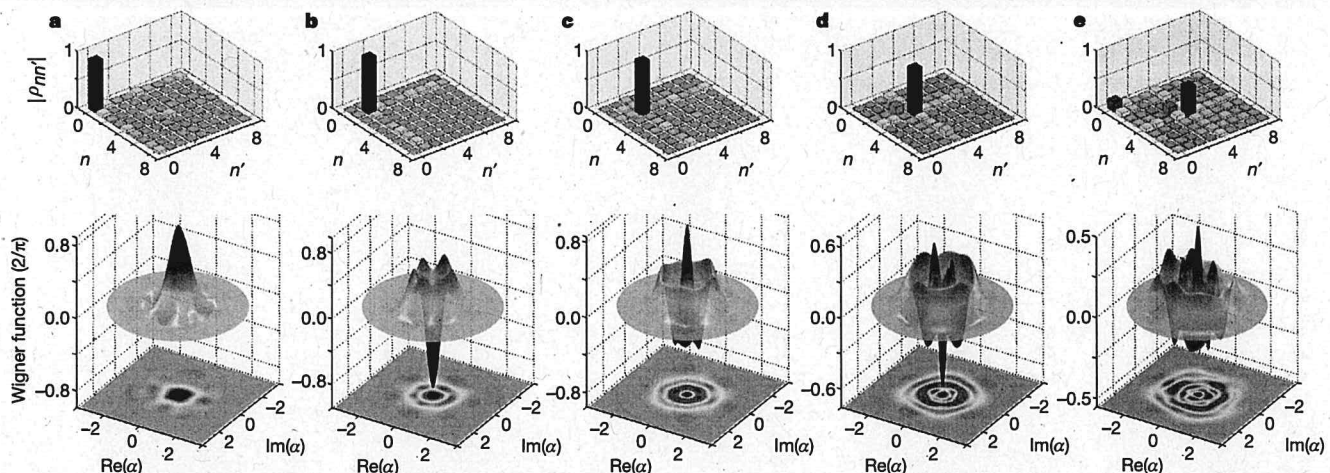


**Figure 2 | Reconstructing Fock states.** a–e, Reconstructed density matrices (modulus of matrix elements) and Wigner functions (in units of  $2/\pi$ ) of the  $n_0 = 0, 1, 2, 3, 4$  Fock states prepared by quantum non-demolition projection of an initial coherent field ( $n_m = 1.5$  for  $n_0 = 0, 1, 2, 3$ ;  $n_m = 5.5$  for  $n_0 = 4$ ). The Wigner functions are shown as three-dimensional plots and two-dimensional projections. We select a photon number  $n_0$  if, after the detection of  $\sim 60$  preparation atoms, the measurement has converged to a Fock state having a probability  $> 0.9$  for  $n_0 = 0, 1, 2, 3$  and  $> 0.8$  for  $n_0 = 4$ . The same detuning ( $\delta/2\pi = 120$  kHz) is used for state preparation and reconstruction, corresponding to  $\partial\Phi/\partial n \approx \pi/2$  at  $n = 3$ . Two values of  $\phi$  ( $-\Phi(0, \delta) + \pi$  and  $-\Phi(0, \delta) + \pi/2$ ) are used for state preparation and reconstruction, which is made in a nine-dimensional Hilbert space. We

$$\text{Tr}[\rho G(\alpha, \phi, \delta)] = g(\alpha, \phi, \delta) \quad (1)$$

Provided that we sample a large enough number of points  $\alpha$  in phase space, equation (1) allows us to reconstruct  $\rho$ . To ensure that the reconstructed state does not contain any information other than that extracted from the data, we also maximize the field entropy,  $-\text{Tr}[\rho \ln \rho]$ , during the reconstruction procedure (principle of maximum entropy<sup>16</sup>).

The Wigner function associated with the state described by the density matrix  $\rho$  is defined at point  $\alpha$  in phase space as<sup>14</sup>

$$W(\alpha) = \frac{2}{\pi} \text{Tr}[D(-\alpha)\rho D(\alpha)e^{i\pi N}] \quad (2)$$

and (to within a normalization) is the expectation value of the photon number parity operator  $\exp(i\pi N)$  in the state translated by  $-\alpha$ . The Wigner function could be determined directly<sup>17</sup> if the atoms underwent an exact phase shift of  $\pi$  per photon, realizing the measurement of  $\exp(i\pi N)$  after field translation by different values of  $\alpha$ . This would be a special case of reconstruction corresponding to  $\Phi(N, \delta) - \Phi(0, \delta) = \pi N$ . This relation cannot be satisfied, owing to nonlinear atom-field phase shift. Instead of a direct determination of the Wigner function, we thus reconstruct  $\rho$  first and then obtain the Wigner function using equation (2).

Figure 1b shows the reconstructed density matrix of a coherent state. Along its diagonal, we recognize the Poisson photon number distribution  $\rho_{nn}$ . The off-diagonal elements describe the classical coherence of the state. The corresponding Wigner function, shown in Fig. 1c, is, as expected, a Gaussian peak with a circular symmetry.

As a first non-classical example, we have reconstructed Fock states. To generate them, we prepare a coherent field and let it interact with atoms, achieving a quantum non-demolition measurement of the photon number that progressively projects the field onto a Fock state  $|n_0\rangle$ . This procedure is adapted from ref. 15, taking into account the known effect of cavity damping during state projection. Following this preparation, we apply our reconstruction method with subsequent probe atoms and reconstruct the Fock states present in the expansion of the initial coherent state.

sample  $\sim 400$  points in phase space and, for each point, average between about 50 (for  $n_0 = 3$ ) and 500 ( $n_0 = 0, 1$ ) realizations, with  $\sim 10$  atoms in each realization. In addition to the main peak in the density matrices, for  $n_0 > 1$  we observe a small diagonal peak at  $n = n_0 - 1$  due to cavity damping during reconstruction. A peak at  $n = 0$  also appears in the  $n_0 = 4$  density matrix, because of imperfections in the state preparation process that selects the photon number modulo four (as  $\Phi(n+4, \delta) \approx \Phi(n, \delta) + 2\pi$ ). The off-diagonal elements in the density matrices and the corresponding fluctuations in the angular distributions of the Wigner functions mainly reflect statistical noise (fewer atoms detected for reconstructing  $n_0 = 2, 3, 4$  than for  $n_0 = 0, 1$ ). The fidelities,  $F = \langle n_0 | \rho | n_0 \rangle$ , of the reconstructed states are 0.89, 0.98, 0.92, 0.82, 0.51 for  $n_0 = 0, 1, 2, 3, 4$ , respectively.

Figure 2 displays the obtained density matrices together with the corresponding Wigner functions for  $n_0 = 0$  (vacuum), 1, 2, 3, 4. As expected, the density matrices mainly exhibit a single diagonal peak. Each Wigner function shows circular rings around the origin of phase space, where it is positive for even  $n_0$  and negative for odd  $n_0$ . The number of rings and their size increases as expected with  $n_0$ . Photonic Fock states with small values of  $n_0$  have already been reconstructed in free space<sup>18–20</sup> and in a cavity<sup>21</sup>, but to our knowledge this is the first Fock state reconstruction with  $n_0 > 2$ .

To generate a Schrödinger cat state<sup>22</sup>, we first inject into C a coherent field of amplitude  $\beta = \sqrt{n_m}$ . We then prepare an atom in the state  $(|e\rangle + |g\rangle)/\sqrt{2}$  using  $R_1$  and send it into C. The two atomic components shift the phase of the field in opposite directions. Neglecting atom–field phase shift nonlinearity, the field is split into two coherent states of complex amplitudes  $\beta \exp(\pm i\chi)$ , where  $\chi = (\partial\Phi(n, \delta)/\partial n)/2$  evaluated at  $n = n_m$ . The atom is entangled with the field in the state  $(|e\rangle|\beta \exp(i\chi)\rangle + |g\rangle|\beta \exp(-i\chi)\rangle)/\sqrt{2}$ . The  $R_2$  pulse then mixes  $|e\rangle$  and  $|g\rangle$  again. Last, the atomic detection, depending upon its outcome ( $|g\rangle$  or  $|e\rangle$ ), projects the field onto one of the two Schrödinger cat states  $(|\beta \exp(i\chi)\rangle \pm |\beta \exp(-i\chi)\rangle)/\sqrt{2}$ . We call these ‘even’ (plus sign) and ‘odd’ (minus sign) Schrödinger cat states because they contain, for  $\chi = \pi/2$ , only even and odd photon numbers, respectively. After this preparation, we apply our reconstruction procedure.

Figure 3a, b shows the Wigner functions of the even and odd Schrödinger cat states obtained from the same coherent field ( $n_m = 3.5$ ,  $\chi = 0.37\pi$ ). They exhibit two well-separated positive peaks that are associated with the classical components and whose slightly elongated shapes are due to the phase shift nonlinearity neglected above. The ‘size’ of each of these states, defined as the squared distance between the peaks (and expressed as a number of photons), is  $d^2 \approx 4n_m \sin^2 \chi = 11.8$  photons. Between these peaks, oscillating features with alternating positive and negative values are the signatures of the state’s quantum interference. The even and odd Schrödinger cat states have nearly identical classical components and only differ in the sign of their quantum interferences. The theoretical Wigner functions, taking the nonlinearity in the preparation of the Schrödinger cat states into account, are shown for comparison in the insets. The fidelity of the two states (overlap between the reconstructed  $\rho$  and the expected  $\rho$ ) is  $F = 0.72$ . It is mainly limited by imperfections in the  $R_1$  and  $R_2$  pulses applied to the preparation atom, which reduce the

contrast of the quantum interference feature. If the preparing atom is detected without discriminating  $|e\rangle$  and  $|g\rangle$ , we obtain the statistical mixture of even and odd Schrödinger cat states whose Wigner function is shown in Fig. 3c. Equivalently, this is a statistical mixture of the two classical components. Although non-classical states of propagating light with similar Wigner functions have previously been observed<sup>23</sup>, here well-separated classical components of a field can be identified in a reconstructed state and unambiguously distinguished from their quantum interference term.

Schrödinger cat states are model states for exploring decoherence, the phenomenon accounting for the transition between quantum and classical behaviours<sup>5</sup>. Our reconstruction method allows us to study this process. Immediately after state preparation, we realize the  $D(\alpha)$  translation and detect a sequence of atoms divided into 4-ms time windows. These atoms record  $P_e - P_g$  as a function of time, without modifying the dynamics of this quantity. We average the results of realizations corresponding to the same translation and time window, and then repeat the process for different values of  $\alpha$ . This provides a direct record of the evolution of the translated states, rather than that of the state itself. The two dynamics are closely related, however. Decoherence acting on the initial density operator  $\rho(0)$  turns it at time  $t$  into  $\rho(t) = L[\rho(0), t]$ . Here  $L$  is the decoherence superoperator<sup>14</sup>, which can be shown to satisfy the following relation:

$$D(\alpha e^{-t/2T_c})L[\rho(0), t]D(-\alpha e^{-t/2T_c}) = L[D(\alpha)\rho(0)D(-\alpha), t]$$

Translating the initial field by  $\alpha$  and letting it evolve over time  $t$  is equivalent to letting it evolve during that time and translating it by  $\alpha \exp(-t/2T_c)$ . We thus analyse the data obtained at time  $t$  as if they corresponded to a translation rescaled by  $\exp(-t/2T_c)$ . This is more efficient than letting the field evolve before translating it, because we exploit all the data of a long sequence instead of recording only a short time window for each delay. We have experimentally checked the equivalence between the two methods by comparing the results for one time delay and have verified that the reconstructed Schrödinger cat states are, within the effects of noise, undistinguishable.

Figure 4a shows four snapshots of the Wigner function of an odd Schrödinger cat at increasing times, clearly revealing decoherence. Although the classical components have hardly decayed after 50 ms,

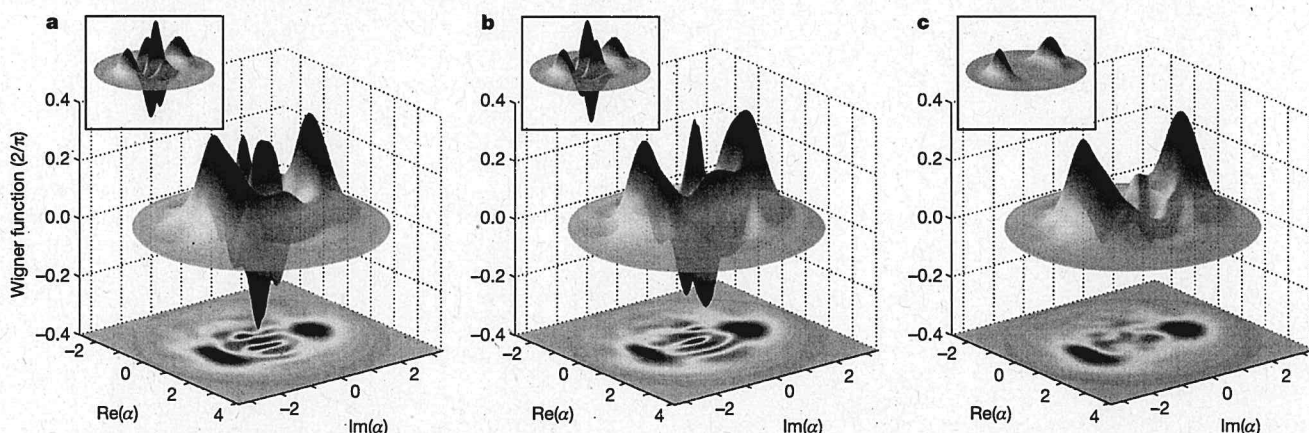


**Figure 3 | Reconstructing Schrödinger cat states.** **a, b**, The Wigner functions (in units of  $2/\pi$ ) of even (a) and odd (b) Schrödinger cat states with  $n_m = 3.5$  and  $\chi = 0.37\pi$  are reconstructed, following state preparation. The same detuning ( $\delta/2\pi = 51$  kHz) and interferometer phase ( $\phi = -\Phi(0, \delta) + \pi$ ) are used for state preparation and reconstruction. The number of sampling points is  $\sim 500$ , with  $\sim 2,000$  atoms detected at each point, in 400 realizations. The dimension of the Hilbert space used for reconstruction is 11. The small insets present for comparison the theoretical Wigner functions computed in the case of ideal preparation and detection of

the atomic state superpositions. Decoherence during state preparation is taken into account. The maximum theoretical values of the classical components and interference fringes are close to 0.5 and 1, respectively. In the reconstructed states, the quantum interference is smaller, mainly owing to imperfections of the Ramsey interferometer that affect the preparation of the Schrödinger cat state (but not its reconstruction). **c**, Reconstructed Wigner function of the field prepared in C when the state of the preparation atom is not read-out (statistical mixture of two classical fields). Inset, corresponding theoretical Wigner function.

the interference feature has vanished, turning the initial state into a statistical mixture similar to that shown in Fig. 3c. A complete movie of the evolution of the Wigner function of a Schrödinger cat state is

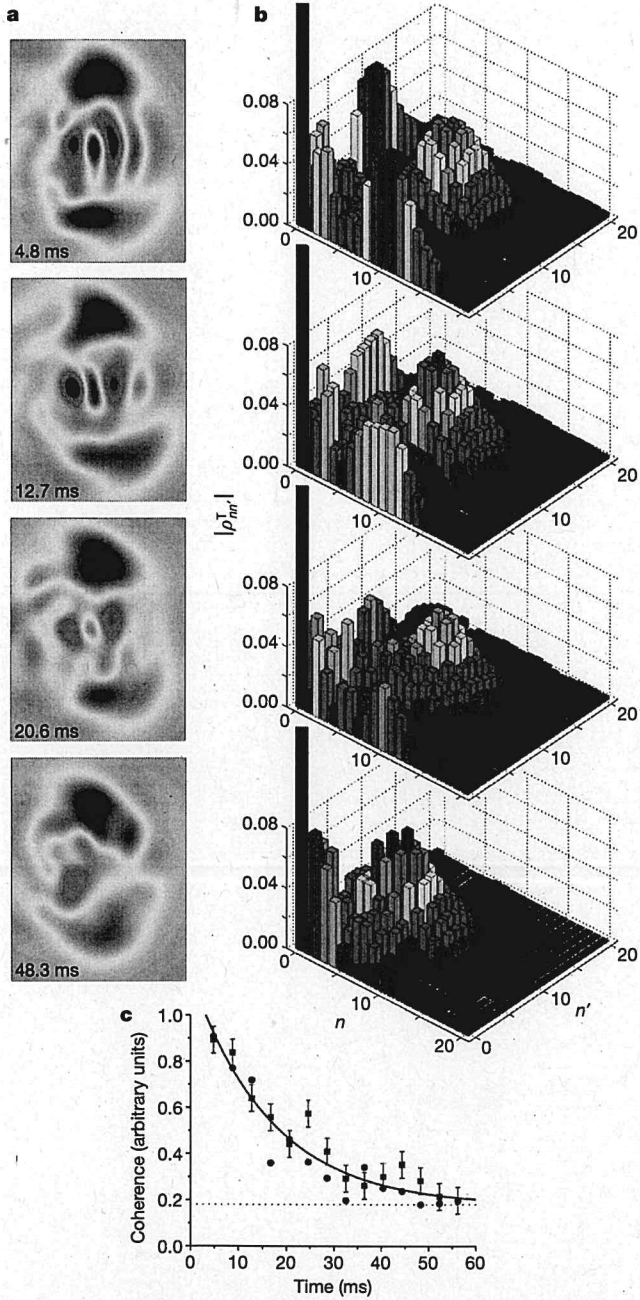


**Figure 4 | Movie of decoherence.** **a**, Snapshots of the Wigner function of the odd Schrödinger cat state in Fig. 3b at four successive times after state preparation. **b**, Corresponding snapshots of the translated density matrix  $\rho^T$  (modulus of matrix elements). The dimension of the Hilbert space is enlarged to 30. The  $n = 0$  peak is clipped, its amplitude being  $\sim 0.38$  in each snapshot. In all frames, the small matrix elements for  $n < 5$  are due to the deviation of the classical component of the Schrödinger cat state from an ideal coherent state. **c**, The quantum coherence of the Schrödinger cat states (even, red; odd, blue), defined as the sum of the  $|\rho_{nn'}^T|$  for  $n \geq 5$ , plotted as a function of time. The statistical error bars (shown, for clarity, for the even Schrödinger cat states only) are obtained by analysing the state reconstructions performed on different subsamples of measured data. The solid line is a common exponential fit, including an offset (dotted line) accounting for residual noise in the modulus of the density matrix elements.

presented in the Supplementary Information. By subtracting the Wigner functions of the even and odd Schrödinger cat states corresponding to the same preparation sequence, we isolate their interference features by cancelling their equal, classical, parts. A movie showing the progressive vanishing of this interference is also provided in the Supplementary Information.

It is also instructive to observe decoherence directly in the density matrix. To distinguish the classical coherence of each component of the Schrödinger cat state from their mutual quantum coherence, we consider the mathematically translated reconstructed density matrix  $\rho^T = \rho^{-\beta \exp(i\chi)}$ , whose classical components are close to the vacuum  $|0\rangle$  and to  $|-2i\beta \sin \chi\rangle$ . This formal translation leaves unchanged the distance between the two classical components in the phase plane as well as their mutual coherence.

In Fig. 4b, we present the density matrix  $\rho^T(t)$  of the Schrödinger cat state in Fig. 4a, reconstructed for the same times. In each frame, the diagonal elements present two maxima around  $n = 0$  and  $n = 11$ . The off-diagonal elements are of two kinds. Those for which  $|n - n'| \approx \sqrt{11}$  describe the classical coherence of the non-vacuum component and remain nearly unchanged on the observed timescale. The off-diagonal terms in the first row and column of the matrix (respectively  $\rho_{0n}^T$  and  $\rho_{n0}^T$ ) initially exhibit a bell-shaped variation with  $n$ , centred at  $n \approx 11$ . These terms correspond to the quantum coherence of the Schrödinger cat state responsible for the oscillations observed in the Wigner function. Their fast decay is the signature of decoherence.

The measured quantum coherence of the even and odd Schrödinger cat states is plotted as a function of time in Fig. 4c. A common exponential fit yields a decoherence time of  $T_d = 17 \pm 3$  ms. A simple analytical model of decoherence<sup>14</sup> predicts that  $T_d = 2T_c/d^2 = 22$  ms at  $T = 0$  K, reduced to<sup>24</sup>  $T_d = 2T_c/(d^2(1+2n_b)+4n_b) = 19.5$  ms when including a thermal background at  $T = 0.8$  K, in good agreement with the measured value. A movie of a smaller Schrödinger cat state ( $d^2 = 8$ ) yields  $T_d = 28$  ms, illustrating the dependence of the decoherence time on the Schrödinger cat state size<sup>5,14</sup>. Earlier experiments have studied the relaxation of photonic<sup>22</sup> and atomic<sup>25</sup> Schrödinger cat states by observing some of their specific features, but this experiment allows us to produce a movie of decoherence in a fully reconstructed Schrödinger cat state.

We have shown that atoms interacting with a cavity field can be used to engineer and reconstruct a wide variety of photonic states and to study their evolution. Going one step farther, we plan to use information provided by the atoms to implement feedback procedures and preserve the quantum coherence over longer time intervals<sup>26</sup>. We will also extend these studies to fields stored in two cavities. Atoms will be used to entangle the cavity fields into non-local quantum states<sup>27,28</sup>, reconstruct these states and protect them against decoherence by means of quantum feedback operations.

Received 25 June; accepted 23 July 2008.

1. Paris, M. G. A. & Řeháček, J. (eds) *Quantum State Estimation* (Springer, 2004).
2. Smithey, D. T., Beck, M., Raymer, M. G. & Faridani, A. Measurement of the Wigner distribution and the density matrix of a light mode using optical homodyne tomography: Application to squeezed states and the vacuum. *Phys. Rev. Lett.* **70**, 1244–1247 (1993).
3. Dunn, T. J., Walmsley, I. A. & Mukamel, S. Experimental determination of the quantum-mechanical state of a molecular vibrational mode using fluorescence tomography. *Phys. Rev. Lett.* **74**, 884–887 (1995).
4. Kurtsiefer, C., Pfau, T. & Mlynek, J. Measurement of the Wigner function of an ensemble of helium atoms. *Nature* **386**, 150–153 (1997).
5. Zurek, W. Decoherence, einselection, and the quantum origins of the classical. *Rev. Mod. Phys.* **75**, 715–775 (2003).
6. Leibfried, D. et al. Experimental determination of the motional quantum state of a trapped atom. *Phys. Rev. Lett.* **77**, 4281–4285 (1996).
7. Häffner, H. et al. Scalable multiparticle entanglement of trapped ions. *Nature* **438**, 643–646 (2005).
8. Morinaga, M., Boucoubou, I., Karam, J.-C. & Salomon, C. Manipulation of motional quantum states of neutral atoms. *Phys. Rev. Lett.* **83**, 4037–4040 (1999).
9. Glauber, R. J. Coherent and incoherent states of the radiation field. *Phys. Rev.* **131**, 2766–2788 (1963).

10. Bužek, V. & Knight, P. L. Quantum interference, superposition states of light, and nonclassical effects, in *Progress in Optics XXXIV* (ed. Wolf, E.) 1–158 (Elsevier, 1995).
11. Schleich, W. P. *Quantum Optics in Phase Space* (Wiley, 2001).
12. Kuhr, S. et al. Ultrahigh finesse Fabry-Pérot superconducting resonator. *Appl. Phys. Lett.* **90**, 164101 (2007).
13. Raimond, J.-M., Brune, M. & Haroche, S. Colloquium: manipulating quantum entanglement with atoms and photons in a cavity. *Rev. Mod. Phys.* **73**, 565–582 (2001).
14. Haroche, S. & Raimond, J.-M. *Exploring the Quantum: Atoms, Cavities and Photons* (Oxford Univ. Press, 2006).
15. Guerlin, C. et al. Progressive field state collapse and quantum non-demolition photon counting. *Nature* **448**, 889–893 (2007).
16. Bužek, V. & Drobny, G. Quantum tomography via the MaxEnt principle. *J. Mod. Opt.* **47**, 2823–2839 (2000).
17. Lütterbach, L. G. & Davidovich, L. Method for direct measurement of the Wigner function in cavity QED and ion traps. *Phys. Rev. Lett.* **78**, 2547–2550 (1997).
18. Lvovsky, A. I. et al. Quantum state reconstruction of the single-photon Fock state. *Phys. Rev. Lett.* **87**, 050402 (2001).
19. Zavatta, A., Viciani, S. & Bellini, M. Tomographic reconstruction of the single-photon Fock state by high-frequency homodyne detection. *Phys. Rev. A* **70**, 053821 (2004).
20. Ourjoumtsev, A., Tualle-Brouri, R. & Grangier, P. Quantum homodyne tomography of a two-photon Fock state. *Phys. Rev. Lett.* **96**, 213601 (2006).
21. Bertet, P. et al. Direct measurement of the Wigner function of a one-photon Fock state in a cavity. *Phys. Rev. Lett.* **89**, 200402 (2002).
22. Brune, M. et al. Observing the progressive decoherence of the ‘meter’ in a quantum measurement. *Phys. Rev. Lett.* **77**, 4887–4890 (1996).
23. Ourjoumtsev, A., Jeong, H., Tualle-Brouri, R. & Grangier, P. Generation of optical ‘Schrödinger cats’ from photon number states. *Nature* **448**, 784–786 (2007).
24. Kim, M. S. & Bužek, V. Schrödinger cat states at finite temperature: Influence of a finite temperature heat bath on quantum interferences. *Phys. Rev. A* **46**, 4239–4251 (1992).
25. Myatt, C. J. et al. Decoherence of quantum superpositions through coupling to engineered reservoirs. *Nature* **403**, 269–273 (2000).
26. Zippilli, S., Vitali, D., Tombesi, P. & Raimond, J.-M. Scheme for decoherence control in microwave cavities. *Phys. Rev. A* **67**, 052101 (2003).
27. Davidovich, L., Brune, M., Raimond, J.-M. & Haroche, S. Mesoscopic quantum coherences in cavity QED: preparation and decoherence monitoring schemes. *Phys. Rev. A* **53**, 1295–1309 (1996).
28. Milman, P. et al. A proposal to test Bell’s inequalities with mesoscopic non-local states in cavity QED. *Eur. Phys. J. D* **32**, 233239 (2005).

**Supplementary Information** is linked to the online version of the paper at [www.nature.com/nature](http://www.nature.com/nature).

**Acknowledgements** This work was supported by the Agence Nationale pour la Recherche (ANR), by the Japan Science and Technology Agency (JST) and by the European Union under the Integrated Projects SCALA and CONQUEST. S.D. is funded by the Délégation Générale pour l’Armement (DGA).

**Author Contributions** S.D., I.D. and C.S. contributed equally to this work.

**Author Information** Reprints and permissions information is available at [www.nature.com/reprints](http://www.nature.com/reprints). Correspondence and requests for materials should be addressed to S.H. ([haroche@lkb.ens.fr](mailto:haroche@lkb.ens.fr)).

- the time-evolution operator is then given by
- $$U(t) = \underbrace{e^{-i\omega_{\text{ex}} t}}_{U_0(t)} \underbrace{\exp \left( -i \int_0^t d\tau \lambda(\tau) [a^\dagger \sigma^- + a \sigma^+] \right)}_{V(t)}$$

- note, operator splits into two parts because  $\hat{N}_{\text{ex}}$  commutes with interaction term
- no time-ordering necessary, since  $[H_{\text{ex}}(t), H_{\text{ex}}(t')] = 0$
- with  $\mathcal{L} = \frac{i}{\hbar} \int_0^t d\tau \lambda(\tau)$  we can write

$$\begin{aligned} V(t) &= \exp(-i\varphi [a^\dagger \sigma^- + a \sigma^+]) = \exp \left( -i\varphi \begin{pmatrix} 0 & a \\ a^\dagger & 0 \end{pmatrix} \right) \\ &= \sum_{m=0}^{\infty} \frac{1}{m!} (-i\varphi)^m \begin{pmatrix} 0 & a \\ a^\dagger & 0 \end{pmatrix}^m \\ &= \sum_{m=0}^{\infty} \frac{1}{(2m)!} (-i\varphi)^{2m} \begin{pmatrix} (aa^\dagger)^m & 0 \\ 0 & (a^\dagger a)^m \end{pmatrix} + \sum_{m=0}^{\infty} \frac{1}{(2m+1)!} (-i\varphi)^{2m+1} \begin{pmatrix} 0 & a(a^\dagger)^m \\ a^\dagger (aa^\dagger)^m & 0 \end{pmatrix} \\ &= \begin{pmatrix} \cos(\varphi \sqrt{a a^\dagger}) & 0 \\ 0 & \cos(\varphi \sqrt{a a^\dagger}) \end{pmatrix} + \begin{pmatrix} 0 & -ia \frac{\sin(\varphi \sqrt{a a^\dagger})}{\sqrt{a a^\dagger}} \\ -ia \frac{\sin(\varphi \sqrt{a a^\dagger})}{\sqrt{a a^\dagger}} & 0 \end{pmatrix} = \begin{pmatrix} \hat{C} & -\hat{S}' \\ -\hat{S} & \hat{C}' \end{pmatrix} \end{aligned}$$

- let us now consider an atom that enters the cavity in the state

$$S_a = |a\rangle \langle a| = \begin{pmatrix} 1 & 0 \\ 0 & 0 \end{pmatrix}$$

- the cavity shall be in the state  $S_f$

- after the atom has traversed the cavity, (140)  
we find the state

$$\begin{aligned}
 \hat{\rho}'_{af} &= U(+)\hat{\rho}_a \otimes \hat{\rho}_f U^+(+) = U(+)
 \begin{pmatrix} \hat{\rho}_f & 0 \\ 0 & 0 \end{pmatrix} U^+(+) \\
 &= U_0(+)
 \begin{pmatrix} \hat{C} - \hat{S}^\dagger \\ -\hat{S} \hat{C}^\dagger \end{pmatrix}
 \begin{pmatrix} \hat{\rho}_f & 0 \\ 0 & 0 \end{pmatrix}
 \begin{pmatrix} \hat{C}^\dagger - \hat{S}^\dagger \\ -\hat{S}^\dagger \hat{C}^\dagger \end{pmatrix} U_0^+(+) \\
 &= U_0(+)
 \begin{pmatrix} \hat{C} \hat{\rho}_f \hat{C}^\dagger - \hat{C} \hat{\rho}_f \hat{S}^\dagger \\ -\hat{S} \hat{\rho}_f \hat{C}^\dagger + \hat{S} \hat{\rho}_f \hat{S}^\dagger \end{pmatrix} U_0^+(+) \\
 &= e^{-it\omega_a t} \underbrace{\begin{pmatrix} e^{-it\omega_e} & 0 \\ 0 & 1 \end{pmatrix}}_{\omega = \omega_e, \text{since } \Delta = 0}
 \begin{pmatrix} \hat{C} \hat{\rho}_f \hat{C}^\dagger - \hat{C} \hat{\rho}_f \hat{S}^\dagger \\ -\hat{S} \hat{\rho}_f \hat{C}^\dagger + \hat{S} \hat{\rho}_f \hat{S}^\dagger \end{pmatrix}
 \underbrace{\begin{pmatrix} e^{it\omega_e} & 0 \\ 0 & 1 \end{pmatrix}}_{\text{itwata}}
 e^{it\omega_a t}
 \end{aligned}$$

- in the following we are only interested in the evolution of the cavity, i.e. we "do not care" what happens to the atom afterwards
- the state of the cavity is then obtained by tracing over the atom

$$\begin{aligned}
 \hookrightarrow \hat{\rho}'_f &= \text{tr}_a \hat{\rho}'_{af} = \langle g | \hat{\rho}'_{af} | g \rangle + \langle e | \hat{\rho}'_{af} | e \rangle \\
 &= \underbrace{e^{-it\omega_a t}}_{\text{free evolution of the cavity}} \underbrace{(\hat{S} \hat{\rho}_f \hat{S}^\dagger + \hat{C} \hat{\rho}_f \hat{C}^\dagger)}_{\substack{\text{atom leaves cavity deexcited} \\ \text{evolution under the interaction with the atom}}} e^{it\omega_a t}
 \end{aligned}$$

- this evolution equation has the form of a Kraus map (actually, two concatenated Kraus maps)

$$S_f' = U_{\text{free}} \left( \sum_{m=0}^1 K_m S_f K_m^+ \right) U_{\text{free}}^+$$

- here the Kraus operators are

$$K_0 = \cos(\varphi \sqrt{\alpha a^\dagger}) \quad \text{and} \quad K_1 = -ia^\dagger \frac{\sin(\varphi \sqrt{\alpha a^\dagger})}{\sqrt{\alpha a^\dagger}}$$

- they obey the normalisation condition

$$\sum_m K_m^+ K_m = \mathbb{1}$$

- for the case of unitary evolution there is only one Kraus operator, which corresponds to the unitary time-evolution operator,  $K=U$

- Kraus maps generalise unitary evolution to so-called quantum channels, which allow to model not only coherent dynamics but also dissipative processes

- to get a first idea about how this works let's consider a situation in which the atom couples weakly to the cavity
- this regime is characterised by  $\varphi \ll 1$
- expanding the Kraus operator to lowest order then yields  $K_0 \approx 1 - \frac{1}{2} \varphi^2 a a^\dagger$ ,  $K_1 \approx -i \varphi a^\dagger$

- let us now parametrise the angle  $\varphi$  in a way, such that  $\varphi = \sqrt{\gamma_1 \Delta t}$  where  $\gamma_1$  is a rate and  $\Delta t$  is the (short) time which the atom takes to pass through the cavity

- since  $\Delta t$  is short, we can also expand the unitary operator of the free evolution:

$$U_{\text{free}} \approx 1 - i \Delta t w_a a^\dagger$$

- we then find

$$\begin{aligned} S_f' &= S_f + \underbrace{\Delta g_f}_{\text{change of } S_f} = (1 - i \Delta t w_a a^\dagger) \left[ \left( 1 - \frac{\gamma_1 \Delta t}{2} a a^\dagger \right) S_f \left( 1 - \frac{\gamma_1 \Delta t}{2} a a^\dagger \right)^\dagger \right. \\ &\quad \left. \dots + \gamma_1 \Delta t a^\dagger g_f a \right] (1 + i \Delta t w_a a^\dagger) \\ &= S_f - i \Delta t w_a g_f + i \Delta t w_g g_a \\ &\quad - \frac{\gamma_1 \Delta t}{2} a a^\dagger g_f - \frac{\gamma_1 \Delta t}{2} S_f a a^\dagger + \gamma_1 \Delta t a^\dagger g_f a + \mathcal{O}(\Delta t^2) \end{aligned}$$

$$\hookrightarrow \Delta g_f = -i [w_a a^\dagger, g_f] \Delta t + \gamma_1 \Delta t \left( a^\dagger g_f - \frac{1}{2} \{a a^\dagger, g_f\} \right) + \mathcal{O}(\Delta t^2)$$

free Hamiltonian

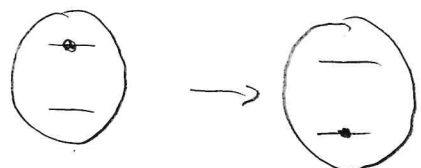
$$\hookrightarrow \frac{\Delta g_f}{\Delta t} \xrightarrow{\Delta t \rightarrow 0} \frac{\partial g_f}{\partial t} = - \underbrace{i}_{\text{dissipator}} \underbrace{[w_a a^\dagger, g_f]}_{\text{dissipator}} + \gamma_1 \underbrace{\left( a^\dagger g_f - \frac{1}{2} \{a a^\dagger, g_f\} \right)}_{\text{dissipator}}$$

- the evolution of the density matrix of the light field is (approximately) governed by a so-called Lindblad master equation

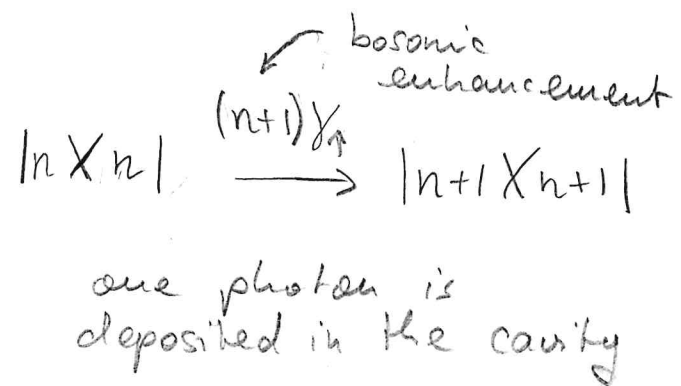
the general form of a Lindblad master equation is given by (143)

$$\frac{\partial \rho}{\partial t} = -\frac{i}{\hbar} [H, \rho] + \sum_k \gamma_k (L_k \rho L_k^\dagger - \frac{1}{2} \{ L_k^\dagger L_k, \rho \})$$

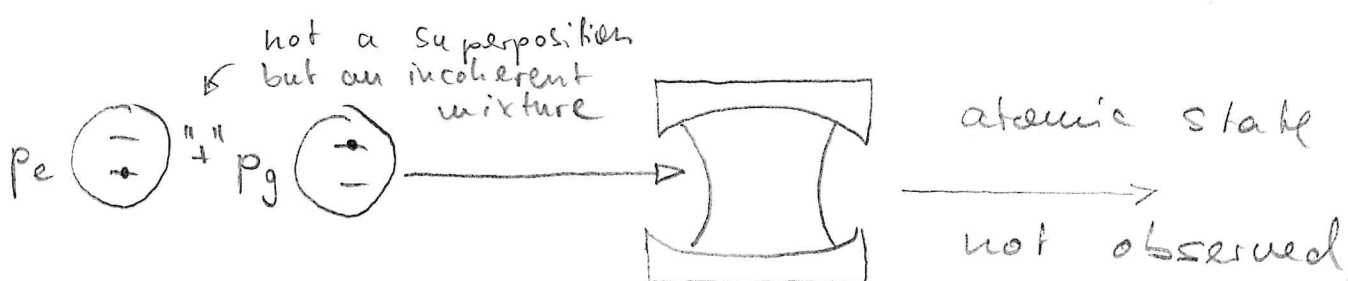
- here  $H$  is the quantum Hamiltonian
- the operators  $L_k$  are called jump operators
- they implement incoherent / dissipative processes, which occur with the rate  $\gamma_k$
- in the example here, we have only a single jump operator  $L = a^\dagger$  with the corresponding rate  $\gamma_\uparrow$
- its interpretation is that the cavity light field acquires spontaneously a photon at rate  $\gamma_\uparrow$
- in the considered physical implementation this means that the atom deposits its excitation inside the cavity and leaves the cavity in the ground state:



atom leaves cavity  
in ground state



- performing the calculation for an initial state in which the atom is in its ground state, and parametrising the small rotation angle as  $\varphi = \sqrt{\gamma \Delta t}$ , yields the jump operator  $L = a$  with the rate  $\gamma$ .
- this process removes a photon from the cavity and leaves an excited atom.
- let us now assume that we send atoms (one by one) through the cavity, which are with probability  $p_e / p_g = 1 - p_e$  in their excited / ground state



- the evolution of the light field's state  $\rho_f$  then follows the master equation

$$\frac{\partial \rho_f}{\partial t} = -i [w_{ata}, \rho_f] + p_e \gamma (a^\dagger a - \frac{1}{2} \{a^\dagger a, \rho_f\}) + p_g \gamma (a a^\dagger - \frac{1}{2} \{a a^\dagger, \rho_f\})$$

absorption of a photon      removal of a photon

- this equation can be solved with the ansatz  $\rho_f = \sum_n p_n |n\rangle \langle n|$  where probability to be in Fock state  $|n\rangle$

(145)

$$\hookrightarrow \sum_n \frac{\partial p_n}{\partial t} |\ln x_n| = -i \sum_n p_n (\underbrace{\omega_n |\ln x_n| - |\ln x_n| \omega_n}_{=0})$$

$$+ Pe\gamma \sum_n p_n \left( \sqrt{n+1} |\ln (n+1) x_{n+1}| / \sqrt{n+1} - \frac{1}{2} ((n+1) |\ln x_n| + |\ln x_n| (n+1)) \right)$$

$$+ Pg\gamma \sum_n p_n \left( \sqrt{n} |\ln n x_{n-1}| / \sqrt{n} - \frac{1}{2} (n |\ln x_n| + |\ln x_n| n) \right)$$

$$\hookrightarrow \frac{\partial p_n}{\partial t} = Pe\gamma (n p_{n-1} - (n+1) p_n) + Pg\gamma ((n+1) p_{n+1} - n p_n)$$

- we are interested in the stationary state of this equation, i.e. we want to find  $p_n$  such that  $\frac{\partial p_n}{\partial t} = 0$

$$\hookrightarrow 0 = \frac{Pe}{Pg} (n p_{n-1} - (n+1) p_n) + (n+1) p_{n+1} - n p_n$$

- making the ansatz  $p_n = c \lambda^n$  yields

$$0 = \lambda^{n-1} \left( \lambda - \frac{Pe}{Pg} \right) (n(\lambda-1) + \lambda), \text{ which is}$$

solved for  $\lambda = \frac{Pe}{Pg}$

- the constant  $c$  is found by requiring

$$1 = \sum_{n=0}^{\infty} p_n = c \sum_{n=0}^{\infty} \left( \frac{Pe}{Pg} \right)^n = c \frac{1}{1 - \frac{Pe}{Pg}}$$

- we thus find for the stationary state of the cavity light field

$t \rightarrow \infty$

$$S_f(\infty) = (1 - \frac{p_e}{p_g}) \sum_{n=0}^{\infty} \left( \frac{p_e}{p_g} \right)^n |n\rangle \langle n|$$

$$= (1 - \frac{p_e}{p_g}) \left( \frac{p_e}{p_g} \right)^{\text{ata}}$$

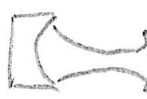
- if we assume that the energies of the atoms that are sent into the cavity are distributed according to a thermal equilibrium state, i.e.

$$\frac{p_e}{p_g} = \exp(-\beta \hbar \omega), \text{ with } \beta = \frac{1}{k_B T}$$

and to the energy difference between  $|g\rangle$  and  $|e\rangle$ , we find that also the cavity state becomes a thermal equilibrium state

$$\hookrightarrow S_f(\infty) = (1 - e^{-\beta \hbar \omega}) e^{-\beta \hbar \omega \text{ata}}$$

- the cavity acquires the same temperature as the atomic ensemble, i.e. the atoms take the role of a bath
- note, that a master equation of the type we consider here is also describing the situation, in which the cavity mode couples to an external thermal light field

 gain of a thermal photon  
loss of a cavity photon

- next, we investigate the dynamics of the cavity field operators
- an operator  $Y$  evolves under the Heisenberg equation of motion

$$\frac{\partial}{\partial t} Y = +i[\omega a, Y] + \overbrace{p_{\text{ex}}^{\dagger} (\alpha Y a^{\dagger} - \frac{1}{2} \{a a^{\dagger}, Y\})}^{\gamma_{\uparrow} \text{ sign change}} + \overbrace{p_g^{\dagger} Y (a^{\dagger} Y a - \frac{1}{2} \{a a^{\dagger}, Y\})}^{\gamma_{\downarrow} \text{ left} \leftrightarrow \text{right swap of the operators}}$$

- the general expression is the so-called adjoint master equation

$$\frac{\partial}{\partial t} Y = \frac{i}{\hbar} [H, Y] + \sum_k \gamma_k \left( L_k^+ Y L_k^- - \frac{1}{2} \{L_k^+ L_k^-, Y\} \right)$$

- for the evolution of the field lowering operator we find
- $$\frac{1}{2} a a a^{\dagger} - \frac{1}{2} a a^{\dagger} a = \frac{1}{2} [a, a a^{\dagger}] = \frac{1}{2} a$$

$$\frac{\partial}{\partial t} a = i [\omega a, a] + \gamma_{\uparrow} \left( a a a^{\dagger} - \frac{1}{2} a a^{\dagger} a - \frac{1}{2} a a a^{\dagger} \right)$$

$$+ \gamma_{\downarrow} \left( a a a a - \frac{1}{2} a a a a - \frac{1}{2} a a a a \right)$$

$$\frac{1}{2} a a a a - \frac{1}{2} a a a a = \frac{1}{2} [a a a, a] = -\frac{1}{2} a$$

$$= -i \omega a - \frac{1}{2} (\gamma_{\downarrow} - \gamma_{\uparrow}) a$$

$$\hookrightarrow a(t) = e^{-i \omega t - \frac{1}{2} (\gamma_{\downarrow} - \gamma_{\uparrow}) t} a(0)$$

- "coherences decay exponentially", i.e. when starting in a coherent state with  $\langle a(0) \rangle \neq 0$ , this initially non-zero expectation value will go to zero

for the number operator we obtain

$$\frac{1}{2}aa^{\dagger}aa^{\dagger} - \frac{1}{2}aa^{\dagger}$$

$$\frac{\partial}{\partial t}aa^{\dagger} = \gamma_r \underbrace{(aa^{\dagger}aa^{\dagger} - \frac{1}{2}aa^{\dagger}aa^{\dagger} - \frac{1}{2}aa^{\dagger}aa)}_{\frac{1}{2}aa^{\dagger}aa^{\dagger} - \frac{1}{2}aa^{\dagger}} + \gamma_i \underbrace{(aa^{\dagger}aa^{\dagger} - \frac{1}{2}aa^{\dagger}aa^{\dagger} - \frac{1}{2}aa^{\dagger}aa)}_{aa^{\dagger}aa^{\dagger} - aa^{\dagger}}$$

$$= \gamma_r aa^{\dagger} - \gamma_i aa^{\dagger} = -(\gamma_i - \gamma_r)aa^{\dagger} + \gamma_r$$

this equation has the solution

$$aa^{\dagger}(t) = \frac{1}{\gamma_i - \gamma_r} (\gamma_r (1 - e^{-(\gamma_i - \gamma_r)t}) + (\gamma_i - \gamma_r) e^{-(\gamma_i - \gamma_r)t} aa^{\dagger}(0))$$

in the stationary state ( $t \rightarrow \infty$ ) we thus obtain the average photon number

$$\bar{n} \equiv \langle aa^{\dagger}(\infty) \rangle = \frac{\gamma_r}{\gamma_i - \gamma_r} = \frac{p_e}{p_e - p_g} = \frac{e^{-\beta \hbar \omega}}{1 - e^{-\beta \hbar \omega}}$$

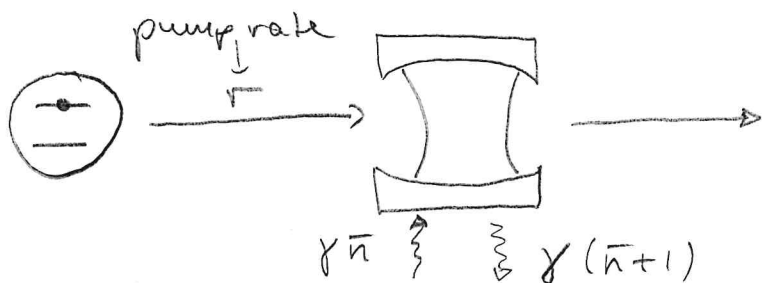
we can also express the Boltzmann factors in terms of  $\bar{n}$ :  $e^{-\beta \hbar \omega} = \frac{\bar{n}}{1 + \bar{n}} = \frac{p_e}{p_g}$

choosing  $p_e \propto \bar{n}$  and  $p_g \propto 1 + \bar{n}$  leads to a thermal stationary state with average photon number  $\bar{n}$

## IV. 5 Micromaser theory

(149)

- the micromaser is constituted by a high-quality cavity which is "pumped" by excited atoms that enter one by one at a rate  $\Gamma$



- we will also consider gain and loss of cavity photons that would thermalise the cavity (in the absence of the pumping) to a thermal state with average photon number  $\bar{n}$
- let us first consider the pumping dynamics
- the change of the cavity state,  $\Delta g$ , after a transit of an atom is given by

$$\Delta g = \left[ g(\Delta t) - g(0) \right] \Gamma \Delta t$$

$\uparrow$                        $\uparrow$                        $\uparrow$   
 cavity state when atom has left      cavity state before atom enters      interaction time

- using our previous results, we find

$$\Delta g = \left[ U_{\text{free}} \sum_{m=0}^1 K_m g(0) K_m U_{\text{free}}^* - g(0) \right] \Gamma \Delta t$$

with  $K_0 = \cos(\varphi \sqrt{\omega} \Delta t)$ ,  $K_1 = -i \Delta t \frac{\sin(\varphi \sqrt{\omega} \Delta t)}{\sqrt{\omega}}$ ,  $\varphi = \frac{1}{\hbar} \int_0^{\Delta t} d\tau \lambda(\tau)$

$$\hookrightarrow \frac{\Delta g}{\Delta t} \Big|_{\text{pumping}} = \Gamma \left( U_{\text{free}} \sum_{m=0}^1 K_m g K_m^+ U_{\text{free}} - g \right) \underbrace{\qquad}_{\text{jump operators}}$$

- note, the right-hand side is actually in Lindblad form:  $L_m = U_{\text{free}} K_m$
- we now make the simplifying assumption that thermal gain and loss can simply be added to the pumping (independent rate approximation)
- the density matrix of the cavity field then evolves (phenomenologically) according to

$$\frac{\partial \rho}{\partial t} = \frac{\Delta g}{\Delta t} \Big|_{\text{pumping}} + \gamma \bar{n} (a^\dagger \rho a - \frac{1}{2} \{ \rho a^\dagger, a \}) + \gamma (\bar{n}+1) (a \rho a^\dagger - \frac{1}{2} \{ \rho a^\dagger, a \})$$

- to find the solution of this equation we make the diagonal ansatz

$$\rho = \sum_{n=0}^{\infty} p_n |n\rangle \langle n|$$

$$\begin{aligned} \sum_n \dot{p}_n |n\rangle \langle n| &= \sum_n p_n \left( \Gamma \cos(\varphi \sqrt{n+1}) |n\rangle \langle n| \cos(\varphi \sqrt{n+1}) \right. \\ &\quad \left. + \Gamma \sqrt{n+1} \frac{\sin(\varphi \sqrt{n+1})}{\sqrt{n+1}} |n+1\rangle \langle n+1| \right. \\ &\quad \left. - \Gamma |n\rangle \langle n| \right. \\ &\quad \left. + \gamma \bar{n} \left( \Gamma \sqrt{n+1} |n+1\rangle \langle n+1| \Gamma \sqrt{n+1} - (n+1) |n\rangle \langle n| \right) \right. \\ &\quad \left. + \gamma (\bar{n}+1) \left( \Gamma_n |n-1\rangle \langle n-1| \Gamma_n - n |n\rangle \langle n| \right) \right) \end{aligned}$$

(151)

$$-r \sin^2(\varphi \sqrt{n+1}) p_n$$

$$\hookrightarrow r \cos^2(\varphi \sqrt{n+1}) p_n - r p_n + r \sin^2(\varphi \sqrt{n}) p_{n-1} + \gamma \bar{n} n p_{n-1} - \gamma \bar{n} (n+1) p_n + \gamma (\bar{n}+1) (n+1) p_{n+1} = \dot{p}_n$$

for the stationary state we set  $\dot{p}_n = 0$

$$\hookrightarrow r \sin^2(\varphi \sqrt{n}) p_{n-1} + \gamma \bar{n} n p_{n-1} - \gamma (\bar{n}+1) n p_n$$

$$= r \sin^2(\varphi \sqrt{n+1}) p_n + \gamma \bar{n} (n+1) p_n - \gamma (\bar{n}+1) (n+1) p_{n+1}$$

- both lines are equal for all  $n$ , and choosing the particular case  $n=0$ , we find that they are in fact both equal to zero

- this yields the simpler relation

$$\gamma (\bar{n}+1) n p_n = (r \sin^2(\varphi \sqrt{n}) + \gamma \bar{n} n) p_{n-1}$$

$$\hookrightarrow p_n = \left( \frac{r}{\gamma} \frac{1}{\bar{n}+1} \frac{\sin^2(\varphi \sqrt{n})}{n} + \frac{\bar{n}}{\bar{n}+1} \right) p_{n-1}$$

- the solution of this recurrence relation is

$$p_n = p_0 \prod_{l=1}^n \left( \frac{r}{\gamma} \frac{1}{\bar{n}+1} \frac{\sin^2(\varphi \sqrt{l})}{l} + \frac{\bar{n}}{\bar{n}+1} \right)$$

- the value for  $p_0$  is found through the normalisation condition  $\sum_{n=0}^{\infty} p_n = 1$

- now that we have an explicit expression for  $p_n$  we can calculate all stationary properties of the cavity field, e.g.  $\langle n \rangle = \sum_{n=0}^{\infty} n p_n$  and  $\langle n^2 \rangle = \sum_{n=0}^{\infty} p_n n^2$

before we do this we briefly come back to the dynamics in order to see that there is a so-called "threshold" at which the stationary state properties change dramatically

- to this end we expand  $\sin^2(\varphi \bar{n}) \approx \varphi^2 \bar{n}$  and consider zero temperature, i.e.  $\bar{n} = 0$

$$\begin{aligned} \hookrightarrow \dot{p}_n &\approx -\Gamma \varphi^2 (n+1) p_n + \Gamma \varphi^2 n p_{n-1} + \gamma (n+1) p_{n+1} - \gamma n p_n \\ \hookrightarrow \langle n \rangle &= \sum_{n=0}^{\infty} n \dot{p}_n = -\Gamma \varphi^2 \sum_n n(n+1) p_n + \Gamma \varphi^2 \sum_n (n+1)^2 p_n \\ &\quad + \gamma \sum_n (n-1)n p_n - \gamma \sum_n n^2 p_n \\ &= \Gamma \varphi^2 \sum_n (n+1) p_n - \gamma \sum_n n p_n = (\underbrace{\Gamma \varphi^2 - \gamma}_{\text{growth/decay rate}}) \langle n \rangle + \Gamma \varphi^2 \end{aligned}$$

- apparently the mean photon number starts to grow exponentially as soon as  $\Gamma \varphi^2 > \gamma$ , i.e. the pumping is stronger than the cavity photon loss
- below this threshold the mean photon number is decaying exponentially with time
- to analyse the microwave one often uses the so-called pump parameter:  $\Theta = \sqrt{\frac{\Gamma}{\gamma}} \varphi$
- the threshold is then found at the critical value  $\Theta_c = 1$  (note, that this is only a perturbative result)

- the maximum number of photons that can be accumulated by the cavity field is given by  $N_{\text{ex}} = \frac{\Gamma}{\gamma} = \frac{\text{pump rate}}{\text{decay rate}}$
- at small values of  $\Theta$  the cavity is almost empty in the stationary state
- here the Mandel Q-parameter;  $Q = \frac{\langle n^2 \rangle - \langle n \rangle^2}{\langle n \rangle}$  - 1, is close to zero indicating approximately Poissonian photon statistics
- when passing the threshold  $\langle n \rangle$  shoots up, reaching  $N_{\text{ex}}$
- here the Q-parameter reaches large value, signalling a super-Poissonian statistics
- increasing  $\Theta$  further leads to a series of peaks in both Q and  $\langle n \rangle$ , due to the quasi-periodic nature of the microwave pump rates
- near those peaks the photon number distribution may become bi-modal, reminiscent of a first order phase transition

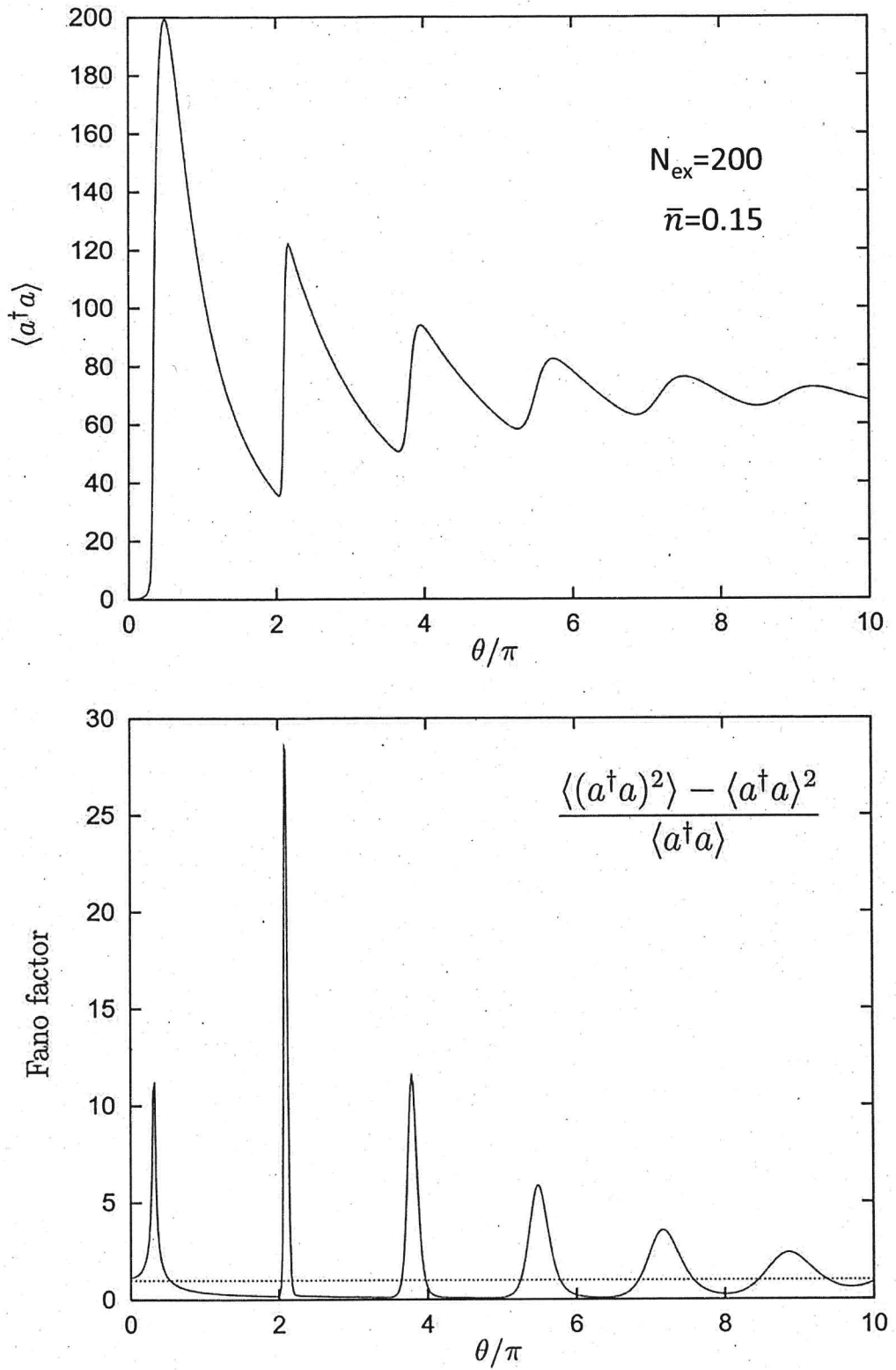


FIG. 9: Mean photon number and Fano factor in the OAM steady state for an effective rate of  $r/A = 200$  and a thermal photon number of  $\nu = 0.15$ , as a function of the pump parameter  $\theta$  in the range from  $\theta = 0$  to  $\theta = 10\pi$ .

Taken from

Berthold-Georg Englert, Elements of micromaser physics, arXiv:quant-ph/0203052 (2002)

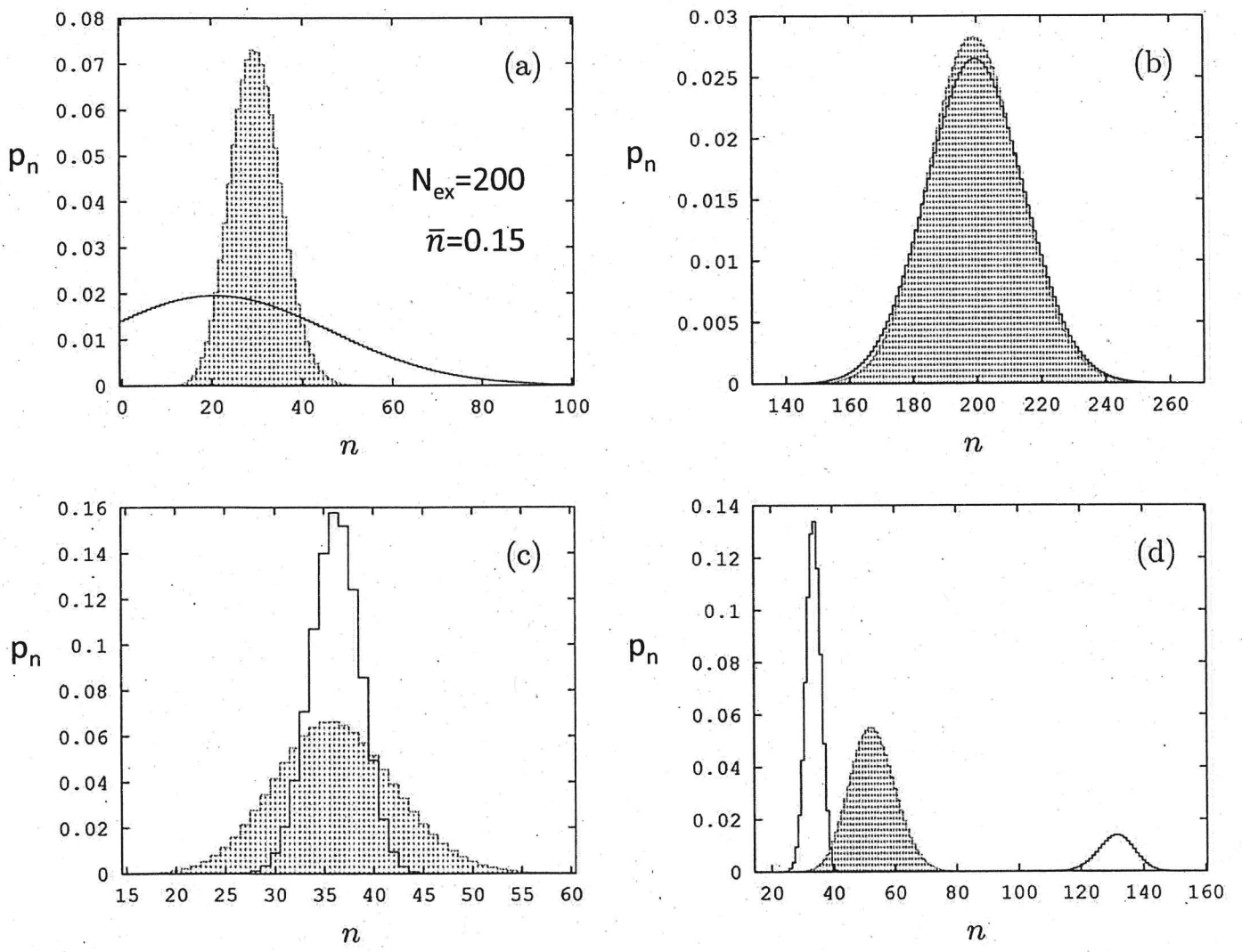


FIG. 11: Histograms for the photon number distribution in the OAM steady state for an effective rate of  $r/A = 200$  and a thermal photon number of  $\nu = 0.15$ . The plots are for (a)  $\theta = 0.32442\pi$  (i.e.,  $\varphi = 4.129^\circ$ ), (b)  $\theta = \pi/2$  (i.e.,  $\varphi = 6.364^\circ$ ), (c)  $\theta = 2\pi$  (i.e.,  $\varphi = 25.46^\circ$ ), and (d)  $\theta = 2.09\pi$  (i.e.,  $\varphi = 26.60^\circ$ ). The solid line shows the actual distribution. The broken line with the shaded area underneath shows the corresponding Poisson distribution with the same mean photon number. The respective mean photon numbers  $\langle a^\dagger a \rangle$  are (a) 30.14, (b) 199.44, (c) 36.25, and (d) 52.72. The Fano factors equal (a) 12.56, (b) 1.153, (c) 0.214, and (d) 28.68.

Taken from

Berthold-Georg Englert, Elements of micromaser physics, arXiv:quant-ph/0203052 (2002)

- next, we show that the peculiar form of the transition rates in the micromaser allows the preparation of Fock states
- to this end we consider the case of an extremely high quality cavity for which we can neglect spontaneous photon loss (and gain), i.e. we set  $\gamma = 0$
- the photon number probability distribution then evolves according to

$$\dot{p}_n = \underbrace{-r \sin^2(\varphi \sqrt{n+1}) p_n}_{= a_n p_n} + \underbrace{r \sin^2(\varphi \sqrt{n}) p_{n-1}}_{= a_{n-1} p_{n-1}}$$

- we now set the atom-light coupling strength such that for a certain number  $n_q$  inside the cavity, it becomes  $\varphi \sqrt{n_{q+1}} = q\pi$  ( $q=1, 2, 3, \dots$ )
- this means that an excited atom will undergo  $q$  Rabi oscillations when  $n_q$  photons are inside the cavity and thus also leaves the cavity in its excited state
- in this situation the cavity is said to be in an (upward) trapping state, since no transition from  $|n_q\rangle$  to  $|n_{q+1}\rangle$  can take place
- in the following we consider  $q=1$  and show that under the condition  $\varphi \sqrt{n_{q+1}} = \pi$  the Fock state  $|n_1\rangle$  is the stationary state of the micromaser

$$\frac{\partial}{\partial t} \vec{p} = M \vec{p}$$

eigenvalues and eigenvectors of  $M$   
 right left

$$M \vec{\alpha}^{(e)} = \lambda_e \vec{\alpha}^{(e)}$$

$$\vec{\beta}^{(e)T} M = \lambda_e \vec{\beta}^{(e)T}$$

$$\text{normalisation: } \vec{\beta}^{(e)T} \vec{\alpha}^{(e)} = 1$$

$$\text{completeness: } \sum_e \vec{\alpha}^{(e)} \vec{\beta}^{(e)T} = 1$$

spectral expansion

$$M = \sum_e \lambda_e \vec{\alpha}^{(e)} \vec{\beta}^{(e)T}$$

time evolution

$$\vec{p}(t) = e^{Mt} \vec{p}(0) = \sum_e e^{\lambda_e t} \vec{\alpha}^{(e)} \vec{\beta}^{(e)T} \vec{p}(0)$$

$$p_n(t) = \sum_e e^{\lambda_e t} \vec{\alpha}_n^{(e)} \sum_q \vec{\beta}_q^{(e)T} p_q(0)$$

- to this end we write the evolution equation as

$$\frac{\partial}{\partial t} \vec{p} = M \vec{p} \quad \text{with} \quad M = \begin{pmatrix} a_0 & & & 0 \\ -a_0 & a_1 & & \\ & -a_1 & a_2 & \\ 0 & & -a_2 & \end{pmatrix}$$

- the matrix  $M$  has the eigenvalues  $\lambda_e = a_e$
- the corresponding left- and right-hand eigenvectors are  $\vec{\beta}^{(e)}$  and  $\vec{\alpha}^{(e)}$ :  $M \vec{\alpha}^{(e)} = \lambda_e \vec{\alpha}^{(e)}$ ,  $\vec{\beta}^{(e)T} M = \lambda_e \vec{\beta}^{(e)T}$
- their components obey the recurrence relations

$$-a_{n-1} \alpha_{n-1}^{(e)} + a_n \alpha_n^{(e)} = a_e \alpha_n^{(e)}$$

$$a_{q-1} \beta_{q-1}^{(e)} - a_q \beta_q^{(e)} = a_e \beta_{q-1}^{(e)},$$

which are solved by

$$\alpha_n^{(e)} = \begin{cases} \prod_{r=0}^n \frac{a_{r+1}}{(a_r - a_e)} & , n > l \\ 1 & , n = l \\ 0 & , n < l \end{cases}$$

$$\beta_n^{(e)} = \begin{cases} \prod_{r=q}^{l-1} \frac{a_r}{a_r - a_e} & , q < l \\ 1 & , q = l \\ 0 & , q > l \end{cases}$$

- with these solutions, we can now write the evolution of the probabilities as

$$p_n(t) = \sum_{e=0}^{\infty} \sum_{q=0}^{\infty} \beta_n^{(e)} \alpha_q^{(e)} e^{i \omega_e t} p_q(0)$$

$$\hookrightarrow p_n(t) = \begin{cases} e^{a_0 t}, & n=0 \\ \sum_{l=0}^n \frac{\prod_{r=0}^{n-1} (a_r - a_l)}{\prod_{\substack{r=0 \\ r \neq l}}^n (a_r - a_l)} e^{a_l t}, & n \geq 1 \end{cases}$$

- Now note, that for a given  $n$ , all contributions in the sum with  $n > n_i$  are zero since  $a_{n_i} = -r \sin^2(\varphi \sqrt{n_i+1}) = 0$
- Moreover, all terms with  $n < n_i$  are exponentially decaying in time as they are proportional to  $e^{a_n t}$
- $\hookrightarrow$  in the limit  $t \rightarrow \infty$  the cavity state thus becomes the Fock state  $|n_i\rangle$ :

$$\lim_{t \rightarrow \infty} p_n(t) = \delta_{nn_i}$$